UNIVERSITAT DE BARCELONA

Desenvolupament de models d'*Orthoxenografts (PDOX)* per al seu ús en oncologia

August Vidal i Bel

DESENVOLUPAMENT DE MODELS D'*ORTHOXENOGRAFTS* (*PDOX*) PER AL SEU ÚS EN ONCOLOGIA

Memòria de Tesi Doctoral presentada per **August Vidal i Bel** per a optar al grau de Doctor per la Universitat de Barcelona

Dirigida per

Enric Condom i Mundó, Facultatiu Emèrit del Servei d'Anatomia Patològica de l'Hospital Universitari de Bellvitge

Alberto Villanueva Garatachea, Investigador del Programa contra la resistència terapèutica del càncer (PROCURE) de l'Institut Català d'Oncologia, cap del grup de Quimioresistència i factors predictors de resposta tumoral i medi ambient estromal de l'àrea de Càncer i genètica molecular humana de l'Institut d'investigació biomèdica de Bellvitge

Tutora

Mireia Martín Satué, Catedràtica del Departament de Patologia i Terapèutica Experimental de la Universitat de Barcelona

Programa de Doctorat Medicina i Recerca Translacional (2020-2024)

Facultat de Medicina i Ciències de la Salut. Universitat de Barcelona

Juny de 2024

Als meus pares,
a Xavier i a Enric
i a Iolanda

AGRAÏMENTS

La realització d'aquest treball d'investigació ha estat fruit de temps de la meva dedicació a l'anatomia patològica, especialitat que m'apassiona i que fa gairebé 30 anys que desenvolupo en el servei d'Anatomia Patològica de l'Hospital Universitari de Bellvitge. L'amor a la meva professió i el respecte que em mereix cadascun dels pacients, fa de cada cas un nou motiu d'estudi i aprenentatge, tractant de treballar-lo amb la vivor de la seva singularitat. A tots aquests pacients la meva consideració i l'agraïment.

Aquesta labor diària m'ha aportat ritme i immersió, condicions necessàries per a orientar el desig de recerca cap a aquesta àrea. El meu interès per cada procés diagnòstic m'ha anat despertant el desig d'elaborar una recerca que reculli part de la meva experiència d'aquests anys.

Vull fer arribar el meu més sincer agraïment als companys de l'HUB amb els qui he compartit l'experiència de la medicina en un ambient gran i exigent, una sort que permet tractar un volum de clínica important alhora que consultar amb altres col·legues que ajuden a pensar els casos difícils. Un agraïment especial a tot el personal del servei d'Anatomia Patològica de Bellvitge, cel·ladors, tècnics, administratius i col·legues d'especialitat, he pogut comptar amb tots ells pel què he necessitat.

La meva consideració i estima a tots els patòlegs de l'Hospital de Bellvitge amb els que he compartit professió i vivències; alguns d'ells ara ja no hi són, bé perquè han marxat o bé perquè ja ens han deixat. El seu record reactiva en mi els moments compartits, tant a nivell personal com en els espais clínics i d'aprenentatge dintre de l'hospital.

Així mateix als residents d'aquest servei pel que signifiquen d'il·lusió i projecte de futur. Ells són les noves generacions de patòlegs als qui tenim la responsabilitat de saber arribar-los de la bona manera i animar en ells el desig de seguir cuidant, estimant i millorant la nostra especialitat.

En el que ha estat el llarg recorregut d'aquesta tesi, amb els seus diversos moments d'impàs i reactivació, em cal fer uns altres compliments, francs i amb estima, a les persones que han estat incondicionals en el seu suport actiu i confiat cap a mi i cap al projecte que he acabat desenvolupant. Sense totes elles, una per una, no hagués pogut culminar aquest treball de la mateixa manera.

A la Dra. Mireia Martín Satué li agraeixo la seva excel·lent disposició en la tutoria i en orientar-me en el que ha implicat per a mi la construcció i la realització d'aquesta tesi.

A l'Alberto Villanueva Garatachea perquè des del moment en què ens vàrem conèixer m'ha transmès un entusiasme alegre per la recerca i és, avui, un amic i un bon company amb qui compartim projectes professionals i altres aventures.

Al qui és, des de fa molts anys ja, el meu molt bon amic i mestre Enric Condom i Mundó. Ell ha estat el meu company a l'hospital i hem pogut compartir molts anys d'experiències de recerca, treball i d'estudi, així com la vivència de temps personals que ens han apropat. Amic íntim, familiar i referent. Amb ell hem mantingut moltes converses, dins i fora de l'hospital, que m'han fet créixer com a patòleg i com a persona. Gairebé cada paraula i cada silenci d'aquestes trobades han tingut el seu efecte per a mi.

Al Dr. Joan Josep Sirvent Calvera, el meu primer professor i mestre que, amb el seu respecte per la professió, entusiasme i cura per la bona transmissió d'aquesta especialitat, va saber despertar en mi l'amor per l'anatomia patològica. Avui, també, un vell amic a qui li tinc un gran afecte.

Em cal, encara, dedicar unes paraules a les persones amb les qui comparteixo la meva vida i que han estat, i són, els meus suports fonamentals i alè del què m'anima. El meu profund agraïment als meus fills i a la meva dona.

A Xavier perquè amb el seu fer enèrgic i alegre em fa arribar humor i plena confiança.

A Enric perquè en les nostres converses m'aporta reflexió i desig de seguir aprenent.

I a Iolanda per la paciència d'aguantar-me en els meus moments difícils; trobo en ella el gest de l'amor i la paraula que em desperta.

No m'oblido, mai, dels meus pares, Joaquim i Teresa; ells van encendre la meva primera espurna, llum que continua ben viva dintre meu.

FINANÇAMENT

Aquest treball ha estat en part finançat per:

August Vidal ha rebut una beca BAE (BAE11/00073) de l'Instituto de Salud Carlos III.

Alberto Villanueva ha rebut FIS PI10-0222, CDTI IDI 2010 1640, SAF 2002-02265, FIS BFU 2007-67123, FIS PI13-01339, FIS PI16-01898.

ÍNDEX

ÍNDEX

GLOSSARI **23**
ABREVIATURES **27**
ENUMERACIÓ DELS ARTICLES QUE COMPOSEN LA TESI **31**
INTRODUCCIÓ **37**
CÀNCER D'OVARI 39
TUMORS TESTICULARS DE CÈL·LULES GERMINALS (TTCG) 45
CÀNCER DE PULMÓ 51
CÀNCER D'ENDOMETRI 55
MODELS PRECLÍNICS EN LA RECERCA DEL CÀNCER. 62
GENERACIÓ DE MODELS PDX (Patient Derived Xenografts) 65
CARACTERÍSTIQUES DESTACADES DELS MODELS PDX 69
APLICACIONS DELS MODELS PDX EN LA INVESTIGACIÓ DEL CÀNCER 73
LIMITACIONS EN L'ÚS DELS MODELS PDX 78
PREMISSES **81**
HIPÒTESI **85**
OBJECTIUS **89**
MATERIAL I MÈTODES I RESULTATS **93**
ARTICLE 1: 95
ARTICLE 2: 113
ARTICLE 3 147
ARTICLE 4 175
DISCUSSIÓ **225**
CONSIDERACIONS FINALS 236
CONCLUSIONS **237**
BIBLIOGRAFIA **241**

GLOSSARI

Orthoallografts (Ortoal·loempelt): models consistents en la implantació d'un fragment de tumor murí al mateix òrgan d'origen d'un ratolí. El prefix ortho- significa al mateix òrgan i allo- significa que el trasplantament de l'empelt es realitza entre individus de la mateixa espècie.

Orthoxenografts (Ortoxenoempelt): models consistents en la implantació d'un fragment de tumor humà al mateix òrgan d'origen d'un ratolí. El prefix ortho- significa al mateix lloc i xeno- significa que el trasplantament de l'empelt es realitza entre espècies diferents (tumors humans en ratolins).

PDOX: sigles derivades de l'anglès "Patient Derived Orthotopic Xenograft": empelt ortotòpic derivat de pacient. És la manera en què més freqüentment estan citats aquesta mena de models a la literatura. Són models en què s'ha fet créixer un tumor d'un pacient al mateix òrgan d'origen d'un ratolí immunodeficient.

PDX: sigles derivades de l'anglès "Patient Derived Xenograft": empelt derivat de pacient. És la manera en què més freqüentment estan citats aquesta mena de models a la literatura. Són models en què s'ha fet créixer un tumor d'un pacient en un ratolí immunodeficient. En general se sol referir a implantacions subcutànies.

ABREVIATURES

ADN: Àcid desoxiribonucleic.

AFP: Alfa Fetoproteïna.

ARN: Àcid ribonucleic.

CCR: Càncer colorectal.

CDX: *Cell Derived Xenograft*.

CE: Càncer d'endometri.

CEO: Càncer epitelial d'ovari.

CNA: Copy Number Alteration.

CPNCP: Carcinoma de pulmó no cèl·lula petita.

EMA: European Medicines Agency.

FDA: Food and Drug Administration

GCS: Glucosil Ceramida Sintasa.

GEMM: Genetically Engineered Mouse Models.

hCG: Gonadotrofina coriònica humana.

HRD: Homologous Recombination Deficiency.

ILV: Invasió limfovascular.

LDH: Lactat deshidrogenasa.

NCI: National Cancer Institute.

NGS: Next Generation Sequencing.

PARP: Poly (ADP-ribose) Polimerase.

PDX: Patient Derived Xenograft.

PDOX: Patient Derived Orthotopic Xenograft.

PFS: Progression Free Survival.

QMT: Quimioteràpia.

SCID: Severe Combined Immunodeficiency.

STIC: Serous Tubal Intraepithelial Carcinoma.

TCGA: The Cancer Genome Atlas.

TILs: Tumor infiltrating lymphocytes.

TTCG: Tumor Testicular de Cèl·lules Germinals.

UCEC: Uterine Corpus Endometrial Carcinoma.

WES: Whole Exome Seguencing.

5-FU: 5-Fluorouracil.

ENUMERACIÓ DELS ARTICLES QUE COMPOSEN LA TESI

Tesi en format de compendi de publicacions

La Tesi consta d'un objectiu general, sis objectius específics i quatre articles.

ARTICLE 1

Vidal, A.*; Muñoz, C.*; Guillem, M.J.; Moreto, J.; Sara, P.; Martínez-Iniesta, M.; Figueras, A.; Padullés, L.; Rodriguez, F.G.; Berdiel-Hacer, M.; Pujana, M.A.; Salazar, R.; Gil-Martín, M.; Martí, L.; Ponce, J.; Molleví, D.G.; Capellà, G.; Condom, E.; Viñals, F.; Huertas, D.; Cuevas, C.; Esteller, M.; Avilés,P.; Villanueva, A. Lurbinectedin (PM01183), a New DNA Minor Groove Binder, Inhibits Growth of Orthotopic Primary Graft of Cisplatin-Resistant Epithelial Ovarian Cancer. Clinical Cancer Research 2012; 18: 5399 - 5411.

PMID: 22896654 DOI: 10.1158/1078-0432.CCR-12-1513

*Aquests autors han contribuït igualment a aquest article

Factor d'impacte: 7,837; Quartil: 1er; Decil: 1er; Àrea de coneixement: Oncology; Posició de la revista: 12 de 197.

ARTICLE 2

Piulats, J.M.*; **Vidal, A.***; García-Rodríguez, F.J.; Muñoz, C.; Nadal, M.; Moutinho, C.; Martínez-Iniesta, M.; Mora, J.; Figueras, A.; Guinó, E.; Padullés, L.; Aytés, À.; Mollevi, D.G.; Puertas, S.; Martínez-Fernández, C.; Castillo, W.; Juliachs, M.; Moreno, V.; Muñoz, P.; Stefanovic, M.; Pujana, M.A.; Condom, E.; Esteller, M.; Germà-LLuch, J.R.; Capella, G.; Farré, L.; Morales, A.; Viñals, F.; Garcia Del Muro, X.; Cerón, J.; Villanueva, A. Orthoxenografts of testicular germ cell tumors demonstrate genomic changes associated with cisplatin resistance and identify PDMP as a re-sensitizing agent. Clinical Cancer Research 2018; 24: 3755 - 3766.

PMID: 29618620 DOI: 10.1158/1078-0432.CCR-17-1898

*Aquests autors han contribuït igualment a aquest article

Factor d'impacte: 8,911; Quartil: 1er; Decil: 1er; Àrea de coneixement: Oncology; Posició de la revista: 16 de 229.

ARTICLE 3

Ambrogio, C.; Carmona, F.J.; **Vidal, A.**; Falcone, M.; Nieto, P.; Romero, O.A.; Puertas, S.; Vizoso, M.; Nadal, E.; Poggio, T.; Sánchez-Céspedes, M.; Esteller, M.; Mulero, F.; Voena, C.; Chiarle, R.; Barbacid, M.; Santamaria,D.; Villanueva, A. Modeling lung càncer evolution and preclinical response by orthotopic mouse allografts. Cancer Research 2014; 74: 5978 – 5988.

PMID: 25217522 DOI: 10.1158/0008-5472.CAN-14-1606

Factor d'impacte: 9,329; Quartil: 1er; Decil: 1er; Àrea de coneixement: Oncology; Posició de la revista: 11 de 211.

ARTICLE 4

Devis-Jauregui, L*; **Vidal, A.***; Plata-Peña, L.*; Santacana, M.; García-Mulero, S.; Bonifaci, N.; Noguera-Delgado, E.; Ruiz, N.; Gil, M.; Dorca, E.; Llobet, F.J.; Coll-Iglesias, L.; Gassner, K.; Martinez-Iniesta, M.; Rodriguez-Barrueco, R.; Barahona, M.; Marti, L.; Viñals, F.; Ponce, J.; Sanz-Pamplona, R.; Piulats, J.M.; Vivancos, A.; Matias-Guiu, X.; Villanueva, A.; Llobet-Navas, D. Generation and Integrated Analysis of Advanced Patient-Derived Orthoxenograft Models (PDOX) for the Rational Assessment of Targeted Therapies in Endometrial Cancer. Advanced Science 2023; 10: 2204211.

PMID: 36373729 PMCID: PMC9811454 DOI: 10.1002/advs.202204211

*Aquests autors han contribuït igualment a aquest article

Factor d'impacte (2022): 15,1

Quartil: 1er; Decil: 1er; Àrea de coneixement: Chemistry, Multidisciplinary; Posició de la revista: 16/178.

Quartil: 1er; Decil: 1er; Àrea de coneixement: Materials Science, Multidisciplinary; Posició de la revista: 24/344.

Quartil: 1er; Decil: 2on; Àrea de coneixement: Nanoscience & Nanotechnology; Posició de la revista: 14/108.

INTRODUCCIÓ

El tractament del càncer es basa en la combinació de diferents opcions terapèutiques que inclouen cirurgia, diferents tipus de fàrmacs entre els que hi ha agents quimioteràpics, teràpia hormonal i agents biològics, i radioteràpia. L'elecció d'una o vàries d'aquestes alternatives dependrà del tipus de càncer i de l'estadi de la malaltia al moment del diagnòstic. Així, en general, els càncers localitzats es tracten primàriament amb cirurgia, podent afegir alguna mena d'adjuvància, mentre que en els tumors disseminats el tractament comença amb alguna mena de teràpia sistèmica. Si bé la mortalitat per càncer pot ser deguda al creixement local de les neoplàsies, per exemple en tumors del sistema nerviós central, en general està causada per disseminació de la malaltia i per manca de resposta dels tumors a aquests tractaments sistèmics.

En les darreres dècades s'ha avançat força en el coneixement de les bases moleculars i cel·lulars del càncer. Això ha contribuït a entendre els mecanismes de carcinogènesi i progressió de la malaltia però, excepte en comptades excepcions com són el cas de la teràpia anti-her2 en càncer de mama (1–3) i l'imatinib en la leucèmia mieloide crònica (4–6), ha contribuït poc en la millora de la supervivència a llarg termini de la majoria de càncers. Es calcula que únicament un 10% de les molècules que s'estudien arribaran finalment a la clínica. Aquesta elevada taxa de fracassos és deguda, en part a la manca de bons models preclínics.

CÀNCER D'OVARI

El càncer d'ovari és molt variat i heterogeni incloent tumors derivats de cèl·lules germinals, dels cordons sexuals i de l'estroma, però més del 90% correspon a tumors epitelials. Cada vegada hi ha més evidència que aquests darrers s'originen majoritàriament de cèl·lules epitelials de la trompa uterina o bé de focus d'endometriosi.

EPIDEMIOLOGIA

El càncer d'ovari és el vuitè més freqüent en dones, entre les que representa aproximadament el 3,7% de diagnòstics de càncer i el 4,7% del total de morts

per càncer el 2020, essent la cinquena causa de mort per càncer en dones i la principal causa de mort per càncer ginecològic pelvià a Europa i els Estats Units (7).

Històricament la seva incidència ha estat més elevada en països desenvolupats i rics del nord d'Europa i Amèrica, però les darreres dècades hi ha hagut un descens en la incidència en aquestes àrees probablement en relació amb l'ús d'anticonceptius hormonals i amb el canvi en la manera de registrar-lo des de que s'ha vist que molts dels tumors tenen origen en les trompes uterines (8). Per contra, sembla que la incidència augmenta en països d'Europa de l'est i en algunes parts d'Àsia. En altres regions com l'Àfrica subsahariana es manté una incidència baixa (9).

ETIOLOGIA I PATOGÈNIA

S'han identificat diversos factors de risc per a desenvolupar càncer d'ovari, associats als diferents tipus histològics. Així, la història familiar en familiars de primer grau incrementa 3-5 vegades el risc de desenvolupar carcinoma serós d'alt grau, una història d'endometriosi s'associa amb més risc de desenvolupar carcinoma endometrioide i de cèl·lules clares i, en menor proporció, de carcinoma serós de baix grau i el consum de tabac incrementa el risc de carcinoma mucinós. Per contra, els embarassos , la lactància materna i l'ús d'anticonceptius hormonals sembla que poden tenir un efecte protector (10).

Un dels factors de risc més robust per a càncer d'ovari és la història familiar de la malaltia en un familiar de primer grau. Una quarta part d'aquestes pacients són portadores de variants patogèniques de *BRCA1* i *BRCA2* en línia germinal. Les dones portadores de mutacions a *BRCA1* tenen entre un 44% i un 61% de risc de desenvolupar càncer d'ovari al llarg de la vida. En les portadores de *BRCA2* mutat el risc es de 17-24% (11,12). La majoria d'aquests casos seran carcinomes serosos d'alt grau. També hi ha casos en què la mutació afecta altres gens implicats en la recombinació homòloga com ara *RAD51C/D*, *PALB2* i *BRIP1* (13). En pacients amb síndrome de Lynch, portadores de mutacions en línia germinal a *MLH1*, *MSH2*, *MSH6* i *PMS2*, hi ha un increment en el número de casos i la

majoria corresponen a carcinomes endometrioides o de cèl·lules clares, encara que també hi ha casos de carcinomes serosos d'alt grau (12,14,15).

La lesió precursora en el carcinoma serós d'alt grau és el carcinoma serós intraepitelial tubàric (STIC de les seves sigles en anglès) normalment present a les fímbries tubàriques. Lesions similars es poden veure a l'escorça ovàrica en inclusions epitelials d'epiteli de tipus tubàric (16,17). Aquestes lesions ja tenen les mateixes mutacions que es poden veure en els carcinomes infiltrants (18,19). De fet, aquesta lesió és la que se sol trobar en les salpingo-ooforectomies profilàctiques en pacients portadores de mutacions en *BRCA1* o *BRCA2* (20,21).

TIPUS HISTOLÒGICS

La classificació histològica vigent dels tumors d'ovari contempla 5 tipus principals, responsables del 98% de tots els carcinomes d'ovari: carcinoma serós d'alt grau, carcinoma de cèl·lula clara, carcinoma endometrioide, carcinoma mucinós i carcinoma serós de baix grau (22). Cadascun d'aquests tipus presenta característiques diferencials des del punt de vista histològic, molecular i carcinogènic que es tradueixen en comportaments clínics i respostes als tractaments diferents. El carcinoma serós d'alt grau és el tipus més freqüent (9) i més del 80% dels casos diagnosticats en estadis III o IV corresponen a aquest tipus histològic (23). Està constituït per cèl·lules molt atípiques, amb marcada anisocitosi, que es disposen en patró papil·lar, glandular o sòlid i tenen un elevat índex mitòtic. Sempre són tumors de grau 3/3. Des del punt de vista immunohistoquímic es caracteritzen per expressar WT1 i mostrar un patró anormal d'expressió de p53 (24). El carcinoma de cèl·lula clara es caracteritza pel patró arquitectural que pot ser papil·lar, túbulo-quístic o sòlid, amb papil·les i túbuls revestits per una sola capa de cèl·lules que tenen un atípia citològica homogènia i, en general, poques figures de mitosi. Són tumors d'alt grau. Aquestes cèl·lules poden tenir abundant glucogen intracitoplasmàtic, que li confereix l'aspecte clar. Des del punt de vista immunohistoquímic no expressen WT1 ni receptors d'estròGens i progesterona, tenen patró normal d'expressió de p53 i poden mostrar expressió intracitoplasmàtica de Napsina-A (24). El carcinoma endometrioide és semblant al de l'endometri. Pot tenir diferenciació

escamosa i es grada en funció de la proporció de component sòlid, així, si aquest representa <5% del volum tumoral és un grau 1, entre el 5 i el 50% grau 2 i més del 50% de component sòlid és un grau 3. Els graus 1 i 2 es consideren tumors de baix grau. En general no expressen WT1, 14-15% de casos tenen patró anormal de p53, no expressen Napsina-A i solen expressar receptors d'estròg ens i progesterona (24). El carcinoma serós de baix grau sol tenir una morfologia papil·lar i micropapil·lar, però també pot ser glandular. Està constituït per unes cèl·lules poc atípiques, de grandària homogènia i escasses figures de mitosi que expressen WT1 i tenen un patró normal d'expressió de p53 (24). El carcinoma mucinós està constituït per cèl·lules caliciformes semblants a les del tracte gastro-intestinal. Pot tenir dos patrons de creixement: expansiu i infiltrant, essent el segon més agressiu. Poden tenir expressió anormal de p53 i poden expressar marcadors propis de tumors gastro-intestinals com citoqueratina 20 i CDX2 . Davant d'un carcinoma mucinós a l'ovari sempre s'ha de descartar que es tracti d'una metàstasi d'origen extrínsec (24).

ESTADIFICACIÓ

El càncer d'ovari, trompa uterina i peritoneu s'estadifica de la mateixa manera i té en compte les característiques del tumor primari (T), l'afectació dels ganglis regionals (N), la presència de metàstasis a distància (M) (Taula 1)(25,26) .

T	Tumor primari
Tx	El tumor primari no pot ser avaluat.
T0	No hi ha evidència de tumor primari.
T1	Tumor limitat als ovaris (un o els dos) o les trompes de Fal·lopi.
T1a	Tumor limitat a un ovari (càpsula intacta) o trompa de Fal·lopi, sense tumor a la superficie ovárica o de la trompa i sense cèl·lules malignes a l'ascites o als rentats peritoneals.
T1b	Tumor limitat als dos ovaris (càpsula intacta) o trompes de Fal·lopi, sense tumor a la superficie ovárica o de la trompa i sense cèl·lules malignes a l'ascites o als rentats peritoneals.
T1c	Tumor limitat a un o els dos ovaris o trompes de Fal·lopi amb alguna de les següents dades:
T1c1	Trencament intraquirúrgic de la càpsula.
T1c2	Càpsula trencada abans de la cirurgia o tumor sobre la superfície ovàrica o tubàrica.
T1c3	Cèl·lules malignes a l'ascites o als rentats peritoneals.
T2	Tumor afectant un o tots dos ovaris o trompes de Fal·lopi amb extensió peritoneal per sota de la vora pelviana o càncer primari peritoneal.
T2a	Extensió i/o implants sobre l'úter i/o les trompes de Fal·lopi i/o els ovaris.
T2b	Extensió i/o implants sobre altres teixits pelvians.

T3	Tumor afectant un o tots dos ovaris o les trompes de Fal·lopi o càncer primari peritoneal amb metàstasis peritoneals fora de la pelvis i/o metàstasis a ganglis limfàtics retroperitoneals (pelvians i/o para-aòrtics).
T3a	Afectació microscòpica peritoneal extra-pelviana (per damunt de la vora pelviana) amb o sense ganglis limfàtics retroperitoneals positius.
T3b	Metàstasi peritoneal macroscòpica ≤ 2cm més enllà de la pelvis amb o sense metàstasis a ganglis limfàtics retroperitoneals.
T3c	Metàstasi peritoneal macroscòpica > 2cm més enllà de la pelvis amb o sense metàstasis a ganglis limfàtics retroperitoneals.

N	Ganglis limfàtics regionals
px	Els ganglis regionals no poden ser avaluats.
N0	No hi ha metàstasi a ganglis regionals
N0(i+)	Cèl·lules tumorals aïllades ≤ 0,2 mm
N1	Metàstasi a ganglis limfàtics retroperitoneals.
N1a	Metàstasi ≤ 10 mm.
N1b	Metàstasi > 10 mm.

M	Metàstasi a distància
M1	Metàstasi a distància incloent vessament pleural amb citologia positiva, metàstasis parenquimatoses hepàtiques o esplèniques o metàstasis a òrgans extra-abdominals (incloent ganglis limfàtics inguinals i ganglis limfàtics de fora de la cavitat abdominal.
M1a	Vessament pleural amb citologia positiva
pM1b	Metàstasis parenquimatoses hepàtiques o esplèniques o metàstasis a òrgans extra-abdominals (incloent ganglis limfàtics inguinals i ganglis limfàtics de fora de la cavitat abdominal)

Taula 1. Classificació TNM del càncer d'ovari, trompa uterina i peritoneu. Adaptat de (25)

En base a aquestes característiques s'estableixen els estadis clínics amb correlació pronòstica que estan representats a la taula 2.

ESTADI FIGO	**Definició**
I	Tumor limitat als ovaris (un o els dos) o les trompes de Fal·lopi.
IA	Tumor limitat a un ovari (càpsula intacta) o trompa de Fal·lopi, sense tumor a la superficie ovárica o de la trompa i sense cèl·lules malignes a l'ascites o als rentats peritoneals.
IB	Tumor limitat als dos ovaris (càpsula intacta) o trompes de Fal·lopi, sense tumor a la superficie ovárica o de la trompa i sense cèl·lules malignes a l'ascites o als rentats peritoneals.
IC	Tumor limitat a un o els dos ovaris o trompes de Fal·lopi amb alguna de les següents dades:
IC1	Vessament quirúrgic intraoperatori.
IC2	Càpsula trencada abans de la cirurgia o tumor sobre la superfície ovàrica o tubàrica.
IC3	Cèl·lules malignes a l'ascites o als rentats peritoneals.
II	Tumor afectant un o tots dos ovaris o trompes de Fal·lopi amb extensió peritoneal per sota de la vora pelviana o càncer primari peritoneal.
IIA	Extensió i/o implants sobre l'úter i/o les trompes de Fal·lopi i/o els ovaris.
IIB	Extensió i/o implants sobre altres teixits pelvians.
III	Tumor afectant un o tots dos ovaris o les trompes de Fal·lopi o càncer primari peritoneal amb metàstasis peritoneals fora de la pelvis i/o metàstasis a ganglis limfàtics retroperitoneals (pelvians i/o para-aòrtics).
IIIA	Metàstasis a ganglis limfàtics retroperitoneals amb o sense afectació peritoneal microscòpica més enllà de la pelvis.
IIIA1	Només ganglis limfàtics retroperitoneals positius.

IIIA1(i)	Metàstasi ≤ 10 mm.
IIIA1(ii)	Metàstasi > 10 mm.
IIIA2	Afectació microscòpica peritoneal extra-pelviana (per damunt de la vora pelviana) amb o sense ganglis limfàtics retroperitoneals positius.
IIIB	Metàstasis peritoneal macroscòpica ≤ 2cm més enllà de la pelvis amb o sense metàstasis a ganglis limfàtics retroperitoneals.
IIIC	Metàstasis peritoneal macroscòpica > 2cm més enllà de la pelvis amb o sense metàstasis a ganglis limfàtics retroperitoneals.
IV	Metàstasi a distància excloent metàstasis peritoneals.
IVA	Vessament pleural amb citologia positiva
IVB	Metàstasis parenquimatoses hepàtiques o esplèniques, metàstasis a òrgans extra-abdominals (incloent ganglis limfàtics inguinals i ganglis limfàtics de fora de la cavitat abdominal) o afectació transmural del budell.

Taula 2. Estadis del càncer d'ovari, trompa uterina i peritoneu. Adaptat de (Bhatla Int J Gynecol Obstat 2018-FIGO report 2018)

En resum, l'estadi I correspon a tumors d'ovari o trompa de Fal·lopi que no afecten altres estructures, que poden tenir o no cèl·lules al líquid ascític o als rentats peritoneals, l'estadi II són tumors d'ovari, trompa o peritoneu amb afectació d'altres estructures pelvianes, l'estadi III representa tumors d'ovari, trompa o peritoneu amb afectació de peritoneu extra pelvianes o bé amb metàstasis a ganglis regionals i l'estadi IV correspon a tumors amb disseminació extraabdominal o bé amb metàstasis intraparenquimatoses hepàtiques o esplèniques.

MANEIG CLÍNIC

Les estratègies de cribratge per tal d'assolir un diagnòstic precoç no han donat resultats quant a impacte en la supervivència, de manera que actualment l'optimització del tractament continua essent la única via per tal de millorar aquests resultats. L'estratègia actual de maneig en el càncer d'ovari requereix l'abordatge amb un equip multidisciplinari que dugui a terme un apropiat estudi d'imatge preoperatori, una cirurgia reglada d'estadificació i cito-reducció realitzada per ginecòlegs entrenats en cirurgia oncològica, un acurat diagnòstic histopatològic i l'administració òptima de quimioteràpia (QMT) basada en platí, concretament l'estàndard dels darrers anys ha estat carboplatí i paclitaxel (27–29). L'objectiu de la cirurgia és l'assoliment de la citoreducció completa, definida com l'absència de tumor macroscòpic residual. Aquesta cirurgia es pot fer inicialment o després d'administrar QMT neoadjuvant en les pacients inicialment

considerades irressecables (30). L'addició de l'anticòs monoclonal bevacizumab al carboplatí i paclitaxel en primera línia i un manteniment durant un any en monoteràpia va suposar una millora significativa en la supervivència global mitjana de pacients amb càncer d'ovari estadi IV en comparar-ho amb el tractament estàndard sense l'anti-angiogènic, mostrant a més a més beneficis en termes de supervivència tant en malaltes sensibles com resistents al platí (31–33). Més recentment s'han afegit els inhibidors de PARP com a teràpia de manteniment en primera línia en aquelles malaltes amb mutacions en *BRCA1/2* o que presenten deficiència en la recombinació homòloga ja que diferents estudis han demostrat millora en supervivència lliure de progressió en aquest tipus de pacients (34–36). Tot i l'elevada resposta al tractament de QMT inicial, la majoria de casos, sobretot avançats, recidivaran en el curs de la malaltia. Alguns d'ells es podran beneficiar d'una cirurgia de citoreducció. Quan això no sigui possible, el tractament de la recurrència dependrà de l'interval lliure de malaltia després de finalitzar la quimioteràpia, que defineix les possibilitats de resposta al re-tractament amb combinacions de platí. Aquesta sensibilitat disminueix amb les subsegüents recaigudes amb la inevitable progressió o resistència a platí. En aquesta situació, les possibilitats de resposta al tractament estàndard està en torn al 20%, essent el pronòstic en general pobre (37).

TUMORS TESTICULARS DE CÈL·LULES GERMINALS (TTCG)

Els tumors de cèl·lules germinals constitueixen un grup variat de neoplàsies que es desenvolupen principalment a les gònades (ovaris i testicles) però també a localitzacions extragonadals, sobre tot seguint la línia mitja del cos, com ara retroperitoneu, mediastí i la regió central del cervell. L'origen d'aquest tipus de tumor a partir de cèl·lules germinals pot deduir-se per l'expressió per part de les cèl·lules que els composen de proteïnes específiques de línia germinal com ara VASA o pel patró d'empremta genòmica que mostren aquestes cèl·lules (38).

EPIDEMIOLOGIA

El càncer testicular va representar l'1,8% de càncers en homes el 2020 amb uns 74.000 nous casos diagnosticats a tot el món i va ocasionar el 0.2% de les morts

per càncer el mateix any (7). El 95% dels tumors testiculars són TTCG. Els TTCG constitueixen el tipus de neoplàsia maligna més freqüent en homes entre 15 i 35 anys (39,40). La incidència dels TTCG és baixa en països poc desenvolupats, amb < 2 casos nous per 100.000 homes i per any a Àfrica, Carib i Àsia. Els nivells d'incidència més elevats es troben a Dinamarca, Alemanya, Noruega, Hungria i Suïssa amb 8-10 casos nous per 100.000 homes i per any. Fora de poblacions europees, només trobem dades d'incidència similars a la població maorí de Nova Zelanda amb aproximadament 7 nous casos per 100.000 homes i per any (40). Els darrers anys del segle XX s'ha produït un increment progressiu en la incidència d'aquests tumors a països industrialitzats (41,42). Aquesta variabilitat geogràfica caracteritzada, en general, per dades d'incidència més elevades en països desenvolupats, ha fet plantejar la possibilitat de que es tracti de neoplàsies relacionades amb l'estil de vida occidental (abús de dietes hipercalòriques i poc exercici físic) (43). L'edat de distribució dels TTCG és diferent de l'edat de distribució de la majoria de tumors. Així la incidència d'aquest tipus de neoplàsia s'incrementa just després de l'inici de la pubertat i disminueix fins a nivells molt baixos més enllà dels 60 anys. Assoleix el seu màxim entre el final de la dècada dels 20 i la dècada dels 30 anys. En general no hi ha diferències en aquesta corba d'incidència per edats entre poblacions amb alt o baix risc. La corba d'incidència per edats és similar en seminomes i no seminomes, encara que el pic de màxima incidència se situa 10 anys abans en no seminomes (al voltant de la tercera dècada de la vida), probablement reflectint la major agressivitat i el creixement més ràpid d'aquesta mena de tumors (44,45).

ETIOLOGIA I PATOGÈNIA

La incidència de TTCG està incrementada 3-5 vegades en homes amb història de criptorquídia. La presència d'atròfia en aquests testicles no descendits incrementa el risc de desenvolupar càncer testicular (46,47). Hi ha estudis que indiquen que el retard de creixement intrauterí podria afavorir l'aparició de TTCG (48,49). S'ha demostrat increment de la incidència de TTCG en malalts immunodeficients (trasplantats renals i malalts de SIDA) (50,51). No s'han trobat diferències en factors etiològics entre seminomes i no seminomes (49,52).

La lesió precursora és la neoplàsia de cèl·lules germinals in situ en què hi ha activació de KIT i sobreexpressió de factors de transcripció embrionaris com NANOG i OCT4 (53,54). A la neoplàsia infiltrant a més a més apareixen guanys a 12p que no estan presents en les lesions in situ, però no s'ha pogut demostrar que els gens presents en aquesta regió estiguin implicats en la progressió de la malaltia (55). La càrrega mutacional dels TTCG és baixa comparada amb altres tumors sòlids dels adults. Hi ha poques mutacions somàtiques recurrents, en gens com *KRAS*, *NRAS*, *KIT* o *PIK3CA*, però es detecten més freqüentment en seminomes que en no seminomes (56). Les mutacions de *TP53* són poc freqüents en TTCG, excepte en casos resistents al tractament amb platí (57). S'han observat diferències en patrons de metilació entre tipus histològics, així, els seminomes mostren poca metilació global mentre que és extensa en carcinomes embrionaris i tumors mixtes (56). En no seminomes s'ha demostrat silenciament epigenètic de diferents gens supressors com *BRCA1* i *RAD51C* que indiquen que les deficiències en la reparació homòloga poden tenir un paper en els TTCG, obrint noves possibilitats terapèutiques (56,57).

TIPUS HISTOLÒGICS

Els tumors de cèl·lules germinals es divideixen en 2 grans grups: aquells que deriven de neoplàsia de cèl·lules germinals in situ i els que no (38,58). La neoplàsia de cèl·lules germinals in situ està constituïda per cèl·lules semblants a les del seminoma amb nuclis grans, hipercromàtics, cromatina grumosa i un o diversos nuclèols prominents que estan disposades sobre la membrana basal dels túbuls seminífers (58,59). Els TTCG derivats de neoplàsia de cèl·lules germinals in situ són seminoma, carcinoma embrionari, tumor del si endodèrmic de tipus post-puberal, tumors trofoblàstics, els teratomes post-puberals i els tumors mixtes de cèl·lules germinals que poden contenir proporcions variables de qualsevol dels altres tipus en qualsevol combinació (58). El tumor més freqüent és el seminoma que representa el 50-55% del total de TTCG, seguit pel carcinoma embrionari, representant el 4-16% i el teratoma post-puberal el 2,7-7% (58,60,61). El tumor del si endodèrmic post-puberal i el coriocarcinoma es presenten rarament com a formes pures, representant <1% i 0,3% dels TTCG respectivament (62,63). El segon tipus de TTCG més freqüent són els tumors

mixtes de cèl·lules germinals i representen aproximadament el 35% dels casos (62). Des del punt de vista clínic, en termes de maneig, tractament i pronòstic, els TTCG es divideixen en seminomes i no seminomes. Els primers són els seminomes purs, i els segons són qualsevol dels altres tipus histològics de forma pura o qualsevol tumor mixt de cèl·lules germinals, incloent els que tenen un component de seminoma (64).

ESTADIFICACIÓ I GRUPS PRONÒSTICS

L'estadificació dels tumors testiculars té en compte les característiques del tumor primari (T), l'afectació dels ganglis regionals (N), la presència de metàstasis a distància (M) i els nivells a sèrum dels marcadors LDH, hCG i AFP (S) (Taula 3)(25,26) .

pT- Tumor primari	
pTX	No s'ha pogut avaluar el tumor primari
pT0	No hi ha evidència de tumor primari (Exemple: cicatriu histològica al testicle)
pTis	Neoplàsia de cèl·lules germinals in situ
pT1	Tumor limitat al testicle i a l'epidídim sense invasió vascular o limfàtica; el tumor por infiltrar la túnica albugínia però no la túnica vaginal
pT2	Tumor limitat al testicle i a l'epidídim amb invasió vascular o limfàtica o tumor extenent-se a través de la túnica albugínia amb afectació de la túnica vaginal
pT3	Tumor envaint cordó espermàtic amb o sense invasió vascular o limfàtica
pT4	Tumor envaint l'escrot amb o sense invasió vascular

pN- Ganglis limfàtics regionals	
pNX	No s'han pogut avaluar els ganglis limfàtics regionals
pN1	Metàstasi a un gangli limfàtic menor o igual a 2 cm de diàmetre màxim y 5 o menys ganglis limfàtics positius, cap d'ells de més de 2 cm de diàmetre màxim
pN2	Metàstasi a un gangli limfàtic de més de 2 cm pero no més de 5 cm de diàmetre màxim; o més de 5 ganglis limfàtics positius, cap d'ells de més de 5 cm de diàmetre màxim; o evidència d'extensió extranodal del tumor
pN3	Metàstasi a un gangli limfàtic de més de 5 cm de diàmetre màxim

M- Metàstasis a distància	
MX	No s'han pogut avaluar les metàstasis a distància
M0	No hi ha metàstasis a distància
M1	Presència de metàstasis a distància
M1a	A ganglis limfàtics no regionals o pulmó
M1b	A altres localitzacions

S- Marcadors tumorals en sèrum (pre-quimioteràpia)			
	LDH	hCG (mUI/mL)	AFP (ng/mL)
S1	<1.5 x N	i < 5000	i < 1000
S2	1.5-10 x N	o 5000 - 50000	o 1000 - 10000
S3	>10 x N	o > 50000	o > 10000

N correspon al límit alt dels valors normals de la determinació d'LDH

Taula 3. Classificació TNM del càncer testicular. Adaptat de (25)

En base a aquestes característiques s'estableixen els estadis clínics amb correlació pronòstica que estan representats a la taula 4.

Estadi	T	N	M	S
Estadi 0	pTis	N0	M0	S0, SX
Estadi I	pT1-4	N0	M0	SX
Estadi IA	pT1	N0	M0	S0
Estadi IB	pT2	N0	M0	S0
	pT3	N0	M0	S0
	pT4	N0	M0	S0
Estadi IS	Qualsevol pT/TX	N0	M0	S1-3
Estadi II	Qualsevol pT/TX	N1-3	M0	SX
Estadi IIA	Qualsevol pT/TX	N1	M0	S0
	Qualsevol pT/TX	N1	M0	S1
Estadi IIB	Qualsevol pT/TX	N2	M0	S0
	Qualsevol pT/TX	N2	M0	S1
Estadi IIC	Qualsevol pT/TX	N3	M0	S0
	Qualsevol pT/TX	N3	M0	S1
Estadi III	Qualsevol pT/TX	Qualsevol N	M1	SX
Estadi IIIA	Qualsevol pT/TX	Qualsevol N	M1a	S0
	Qualsevol pT/TX	Qualsevol N	M1, M1a	S1
Estadi IIIB	Qualsevol pT/TX	N1-3	M0	S2
	Qualsevol pT/TX	Qualsevol N	M1a	S2
Estadi IIIC	Qualsevol pT/TX	N1-3	M0	S3
	Qualsevol pT/TX	Qualsevol N	M1a	S3
	Qualsevol pT/TX	Qualsevol N	M1b	Qualsevol S

Taula 4. Estadis del càncer testicular. Adaptat de (26)

Els TTCG es classifiquen en diferents grups de risc segons el tipus histològics, l'extensió de la malaltia i els nivells de marcadors en sèrum (64). Els tumors de bon pronòstic engloben els seminomes sense metàstasis viscerals amb nivells normals de marcadors tumorals i els no seminomes de localització testicular o retroperitoneal sense metàstasis, amb AFP <1000 ng/ml i hCG <5000 mUI/ml i LDH < 1,5 vegades el valor normal. Els tumors de pronòstic intermedi són els seminomes amb metàstasis que no siguin pulmonars amb nivells normals de marcadors tumorals i els no seminomes de localització testicular o retroperitoneal amb metàstasis que no siguin pulmonars i una de les següents característiques: AFP entre 1000 i 10000 ng/ml, hCG entre 5.000 i 50.000 mUI/ml o LDH entre 1,5 i 10 vegades el seu valor normal. Finalment, els tumors de mal pronòstic són aquells no seminomes amb afectació mediastínica o amb metàstasis viscerals extrapulmonars o amb nivells alts d'algun dels marcadors tumorals: AFP < 10.000 ng/ml o hCG > 50.000 mUI/ml o LDH > 10 vegades el valor normal (64).

MANEIG CLÍNIC

La primera maniobra terapèutica a tots els TTCG és l'orquiectomia inguinal, excepte en aquells malalts amb malaltia disseminada i risc vital als que es pot començar tractament quimioteràpic, diferint-se la orquiectomia per a un altre moment. El tractament post-orquiectomia depèn de l'estadi i la histologia del tumor. Els pacients amb seminoma en estadi I sense altres factors de mal pronòstic com ara invasió de rete testis o tumors grans tenen un risc de recidiva molt baix i per tant la tendència actual és no afegir tractament adjuvant (65,66). Els pacients amb seminoma estadis II o III es tracten amb quimioteràpia basada en platí, obtenint en general bons resultats (66,67). En pacients amb no seminoma en estadi I també es contempla l'opció de no afegir tractament adjuvant, excepte si hi ha algun factor de mal pronòstic com ara abundant component de carcinoma embrionari o coriocarcinoma (68–71), en què es pot afegir quimioteràpia basada en platí. Els pacients amb no seminoma en estadi II o III sempre reben alguna mena de tractament quimioteràpic basat en platí (66).

Al moment del diagnòstic el 80% dels seminomes i el 60% dels no seminomes estan localitzats (estadi I), però durant el seguiment el 18% dels pacients amb

seminoma i aproximadament el 30% dels pacients amb no seminoma en aquest estadi recidivaran (70,72). Per tant, aproximadament el 50% dels pacients amb TTCG rebran tractament basat en platí en algun moment de l'evolució de la malaltia (65,66,70).

CÀNCER DE PULMÓ

El càncer de pulmó és un dels càncers més prevalents i la principal causa de mort per càncer a nivell mundial.

EPIDEMIOLOGIA

L'any 2020 van haver-hi dos milions de casos nous i es van produir 1,7 milions de morts per càncer de pulmó al món (7). Tradicionalment el càncer de pulmó tenia les taxes d'incidència i mortalitat més elevades en països rics però actualment hi ha una tendència a la disminució d'aquestes taxes, particularment entre els joves sobre tot degut al descens de l'hàbit tabàquic. Per contra, en regions en què està augmentant el consum de tabac com ara Àsia, la incidència del càncer de pulmó està augmentant (73). Durant molt de temps el càncer de pulmó ha estat més freqüent en homes que en dones, però en països de renda alta aquestes diferències entre sexes s'han anat igualant degut a l'augment de dones fumadores (74).

ETIOLOGIA I PATOGÈNIA

S'han identificat diversos factors de risc per a desenvolupar càncer de pulmó com ara exposició ocupacional a substàncies com el radó i l'asbest o exposició a contaminació ambiental, però el factor de risc més important és el consum de tabac i sobretot de cigarretes. El risc en fumadors es va incrementant amb la duració i el nombre de cigarretes fumades al dia i disminueix després de deixar de fumar, encara que mai s'arriba al nivell de risc que tenen els que no han estat mai fumadors. El risc és 20-30 vegades més gran en fumadors que en no fumadors. Els factors de risc en no fumadors són l'exposició passiva al fum del

tabac (fumadors passius) i exposicions laborals o ambientals, però en la majoria de casos en no fumadors no es pot identificar una causa específica.

El rol del tabac en la carcinogènesi pulmonar està mediat per les més de 80 substàncies carcinògenes presents al fum del tabac que tenen un efecte pro-inflamatori i mutagènic en els teixits de les vies respiratòries i del parènquima pulmonar (75). Alguns d'aquests carcinògens generen adductes amb l'ADN que acaben ocasionant mutacions en gens que afavoreixen la iniciació i la progressió de les neoplàsies, com per exemple mutacions en *TP53* i *KRAS* (76).

La majoria dels adenocarcinomes de pulmó en malalts que no han fumat mai presenten mutacions als gens *EGFR* o *HER2* o bé fusions que impliquen els gens *ALK* o *ROS1* (77). També s'han descrit mutacions *driver* en altres gens com *KRAS*, *BRAF* o *PIK3CA*. En general les mutacions a *EGFR* i *KRAS* són mútuament excloents (78,79). Els tumors que presenten mutacions a *EGFR* o fusions amb *ALK* o *ROS1* actualment tenen teràpies dirigides contra aquestes alteracions que ja són emprades de manera habitual en la pràctica clínica (80).

TIPUS HISTOLÒGICS

Des del punt de vista clínic el càncer de pulmó es divideix en dos grups: carcinoma de cèl·lula petita (15% dels casos) i el carcinoma no cèl·lula petita que representa el 85% dels pacients. Dintre del carcinoma no cèl·lula petita es reconeixen 3 tipus histològics: adenocarcinoma, carcinoma escamós i carcinoma de cèl·lula gran (81,82). En aquesta revisió ens centrarem en aquest segon grup.

L'adenocarcinoma és el tipus més freqüent i representa aproximadament el 40% del total de càncers de pulmó (Pesch, et al., 2012). S'origina de les cèl·lules alveolars i es caracteritza per l'expressió immunohistoquímica de TTF-1 i Napsina A. Es reconeixen fases incipients de la malaltia com l'adenocarcinoma *in situ* i l'adenocarcinoma mínimament invasiu en què la lesió creix en patró lepídic, però la majoria corresponen a adenocarcinomes infiltrants. Histològicament poden tenir patró lepídic, acinar, papil·lar, micropapil·lar, sòlid o mucinós, de forma pura o, més freqüentment, en combinacions d'algun d'ells en proporcions diverses (81,84).

El carcinoma escamós constitueix el 25-30% dels càncers de pulmó. S'origina de l'epiteli de revestiment bronquial i des del punt de vista immunohistoquímic expressa CK5/6 i p40 i no expressa TTF-1. La lesió precursora és la displàsia escamosa i el carcinoma escamós *in situ* de l'epiteli bronquial (81,84)l.

El carcinoma de cèl·lula gran representa el 5-10% dels càncers de pulmó i la seva inciència va disminuint en la mesura en què es van afegint tècniques immunohistoquímiques en el diagnòstic de les lesions. Són neoplàsies poc diferenciades constituïdes per cèl·lules grans amb abundant citoplasma i nucléols prominents que des del punt de vista immunohistoquímic no mostren un patró d'expressió característic d'adenocarcinoma ni de carcinoma escamós (85,86).

ESTADIFICACIÓ

L'estadificació dels tumors pulmonars té en compte les característiques del tumor primari (T), l'afectació dels ganglis regionals (N), la presència de metàstasis a distància (M).(Taula 5)(25,26)

pT	Tumor primari
Tx	El tumor primari no pot ser avaluat.
T0	No hi ha evidència de tumor primari.
Tis	Carcinoma in situ
T1	Tumor ≤ 3 cm envoltat per pulmó o pleura visceral, sense evidència broncoscòpica d'invasió més proximal al bronqui lobar.
T1mi	Adenocarcinoma mínimament invasiu.
T1a	Tumor ≤ 1 cm
T1b	Tumor > 1 cm i ≤ 2 cm.
T1c	Tumor > 2 cm i ≤ 3 cm.
T2	Tumor > 3 cm i ≤ 5 cm o tumor amb qualsevol dels següents característiques: Afectació del bronqui principal independentment de la distància a la carina, però sense afectació de la carina Infiltració de pleura visceral Associat amb atelectàsia o pneumonitis obstructiva que s'estén a la regió hilar afectant part o tot el pulmó.
T2a	Tumor > 3 cm i ≤ 4 cm
T2b	Tumor > 4 cm i ≤ 5 cm
T3	Tumor > 5 cm i ≤ 7 cm o que infiltra directament qualsevol de les següents estructures: pleura parietal, paret toràcica, nervi frènic, pericardi parietal; o nòduls tumorals separats al mateix lòbul que el primari.

T4	Tumor > 7 cm o de qualsevol grandària que infiltra qualsevol de les següents estructures: diafragma, mediastí, cor, grans vasos, tràquea, nervi recurrent laringi, esòfag, cos vertebral, carina; o nòduls separats del tumor a lòbuls ipsilaterals diferents del del primari.

N	Ganglis limfàtics regionals
Nx	Els ganglis regionals no poden ser avaluats.
N0	No hi ha metàstasi a ganglis regionals.
N1	Metàstasis a ganglis peribronquials ipsilaterals i/o a ganglis hilars ipsilaterals i ganglis intrapulmonars, incloent afectació per extensió directa.
N2	Metàstasis a ganglis mediastínics ipsilaterals i/o a ganglis subcarinals.
N3	Metàstasis a ganglis mediastínics contralaterals, hilars contra laterals, escalens ipsilaterals o contralaterals o supraclaviculars.

M	Metàstasi a distància
M0	No hi ha metàstasis a distància.
M1	Metàstasis a distància.
M1a	Nòdul separat del tumor en un lòbul contralateral; tumor amb nòduls pleurals o pericàrdics o vessament pleural o pericàrdic malignes.
M1b	Metàstasi única extratoràcica a un sol órgan.
M1c	Múltiples metàstasis extratoràciques en un o múltiples òrgans.

Taula 5. Classificació TNM del càncer de pulmó. Adaptat de (25)

En base a aquestes característiques s'estableixen els estadis clínics amb correlació pronòstica que estan representats a la taula 6.

ESTADI	Definició
0	Tis N0 M0
IA1	T1mi-T1a N0 M0
IA2	T1b N0 M0
IA3	T1c N0 M0
IB	T2a N0 M0
IIA	T2b N0 M0
IIB	T1a-T2b N1 M0 o T3 N0 M0
IIIA	T1a-T2b N2 M0 o T3 N1 M0 o T4 N0-N1 M0
IIIB	T1a-T2b N3 M0 o T4 N2-N3 M0
IIA	Extensió i/o implants sobre l'úter i/o les trompes de Fal·lopi i/o els ovaris.
IIB	Extensió i/o implants sobre altres teixits pelvians.
IVA	Qualsevol T Qualsevol N M1a-M1b
IVB	Qualsevol T Qualsevol N M1c

Taula 6. Estadis del càncer de pulmó. Adaptat de (26)

MANEIG CLÍNIC

El tractament del carcinoma no cèl·lula petita de pulmó depèn de l'estadi i es basa en una combinació de cirurgia, radioteràpia, quimioteràpia, immunoteràpia i teràpies dirigides. En general, els pacients en estadi I, II o IIIA es tracten amb resecció quirúrgica, sempre i quan aquesta no estigui contraindicada. En estadis II o IIIA s'afegeix quimioteràpia basada en platí (Pignon et al., 2008). En pacients elegibles per a tractament quirúrgic però amb contraindicació mèdica per a la cirurgia es pot fer tractament radioteràpic amb finalitats curatives (88,89). No està clar el paper que pugui tenir la quimioteràpia neoadjuvant en aquest grup de pacients (90–92). En pacients en estadis avançats inoperables es recomana el tractament amb radioteràpia i quimioteràpia concomitant basada en platí (93). A més a més, a mesura que es va avançant en el coneixement de la biologia dels tumors i es van detectant alteracions moleculars específiques, paral·lelament es van desenvolupant teràpies dirigides cap a aquestes alteracions que s'afegeixen a la quimioteràpia convencional. Així, davant d'un carcinoma de pulmó no cèl·lula petita s'ha d'estudiar si té alguna d'aquestes possibles dianes terapèutiques per a les quals hi ha fàrmacs específics: mutacions d'*EGFR* (94) , translocació d'*ALK* (95), fusions de *ROS1* (96), fusions de *NTRK* (97), fusions de *RET* (98), mutacions de *MET* (99), *KRAS* (100)o *BRAF* (101),...). A excepció de les mutacions de KRAS, presents en 25-30% d'adenocarcinomes (102) i les d'*EGFR* presents en 15-20% de carcinomes de pulmó no cèl·lula petita, sobre tot adenocarcinomes (103), la resta d'alteracions són molt poc freqüents i per tant, la quimioteràpia continua sent la principal eina terapèutica per a aquest tipus de càncer.

CÀNCER D'ENDOMETRI

El càncer d'endometri és el tumor ginecològic maligne més freqüent en els països desenvolupats. La majoria de casos tenen bon pronòstic degut a que produeix manifestacions clíniques en forma de metrorràgia en fases molt inicials del seu desenvolupament, això permet diagnosticar-lo en estadis incipients en què el tractament quirúrgic acostuma a ser curatiu, assolint taxes de supervivència global als 5 anys del 80-95%. Malgrat això, 15-20% de casos estan disseminats

al diagnòstic o bé acaben recidivant i en aquest moment les opcions terapèutiques són limitades, comprometent el pronòstic de les pacients.

EPIDEMIOLOGIA

El càncer d'endometri és el sisè càncer més freqüent en dones. L'any 2020 es van diagnosticar gairebé 420.000 casos a nivell mundial. Les taxes d'incidència són més elevades en països desenvolupats com Europa i els Estats Units i sembla que hi hagi una tendència al seu increment, probablement relacionat amb l'estil de vida i especialment amb l'obesitat (104). La incidència a Europa el 2020 va ser de 12,9-20,2 casos per cada 100.000 dones, amb una mortalitat de 2,0-3,7 per cada 100.000 dones (7). Les taxes més baixes es troben en països amb baix nivell d'ingressos com els del continent africà i l'Índia. Es diagnostica sovint en dones menopàusiques o perimenopàusiques amb una edat mitjana de 63 anys. Els casos en el context de síndromes de predisposició hereditària al càncer com la síndrome de Lynch o la síndrome de Cowden se solen diagnosticar en dones aproximadament 10 anys més joves (105,106). En pacients amb síndrome de Lynch, en què les pacients són portadores d'una mutació en línia germinal en gens implicats en reparació d'errors d'aparellament com ara *MLH1*, *MSH2*, *MSH6 o PMS2,* el risc de desenvolupar càncer d'endometri al llarg de la vida és del 13-54%, depenent de quin és el gen mutat, amb riscs de 46-54% en dones amb mutacions d'MLH1, 21-51% en dones portadores de mutacions d'MSH2, 16-49% en dones portadores de mutacions d'MSH6 i 13-24% en portadores de mutacions de PMS2 (105,107,108).

ETIOLOGIA I PATOGÈNIA

Els factors de risc que estan associats amb el desenvolupament del càncer d'endometri són l'obesitat, la diabetis, la síndrome d'ovaris poliquístics i, en general, situacions en què es produeix una hiperestimulació estrogènica no compensada amb gestàgens, com ara certes neoplàsies ovàriques, tractament hormonal substitutiu basat únicament en estròtgens i tractament amb tamoxifè (109). Aquestes condicions afavoreixen el desenvolupament d'hiperplàsia atípica

que és la lesió precursora del carcinoma endometrioide, que és el tipus histològic més freqüent (110). Altres tipus histològics com carcinoma serós, carcinoma de cèl·lules clares i carcinosarcoma no estan associats a hiperestrogenisme (111). En les lesions precursores ja hi trobem algunes de les alteracions moleculars que caracteritzen el carcinoma, com ara mutacions en *PTEN*, *KRAS* i *CTNNB1* o inestabilitat de microsatèl·lits. La progressió a carcinoma endometrioide és conseqüència de l'acumulació d'altres alteracions com ara inactivació d'ARID1A i de TGFB (112,113).

En el carcinoma serós la lesió més incipient que es troba és el carcinoma serós intraepitelial i en aquests moment ja hi ha mutacions de *TP53* que és l'alteració que caracteritza aquest tipus histològic (114).

Recentment s'ha plantejat una classificació del càncer d'endometri en quatre grups, basada en la càrrega mutacional i les alteracions en el número de còpies dels gens que presenten els tumors, que té implicacions pronòstiques (115):

Al grup anomenat anomenat amb **alt número de còpies** els tumors presenten alteracions genòmiques generalitzades i extenses amplificacions i deleccions. Aquest grup conté la majoria dels tipus histològics més agressius i el 25% dels carcinomes endometrioides d'alt grau. El pronòstic d'aquests tumors és pobre i la majoria dels casos tenen mutacions patogèniques de *TP53* (115).

Tumors hipermutats que tenen una càrrega mutacional unes 10 vegades més elevada que el conjunt dels tumors, es caracteritzen per tenir inestabilitat de microsatèl·lits com a conseqüència de la falta d'expressió per mutació o per silenciament epigenètic d'algun dels gens implicat en la reparació d'errors d'aparellament com ara *MLH1*, *MSH2*, *MSH6 o PMS2.* Aquests tumors gairebé sempre són endometrioides i acostumen a tenir abundants limfòcits intratumorals (TILs) (115).

Tumors ultramutats que tenen una càrrega mutacional unes 100 vegades més elevada que el conjunt dels tumors. Representen el 7% del total de càncer d'endometri. També tenen abundants TILs. Es caracteritzen per tenir mutacions recurrents al domini exonucleasa del gen *POLE*. Són els tumors que com a grup presenten el millor pronòstic, pràcticament sense presentar mai recurrències (115).

Finalment hi ha un quart grup que no té cap de les alteracions descrites anteriorment i que s'anomenen tumors amb **baix número de còpies** o **tumors amb perfil molecular no específic**. Gairebé tots els tumors són carcinomes endometrioides de baix grau (115).

Aquesta classificació molecular dels tumors ha canviat la manera d'estratificar les pacients de cara al tractament (116).

TIPUS HISTOLÒGICS

El tipus més freqüent és el carcinoma endometrioide que representa al voltant del 80% dels casos, mentre que el 20% restant correspon al tipus no endometrioide que majoritàriament comprèn el carcinoma serós, el carcinoma de cèl·lula clara i el carcinosarcoma (24). Es grada en 3 graus, en base a la proporció de component sòlid i glandular: els tumors amb <5% de component sòlid són grau 1, entre 5 i 50% de component sòlid són grau 2 i >50% de component sòlid són grau 3. Els tumors de grau 1 i 2 es consideren de baix grau. Per contra, els tipus no endometrioide són tots d'alt grau i es diagnostiquen en dones aproximadament més 10 anys més grans (24). Durant molts anys s'ha fet servir una classificació dual del càncer d'endometri que tenia sentit clínic en tipus 1 i tipus 2 (117). El tipus 1 corresponia als carcinomes endometrioides de bon pronòstic, freqüentment limitats a l'úter en el moment del diagnòstic, i el tipus 2 corresponent als tipus histològics més agressius, representats sobre tot pel carcinoma serós, que sovint es presenta amb disseminació peritoneal al moment del diagnòstic. Aquests dos tipus tenen un abordatge diagnòstic i terapèutic i un pronòstic diferent. El problema d'aquesta classificació estava en els carcinomes d'alt grau que de vegades són difícils de classificar i en el maneig dels carcinomes endometrioides d'alt grau, si s'havien de considerar com a tumors de tipus 1 o de tipus 2.

Com ja s'ha comentat, més recentment s'ha proposat una classificació molecular del càncer d'endometri en 4 grups que està basada en la càrrega mutacional i en la variació del número de còpies dels gens que presenten els tumors (115). Aquesta classificació que requereix de seqüenciació massiva sistemàtica dels tumors és difícil d'implementar a la pràctica clínica, per la qual cosa se n'ha

plantejat una classificació subrogada basada en l'estudi immunohistoquímic de proteïnes reparadores de l'ADN (MSH6 i PMS2) i de p53 i la seqüenciació del gen POLE (118–120). De manera que els tumors amb mutació patogènica de POLE es consideren tumors POLE mutats (tumors ultramutats), els que tenen pèrdua d'expressió d'alguna de les proteïnes reparadores es consideren tumors amb dèficit de proteïnes reparadores (tumors hipermutats), els que tenen un patró anormal d'expressió de p53 es consideren tumors amb alt número de còpies i els que no tenen cap de les alteracions descrites anteriorment es consideren tumors amb perfil molecular no específic.

ESTADIFICACIÓ

Se segueix la classificació vigent del Sistema FIGO publicada al 2023 (taula 7), que pren en consideració els diferents tipus moleculars del càncer d'endometri amb el doble objectiu d'una millor definició dels grups pronòstic i una subclassificació dels estadis per a una indicació més acurada dels diferents tractaments .

ESTADI FIGO	Definició
I	Tumor confinat al cos uterí i ovari
IA	Malaltia limitada a l'endometri o, Tipus histològic No agressiu (a) amb invasió miometri <50% i sense ILV (o focal) (b) o, Malaltia de bon pronòstic (c)
IA1	Tipus histològic NO agressiu limitat a un pòlip o confinat a l'endometri
IA2	Tipus histològic NO agressiu amb invasió miometri <50% i sense ILV (o focal)
IA3	Tumor G1-G2 limitat a úter i ovari (c)
IB	Tipus histològic NO agressiu amb invasió miometri >50% i sense ILV (o focal)
IC	Tipus histològic agressiu (d) limitat a un pòlip o confinat a l'endometri
II	Invasió de l'estroma cervical sense extensió extrauterina o, ILV extensa o, Tipus histològic agressiu amb invasió miometrial
IIA	Tipus histològic NO agressiu amb invasió cervical
IIB	Tipus histològic NO agressiu amb ILV extensa
IIC	Tipus histològic agressiu amb qualsevol invasió miometrial
III	Disseminació local i/o regional de qualsevol tipus histològic
IIIA	Invasió de serosa uterina, annexos o ambdós per extensió directa o metàstasi
IIIA1	Afectació d'ovari o trompa (excepte si compleix criteris per IA1)
IIIA2	Afectació de subserosa uterina o extensió a traves de la serosa
IIIB	Extensió o metàstasi a vagina i/o a parametri o peritoneu pelvià
IIIB1	Extensió o metàstasi a vagina i/o a parametri

		IIIB2		Metàstasi a peritoneu pelvià
	IIIC			Metàstasi a ganglis pelvians o paraaòrtics o ambdós
		IIIC1		Metàstasi a ganglis pelvians
			IIIC1i	Micrometàstasi
			IIIC1ii	Macrometàstasi
		IIIC2		Metàstasi a ganglis paraaòrtics fins a vasos renals (amb o sense ganglis pelvians)
			IIIC2i	Micrometàstasi
			IIIC2ii	Macrometàstasi
IV				Extensió a mucosa vesical i/o intestinal i/o metàstasi a distància
	IVA			Extensió a mucosa vesical i/o intestinal
	IVB			Metàstasis peritoneals a abdomen superior
	IVC			Metàstasis a distància (inclou ganglis intraabdominals o extraabdominals per sobre dels vasos renals, pulmó, fetge, cervell y ossos)

Taula 7. Estadis del càncer d'endometri. Adaptat de (121). (a) Tipus histològics No agressius: carcinoma endometrioide G1-G2, carcinoma POLE mutat. (b) ILV extensa segons definició WHO 2020: ≥5 vasos afectats. (c) El carcinoma d'endometri G1-G2 afectant endometri i ovaris (IA3) ha de diferenciar-se de l'extensió del carcinoma d'endometri a l'ovari (IIIA1) seguint els següents criteris:

Infiltració miometrial < 50%

ILV absent o focal

Absència d'altres metástasis

Afectació ovàrica unilateral, limitada a l'ovari i sense invasió/ruptura de la càpsula

(d) Tipus histològics agressius: carcinoma endometrioide G3, carcinoma serós, carcinoma de cèl·lula clara, carcinosarcoma, carcinoma mucinós de tipus intesinal i carcinomes amb p53 anormal.

MANEIG CLÍNIC

En els estadis inicials el tractament principal es la cirurgia a la que en funció de l'estadi i d'altres factors de risc s'hi pot afegir radioteràpia i/o quimioteràpia (QMT) adjuvant per a disminuir el risc de recidiva (122). En malaltia metastàtica les opcions terapèutiques són limitades i inclouen tant la QMT com la teràpia endocrina (123) i més recentment s'ha afegit en determinades circumstàncies la immunoteràpia sola o associada amb QMT (124).

La cirurgia és la base del tractament del càncer d'endometri i ha d'incloure histerectomia i annexectomia. Respecte a la necessitat i extensió de l'estudi dels ganglis limfàtics hi ha certa controvèrsia, i depèn de les característiques de la pacient, sobre tot el grau d'obesitat i de característiques del tumor com ara el tipus histològic, el grau, la profunditat d'invasió, la presència d'invasió limfovascular o la classificació molecular (125). Una pràctica raonable seria estudi del/s ganglis sentinella a més d'extirpació del ganglis sospitosos (109). S'ha d'intentar extirpar la malaltia extrauterina que sigui visible

macroscòpicament i en el cas de carcinomes serosos i carcinosarcomes es recomana realitzar una omentectomia pel risc elevat que tenen aquests tipus histològics de fer disseminació peritoneal, encara que aparentment semblin estadis limitats a l'úter (126).

No està clar el paper que pugui tenir la QMT neoadjuvant en el càncer d'endometri (127).

En malaltia recurrent o metastàtica està indicada la quimioteràpia basada en platí, i la combinació més usada és carboplatí amb paclitaxel (128). En casos en què aquesta no té bons resultats degut essencialment a resistència al platí i es requereix una segona línia de QMT les taxes de resposta són molt pobres, inferiors al 20% (129).

Un 25% dels carcinomes serosos tenen sobreexpressió de HER2 i en aquests casos es pot afegir trastuzumab al carboplatí / paclitaxel (115,130).

Finalment, els tumors deficients en proteïnes reparadores poden beneficiar-se d'immunoteràpia (131).

Per tant, la resistència a la quimioteràpia dels tumors és un dels principals problemes en el tractament de les malalties oncològiques. Per tal d'estudiar aquest fenòmen biològic i, eventualment, provar noves estratègies terapèutiques són necessaris models pre-clínics que imitin al màxim la malaltia humana. La implantació de fragments de tumor en ratolins immunodeficients al mateix òrgan d'origen (implantació ortotòpica) pot proporcionar una eina molt útil en aquest camp, ja que les cèl·lules neoplàstiques es troben en un ambient molt més favorable per al seu creixement que en altres circumstàncies experimentals usades freqüentment (cultius cel·lulars o implants subcutanis) (132).

En aquest treball s'han triat quatre tipus de neoplàsia que es tracten de manera estàndard amb quimioteràpia basada en sals de platí, però que presenten patrons de resposta diferents front al fàrmac. Així, els carcinomes d'ovari, sobre tot el carcinoma serós d'alt grau, responen d'entrada el 60-70% dels casos, però en la mesura en què van recidivant, els tumors esdevenen resistents, resultant en una elevada mortalitat de les malaltes als 5 anys del diagnòstic. D'altra banda hi ha els tumors de cèl·lules germinals testiculars que tenen una sensibilitat molt

gran al platí, assolint la curació en més del 80% de casos. La resta de casos, però, són primàriament resistents o se'n tornen i tenen un pronòstic molt pobre. I per últim el càncer de pulmó i càncer d'endometri que tenen, en general, baixes taxes de resposta.

MODELS PRECLÍNICS EN LA RECERCA DEL CÀNCER.

L'ús de models preclínics és fonamental per a poder desenvolupar la investigació translacional del càncer. Models que s'utilitzen tant per a entendre la biologia de la malaltia com per al desenvolupament de nous fàrmacs, i que només en alguns casos d'èxit acabaran convertint-se en tractaments efectius i aprovats per a l'ús en humans per les agències reguladores.

El desenvolupament de fàrmacs és un procés llarg i complex i que implica tant l'ús de models *in vitro* com de models *in vivo*. L'ús de models de càncer per al cribratge de fàrmacs va començar al **NCI (National Cancer Institute)** a la dècada de 1970. En els darrers 40 anys, s'ha establert una metodologia bàsica i un enfocament molt sistemàtic tant per a realitzar els experiments *in vitro* com l'avaluació preclínica de molècules amb activitat anticancerosa *in vivo* (Abaan et al., 2013).

Actualment, el panell de línies cel·lulars tumorals conegudes com NCI-60 representa la col·lecció més ben caracteritzada i que més freqüentment s'ha utilitzat *in vitro* per al cribratge i desenvolupament dels fàrmacs que avui en dia fem servir per a tractar el càncer. Aquest panell està format per 60 línies cel·lulars representatives de diferents tipus tumorals, incloent-hi línies derivades de leucèmia, melanoma i càncers de pulmó, còlon, cervell, mama, pròstata i ronyó. A més, els xenoempelts generats a partir de la injecció subcutània d'aquestes línies cel·lulars en ratolins immunodeficients, anomenats ***CDX (Cell Derived Xenografts)***, han estat la plataforma preclínica més comuna usada *in vivo* per al desenvolupament dels fàrmacs oncològics.

L'ús de les línies cel·lulars en el desenvolupament preclínic de fàrmacs té importants limitacions, sent la més important el baix valor predictiu que tenen respecte a l'activitat en diferents tipus de càncer que s'observa en els ulteriors assaigs clínics. Tot i que no es coneix la causa subjacent d'aquest baix valor

predictiu, es creu que això és degut a les adaptacions biològiques irreversibles que es donen en les cèl·lules en el procés d'adaptació a créixer *in vitro*. Entre aquestes es troben la pèrdua/guany d'informació genètica, l'alteració de les propietats de creixement local i d'invasió a distància, així com la pèrdua d'heterogeneïtat, i per tant de poblacions cel·lulars específiques del tumor. Un altre aspecte important que pot explicar aquest baix valor predictiu amb les línies cel·lulars que s'utilitzen és que hi ha un biaix important ja que generalment s'estableixen a partir dels tumors més agressius, i per tant no són representatives de la complexa heterogeneïtat cel·lular que tenen els tumors (134,135).

Així, en els darrers anys s'han desenvolupat diferents enfocaments per a intentar millorar tot aquest procés, com són els cultius primaris derivats dels tumors, però sobretot la tecnologia per al desenvolupament de tumoroides/organoides. És important remarcar que tots aquests mètodes no deixen de ser tècniques de creixement de les cèl·lules *in vitro*, això sí, més sofisticats que necessiten per al seu desenvolupament de molts factors de creixement i que poden interferir el procés de cribratge dels fàrmacs. De totes maneres, tots aquests mètodes encara requereixen importants estudis de validació abans de ser considerats com a mètodes generalistes i convencionals per al cribratge preclínic de molècules. En aquest sentit, recentment, investigadors del nostre grup han participat en el primer estudi publicat en què un cribratge amb organoides de tumors colorectals, generats tant a partir de tumors desenvolupats en ratolins modificats genèticament com de PDX (*Patient Derived Xenografts*), ha permés identificar un anticòs bi-específic (MCLA-158) que reconeix tant l'EGFR com LGR5 en tumors epitelials, i que actualment està en procés d'avaluació en diversos assaigs clínics (136).

Així, en un intent per resoldre aquests problemes i millorar la capacitat predictiva preclínica de les línies cel·lulars i els models CDX, en els darrers 30 anys hi ha hagut un gran interès en disposar de models preclínics més avançats. En aquest sentit cal destacar els dos grans grups de models en què s'ha treballat activament: i) Els models de tumors generats en ratolí modificat genèticament (GEMM)(*Genetically Engineered Mouse Models*), i ii) els xenoempelts generats a partir de la implantació de tumors de pacients o PDX.

Els models PDX no són nous. De fet, ja en estudis realitzats a la dècada de 1970-80 van mostrar un alt grau de correlació en estudis en què s'avaluava la resposta clínica a la quimioteràpia i la resposta observada en els PDX (137). En els darrers anys hi ha hagut un renovat interès i esforç en desenvolupar-los per als diferents tipus tumorals. Així, en un intent de millorar l'ineficient procés de desenvolupament de nous fàrmacs/teràpies, aquests models en els últims 10 anys s'han convertit en la eina preclínica preferida tant per la indústria farmacèutica com per l'acadèmia (138).

En paral·lel als PDX, el desenvolupament dels models preclínics de ratolí modificats genèticament (GEMM) s'han convertit en eines indispensables per a comprendre els mecanismes bàsics que contribueixen a l'inici i desenvolupament tumoral. No obstant això, per les seves característiques intrínseques, són models molt menys utilitzats durant el procés de desenvolupament de nous fàrmacs. En el càncer de pulmó no microcític (CPNCP), els models GEMM induïts mitjançant l'activació d'un sol oncogen iniciador (mutació del gen *KRAS*) són molt utilitzats a la literatura però no recapitulen aspectes molt rellevants de la malaltia humana. Els tumors que es generen són lesions predominantment en etapes primerenques, mostrant una variació histològica molt limitada, i metastatitzen amb molt poca freqüència. En aquesta tesi, amb l'objectiu de millorar aquests models, presentarem un treball (Article 3) on hem desenvolupat ***orthoallografts*** que consisteix a implantar al pulmó (ortotòpica) de ratolins immunodeficients els tumors generats al pulmó del GEMM. Aquest és un enfocament versàtil i reproduïble que evita algunes de les importants limitacions que presenten els tumors del GEMM, proporcionant a més una plataforma preclínica ràpida i estandarditzada per a l'avaluació de tractaments terapèutics *in vivo.* D'alguna manera, podem dir que els *orthoallografts* són models híbrids entre els GEMM i els PDX (139).

Al llarg d'aquesta tesi, en quatre articles diferents descriurem el procés de generació en ratolins immunodeficients tant de PDOX (Patient Derived Orthotopic Xenografts) de càncer epitelial d'ovari (CEO), de tumors testiculars de cèl·lules germinals (TTCG) humans i de càncer d'endometri (CE), així com orthoallografts (tumors derivats de GEEM implantats ortotòpicament) de càncer

de pulmó de cèl·lules no petites (CPNCP). Són models preclínics avançats que s'han utilitzat per al desenvolupament de noves aproximacions terapèutiques.

GENERACIÓ DE MODELS PDX (Patient Derived Xenografts)

En la literatura s'ha descrit àmpliament el procés de generació de models PDX tant a partir de material fresc obtingut de tumors primaris com de les metàstasis (140,141). En els últims anys, a part dels processos d'implantació realitzats per molts laboratoris d'una forma individual, s'han creat diferents consorcis internacionals (Taula 1) amb la finalitat de generar col·leccions de PDX. De fet, el Dr. Villanueva del grup en què he realitzat aquesta tesi (Grup de Quimioresistència i Factors Predictius, Subprograma Contra la Resistència Terapèutica en Càncer-ProCURE, Programa Oncobell, IDIBELL) forma part com a membre fundador d'una d'aquests iniciatives, EuroPDX (www.europdx.com), que és el major consorci europeu de generació de models PDX (Manuel Hidalgo et al., 2014; Byrne, Alférez, et al., 2017), i de l'assaig MAPPYACTS, especialitzat en la generació de models pediàtrics (144).

De manera genèrica, podem dir que la majoria dels PDX es generen a partir de fragments sòlids de tumors primaris o de les metàstasis obtingudes mitjançant procediments quirúrgics rutinaris o a partir de biòpsies. Però aquests models també es poden generar a partir de fluids obtinguts de drenatges com l'ascites (p. ex., càncer d'ovari) o els vessaments pleurals (p. ex., tumors de pulmó). També s'ha descrit la generació a partir de cèl·lules tumorals circulants, encara que al nostre grup aquesta aproximació no ha funcionat en diversos tipus de tumors.

Les mostres tumorals recollides en fresc es poden implantar tant com a fragments sòlids, mantenint l'estructura tridimensional del teixit, o com a suspensió de cèl·lules obtingudes per disgregació enzimàtica/mecànica del teixit. A més, la implantació/injecció es pot fer de forma directa o bé amb Matrigel o barrejades amb fibroblasts humans o amb cèl·lules mare mesenquimàtiques.

El lloc d'implantació dels tumors en el ratolí més freqüentment utilitzat és la regió dorsal (**implantació subcutània**), mentre que quan els tumors s'implanten al ratolí en el mateix òrgan d'origen del tumor es diu **implantació ortotòpica.** En

un intent d'augmentar la taxa d'implantació, per a alguns tipus tumorals (tumors de pròstata, neuroblastomes, etc.), s'han desenvolupat aproximacions basades en la injecció (principalment) del disgregat tumoral a la càpsula renal. A més, per als tumors sensibles a hormones, alguns estudis també han utilitzat la suplementació hormonal (p. ex., pellets d'estrògens en càncer de mama) (142).

Per a la generació dels xenoempelts s'utilitzen diferents soques de ratolins amb diferents graus d'immunosupressió. La Taula 8 enumera les característiques de les principals soques de ratolins utilitzades, incloent el seu nivell de supressió immunològica, així com els avantatges i desavantatges del seu ús.

Soca de ratolí	Deficiència	Avantatges	Desavantatges	Aplicacions
Nude (*nu*)	Sense cèl·lules T funcionals	Ben caracteritzat. Alta taxa d'empelt de tumors humans. Sense pèl: millora de la cirurgia i seguiment del tumor.	Cèl·lules B i NK funcionals. La funcionalitat de les cèl·lules T augmenta amb l'edat.	Trasplantament de tumors murins i humans (xenogènics) per a estudis d'imatge, metàstasi i noves teràpies.
SCID (*scid*)	Sense cèl·lules T i B funcionals	Millor empelt de cèl·lules i teixits tumorals al·logènics i xenogènics que en la soca Nude	Cèl·lules NK funcionals. Limfomes espontanis.	Trasplantament de tumors murins i humans (xenogènics) per a estudis d'imatge, metàstasi i noves teràpies. Baixos nivells d'empelt de PBMC humanes i teixits hematopoètics fetals.
NOD-SCID	Sense cèl·lules T i B funcionals, cèl·lules NK deteriorades	Ben caracteritzat. Baixa activitat de cèl·lules NK. Molt baixa permeabilitat amb l'edat	Alta incidència de limfomes. Radiosensible.	Nivells més alts d'empelt de PBMC i cèl·lules mare hematopoètiques en comparació amb la soca SCID.
NOD-SCID-IL2rg null (NSG)	Sense cèl·lules T, B i NK funcionals	Resistent als limfomes. Excel·lent empelt de cèl·lules i teixits tumorals al·logènics i xenogènics. Adequat per a l'anàlisi de cèl·lules mare canceroses humanes i metàstasi.	No ben caracteritzat.	Augment dels nivells de creixement, desenvolupament i diferenciació de cèl·lules mare pluripotents humanes i teixit humà empeltat per injecció intravenosa, intrahepàtica, intraperitoneal i intramedul·la òssia.

Taula 8. Aquesta taula resumeix les característiques principals de les soques de ratolins immunodeficients més comunes utilitzades per generar models PDX. Modificada de "El Laboratori Jackson". Les abreviacions són: NK: Cèl·lules Natural Killer; NOD/SCID: diabètic no obès; NSG: NOD/SCID/IL2 receptor λ nul; PBMC:

Cèl·lules sanguínies mononuclears perifèriques; SCID: trastorn de la immunitat combinada severa; NOD/SCID: diabètic no obès; NSG: NOD/SCID/IL2 receptor λ nul.

Des d'un punt de vista teòric, alguns enfocaments d'implantació poden tenir avantatges en termes d'obtenir taxes d'implantació més altes i ràpides, així com la generació de models que recapitulin molt millor les característiques dels tumors humans i, per tant, siguin més predictius. No obstant això, malgrat que de manera recurrent els investigadors del camp plantegen aquestes qüestions, és important esmentar que molt pocs estudis a la literatura han abordat d'una manera rigorosa estudis comparatius d'implantació. Així, no hi ha estudis en què el mateix tumor s'implanti de forma simultània en diferents soques de ratolins amb diferents graus d'immunosupressió, subcutani vs. ortotòpic, disgregat vs. fragment sòlid, etc.

S'han realitzat estudis en què s'han generat simultàniament models de PDX a partir tant del tumor primari com de les lesions metastàtiques d'un mateix pacient, suggerint que les lesions metastàtiques tenen una taxa més alta d'implantació en el ratolí. Però aquests resultats dependran en gran mesura del tipus tumoral i de les diferents variables d'implantació (soca de ratolí, forma d'implantació etc.). Per exemple, en al nostre grup hem observat que les metàstasis hepàtiques de càncer de colon creixen millor i d'una manera més ràpida si s'implanten en ratolins atímics al teixit subcutani que ortotòpicament al fetge del ratolí. Sembla com si el fetge del ratolí es defensés davant de l'implant. Però, en canvi, quan s'analitzen histològicament, les metàstasis crescudes en fetge s'assemblen molt més a les primàries originals que les crescudes subcutànies, que són molt més fibroses i necròtiques. Un altre exemple el tenim en els carcinomes de pulmó no cèl·lula petita (CPNCP), que creixen molt millor i reprodueixen millor la histopatologia del CPNCP quan s'implanten ortotòpicament al pulmó del ratolí (145).

Decidir les soques de ratolins més apropiades a l'hora de generar els models PDX és un aspecte important però, com hem comentat, és difícil de definir.

S'assumeix que els models més immunodeficients, com són els models NOD/SCID o NOD/SCID/IL2λ-receptor nul (NSG), són millors per a la generació dels PDX, ja que en estar més immunodeficients tindran taxes d'implantació més altes. De fet, si es mira la literatura aquestes són les soques de ratolins utilitzades per molts grups de recerca.

Al nostre grup i al llarg d'aquesta Tesi, hem vist que tenim les mateixes taxes d'implantació utilitzant atímics o aquestes soques de ratolins més immunodeficients. Una qüestió a tenir en compte és que en aquestes soques més immunodeprimides la disseminació del tumor es produeix més freqüentment, però també cal anar amb compte ja que apareixen limfomes a una freqüència més elevada, sobretot per a tumors de creixement lent.

En el càncer de mama s'ha vist que la implantació en ratolins NOD/SCID versus NSG té taxes d'implantació similars. La suplementació amb pellets d'estradiol va augmentar notablement les taxes d'implantació, passant del 2,6% al 21,4%. Mentre que la co-implantació del tumor amb fibroblasts humans va disminuir aquesta taxa d'empelt (146).

Un dels debats més actius és què és millor, la implantació subcutània versus la implantació ortotòpica. En els darrers anys sembla que ja està quedant força demostrat que la implantació ortotòpica aporta importants avantatges, com per altra banda descriurem en aquesta tesi. En la implantació ortotòpica la implantació al ratolí hoste dels fragments tumorals es realitza a la mateixa localització anatòmica on es trobava el tumor original al pacient. El fet que les cèl·lules tumorals així implantades creixin i es desenvolupin en un entorn que s'assembla més fidelment al microambient original del tumor del pacient confereix importants avantatges translacionals. La generació dels models ortotòpics és molt més laboriosa, requereix cirurgia complexa, és més costosa i sovint requereix mètodes d'imatge per a poder monitoritzar en temps real el creixement del tumor. A més, requereix una corba d'aprenentatge important per a poder aconseguir taxes d'implantació acceptables.

Al nostre grup hem vist que per dos dels tipus de tumors objecte d'aquesta tesi, com són el càncer epitelial d'ovari i de pulmó (CPNCP), aquest enfocament augmenta substancialment les taxes d'implantació del tumor. I en el cas dels

tumors de cèl·lules germinals testiculars (TTCG), la implantació ortotòpica al testicle és essencial per al creixement inicial dels tumors, y rarament s'aconsegueix el primoimplant al teixit subcutani.

Pel que fa a la implantació dels tumors a la càpsula renal, s'ha publicat que en CPNCP augmenta d'una forma espectacular la implantació de CPNCP (fins a un 90%) respecte al que passa si es fa subcutani (25%), tot i que aquests resultats només es van obtenir d'un sol estudi comparatiu. A més, la implantació a la càpsula renal escurça el temps de creixement, que és una de les variables més importants per realitzar estudis de medicina de precisió en temps real amb PDX (147). En la nostra experiència d'implantació de CPNCP (>50 tumors), la taxa màxima d'implantació s'aconsegueix de forma ortotòpica al pulmó, però amb rangs del 40-50%, i esbiaixat cap a carcinomes escamosos, tenint l'adenocarcinoma taxes més baixes (25-30%). De manera global, la implantació subcutània redueix el percentatge al 20% en CPNCP a les nostres mans.

CARACTERÍSTIQUES DESTACADES DELS MODELS PDX

La principal limitació que tenen la majoria dels models preclínics és el pobre valor predictiu que tenen a nivell clínic, ja sigui els models preclínics *in vitro,* realitzats amb línies cel·lulars convencionals, com els models *in vivo* de xenoempelts generats mitjançant la implantació d'aquestes mateixes línies cel·lulars en ratolins immunodeficients, anomenats *Cell Derived Xenografts* (CDX) (148). Les raons d'aquesta manca de valor predictiu no s'acaben de comprendre bé, però és probable que el procés d'adaptació a créixer *in vitro* generi canvis en l'equilibri entre els complexos circuits biològics de les cèl·lules tumorals i aquests difereixin del que passa a les cèl·lules tumorals creixent en el pacient. Aquestes modificacions afecten tant a propietats fonamentals com són el contingut en material genètic, la capacitat invasiva i el manteniment de la heterogeneïtat cel·lular, així com la seva dependència de vies de senyalització específiques del creixement i la supervivència cel·lular (135).

La generació dels models preclínics PDX a partir de mostra tumoral fresca proporciona eines que representen una clara millora respecte a l'ús de les línies cel·lulars *in vitro* i els CDX derivats a partir d'elles *in vivo*. Aquests models

representen un pas més i són més predictius tant de la biologia com de la resposta als tractaments dels tumors. A més, la generació dels models PDX ens ofereix el potencial per a poder personalitzar el tractament del càncer d'un pacient en temps real.

Per a demostrar el valor dels models PDX s'han utilitzat diferents aproximacions analitzant diferents aspectes (142):

i) **Anàlisi comparativa de les característiques histopatològiques, biològiques i genètiques** dels PDX respecte del tumor original del pacient. Aquesta aproximació podríem dir que és de validació dels models per al seu ús en diferents estratègies d'investigació. Els tumors així generats retindran les característiques clau del tumor del donant, propietats que es mantindran al llarg de diferents passades del tumor de ratolí a ratolí. La majoria d'estudis mostren que els PDX retenen les característiques histològiques principals dels tumors originals, incloent estructures fines del teixit i detalls microscòpics més subtils com l'arquitectura glandular, producció de mucina o el desenvolupament d'estructures quístiques.

ii) La majoria d'estudis realitzats també mostren una bona correlació d'altres característiques biològiques entre el tumor original i el PDX. Els **estudis comparatius dels perfils d'expressió gènica** mostren que no hi ha canvis substancials entre ells. Sí que es detecten canvis en gens relacionats amb l'estroma tumoral i la funció immunològica, i això es deu al fet que l'estroma del tumor primari en el PDX se substitueix per estroma murí. En les anàlisis de dades de grups no supervisats, els tumors primaris dels donants i els PDX generats en els ratolins a partir d'aquests tumors s'agrupen de forma conjunta en la majoria dels casos. En aquest mateix sentit, tant les anàlisis en les alteracions en el nombre de còpies (CNA) com les dades de seqüenciació de l'exoma (WES) també mostren una extraordinària correlació entre tots dos tipus de mostres. És important ressaltar que, en augmentar la puresa de l'ADN tumoral en el xenoempelt, en eliminar l'estroma humà, s'observen les alteracions a una major freqüència. Per exemple, les pèrdues d'homozigositat es detecten

d'una forma molt clara. És molt important ressaltar que en els models PDX, s'evita la contaminació creuada per ADN normal del teixit estromal humà.

En els PDX s'observa **l'enriquiment de variants d'un sol nucleòtid**, que s'argumenta que podrien ser el resultat d'adaptació del tumor a créixer en el nou microambient, encara que també podrien ja estar presents en el tumor original a freqüències indetectables i que s'amplificarien en créixer el tumor en el ratolí. En un treball realitzat pel nostre grup en CPNCP, vam observar després del tractament amb Osimertinib l'expansió d'un clon amb mutació en *KRAS* (G12C) i que aquesta mutació ja estava present en la mostra original tot i ser indetectable per la majoria de tècniques. En aquest cas va ser necessari fer servir tecnologies de darrera generació per detectar-la en el global de la mostra original (149). També s'han demostrat canvis en les **alteracions en el nombre de còpies (CNA**) en PDX de sarcomes, fet que s'observa freqüentment en els pacients quan progressen, suggerint que en els xenoempelts estan representats els reordenaments intrínsecs que tenen lloc durant la progressió tumoral. En la llarga experiència del grup on he fet la tesi, i en els PDOX generats de tumors de molts tipus (ovari, tumors malignes de beina de nervi perifèric, tumors germinals testiculars, pàncrees, còlon, pulmó, melanoma, tumors hematològics, i recentment pediàtrics, entre d'altres) no hem trobat canvis substancials entre els tumors originals i els PDOX (150,151). És important ressaltar que com a patòleg que ha analitzat més de 700 PDOX diferents de forma comparativa, en molts PDOX veiem reflectida l'heterogeneïtat tumoral que es veu en una peça quirúrgica en les diferents subàrees.

iii) La **propagació dels PDX de ratolí a ratolí** (diferents generacions del tumor) no canvia de manera rellevant les característiques funcionals del tumor implantat. En diversos estudis que han comparat la resposta a tractaments de PDX en diferents passades (fins a 10) han mostrat taxes de respostes estables, la qual cosa recolza l'estabilitat fenotípica d'aquests models. En el nostre cas i com mostrarem en aquesta tesi

en els tumors mixtes de cèl·lules germinals testiculars, compostos per combinacions de diversos tipus histològics, aquests van mantenir la seva heterogeneïtat al llarg de >15 passades. Només quan els tractaven amb cisplatí se'n seleccionaven uns components i en desapareixien d'altres.

iv) Una altra forma d'avaluar la **fidelitat dels models és fixar-se en alteracions genòmiques ben conegudes associades amb un tipus de tumor**. Així, en models de PDX de carcinomes escamosos de cap i coll, la prevalença de mutacions en *TP53* i *NOTCH* és similar a la que s'observa en tumors humans. El mateix succeeix en models de càncer colorectal i d'adenocarcinomes de pàncrees en què la freqüència de mutacions en gens com *TP53* i *KRAS* es correspon amb la freqüència de mutacions observades en mostres humanes.

v) Una altra manera de determinar la vàlua dels PDX és **avaluar el seu valor predictiu respecte a l'eficàcia dels medicaments**. En els estudis en què s'han tractat models de PDX de diferents tipus de càncer amb els medicaments utilitzats a la clínica, malgrat la dificultat d'homogeneïtzar els criteris de resposta utilitzats, existeix una notable concordança amb el que s'observa a la clínica (per exemple, cetuximab en càncer colorectal o gemcitabina en càncer de pàncrees). A més, l'anàlisi en PDX de biomarcadors validats clínicament, com són les mutacions en el gen *KRAS* i la resistència als inhibidors de l'*EGFR*, va arribar a les mateixes conclusions que en els assaigs clínics. En aquest sentit, i malgrat les dificultats en la seva implementació clínica, potser el punt més important i que posa de manifest la rellevància dels models PDX, és el seu ús en el desenvolupament de la Medicina Personalitzada en temps real, on el pacient es pot arribar a tractar amb medicaments seleccionats per la seva activitat en el seu propi model PDX, aquí anomenat Avatar® o Orthoxenograft®.

En aquest sentit, tot i que no és el focus d'aquesta tesi, el nostre grup ha desenvolupat diverses aproximacions de Medicina de Precisió en temps real en què els pacients, majoritàriament adults, tot i que també hi ha algun cas pediàtric, han estat tractats en base al

PDOX/Orthoxenograft generat en el ratolí. La majoria dels casos han estat usos compassius autoritzats pels corresponents comitès d'ètica dels Hospitals on s'han tractat els pacients (152).

Així, a mode de resum podem dir que els PDX en general són valuosos per a estudiar la biologia del càncer, provar l'eficàcia de noves aproximacions terapèutiques, i desenvolupar tractaments personalitzats, ja que conserven moltes de les característiques fenotípiques i genotípiques del tumor original del pacient a partir del qual es generen.

APLICACIONS DELS MODELS PDX EN LA INVESTIGACIÓ DEL CÀNCER

1. Cribratge i desenvolupament de fàrmacs.

Un dels principals problemes en el desenvolupament de fàrmacs oncològics és la baixa taxa d'èxit dels nous agents. Molts compostos que arriben a assajar-se en extensos estudis clínics de fase III amb pacients acaben fallant a causa d'una manca d'eficàcia. La raó perquè això passi és per la baixa capacitat predictiva dels models preclínics sovint utilitzats durant el desenvolupament del fàrmac, així com per l'absència de biomarcadors que permetin fer tant una correcta selecció dels pacients a incloure a l'assaig com una correcta monitorització de la resposta (148).

En aquest context es necessita el desenvolupament d'estratègies que permetin disminuir aquestes altes taxes de fracàs. Així, disposar de models preclínics avançats amb alt valor predictiu, és de gran interès ja que han de permetre afinar al màxim a nivell preclínic, per a després dissenyar i realitzar assaigs clínics de fase II-III amb més possibilitats d'èxit.

En la literatura existeixen cada vegada més exemples en què es demostra que la taxa de resposta en models PDX es correlaciona amb les observades a la clínica, tant per a teràpies dirigides com per als tractaments amb quimioteràpia estàndard. Així per exemple, en 47 PDX de càncer colorectal no seleccionats la taxa de resposta a cetuximab és del 10,6%, essent molt similar a la resposta observada en pacients (153). Igualment en 40 PDX de càncer colorectal amb

mutació en *KRAS* els inhibidors de MEK i PI3K/mTOR van ser poc eficaços, similar al que va passar en l'assaig clínic (154). Respecte a la quimioteràpia, estudis en PDX de diferents tipus de tumors (CPNCP, càncer colorectal (CCR), càncer de mama, càncer de pàncrees) demostren que les taxes de respostes als agents utilitzats clínicament com paclitaxel, carboplatí, gemcitabina, 5-fluorouracil i irinotecan entre d'altres són bastant comparables amb les dades clíniques.

En aquest sentit volem destacar, tal com veurem al llarg d'aquesta tesi, que quant més avançat sigui el model PDX generat possiblement més valor afegit tindrà a l'hora d'ajudar en aquesta faceta de desenvolupament de nous fàrmacs o aproximacions terapèutiques. Quan ens referim a avançat ho fem des de dues perspectives: i) la forma com s'implanta en el ratolí, ortotòpic vs. subcutani, si es fa com teixit mantenint l'estructura tridimensional o ho fem d'un disgregat; i ii) és un tumor primari sense tractament o per contra deriva de biòpsia de pacient a la recaiguda després d'una o més línies de tractament (quimioteràpia, teràpia dirigida, immunoteràpia (ICIs)). Des del nostre punt de vista, quan un fàrmac es mostra efectiu en aquests models avançats té més possibilitats d'èxit de convertir-se en un fàrmac que arribi a ser utilitzat en el tractament dels pacients.

De la mateixa manera, la manca d'eficàcia antitumoral en models PDX es correlaciona amb resultats clínics negatius. En càncer de pàncrees la manca d'eficàcia preclínica de saracatinib (inhibidor de SRC) i sirolimus (inhibidor de mTOR) en PDX es correlaciona amb el fracàs a la clínica.

2. Desenvolupament de Biomarcadors de resposta i per a la selecció de pacients

Un altre aspecte molt important dels estudis preclínics amb PDX és que, a més d'ajudar a prioritzar les possibles indicacions clíniques, també poden facilitar la identificació de biomarcadors d'eficàcia del fàrmac. Existeix una alta concordança entre els models PDX i els assaigs clínics respecte als biomarcadors de susceptibilitat així com de resistència a fàrmacs. Així, per exemple, en càncer colorectal s'ha demostrat que els models PDX amb mutació

en *KRAS* no responen a cetuximab. La presència de *KRAS* no mutat és un biomarcador clínic per a aquesta teràpia dirigida (155,156).

De la mateixa manera, és important descobrir en els PDX marcadors de resistència que puguin ajudar-nos a identificar combinacions clíniques efectives. Un exemple el veurem en aquesta tesi en la identificació de la GCS en TTCG i tumors d'ovari com a diana per tractar tumors resistents als platins. Un altre exemple és en el CCR en què els tumors resistents a la inhibició de l'EGFR presenten amplificacions d'altres gens com *HER2* i *MET*. Els estudis preclínics en PDX van demostrar, i després es va validar clínicament, que l'ús de fàrmacs contra aquestes dues proteïnes va ser efectiu (157).

Els models PDX també són eines molt útils per mimetitzar o simular en el ratolí els mecanismes de resistència que es donen en els tumors quan els pacients es tracten. Així, com mostrem en dos treballs d'aquesta tesi (Article 1 i 2) en TTCG i tumors d'ovari sensibles als tractaments amb cisplatí, quan els ratolins implantats amb aquests tumors s'exposen a tractaments iteratius amb cisplatí això resulta en l'aparició de resistències de forma anàloga al que ocorre en l'entorn clínic. A més, els models així generats són eines molt potents no només per a identificar els mecanismes de resistència, sinó també per avaluar nous fàrmacs com exposarem al llarg de la tesi. Els *PDOX/Orthoxenografts* de càncer d'ovari i TTCG sensibles i els seus aparellats així generats resistents al cisplatí, recapitulen les característiques distintives de la resposta tumoral humana primària, com són els criteris de regressió histopatològica del tumor associada amb la resposta al tractament del pacient.

Des del nostre punt de vista, i tal com mostrarem en aquesta tesi, perquè els models de PDX puguin complir amb els objectius de millorar el desenvolupament de nous fàrmacs o teràpies, així com la cerca de biomarcadors efectius per a selecció de pacients, aquests han de complir diverses premisses bàsiques:

i) Els PDX han d'estar ben caracteritzats tant a nivell histopatològic com genòmic i molecular.

ii) En els estudis a realitzar en els PDX a l'hora d'avaluar nous fàrmacs o combinacions d'aquests amb els tractaments estàndards, és molt important avaluar tant la resposta immediata al tractament o **resposta**

ràpida, avaluada en finalitzar l'esquema de tractament; així com el retard en el recreixement del tumor en el temps una vegada finalitzat el tractament o **resposta a llarg termini**.

iii) Els tractaments efectius no només han de produir una disminució de la mida tumoral sinó que s'ha de traduir en la presència de paràmetres quantificables de resposta histològica.

3. Desenvolupament d'assaigs co-clínics

Un cop que un fàrmac ha entrat en un assaig clínic es molt difícil poder analitzar informació que sigui útil per al desenvolupament del fàrmac, fins i tot en aquells estudis que seleccionen als pacients per entrar en l'assaig basant-se en una alteració molecular i que per tant requereix moltes vegades de teixit tumoral abans i després del tractament. Això succeeix per la naturalesa intrínseca dels assaigs clínics on els pacients són seguits sota criteris molt específics, però també per la manca de materials biològics suficients i d'accés fàcil per realitzar estudis (158).

En els assaigs clínics els pacients poden tenir comportaments extrems, és a dir, arribar a desenvolupar tant respostes extremes com resistències de forma primerenca, sent molt difícil estudiar aquests mecanismes en detall, que permetrien millorar els resultats. En aquest context s'ha plantejat la realització d'assaigs co-clínics, en què de forma paral·lela el PDX o Avatar/Orthoxenograft, generat amb el tumor del pacient que entra en l'assaig, es tracta amb el mateix fàrmac experimental per emular la resposta clínica.

Aquesta estratègia permet l'avaluació de l'eficàcia del fàrmac tant en el pacient com en el model en el ratolí proporcionant una plataforma on investigar marcadors de susceptibilitat/resistència, així com una eina on provar combinacions per superar les resistències.

Tot i que aparentment aquest escenari és factible de realitzar i els PDX podrien aportar una informació molt valuosa, aquesta aproximació és més una

aproximació teòrica que un fet real, ja que molt pocs assaigs clínics compten amb un co-clínic en paral·lel.

4. Desenvolupament d'estratègies de Medicina Personalitzada

La idea de la medicina personalitzada en el camp de l'oncologia és que cada pacient sigui tractat segons les característiques específiques del seu propi tumor, proporcionant-li el tractament més adequat (158). Així, avui en dia, en la majoria d'hospitals, els tumors de càncer colorectal, de pulmó (CPNCP), de mama i d'ovari, entre d'altres, ja es caracteritzen de manera rutinària mitjançant NGS o panells de gens per a identificar les mutacions rellevants i ajudar en el procés de presa de decisions terapèutiques (159).

En ocasions, també s'utilitza la biòpsia líquida o l'anàlisi de l'ADN tumoral circulant per evitar biòpsies complexes i de risc, així com per incloure els pacients en assaigs clínics adequats amb agents dirigits a una determinada alteració molecular (160). Totes aquestes estratègies representen un avanç significatiu en la recerca translacional del càncer, però compliquen cada vegada més el procés terapèutic. Hi ha pacients per als quals en els seus tumors no es detecten biomarcadors d'eficàcia de medicaments, o bé casos en què s'identifiquen múltiples opcions que dificulten molt la selecció del més apropiat.

En aquest context, els models PDX o Avatar/Orthoxenografts es poden utilitzar per a personalitzar el tractament dels pacients en temps real (152,161). Aquesta potser és l'aproximació més complexa, però alhora més fascinant per a la qual es poden utilitzar els PDX. L'estratègia es basa en seleccionar en el PDX la millor teràpia per a tractar un pacient, per la qual cosa s'ha de provar la seva eficàcia en temps real en el PDX generat a partir d'una biòpsia del tumor. Les teràpies son seleccionades basant-se en les característiques moleculars del tumor o en les possibles teràpies disponibles per al tractament del tumor, i tot això es realitza en temps real. Aquest procés és complex, però quan tots els factors involucrats estan correctament alineats, la resposta en els Avatar/Orthoxenografts i els pacients està altament correlacionada.

No obstant això, aquest enfocament no és factible en molts pacients per raons com el fracàs del tumor per implantar-se, la manca d'agents efectius i el temps necessari per a realitzar un estudi complet. Per tant, es necessita el desenvolupament d'estratègies per optimitzar aquest procés. En aquest sentit, el nostre grup ha apostat per generar amplis grups de tumors en els quatre tipus tumorals objecte d'aquesta tesi, que són el Càncer d'Ovari, el Germinal Testicular, el càncer d'endometri i el càncer de pulmó (CPNCP), en què estiguin representats els diferents tipus de tumor tant histològicament com genètica. Models que ens han de permetre identificar subgrups de tumors segons les seves característiques histogenètiques als quals se'ls pugui assignar un tractament òptim. És clar que no es pot generar un Avatar per a cada tumor, però sí que podem generar Avatar/Orthoxenografts prototipus dels diferents subgrups per a així, en un nou cas, assignar-lo a un grup de tractament.

LIMITACIONS EN L'ÚS DELS MODELS PDX

Tot i la rellevància de la incorporació dels PDX en la recerca oncològica, aquests tenen limitacions importants que s'han d'abordar. Algunes d'aquestes són limitacions tècniques que inclouen diversos problemes com són:

i) La selecció del teixit més adequat per generar un PDX com a eina preclínica de màxim valor afegit. Molts dels estudis publicats estan fets amb mostres quirúrgiques en què hi ha molta quantitat de teixit i normalment són tumors primaris obtinguts abans del tractament. Tot i que aquest enfocament és útil per a generar col·leccions de PDX, les mostres complexes que provenen de biòpsies de metàstasi o tumors a la recaiguda després de cicles de tractament són molt més rellevants. Aquestes mostres, però, són molt més difícils d'aconseguir, i la quantitat de teixit tumoral que s'obté sol ser molt petita.

ii) És important definir la millor estratègia d'implantació del tumor en els ratolins (implantació ortotòpica, més complexa, vs. subcutània i més fàcil).

iii) És molt important tenir en compte el temps que es necessita perquè el tumor creixi, sobretot per a les aproximacions de medicina

personalitzada en temps real. Normalment, es triga de 3 a 5 mesos en desenvolupar un model PDX llest per a un estudi preclínic, un temps que molts pacients no tenen.

iv) Aconseguir taxes d'implantació acceptables. Tot i que són altes per a alguns tipus tumorals (pàncrees, còlon, melanoma cutani, etc.), són molt baixes per a d'altres (TTCG, melanoma uveal, pròstata, etc.). Per a poder arribar a fer estratègies de medicina personalitzada es considera que serien acceptables nivells d'implantació del 60% al 70%, sent aquest un dels principals aspectes que requereixen millora.

v) És important generar col·leccions de PDX no esbiaixades cap a certs subtipus de càncer, sinó que representin àmpliament l'heterogeneïtat de la malaltia. Com comentaré més endavant, tot i que no és l'objectiu d'aquesta Tesi, el nostre grup porta anys intentant aconseguir sèries no esbiaixades dels quatre tipus de tumors objecte de la tesi que representin l'heterogeneïtat canviant de la malaltia.

vi) Un aspecte fonamental en el desenvolupament de PDX és l'ús de soques de ratolins immunodeficients, que manquen d'elements funcionals del sistema immunològic. Tot i el desenvolupament de models humanitzats complexos en què es re-introdueixen cèl·lules del sistema immune després de la implantació del tumor, els PDX tenen un ús limitat per a l'avaluació d'immunoteràpies.

vii) Un altre aspecte important és la substitució de l'estroma tumoral humà per estroma murí, que probablement resulti en canvis en la regulació paracrina del tumor, així com en propietats físiques com la pressió intersticial, que poden limitar l'estudi d'agents dirigits contra aquest compartiment tumoral.

viii) L'elevat cost econòmic dels PDX i l'experiència necessària per al seu maneig fan que no sigui gaire factible el seu ús per fer cribratge de fàrmacs, substituint així les línies cel·lulars, que tenen un valor predictiu molt baix. Per això, actualment s'està tendint a l'ús de tumoroides o organoides per millorar aquest procés *in vitro*.

ix) En el procés de generació dels PDX en els diferents tipus de tumors s'ha vist que hi ha un biaix cap a la implantació de tumors de pitjor pronòstic o més agressius.

PREMISSES

1. Els models preclínics són eines fonamentals per a poder desenvolupar la investigació translacional del càncer, i s'utilitzen tant per a entendre la biologia de la malaltia com per al desenvolupament de nous fàrmacs.

2. Aconseguir que una molècula s'arribi a convertir en un fàrmac oncològic és un procés llarg, complex i econòmicament molt costós. Només alguns casos d'èxit (aproximadament 1 de cada 10 fàrmacs en fases clíniques) acabaran convertint-se després de l'aprovació de les agències reguladores (FDA i EMA) en tractaments per a l'ús en humans.

3. En els darrers 30 anys s'ha fet un gran esforç en generar en els ratolins dos tipus diferents de models preclínics tumorals: i) els *Genetically Engineered Mouse Models (GEMM),* en què s'introdueixen diferents alteracions genètiques al genoma del ratolí, i que s'han fet servir sobretot per a estudiar la biologia dels tumors; i ii) els *Patient Derived Xenografts (PDX)* basats en la implantació i perpetuació dels tumors humans en ratolins immunodeficients, i que s'han fet servir entre altres coses per al desenvolupament de fàrmacs.

4. Una de les limitacions més grans que hi ha en el desenvolupament de nous fàrmacs o noves estratègies terapèutiques, tant amb els models *in vitro* basats en línies cel·lulars convencionals, tumoroides, cultius 3D, organoides, etc., com amb els models *in vivo* generats a partir d'aquests models *in vitro* coneguts com a xenoempelts és el baix poder predictiu que tenen respecte al que s'observa als assaigs clínics.

5. La generació dels models preclínics PDX, i més concretament els PDOX, a partir de mostra tumoral fresca, ja sigui a partir d'una peça quirúrgica o d'una biòpsia, representen un pas més en la recerca translacional i una clara millora respecte a l'ús de les línies cel·lulars *in vitro* o dels xenoempelts derivats *in vivo* a partir d'elles. Aquests models reprodueixen les característiques histopatològiques dels tumors primaris i són molt més predictius tant de la biologia del tumor com de la resposta als tractaments dels tumors.

6. A més, com més complexos siguin aquests models, més valor afegit tindran en els diferents estudis en què s'utilitzin, però al mateix temps més

complex serà el seu maneig i més saber fer es necessitarà per manejar-los i treure'ls el màxim rendiment. Així, actualment els models més preats són els models ortotòpics, anomenats PDOX o orthoxenografts, generats a partir de biòpsies obtingudes a la progressió ja sigui de tumors refractaris als tractaments o de metàstasis de diferent localització. Aquests són models que contenen els canvis moleculars que han tingut lloc al tumor a conseqüència dels tractaments.

7. Les diverses modalitats de PDX, generats a partir de diferents tipus de mostres tumorals, però sobretot els PDOX generats de mostres complexes, com ara tumors recidivats / metastàtics, a banda de ser rellevants per al cribratge i desenvolupament de fàrmacs i per al descobriment de biomarcadors, poden permetre el desenvolupament d'estratègies de Medicina de Precisió i assaigs co-clínics que ens permetin fer un pas endavant a l'hora de fer una millor selecció dels tractaments que reben els pacients.

HIPÒTESI

Establir models preclínics que fenocopïin les característiques primàries del tumor dels pacients, que reflecteixin de manera precisa el comportament fenotípic, genotípic i de resposta a la quimioteràpia del tumor, és un pas bàsic en el camí per a identificar noves dianes terapèutiques i per a provar tractaments nous. Pensem que fer l'esforç per la implantació de teixits tumorals primaris de forma ortotòpica en ratolins inmunosuprimits pot ser excepcionalment valuosa per a l'elevada taxa de fracàs que existeix en la translació dels resultats preclínics als pacients. Així, la generació i perpetuació de *PDOX/Orthoxenografts* de Tumors Testiculars de Cèl·lules Germinals (TTCGs), Càncer Epitelial d'Ovari (CEOs), Càncer d'Endometri (CE) i d'*Orthoallografts* de càncer de pulmó, així com el seu desenvolupament posterior com a models tumorals *in vivo* de resistència adquirida al cisplatí, ens ha d'ajudar a millorar el tractament dels pacients. Tots ells, models preclínics avançats que ens han de permetre testar nous fàrmacs i identificar mecanismes de resistència a l'acció del platí.

OBJECTIUS

L'objectiu general d'aquesta tesi és generar i caracteritzar models preclinics de *PDOX/Orthoxenografts* de Tumors Testiculars de Cèl·lules Germinals (TTCGs), Càncer Epitelial d'Ovari (CEOs) i Carcinoma endometrioide d'endometri així com *orthoallografts* de càncer de pulmó (CPNCP). Models que s'evolucionaran a models de resistència adquirida al cisplatí per tal d'identificar tant mecanismes de resistència com noves estratègies terapèutiques.

Els objectius específics d'aquesta tesi són:

1. Generació i caracterització clínico-patològica de models *PDOX/Orthoxenografts* de Tumors Testiculars de Cèl·lules Germinals (TTCG), Càncer Epitelial d'Ovari (CEO) i carcinoma endometrioide d'endometri.

2. Evolució *in vivo* d'alguns d'aquests models preclínics de TTCGs i CEOs com a models de resistència adquirida al tractament amb el cisplatí. Utilització d'aquests models preclínics per a identificació i posterior validació en una sèrie clínica retrospectiva de tumors metastàtics d'alteracions genètiques pronòstiques associades amb l'adquisició de resistència al cisplatí.

3. Identificació en els models preclínics de TTCGs i CEOs i del cuc *Caenorhabditis elegans* (*C. elegans*) dels gens rellevants associats amb l'adquisició de resistència al cisplatí i validació preclínica d'una teràpia resensibilitzant en tumors refractaris.

4. Utilització de models avançats de càncer epitelial d'ovari aparellats sensibles/resistents al cisplatí per al desenvolupament preclínic en col·laboració amb la companyia farmacèutica Pharmamar S.A. de la molècula PM11083 (lurbinectedina).

5. Generació i caracterització d'al·loempelts ortotòpics (*orthoallografts*) mitjançant la implantació en el pulmó de ratolins immunodeficients dels tumors pulmonars generats en el model K-Ras$^{lox/LSLG12Vgeo}$ i el model EML4-ALK de ratolins modificats genèticament.

6. Utilització dels PDOX de carcinoma endometrioide d'endometri per a dissenyar de manera racional una teràpia dirigida a partir de la caracterització transcriptòmica i del perfil mutacional d'aquests models.

MATERIAL I MÈTODES I RESULTATS

ARTICLE 1:

Vidal, A.; Muñoz, C.; Guillem, M.J.; Moreto, J.; Sara, P.; Martínez-Iniesta, M.; Figueras, A.; Padullés, L.; Rodriguez, F.G.; Berdiel-Hacer, M.; Pujana, M.A.; Salazar, R.; Gil-Martín, M.; Martí, L.; Ponce, J.; Molleví, D.G.; Capellà, G.; Condom, E.; Viñals, F.; Huertas, D.; Cuevas, C.; Esteller, M.; Avilés,P.; Villanueva, A. Lurbinectedin (PM01183), a New DNA Minor Groove Binder, Inhibits Growth of Orthotopic Primary Graft of Cisplatin-Resistant Epithelial Ovarian Cancer. Clinical Cancer Research 2012; 18: 5399 - 5411.

RESUM

Objectius:

1. Generació i caracterització clínico-patològica de models *PDOX/Orthoxenografts* de Càncer Epitelial d'Ovari (CEO).
2. Evolució *in vivo* d'alguns d'aquests models preclínics d'CEOs com a models de resistència adquirida al tractament amb el cisplatí.
3. Utilització de models avançats de càncer epitelial d'ovari aparellats sensibles/resistents al cisplatí per al desenvolupament preclínic en col·laboració amb la companyia farmacèutica Pharmamar S.A. de la molècula PM11083 (lurbinectedina).

Introducció: El càncer epitelial d'ovari és la cinquena causa de mort per càncer en dones. La baixa taxa de supervivència és deguda al seu estadi avançat al moment del diagnòstic així com a la resistència intrínseca o adquirida a la quimioteràpia estàndard basada en platí. Així, és altament prioritari el desenvolupament d'estratègies terapèutiques innovatives i efectives per eludir la resistència al cisplatí.

Disseny experimental: Per tal d'investigar nous tractaments en models *in vivo* que reproduexin el creixement del càncer epitelial d'ovari, es va generar un model preclínic de càncer d'ovari després de la implantació ortotòpica d'un carcinoma serós d'alt grau primari en ratolins atímics. A continuació es va derivar en els ratolins una versió del tumor amb resistència adquirida al cisplatí.

Finalment es va testar en ambdós models preclínics l'eficàcia del tractament amb lurbinectedina (PM01183) sola o en combinació amb cisplatí.

Resultats: Els empelts tumorals perpetuats ortotòpicament van imitar les característiques histopatològiques del tumor primari de la pacient així com el patró de resposta del tumor al tractament amb cisplatí. La lurbinectedina, tant en monoteràpia com combinada amb cisplatí, va resultar efectiva tractant els models preclínics de tumor d'ovari sensible i resistent al cisplatí. A més a més, es va demostrar un potent efecte sinèrgic *in vivo* en els tractaments combinats, especialment en tumors resistents al cisplatí. La inhibició del creixement tumoral induïda per la lurbinectedina es va associar amb reducció de la proliferació, increment de la proporció de mitosis aberrants i la subseqüent inducció d'apoptosi.

Conclusions: Els models preclínics d'empelts ortotòpics en ratolins de tumors ovàrics primaris humans són eines útils en el desenvolupament de fàrmacs, aportant evidència consistent que lurbinectedina pot esdevenir una agent terapèutic útil en el tractament del càncer epitelial d'ovari, superant la resistència al cisplatí.

Cancer Therapy: Preclinical

Clinical Cancer Research

Lurbinectedin (PM01183), a New DNA Minor Groove Binder, Inhibits Growth of Orthotopic Primary Graft of Cisplatin-Resistant Epithelial Ovarian Cancer

August Vidal[3], Clara Muñoz[1], María-José Guillén[6], Jemina Moretó[2], Sara Puertas[1], María Martínez-Iniesta[1], Agnés Figueras[1], Laura Padullés[1], Francisco J. García-Rodriguez[1], Mireia Berdiel-Acer[1], Miguel A. Pujana[1], Ramón Salazar[4], Marta Gil-Martin[4], Lola Martí[5], Jordi Ponce[5], David G. Molleví[1], Gabriel Capella[1], Enric Condom[3], Francesc Viñals[1], Dori Huertas[2], Carmen Cuevas[6], Manel Esteller[2], Pablo Avilés[6], and Alberto Villanueva[1]

Abstract

Purpose: Epithelial ovarian cancer (EOC) is the fifth leading cause of death in women diagnosed with gynecologic malignancies. The low survival rate is because of its advanced-stage diagnosis and either intrinsic or acquired resistance to standard platinum-based chemotherapy. So, the development of effective innovative therapeutic strategies to overcome cisplatin resistance remains a high priority.

Experimental Design: To investigate new treatments in *in vivo* models reproducing EOCs tumor growth, we generated a preclinical model of ovarian cancer after orthotopic implantation of a primary serous tumor in nude mice. Further, matched model of acquired cisplatin-resistant tumor version was successfully derived in mice. Effectiveness of lurbinectedin (PM01183) treatment, a novel marine-derived DNA minor groove covalent binder, was assessed in both preclinical models as a single and a combined-cisplatin agent.

Results: Orthotopically perpetuated tumor grafts mimic the histopathological characteristics of primary patients' tumors and they also recapitulate in mice characteristic features of tumor response to cisplatin treatments. We showed that single lurbinectedin or cisplatin-combined therapies were effective in treating *cisplatin-sensitive* and *cisplatin-resistant* preclinical ovarian tumor models. Furthermore, the strongest *in vivo* synergistic effect was observed for combined treatments, especially in cisplatin-resistant tumors. Lurbinectedin tumor growth inhibition was associated with reduced proliferation, increased rate of aberrant mitosis, and subsequent induced apoptosis.

Conclusions: Taken together, preclinical orthotopic ovarian tumor grafts are useful tools for drug development, providing hard evidence that lurbinectedin might be a useful therapy in the treatment of EOC by overcoming cisplatin resistance. *Clin Cancer Res; 18(19); 5399–411. ©2012 AACR.*

Authors' Affiliations: [1]Translational Research Laboratory, Catalan Institute of Oncology - Bellvitge Biomedical Research Institute (IDIBELL); [2]Cancer Epigenetics and Biology Program (PEBC); [3]Department of Pathology, Hospital Universitari de Bellvitge; [4]Department of Medical Oncology, Catalan Institute of Oncology; [5]Department of Gynecology, Hospital Universitari de Bellvitge, Barcelona; and [6]Department of Research and Development (R&D), PharmaMar S.A, Madrid, Spain

Note: Supplementary data for this article are available at Clinical Cancer Research Online (http://clincancerres.aacrjournals.org/).

August Vidal and Clara Muñoz contributed equally to this work.

Corresponding Authors: Alberto Villanueva, Laboratory of Translational Research, Catalan Institute of Oncology - Bellvitge Biomedical Research Institute (IDIBELL), Hospital Duran i Reynals, Avda Gran Via s/n km 2.7, L'Hospitalet de Llobregat, 08907 Barcelona, Spain. Phone: 34-93-260-7952; Fax: 34-93-260-7466; E-mail: avillanueva@iconcologia.net; and Pablo Aviles, Department of Research and Development (R&D), PharmaMar S.A, Avda de los Reyes 1, Polígono Industrial La Mina, Colmenar Viejo, 28770 Madrid, Spain. Phone: 34-91-823 4514. E-mail: paviles@pharmamar.com.

doi: 10.1158/1078-0432.CCR-12-1513

Introduction

Ovarian cancer is the fifth leading cause of death among women, and is the most common cause arising from gynecologic malignancies (1). Although progress has been made in the treatment of epithelial ovarian cancer (EOC) by improved surgical debulking and the introduction of platinum-taxane regimens, overall 5-year survival rate is only 29% in advanced-stage disease (2–6). This low survival rate is because of its frequent diagnosis at an advanced stage and by intrinsic and acquired resistance to platinum-based chemotherapy. In the recurrent disease setting, those patients who experience progression through first-line, platinum-based therapy (*platinum refractory*), or those who experience relapse within 6 months of receiving platinum therapy (*platinum resistant*) are typically treated with a second-line non–platinum-based regimen, such as single-agent doxorubicin (7) gemcitabine (8), paclitaxel,

Translational Relevance

The efficacy of conventional platinum-based chemotherapy for EOCs is limited; most patients show an initial response to treatment but upon relapse, the platinum response rates progressively diminish and they ultimately die. So, the development of effective innovative therapeutic strategies to overcome cisplatin resistance remains a high priority. On the way to identifying novel therapeutic targets and for drug testing, we have developed two paired (*cisplatin-sensitive* and *cisplatin-resistant*) preclinical models of serous carcinoma phenocopying patients' primary tumor features including chemotherapy response behavior. In this study, we show that single lurbinectedin (PM01183), a novel marine-derived DNA minor groove covalent binder, or cisplatin-combined therapies were effective in treating *cisplatin-sensitive* and *cisplatin-resistant* preclinical models. Thus, we present hard evidences that lurbinectedin might be a useful therapy in epithelial ovarian cancer overcoming acquired cisplatin resistance providing a rationale for future trials.

topotecan (9), vinorelbine (10), or trabectedin plus pegylated liposomal doxorubicin (11). Agents yielding responses in the range of 15% to 20% that last a median of approximately 4 months, emphasize the great need for novel effective therapeutic strategies for its management (12–15).

DNA structure features 2 well-defined clefts known as the major and minor grooves, and DNA-binding proteins and drugs usually make contacts with the sides of the bases exposed in both grooves (16, 17). The DNA major groove is a site of attack for cisplatin and many alkylating agents, and when cisplatin binds to DNA 3 types of lesions can be formed on purine bases: monoadducts, and intra- and interstrand crosslinks. On the other hand, other antitumor drugs including mitomycin C, chromomycin A_3, and ecteinascidins, bind to the minor groove (18). One of the best examples is trabectedin (Yondelis), which reacts with certain guanines in the minor groove of DNA to form a covalent bond (19–21). The adduct is stabilized by van der Waals interactions with nucleotides in the opposite DNA strand, creating the equivalent of a functional interstrand crosslink (22). Lurbinectedin (PM01183) is a new synthetic alkaloid that is structurally related to ecteinascidins (23), which, with the exception of a module addition (ring C), confer important pharmacokinetic and pharmacodynamics properties benefits as well intrinsic activity (24–26).

Establishment of preclinical models phenocopying patients' primary tumor features, which accurately reflect phenotypic, genotypic, and tumor chemotherapy response behavior, is a basic step on the way to identifying novel therapeutic targets and for testing novel treatments (27, 28). Several lines of evidence indicate that engrafting primary tumor tissues orthotopically into immune-deficient mice (termed "tumor grafts") may be outstandingly valuable preclinical models for new drug development, and for reducing the high failure rate that exists in translating preclinical results to patients (29–33).

Here, we report the establishment and characterization of a serially transplantable, orthotopic, subject-derived epithelial ovarian tumor graft that retains crucial characteristics of the original primary tumor specimen, and its further development as an *in vivo* cisplatin-resistance tumor model. We show in engrafted preclinical models that lurbinectedin, a new minor groove DNA binder, is effective in the treatment of experimental ovarian tumors as a single or a combined-cisplatin agent. Overall, we present evidence of the efficacy of a therapeutic strategy based on the idea that a combination of 2 drugs that bind differentially to each DNA groove could overcome frequent cisplatin resistance in advanced-stage ovarian cancer.

Materials and Methods

Drugs and cell lines

Lyophilized lurbinectedin (PM01183) vials (1 mg/mL) were obtained from PharmaMar (Colmenar Viejo) and cisplatin (1 mg/mL) from Ferrer-Farma. The A2780 human ovarian carcinoma cell line was obtained from the European Collection of Cell Cultures. Cell cultures were grown *in vitro* at 37°C in a humidified atmosphere of 5% CO_2 in RPMI-1640 (Sigma-Aldrich Co.) supplemented with 10% FBS.

Animals

Female athymic *nu/nu* mice (Harlan) between 4 to 6 weeks of age were housed in individually ventilated cages on a 12-hour light-dark cycle at 21 to 23°C and 40% to 60% humidity. Mice were allowed free access to an irradiated diet and sterilized water. All animal protocols were reviewed and approved according to regional Institutional Animal Care and Use Committees.

Primary sample and orthotopic tumor engrafted in mice

The primary tumor specimen was obtained at Hospital Universitari de Bellvitge (L'Hospitalet de Llobregat, Barcelona, Spain). The study was approved by the Institutional Review Board. Written informed consent was collected from a patient who had not received cisplatin-based chemotherapy. Nonnecrotic tissue pieces (*ca.* 2–3 mm^3) from resected serous human epithelial ovarian tumor were selected and placed in DMEM (BioWhittaker) supplemented with 10% FBS and penicillin/streptomycin at room temperature. Under isofluorane-induced anesthesia, animals were subjected to a lateral laparotomy, their ovaries exposed and tumor pieces anchored to the ovary surface with prolene 7.0 sutures. Tumor growth was monitored 2 to 3 times per week and when the tumor grew, it was harvested, cut into small fragments, and transplanted into 2 to 5 new animals. Engrafted tumors at early mouse passages were cut in 6 to 8 mm^3 pieces and stored in liquid nitrogen in a solution of

90% FBS and 10% dimethyl sulfoxide for subsequent implantation.

Histology and immunohistochemical tumor characterization

The morphology of the primary patient's tumor and of the both engrafted tumors (OVA1X and OVA1XR) was compared by H&E staining in paraffin-embedded sections. Determination of cytokeratin (CK) 7, Ki67, WT1, alpha estrogen, and progesterone receptors status by immunohistochemistry, in accordance with the standard clinical protocols of the Department of Pathology (see Fig. 1 legend).

In vivo establishment of cisplatin-resistant xenografted tumor

Cisplatin-resistant tumor (named OVA1XR) was developed by iterative cycles of *in vivo* exposure to cisplatin of OVA1X. Briefly, orthotopically engrafted OVA1X tumors (at mouse passage #3) were allowed to grow until intra-abdominal palpable masses were noted. Then, animals were intravenously (i.v.) administered with cisplatin at a dose of 2 mg/kg for 3 consecutive weeks (Days 0, 7 and 14; cycle#1 of treatment). Post-cisplatin tumor relapse were harvested, prepared as previously described, and engrafted in new animals. This process was repeated up to five times by treating tumor-bearing mice with stepwise increasing doses of cisplatin: cycle#2, 3 mg/kg; cycle#3, 3.5 mg/kg; cycle#4, 4 mg/kg; and cycle#5, 5 mg/kg (see Fig. 1C). Cisplatin-resistant tumors were obtained in three independent experiments (OVA1XR-L1, -L2 and -L3). At doses higher than 3.5 mg/kg, signs of cisplatin-induced toxicity were ameliorated by 2 days administration of saline containing 5% glucose.

Drug treatment of engrafted cisplatin-sensitive and cisplatin-resistant tumor models

Mice were transplanted with fragments of OVAX1 and OVAX1R tumors, and when tumors reached a homogeneous palpable size were randomly allocated into the treatment groups (n = 8–12/group): i) Placebo; ii) Lurbinectedin (0.18 mg/kg); iii) Cisplatin (3.5 mg/kg); and iv) Lurbinectedin plus cisplatin (0.18 + 3.5 mg/kg). Drugs were i.v. administered once per week for 3 consecutive weeks (days 0, 7, and 14). Seven days after the final dose (day 21), animals were sacrificed, their ovaries dissected out, and weighed. Representative fragments were either frozen in nitrogen or fixed and then processed for paraffin embedding.

Evaluation of histologic response after chemotherapeutic treatment

Regressive histopathological features were evaluated (34–37), and 3 histologic response categories were established (38): (i) *NHR*, no histopathological response ($\leq$1 regression criterion [3+] present); (ii) *MHR*, moderate (2 regression criteria [3+] present); and (iii) *GHR*, good histopathological response ($\geq$3 regression criteria [3+] present).

In vivo evaluation of synergism among lurbinectedin and cisplatin treatments

Female mice were subcutaneously implanted with 10^7 A2780 cells suspended in a 1:1 solution of RPMI-1640: Matrigel (Becton, Dickinson & Co.). Mice bearing tumors (*ca.* 150 mm^3) were randomly allocated to 13 treatment groups (see Fig. 3 legend). All treatments were intravenously administered once per week for 2 consecutive weeks (days 0 and 7). Tumor growth was recorded 2 to 3 times per week starting from the first day of treatment (day 0) and tumor volume (in mm^3), estimated according to the formula $V = (a \cdot b^2)/2$, (a: length or biggest diameter; b: width or smallest diameter). Antitumor drug activity was measured with respect to the T/C index, and the fraction affected (F_a) by treatment was calculated ($F_a = 1 - T/C$). A CI was determined by the CI-isobol method (39).

Determination of tumor proliferation, apoptosis, and angiogenesis

Proliferation was assessed by quantifying the anti-phospo-Histone H3 (S10; Millipore) mitosis marker as described (40). Aberrant mitotic figures were identified by double immunostaining with α-tubulin (1:200) and anti-phospo-Histone H3 (S10; ref. 40). Apoptotic cells were quantified with two approaches: (i) immunostaining in paraffin-embedded samples with anti-Cleaved Caspase-3 (Asp175) antibody (Cell Signaling) at 1:200; and (ii) by terminal deoxynucleotidyl transferase-mediated biotin-dUTP nick end labeling (TUNEL) staining kit (Promega) in frozen OCT tissues (41).

Statistical analysis

Postchemotherapy tumor weight data were analyzed using a 2-tailed Mann–Whitney U test. The data are presented as medians and interquartile ranges (IQR) or means $\pm$ SD. Statistical analyses were done and graphs plotted using GraphPad Prism, version 5.02 (GraphPad Software Inc.). Synergism analyses were done by CompuSyn, version 1.0 (ComboSyn Inc.).

Results

Orthotopic model of epithelial ovarian cancer mimics the histopathological characteristics of primary patients' tumors

Primary tumors engrafted in the ovarian surface of athymic female mice (named OVA1X) grew as large solid masses. Ovarian infiltration and neighboring organ invasion were not seen in any of the implanted animals (Fig. 1A). The engrafted rate was close to 95% in all mouse-to-mouse passages, with a mean time of *ca.* 1,000 to 1,500 mm^3 during the first 6 passages of 84 $\pm$ 8 days. As shown in Fig. 1A, a very high histologic correlation was found between primary and engrafted tumors. Indeed, OVA1X had a typical serous adenocarcinoma appearance showing high cellularity, cellular papillae formation, and irregular slit-like spaces, and it remained stable throughout multiple rounds of serial mouse-to-mouse transplantation.

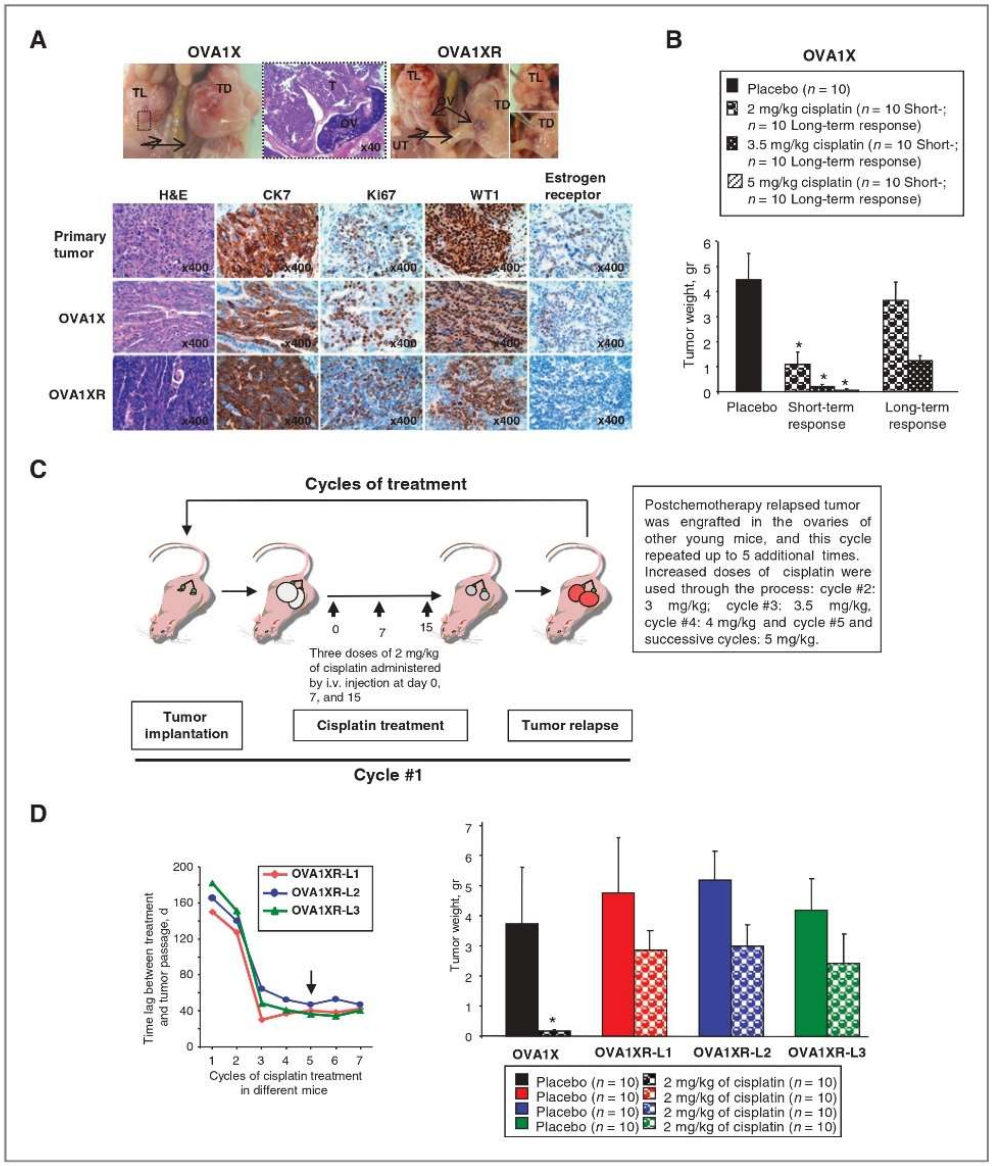

Figure 1. Establishment, and comparative histopathological characterization of primary and engrafted OVA1X and its paired developed cisplatin-resistant OVA1XR tumor. A, top, lateral laparatomy was conducted in isofluorane-anesthetized mice, the ovary mobilized and small tumor pieces of primary tumor anchored on the ovarian mouse surface with prolene 7.0 sutures. Engrafted tumors grew as large solid masses (usually 1,000–1,500 mm^3) in diameter at the time of sacrifice, and ovarian infiltration/invasion or ascitis were not seen. Bottom, representative H&E and immunohistochemical staining reveals a high correlation between primary and paired engrafted tumors. Primary antibodies were monoclonal antibodies: CK7 (clone OV-TL 12/30, Dako); Ki67 (clone MIB-1, Dako); WT1 (clone 6F-H2, Dako) and estrogen receptor alpha (clone SP1, Dako) OV, ovary; TL, tumor engrafted in the left ovarian; TD, engrafted in the right ovarian; UT, uterus. B, mice engrafted with OVA1X tumor were treated intravenously with low (2 mg/kg), intermediate (3.5 mg/kg), and high (5 mg/kg) cisplatin doses, and either short- or long-term responses were

Ki-67 immunostaining revealed a similar proliferative rate in primary and engrafted tumors, and they both preserved the same cytokeratin 7 (CK7) and Wilm's tumor susceptibility gene 1 (WT1) immunostaining pattern. Engrafted OVA1X tumor also retained their levels of positive immunostaining for estrogen receptor through mouse-to-mouse passages. Ascitis or synchronic peritoneal implants arising through tumor perpetuation were rarely identified in mice (data not shown).

Cisplatin treatment of engrafted tumor recapitulates characteristic features of primary tumor response in mice

OVA1X-implanted mice were treated with low (2 mg/kg), intermediate (3.5 mg/kg), and high (5 mg/kg) doses of cisplatin, and short- and long-term responses were evaluated (Fig. 1B). Low or intermediate doses of cisplatin were associated with a good short-term response, characterized by significant tumor weight reduction relative to the control group, whereas there was a complete response at high doses. Long-term response was investigated in a subgroup of mice ($n = 4$–6 mice/treatment/dose) that were kept alive for a postchemotherapy follow-up of 6 to 12 months. Tumors relapsed in 5 of 10 (50%) mice treated with 2 mg/kg and in 3 of 10 (30%) treated with 3.5 mg/kg at 6 months, whereas all animals treated with 5 mg/kg were disease-free after a 12-month follow-up. Postchemotherapy, histologic and immunohistochemical analysis of relapsed masses exhibited a viable serous adenocarcinoma that preserved the morphology and the main immunophenotypical characteristics of untreated engrafted tumors.

In vivo development of a cisplatin-resistant engrafted tumor model that recapitulates cisplatin primary tumor behavior response is a feasible model for pharmacologic drug evaluations

The general approach use to obtain the cisplatin-resistant engrafted tumor model is illustrated in Fig. 1C. OVA1X-implanted mice were initially treated with low doses (2 mg/kg) of cisplatin. When tumors relapsed, they were harvested and implanted in new animals (mouse-to-mouse passage). The process was repeated up to 5 times by treating tumor-bearing mice with stepwise increasing doses of cisplatin (Fig. 1C). A progressively shortened time lag between treatment and tumor relapse was noted for the 3 independent tumor lines (named OVA1XR-L1, -L2, and -L3) generated after iterative cycles of treatment. Indeed, a shortened time lag was mainly noted after the third or fourth cycle, and became stabilized (41 ± 6.1 days) subsequently for successive cycles of cisplatin treatment (Fig. 1D, left). Next, we evaluated the levels of cisplatin tumor resistance by comparative assays of OVA1X and each of the 3 independent lines of resistant tumors and homogeneous resistance was reproduced with each individual OVA1XR tumors (Fig. 1D, right). Thus, we selected OVA1XR-L2 for all further experiments, hereafter referred to as OVA1XR. Figure 1A shows that OVA1X and OVA1XR both recapitulated the histologic and immunohistochemical patterns found in the original patient-derived tumor. Interestingly, a consistent loss of estrogen expression was observed among resistant OVA1XR tumor respect to primary and OVA1X.

Lurbinectedin is effective in the treatment of cisplatin-sensitive and cisplatin-resistant ovarian tumor models

OVA1X and OVA1XR were orthotopically implanted in mice and when homogeneous tumor sizes (300–500 mm^3) were identified at palpation (on days 60 and 64 for OVA1X and OVA1XR, respectively) animals bearing tumors were randomized to the following groups ($n = 8$–12 mice/group): (i) placebo; (ii) cisplatin (3.5 mg/kg); (iii) lurbinectedin (0.180 mg/kg); and (iv) lurbinectedin + cisplatin (0.180 + 3.5 mg/kg). On day 21, cisplatin-sensitive tumor OVA1X experienced reductions of 95.3%, 88.3%, and 87.2% following the treatment with cisplatin, lurbinectedin, and lurbinectedin + cisplatin, respectively (Fig. 2A, left). Although, as single agents both cisplatin and lurbinectedin had a significant response with respect to the placebo-treated animals, nonsignificant differences were observed between both individual treatments. Likewise, combined lurbinectedin + cisplatin treatment had no additional significant benefit with respect to each individual treatment (lurbinectedin + cisplatin vs. cisplatin, $P = 0.15$; lurbinectedin + cisplatin vs. lurbinectedin, $P = 0.85$).

Figure 2B summarizes the results obtained for treatments of cisplatin-resistant tumor (OVA1XR), showing important differences between both tumors for lurbinectedin-based treatments. Thus, 48.2%, 93.6%, and 96.7% reductions in tumor weight were recorded following cisplatin, lurbinectedin, or lurbinectedin + cisplatin treatments, respectively. Lurbinectedin, as a single therapy was a significantly better response than with cisplatin ($P = 0.003$). Notably, the combined lurbinectedin + cisplatin treatment proved to be more active than either drug separately, suggesting a synergistic drug effect (lurbinectedin + cisplatin vs. lurbinectedin, $P = 0.022$; or vs. cisplatin, $P = 0.002$).

Histopathological changes were assessed for the different treatments within the tumor as surrounding stromal tissue in both cisplatin-sensitive (Fig. 2A, right, and Supplementary Table S1) and cisplatin-resistant tumors (Fig. 2B, right, and Table 1). Thus, enlargement of tumor cells, presence of

analyzed for each treatment. For short-term response studies, all dose-response mice were sacrificed on day 21 after treatment, whereas for long-term studies they were sacrificed after 6 months. C, experimental approach used for cisplatin-resistant tumor generation combines: (i) iterative cycles of cisplatin treatment (3 doses of cisplatin administered by i.v. injection on days 0, 7, and 15); and (ii) successive increase of administered doses through the process. D, left, illustrates a short time lag between successive cycles of treatment for 3 independent OVA1XR-L1, -L2, and -L3 tumor lines. For each line, tumors at cycle #5 of cisplatin treatment (arrow), were selected for further cisplatin assays. Right, shows comparative short-time cisplatin response between untreated OVA1X tumor versus each independent cisplatin-resistant OVA1XR-L1, -L2, and -L3 tumors. All mice were treated with 2 mg/kg of cisplatin administered by i.v. injection on days 0, 7, and 15 and sacrificed on day 21. *, $P < 0.05$.

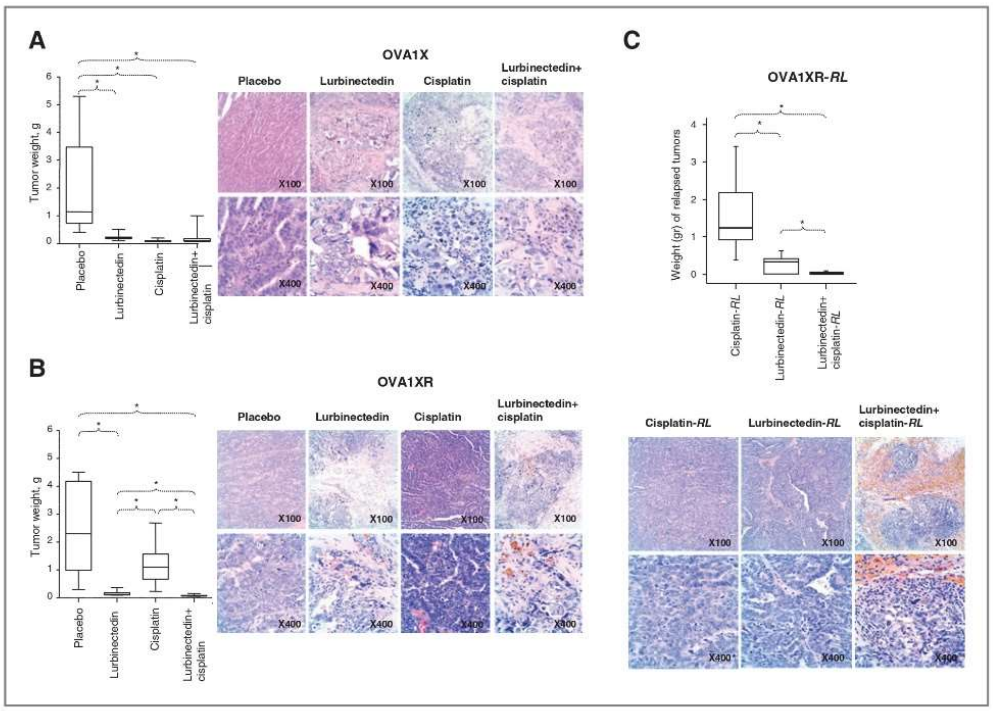

Figure 2. Response of engrafted OVA1X and OVA1XR tumors after lurbinectedin-based chemotherapy treatments. Animals were treated with placebo, cisplatin (3.5 mg/kg), or lurbinectedin (0.180 mg/kg) administered following the same schedule in three doses by i.v. tail vein injection on Days 0, 7, and 15 and sacrificed on day 21 ($n = 8$ placebo; $n = 10$ cisplatin; $n = 12$ lurbinectedin; and $n = 12$ combined lurbinectedin + cisplatin treatments). The doses of the combination (0.180 mg/kg + 3.5 mg/kg; lurbinectedin plus cisplatin) were selected on the basis of the optimal treatment tolerability in mice bearing tumors (data not shown). A and B, graphs illustrate responses of cisplatin-sensitive OVA1X and cisplatin-resistant OV1XR tumors on day 21 of treatment. Histopathological characterization of residual tumor masses postchemotherapy of cisplatin-sensitive OVA1X and cisplatin-resistant OVA1XR tumors, respectively. Sections were stained with H&E and an extensive study of tumor regression characteristics done, as an indicator of chemotherapeutic response (see Supplementary Table S1 and Table 1). C, characterization of the long-term response of cisplatin-resistant OVA1XR tumor. A subgroup of mice ($n = 5$) for each treatment was kept alive postchemotherapy, and was simultaneously sacrificed upon tumor relapse of the cisplatin-treated group. The graph illustrates differences in the weight of relapsed tumor masses for the different treatments. Histopathological characterization of relapsed tumor masses (*-RL*) from mice treated with cisplatin, lurbinectedin, and lurbinectedin + cisplatin. Sections were stained with H&E and an extensive study of tumor regression characteristics done, as an indicator of chemotherapeutic response (see Supplementary Table S1 and Table 1). Cisplatin-*RL*, lurbinectedin-*RL*, lurbinectedin + cisplatin-*RL*, tumor relapsed after cisplatin, lurbinectedin, or combined treatments, respectively. *, $P < 0.05$.

multinucleated giant cells, lymphocytic and histiocytic infiltrates with the presence of hemosiderin and fibrosis, and the scarring of tumoral stroma were observed associated with treatments. Interestingly, cisplatin treatment did not induce morphologic changes in the cisplatin-resistant OVA1XR tumors (Fig. 2B).

To investigate the long-term response a subgroup of treated mice ($n = 4$–6 mice/group) were kept alive postchemotherapy. Thus, OVA1XR tumor relapse took place more than a period of 42 days in all cisplatin-treated mice, whereas in cisplatin-sensitive OVA1X regrowth was found in only 1 cisplatin-treated mouse after eight months follow-up. At sacrifice of OVA1XR, significant differences were found in the weight and histology of relapsed masses (*-RL*) for lurbinectedin-based treatments compared with the cisplatin-*RL* group (lurbinectedin-*RL* vs. cisplatin-*RL*, $P = 0.0020$; or lurbinectedin + cisplatin-*RL* vs. cisplatin-*RL*, $P = 0.0008$; Fig. 2C, top). Furthermore, combined lurbinectedin + cisplatin treatment was more active than lurbinectedin monotherapy ($P = 0.046$), suggesting a long-term synergistic antitumor response for combined therapy. This finding is reinforced by the histology of lurbinectedin + cisplatin-*RL* masses (Fig. 2C, bottom). Together, although our results showed the efficacy of lurbinectedin treatment in the treatment of cisplatin-sensitive and cisplatin-resistant orthotopic engrafted tumor models, it is of note that they also suggest a synergistic effect with cisplatin in cisplatin-resistant OVA1XR.

Table 1. Extensive histopathological tumor regression criteria analyses in postchemotherapy engrafted OVA1XR tumor

	Mice	Fibrosis	Necrosis	Inflammation	Foamy macrophages	Calcification	Hemosiderin	Foreign-body giant cells	Giant tumor cells	Pattern of tumor infiltration[b]	Chemotherapy response based on histopathological features[e]
Short-term response[a]											
Placebo	1	0	1+	0	0	0	0	0	1+	1+	*NHR*
	2	0	1+	1+	0	0	0	0	1+	1+	*NHR*
	3	1+	1+	0	0	CD[c]	0	0	1+	1+	*NHR*
	4	1+	0	1+	0	0	0	0	1+	1+	*NHR*
	5	1+	1+	0	0	0	0	0	1+	1+	*NHR*
Cisplatin	6	2+	0	0	0	0	1+	0	0	1+	*NHR*
	7	2+	0	0	0	0	1+	0	1+	1+	*NHR*
	8	1+	0	0	0	0	1+	0	1+	1+	*NHR*
	9	1+	0	0	0	0	0	0	1+	1+	*NHR*
	10	1+	1+	0	0	0	0	0	1+	1+	*NHR*
Lurbinectedin	11	2+	1+	1+	0	0	2+	0	2+	2+	*NHR*
	12	2+	0	1+	0	CD	2+	0	2+	2+	*NHR*
	13	2+	0	2+	0	0	2+	0	2+	2+	*NHR*
	14	1+	0	1+	0	0	1+	0	1+	1+	*NHR*
	15	2+		1+	0	0	2+	0	2+	1+	*NHR*
Lurbinectedin + cisplatin	16	3+	0	2+	0	0	2+	0	3+	2+	*MHR*
	17	3+	0	1+	0	0	2+	0	3+	3+	*GHR*
	18	3+	0	2+	0	CD	2+	0	3+	3+	*GHR*
	19	1+	0	2+	0	0	1+	0	3+	3+	*MHR*
	20	3+	0	1+	1+	CD	2+	0	3+	3+	*GHR*
Long-term response[a]											
Cisplatin-RL	21	1+	1+	0	0	0	0	0	1+	1+	*NHR*
	22	1+	2+	1+	0	0	0	0	1+	1+	*NHR*
	23	1+	0	0	0	0	0	0	1+	1+	*NHR*
Lurbinectedin-RL	24	1+	0	1+	0	0	1+	0	1+	1+	*NHR*
	25	1+	0	1+	0	0	0	0	1+	1+	*NHR*
	26	3+	0	1+	0	0	2+	0	3+	2+	*MHR*
	27	NV[d]	NV	NV	NV	NV	NV	NV	NV	NV	*GHR*
Lurbinectedin + cisplatin-RL	28	3+	0	2+	0	0	2+	0	3+	3+	*GHR*
	29	3+	0	1+	0	0	0	0	3+	3+	*GHR*
	30	NV	NV	NV	NV	NV	NV	NV	NV	NV	*GHR*
	31	NV	NV	NV	NV	NV	NV	NV	NV	NV	*GHR*

[a]For short-term response studies, animals were sacrificed on day 21 of treatment, whereas for long-term-response studies, mice were sacrificed 42 days after the end of treatment when the tumor had relapsed.

[b]Pattern and extent of tumor infiltration was classified as follows: 1+, macroscopic large confluent tumor mass(es); 2+, multiple small tumor foci; 3+, scattered solitary tumor cells or complete absence of residual tumor. The remaining regression criteria were graded as follows: 0/1+, no or only minimally presence of the regression criterion within the specimen; 2+, focal occurrence of the respective regression criterion; 3+, widespread occurrence of the respective regression criterion.

[c]CD, dystrophic calcification.

[d]NV, not evaluated by complete tumor regression. Characterized by the absence of macro- and microscopic lesions.

[e]Three histopathological response categories were defined based on the number of regression criteria: *NHR*, no histopathological response (≤1 regression criteria [3+] present); *MHR*, moderate (2 regression criteria [3+] present), and *GHR*, good histopathological response (≥3 regression criteria [3+] present).

Histopathological tumor regression criteria are associated with treatment response in cisplatin-sensitive OVA1X and cisplatin-resistant OVA1XR tumors

Cytotoxic therapy leads to morphologic and histopathological changes within tumor tissue as well in the involved stroma. Next, we evaluated histopathological tumor regression, which has been established as the gold standard for the assessment of treatment response in several types of solid tumors (42–45). Supplementary Table S1 and Table 1 show extensive analysis of regression criteria for both OVA1X and OVA1XR, to establish whether they are suitable indicators of treatment response, as described for primary neoadjuvant EOC (38). On the basis of these criteria, a moderate histopathological response was observed in OVA1X for single cisplatin and lurbinectedin treatments, whereas a good response with respect to regression criteria was found for the combined treatment (Supplementary Table S1). Taken together, the tumor response and the histopathological regression criteria were evidence of the relevance of the combined treatment in cisplatin-sensitive OVA1X. In this context, in cisplatin-resistant OVA1XR tumor a good histopathological response was confirmed for the combined lurbinectedin + cisplatin treatment (Table 1). Moreover, the relevance of combined treatments was reinforced by the observation that the histopathological response was maintained in relapsed masses (Table 1).

Lurbinectedin and cisplatin treatments are synergistic *in vivo* in A2780-derived tumor xenografts

The synergism of the combined lurbinectedin + cisplatin treatment was further investigated in mice bearing A2780 xenografted tumors. Figure 3A shows the *T*/*C* values,

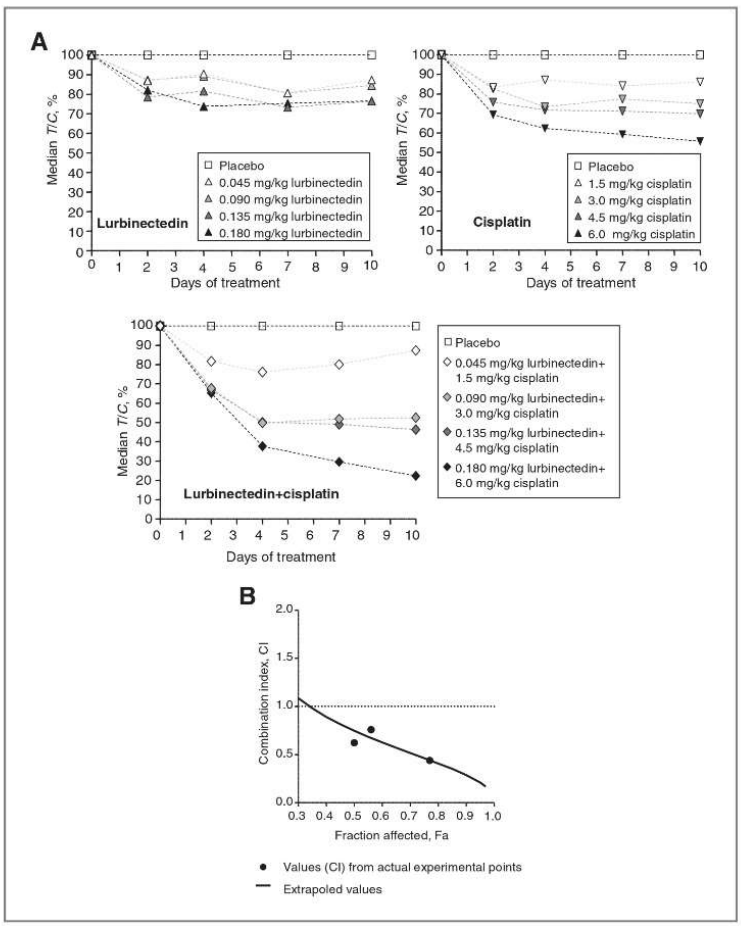

Figure 3. *In vivo* characterization of the synergistic effect among lurbinectedin and cisplatin treatments. Xenografted s.c. tumors were generated in nude mice after injection of 10^7 cells of the A2780 ovarian cancer cell line, and mice bearing tumors (*ca.* 150 mm^3) were randomly allocated to 13 treatment groups (n = 8–10/group): (i) placebo; (ii) lurbinectedin at 4 dose levels, namely MTD (0.180 mg/kg), 0.75 MTD (0.135 mg/kg), 0.5 MTD (0.09 mg/kg), and 0.25 MTD (0.045 mg/kg); (iii) cisplatin, at 4 dose levels MTD (6 mg/kg), 0.75 MTD (4.5 mg/kg), 0.5 MTD (3.0 mg/kg), and 0.25 MTD (1.5 mg/kg); and (iv) lurbinectedin plus cisplatin, administered with the combination at (1 + 1), (0.75 + 0.75), (0.50 + 0.50), and (0.25 + 0.25) of MTD ratios. A, graphs show antitumor activity of each single or combined treatment followed by *T*/*C* values, defined as the change in tumor volume for each treated (*T*) and placebo (*C*) group during the placebo-treated survival period. B, determination of tumor fraction affected (F_a) by treatment, calculated according to the formula $F_a = 1 - T/C$ and CI determined by the CI-isobol method using CompuSyn software, version 1.0 (ComboSyn, Inc. Paramus).

Table 2. Dose-response treatment effect of s.c. xenografts of A2780-derived cell line

			Dose-effect parameters[b]		
Treatment	**Dose, mg/kg**	**Fraction affected[a], F_a**	***m* (SD)**	**D_m**	***r***
Lurbinectedin	0.180	0.29			
	0.135	0.26	1.04 (0.16)	2.12	0.978
	0.090	0.22			
	0.045	0.09			
Cisplatin	6.0	0.45			
	4.5	0.31	1.24 (0.12)	1.29	0.990
	3.0	0.23			
	1.5	0.12			
Lurbinectedin + cisplatin	0.180 + 6.0	0.77			
	0.135 + 4.5	0.56	2.34 (0.36)	1.20	0.977
	0.090 + 3.0	0.50			
	0.045 + 1.5	0.10			

[a]Fraction affected ($F_a = 1-T/C$), defined as the change in tumor volume for each treated (T) and placebo (C) groups during placebo-treated survival period.

[b]Derived from the median-effect plot: [logFa/(1-Fa)] versus log(Dose), where m is the slope (as mean ± SD), D_m is the intercept of the plot, and r is the linear regression coefficient.

defined as the change in tumor volume for each treated (T) and placebo (C) group during the placebo-treated survival period, for mice treated with lurbinectedin, cisplatin or combined lurbinectedin + cisplatin. Animals treated with high cisplatin doses showed the lowest T/C of 55.2% on day 10, whereas there was no antitumor effect induced by the lurbinectedin single-agent treatment (minimal T/C, 70.8% on day 4). The combined lurbinectedin + cisplatin treatment produced lower T/C values than the more active agent in this experiment (cisplatin at 6.0 mg/kg). The antitumor effect seen on day 4 (T/C, 39.8%) for the highest dose of the combination (0.180 + 6.0 mg/kg; lurbinectedin + cisplatin) increased on subsequent days (T/C, 23.4% on day 10). On day 10, lurbinectedin + cisplatin treatment displayed a dose-dependent antitumor effect with median tumor volumes (mm^3) of 572.8, 1,074, 1,233, and 2,199 for animals treated with lurbinectedin + cisplatin at 0.180 + 6.0, 0.135 + 4.5, 0.09 + 3.0, and 0.045 + 1.5 mg/kg levels, respectively. Applying the median-effect principle to the data gave a Combination Index (CI) of 0.17 (at Fa = 0.97), suggesting a synergistic effect of the combination lurbinectedin + cisplatin in ovarian (A2780) xenografted tumors (Fig. 3B and Table 2).

Lurbinectedin-induced tumor response is mediated by antiproliferative and proapoptotic features and causes mitotic catastrophe

Next, we investigated whether tumor response mechanisms were induced by lurbinectedin associated with antiproliferative and proapoptotic features. Two experimental approaches were used: (i) in A2780-derived subcutaneous (s.c.) tumor xenografts treated with cisplatin, lurbinectedin or combined drugs for 24 or 72 hours; and (ii) in cisplatin-sensitive OVA1X and cisplatin-resistant OVA1XR tumors.

We found that 24 hours after treatments of the A2780 xenografts, the anti-phospo-Histone H3 (S10; H3S10ph) mitosis marker significantly decreased in cisplatin ($P = 0.007$), lurbinectedin ($P = 0.002$), or combined ($P < 0.001$) treatments compared with placebo-treated tumors (Fig. 4A). In fact, the decrease was significantly greater for the combined treatment than for each single therapy (lurbinectedin + cisplatin vs. lurbinectedin, $P = 0.005$; or vs. cisplatin, $P = 0.015$). In addition, a proapoptotic effect was associated with lurbinectedin treatments. Thus, a 6.7-fold increase in the number of apoptotic cells (by TUNEL assay) was observed in combined lurbinectedin + cisplatin ($P = 0.013$) treatment compared with the placebo group, and 3.0-fold and 3.7-fold increases with respect to cisplatin and lurbinectedin, respectively (Fig. 4C, left).

Likewise, antiproliferative and proapoptotic effects were confirmed in both engrafted orthotopic models. In OVA1XR (Fig. 4B), all treatments showed a significant decrease in the number of mitoses determined by H3S10ph (cisplatin, $P = 0.007$; lurbinectedin, $P = 0.003$; lurbinectedin + cisplatin, $P < 0.001$). As a single treatment, lurbinectedin was more effective than cisplatin ($P = 0.044$). Combined lurbinectedin + cisplatin treatment significantly diminished the number of mitoses with respect to single lurbinectedin ($P = 0.016$) or cisplatin ($P = 0.003$) treatment (Fig. 4B). This effect was also maintained in relapsed tumor masses (lurbinectedin + cisplatin-*RL* vs. cisplatin-*RL*, $P = 0.005$; or vs. lurbinectedin, $P = 0.012$). Apoptotic drug-induction was assessed in OVA1X and OVA1XR by immunodetection in paraffin-embedded tissues of caspase-3, an early and specific apoptotic marker. In cisplatin-sensitive

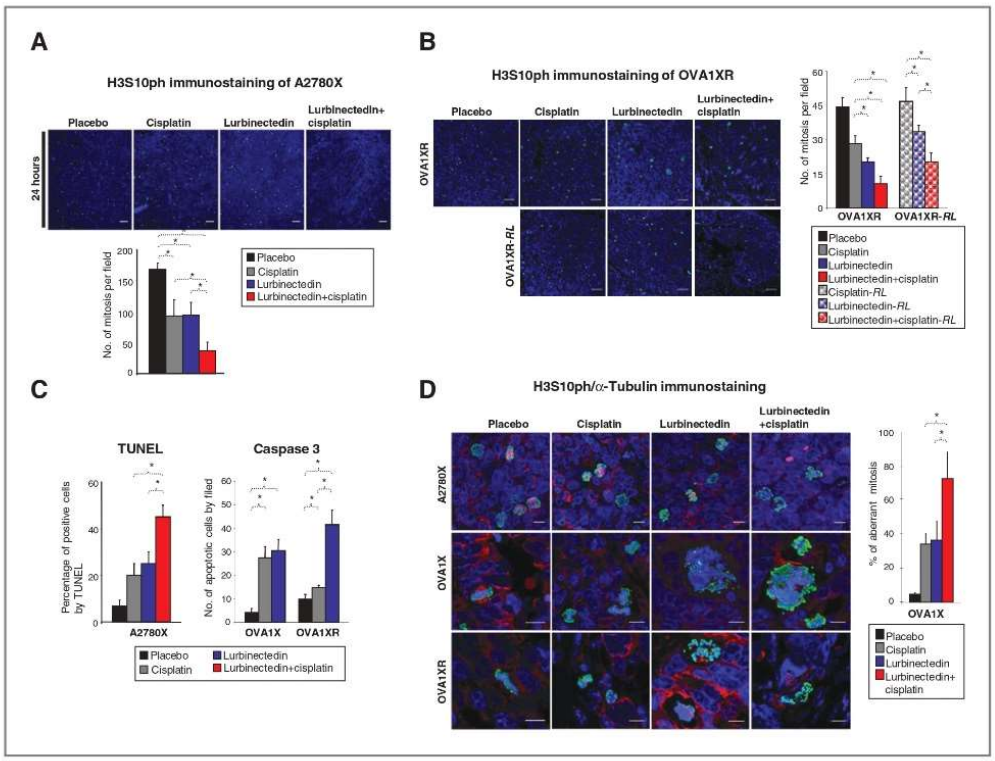

Figure 4. Tumor proliferation was determined after immunostaining mitotic figures with antiphosphorylated histone H3 (S10) antibody (H3S10ph; green staining), and mitotic spindles with anti α-tubulin (red staining). Chromosomes were labeled with 4′, 6-diamidino-2-phenylindole in the blue channel. Treatment doses were: (i) lurbinectedin (0.18 mg/kg); (ii) cisplatin (3.5 mg/kg); and (iii) lurbinectedin plus cisplatin (0.18 + 3.5 mg/kg). A, in A2780-derived s.c. tumors (A2780X) and (B) in residual tumor masses of cisplatin-resistant OVA1XR tumor or in long-term relapsed masses (-RL; 36 days after the sacrifice of the short-term response group). Stained cells were counted in 6 nonoverlapping representative fields. Images were taken with a Leica TCS LP5 spectral confocal microscope (Leica Microsystems) with ×20 and ×63 objectives and 405 Diode, Argon and DPSS 561 lasers, acquiring stacks every 1 mm. Stacks were projected and processed using ImageJ software (MacBiophotonics). Hotspot fields in viable comparable tissues zones at ×400 magnification were captured for each tumor and quantified, also taking the stromal component into consideration. C, apoptosis was evaluated by TUNEL and immunostaining of Caspase 3. Left, TUNEL assay in A2780X s.c. tumors treated with lurbinectedin, cisplatin, or combined lurbinectedin + cisplatin, and mice sacrificed 72-hour posttreatment. Right, cleaved Caspase 3 was analyzed in paraffin sections of residual tumor masses on day 21 of single cisplatin and lurbinectedin treatments of OVA1X and OVA1XR tumors. D, the presence of aberrant mitotic figures was determined by coimmunostaining with anti-H3S10ph and anti-α-tubulin (40) in A2780X s.c. tumors 72-hour posttreatment as in residual masses of OVA1X and OVA1XR tumors on day 21 of treatment. Graphs show the percentage of aberrant mitosis in OVA1X tumor. Scale bar is 10 μm. *, $P < 0.05$.

OVA1X, nonsignificant differences for the proapoptotic-induced effect were observed for the single treatments (cisplatin, 6.3-fold; lurbinectedin, 7.1-fold; $P = 0.45$; Fig. 4C, right). Whereas in cisplatin-resistant OVA1XR tumor the strong proapoptotic effect was noted for lurbinectedin (4.2-fold induction relative to the placebo, $P = 0.014$; and 2.8-fold with respect to cisplatin, $P = 0.007$), cisplatin retaining a moderate capability of inducing apoptosis in OVA1XR tumors (1.5-fold induction relative to placebo, $P = 0.036$; Fig. 4C, right). We did not analyze apoptosis induction in the combined treatment because the extensive histopathological regression prevents the reliable interpretation of the caspase cleaved apoptosis assay (data not shown).

Finally, we investigated whether lurbinectedin treatments affected the morphology of the mitotic spindle by double immunofluorescence staining with α-tubulin (red staining), a protein localized in the spindle, combined with staining with the mitosis marker histone H3S10ph (green staining; Fig. 4D and Supplementary Fig. 1). Thus, in mitotic cells identified by H3S10ph with vehicle-treated tumors, α-tubulin shows that control cells display

normal bipolar mitotic spindles with chromosomes correctly aligned on the metaphase plate. On the other hand, lurbinectedin-treated cells exhibited abnormal mitotic figures, with seriously defective chromosome alignment, and the cells displaying aberrant figures failed to progress through mitosis. The presence of cells displaying aberrant figures was particularly manifested for combined lurbinectedin + cisplatin treatment, in A2780-derived xenografts and both engrafted orthotopic models (Fig. 4D).

Discussion

In this work, we report the generation and characterization of a serous ovarian cancer model based on orthotopic tumor implantation in nude mice, and its further *in vivo* development as a tumor model of cisplatin resistance. Next, as preclinical models, we show that lurbinectedin, a new synthetic alkaloid binder to the DNA minor groove, is effective either in the treatment of *cisplatin-sensitive* and *cisplatin-resistant* ovarian tumors. So, our results show that the combination of 2 compounds that differentially bind the DNA major and minor grooves should be a useful treatment strategy for EOC patients, and suggest its importance for overcoming cisplatin resistance.

Recent data suggest an overall success rate of 10% for oncology products in clinical development, being one of the reasons attributed to this failure the fact that preclinical models used frequently do not predict clinical results (31). Currently, preclinical *in vivo* drug development is mainly realized in s.c. tumor xenografts generated after cell line injection, or in some cases after s.c. engraftment of primary tumor (29, 32, 33), and pure primary orthotopic tumor-based models have rarely been used. Few such tumor models are available: because surgery is often complex, small numbers of mice are used per study, and the models are more expensive (28). Here, we show that these orthotopic-based preclinical ovarian tumor models, which reproduce primary tumor properties, are outstanding resources for the development of new drug therapies. They would also be very valuable for exploring new therapeutic applications for drugs that are currently approved for use in humans, as we recently reported in microsatellite instability (MSI) + colorectal tumors with enoxacin (46). Thus, assessed chemotherapy responses in cisplatin-sensitive and cisplatin-resistant tumor models that maintain the morphologic, histologic, and genetic characteristics of patients' tumors, including the behavior of the stromal component and the tissue architecture, may improve preclinical drug translation to patients.

To overcome cisplatin resistance and reduce the side effects, new agents should have different mechanisms of action and should be non–cross-resistant with platinum (47). Structurally, the DNA duplex gives rise to two well-defined clefts known as the major and minor grooves (25). While the DNA major groove represents a site of attack for cisplatin and many alkylating agents, other antitumor drugs such as ecteinascidins, mitomycin C and chromomycin A3 bind to the minor groove (16, 17). Our work with the new synthetic alkaloid lurbirnectedin strongly suggests that strategies based on dual major and minor DNA groove-targeted therapies should be useful for treating cisplatin-resistant/refractory cases of ovarian carcinomas. Further studies in these models will allow a deeper insight into the cooperative mechanism of action among cisplatin and lubirnectedin, and enable their combined properties with other drugs such olaparib, temozolamide, doxorrubicine, etc. to be evaluated. Although, lurbinectedin is structurally similar to trabectedin (Yondelis), their important different pharmacokinetics properties identified may lead to novel and/or increased antitumor activity compared with original trabectedin (25, 26).

Our preclinical findings in cisplatin-sensitive OVA1X tumor indicate that lurbinectedin monotherapy treatment could be an active first-line drug on the basis of its similar cisplatin response rates and the related long-term behavior response. However, from the clinical standpoint, certainly, the most relevant preclinical result was the capability of lurbinectedin, either on its own or in combination with cisplatin, to overcome the cisplatin resistance of OVA1XR tumor. Its relevance was underlined by the better response and by the histopathological regression found in OVA1XR treated with lurbinectedin alone or combined with cisplatin, both in short- and long-term experiments. All together, our results indicate that combined lurbinectedin treatment should overcome cisplatin resistance, it being an effective second-line treatment for platinum responder patients as a first-line agent for refractory tumors.

In agreement with previously described *in vitro* results (25), we showed that the tumor response produced *in vivo* by lurbinectedin was mediated by an antiproliferative and proapoptotic induction and causes mitotic catastrophe. Previous reports showed common PM01183 (lurbinectedin) effectiveness in the nanomolar range in a panel of representative cell lines of different tumor types, and described that PM01183 (lurbinectedin) and cisplatin acted synergistically when tested *in vitro* on platinum-resistant cells lines (26). In this work, we showed that lurbinectedin synergizes *in vivo* with cisplatin treatments, an effect that is mainly observed in cisplatin-resistant OVA1XR tumors. It has been reported that although DNA lesions generated by lurbinectedin are not repaired by nucleotide excision repair (NER), it can interfere with NER, thereby attenuating the repair of specific NER substrates. Thus, lurbinectedin has enhanced activity in cisplatin-resistant cell lines with higher NER activity (26).

Dissemination in EOCs characteristically involves local invasion of pelvic and abdominal organs, and unlike many epithelial cancers, initial dissemination rarely requires the vasculature, although this is often involved in the advanced stages of disease (48). The tumor model presented here, as happens in their original patient, rarely disseminate in mice. Nevertheless, the generation of other orthotopic-based EOCs tumor models reproducing human dissemination patterns should be very useful for investigating drug action in malignant ascitis formation, the characteristic feature of advanced ovarian cancer at diagnosis. In fact, we have

developed other engrafted primary EOCs models that mimic in mice human local and distal dissemination behaviors (A. Vidal and A. Villanueva, personal communication).

After neoadjuvant chemotherapy, the residual tumor size in ovarian specimens was the only histopathological criterion that was significantly associated with treatment and subsequent overall survival. Histopathological responders defined by the absence of residual tumor, scattered solitary tumor cells, or a residual tumor of 5 mm or less had a significantly longer survival (38). The size of the residual tumor remaining after debulking surgery is known to be an important prognostic factor (49). Likewise, we show in both tumor models that the size of the residual masses and the abundance of regressive criteria correlate with response. The strong correlation between our preclinical tumor models and clinical settings in terms of tumor progression and response to chemotherapy, strongly argues in favor of conducting clinical lurbinectedin trials in resistant/refractory EOC.

In conclusion, we have shown that lurbinectedin, a drug targeting the minor DNA groove, is active and *in vivo* synergizes with cisplatin, which targets the major DNA groove, in the treatment of orthotopic cisplatin-sensitive and cisplatin-resistant patient-derived preclinical tumor models. Overall, our results provide solid evidence supporting clinical trials with lurbinectedin alone or in combination with cisplatin in advanced EOCs.

Disclosure of Potential Conflicts of Interest

M.J. Guillén, C. Cuevas, and P. Avilés are employees and shareholders of PharmaMar, SA (Madrid, Spain). No potential conflicts of interest were disclosed by the other authors.

Grant Support

This work was supported in part by grants FIS PI10-0222 A. Villanueva and Centro para el Desarrollo Tecnológico e Industrial (CDTI) IDI-20101640 (A. Villanueva). A. Vidal received a BAE grant (BAE/00073) from the Instituto de Salud Carlos III. D. Huertas is a Ramon y Cajal Researcher; C. Muñoz is an AGAUR Fellow and F.J. García–Rodriguez was supported by FIS. A. Villanueva has received a Research Grant from PharmaMar, SA.

The costs of publication of this article were defrayed in part by the payment of page charges. This article must therefore be hereby marked *advertisement* in accordance with 18 U.S.C. Section 1734 solely to indicate this fact.

Received May 7, 2012; revised July 31, 2012; accepted August 2, 2012; published OnlineFirst August 15, 2012.

References

1. Jemal A, Siegel R, Ward E, Murray T, Xu J, Thun MJ. Cancer statistics, 2007. CA Cancer J Clin 2007;57:43–66.
2. Alberts DS, Liu PY, Hannigan EV, O'Toole R, Williams SD, Young JA, et al. Intraperitoneal cisplatin plus intravenous cyclophosphamide versus intravenous cisplatin plus intravenous cyclophosphamide for stage III ovarian cancer. N Engl J Med 1996;335:1950–5.
3. Armstrong DK, Bundy B, Wenzel L, Huang HQ, Baergen R, Lele S, et al. Intraperitoneal cisplatin and paclitaxel in ovarian cancer. N Engl J Med 2006;354:34–43.
4. Berkenblit A, Cannistra SA. Advances in the management of epithelial ovarian cancer. J Reprod Med 2005;50:426–38.
5. Bhoola S, Hoskins WJ. Diagnosis and management of epithelial ovarian cancer. Obstet Gynecol 2006;107:1399–410.
6. Hoskins WJ, Bundy BN, Thigpen JT, Omura GA. The influence of cytoreductive surgery on recurrence-free interval and survival in small-volume stage III epithelial ovarian cancer: a Gynecologic Oncology Group study. Gynecol Oncol 1992;47:159–66.
7. Muggia FM, Hainsworth JD, Jeffers S, Miller P, Groshen S, Tan M, et al. J. Phase II study of liposomal doxorubicin in refractory ovarian cancer: antitumor activity and toxicity modification by liposomal encapsulation. J Clin Oncol 1997;15:987–93.
8. Lund B, Hansen OP, Theilade K, Hansen M, Neijt JP. Phase II study of gemcitabine (2′,2′-difluorodeoxycytidine) in previously treated ovarian cancer patients. J Natl Cancer Inst 1994;86:1530–3.
9. ten Bokkel Huinink W, Gore M, Carmichael J, Gordon A, Malfetano J, Hudson I, et al. Topotecan versus paclitaxel for the treatment of recurrent epithelial ovarian cancer. J Clin Oncol 1997;15:2183–93.
10. Rothenberg ML, Liu PY, Wilczynski S, Nahhas WA, Winakur GL, Jiang CS, et al. Phase II trial of vinorelbine for relapsed ovarian cancer: a Southwest Oncology Group study. Gynecol Oncol 2004;95:506–12.
11. Poveda A. Introduction. Trabectedin treatment in GYN cancers. Int J Gynecol Cancer 2011;21 Suppl 1:S1–2.
12. Gonzalez-Martin AJ, Calvo E, Bover I, Rubio MJ, Arcusa A, Casado A, et al. Randomized phase II trial of carboplatin versus paclitaxel and carboplatin in platinum-sensitive recurrent advanced ovarian carcinoma: a GEICO (Grupo Español de Investigación en Cáncer de Ovario) study. Ann Oncol 2005;16:749–55.
13. Pujade-Lauraine E, Wagner U, Aavall-Lundqvist E, Gebski V, Heywood M, Vasey PA, et al. Pegylated liposomal Doxorubicin and Carboplatin compared with Paclitaxel and Carboplatin for patients with platinum-sensitive ovarian cancer in late relapse. J Clin Oncol 2010;28:3323–9.
14. Alberts DS, Liu PY, Wilczynski SP, Clouser MC, Lopez AM, Michelin DP, et al. Randomized trial of pegylated liposomal doxorubicin (PLD) plus carboplatin versus carboplatin in platinum-sensitive (PS) patients with recurrent epithelial ovarian or peritoneal carcinoma after failure of initial platinum-based chemotherapy (Southwest Oncology Group Protocol S0200). Gynecol Oncol 2008;108:90–4.
15. Ushijima K. Treatment for recurrent ovarian cancer-at first relapse. J Oncol 2010;2010:497429.
16. Pabo CO, Sauer RT. Protein-DNA recognition. Annu Rev Biochem 1984;53:293–321.
17. Rohs R, West SM, Sosinsky A, Liu P, Mann RS, Honig B. The role of DNA shape in protein-DNA recognition. Nature 2009;461:1248–53.
18. Susbielle G, Blattes R, Brevet V, Monod C, Kas E. Target practice: aiming at satellite repeats with DNA minor groove binders. Curr Med Chem Anticancer Agents 2005;5:409–20.
19. Guan Y, Sakai R, Rinehart KL, Wang AH. Molecular and crystal structures of ecteinascidins: potent antitumor compounds from the Caribbean tunicate Ecteinascidia turbinata. J Biomol Struct Dyn 1993;10:793–818.
20. Kishi K, Yazawa K, Takahashi K, Mikami Y, Arai T. Structure-activity relationships of saframycins. J Antibiot (Tokyo) 1984;37:847–52.
21. Pommier Y, Kohlhagen G, Bailly C, Waring M, Mazumder A, Kohn KW. DNA sequence- and structure-selective alkylation of guanine N2 in the DNA minor groove by ecteinascidin 743, a potent antitumor compound from the Caribbean tunicate Ecteinascidia turbinata. Biochemistry 1996;35:13303–9.
22. Casado JA, Rio P, Marco E, Garcia-Hernandez V, Domingo A, Perez L, et al. Relevance of the Fanconi anemia pathway in the response of human cells to trabectedin. Mol Cancer Ther 2008;7:1309–18.
23. Manzanares I, Cuevas C, Garcia-Nieto R, Marco E, Gago F. Advances in the chemistry and pharmacology of ecteinascidins, a promising new class of anti-cancer agents. Curr Med Chem Anticancer Agents 2001;1:257–76.
24. Bueren-Calabuig JA, Giraudon C, Galmarini CM, Egly JM, Gago F. Temperature-induced melting of double-stranded DNA in the absence and presence of covalently bonded antitumour drugs: insight from molecular dynamics simulations. Nucleic Acids Res 2011;39:8248–57.

25. Leal JF, Martinez-Diez M, Garcia-Hernandez V, Moneo V, Domingo A, Bueren-Calabuig, et al. PM01183, a new DNA minor groove covalent binder with potent *in vitro* and *in vivo* anti-tumour activity. Br J Pharmacol 2010;161:1099–110.
26. Soares DG, Machado MS, Rocca CJ, Poindessous V, Ouaret D, Sarasin A, et al. Trabectedin and its C subunit modified analogue PM01183 attenuate nucleotide excision repair and show activity toward platinum-resistant cells. Mol Cancer Ther 2010;10:1481–9.
27. de Plater L, Lauge A, Guyader C, Poupon MF, Assayag F, de Cremoux P, et al. Establishment and characterisation of a new breast cancer xenograft obtained from a woman carrying a germline BRCA2 mutation. Br J Cancer 2010;103:1192–200.
28. Teicher BA. Tumor models for efficacy determination. Mol Cancer Ther 2006;5:2435–43.
29. Bibby MC. Orthotopic models of cancer for preclinical drug evaluation: advantages and disadvantages. Eur J Cancer 2004;40:852–7.
30. Derose YS, Wang G, Lin YC, Bernard PS, Buys SS, Ebbert MT, et al. Tumor grafts derived from women with breast cancer authentically reflect tumor pathology, growth, metastasis and disease outcomes. Nat Med 2011;17:1514–20.
31. Hait WN. Anticancer drug development: the grand challenges. Nat Rev Drug Discov 2010;9:253–4.
32. Kerbel RS. Human tumor xenografts as predictive preclinical models for anticancer drug activity in humans: better than commonly perceived-but they can be improved. Cancer Biol Ther 2003;2:S134–9.
33. Teicher BA, Herman TS, Holden SA, Wang YY, Pfeffer MR, Crawford JW, et al. Tumor resistance to alkylating agents conferred by mechanisms operative only *in vivo*. Science 1990;247:1457–61.
34. Becker K, Mueller JD, Schulmacher C, Ott K, Fink U, Busch R, et al. Histomorphology and grading of regression in gastric carcinoma treated with neoadjuvant chemotherapy. Cancer 2003;98:1521–30.
35. Fisher ER, Wang J, Bryant J, Fisher B, Mamounas E, Wolmark N. Pathobiology of preoperative chemotherapy: findings from the National Surgical Adjuvant Breast and Bowel (NSABP) protocol B-18. Cancer 2002;95:681–95.
36. McCluggage WG, Lyness RW, Atkinson RJ, Dobbs SP, Harley I, McClelland HR, et al. Morphological effects of chemotherapy on ovarian carcinoma. J Clin Pathol 2002;55:27–31.
37. Moreno A, Escobedo A, Benito E, Serra JM, Guma A, Riu F. Pathologic changes related to CMF primary chemotherapy in breast cancer. Pathological evaluation of response predicts clinical outcome. Breast Cancer Res Treat 2002;75:119–25.
38. Sassen S, Schmalfeldt B, Avril N, Kuhn W, Busch R, Hofler H, et al. Histopathologic assessment of tumor regression after neoadjuvant chemotherapy in advanced-stage ovarian cancer. Hum Pathol 2007;38:926–34.
39. Chou TC, Talalay P. Quantitative analysis of dose-effect relationships: the combined effects of multiple drugs or enzyme inhibitors. Adv Enzyme Regul 1984;22:27–55.
40. Huertas D, Soler M, Moreto J, Villanueva A, Martinez A, Vidal A, et al. Antitumor activity of a small-molecule inhibitor of the histone kinase Haspin. Oncogene 2012;31:1408–18.
41. Castillo-Avila W, Piulats JM, Garcia Del Muro X, Vidal A, Condom E, Casanovas O, et al. Sunitinib inhibits tumor growth and synergizes with cisplatin in orthotopic models of cisplatin-sensitive and cisplatin-resistant human testicular germ cell tumors. Clin Cancer Res 2009;15:3384–95.
42. Evans DB, Rich TA, Byrd DR, Cleary KR, Connelly JH, Levin B, et al. Preoperative chemoradiation and pancreaticoduodenectomy for adenocarcinoma of the pancreas. Arch Surg 1992;127:1335–9.
43. Honkoop AH, Pinedo HM, De Jong JS, Verheul HM, Linn SC, Hoekman K, et al. Effects of chemotherapy on pathologic and biologic characteristics of locally advanced breast cancer. Am J Clin Pathol 1997;107:211–8.
44. Junker K, Thomas M, Schulmann K, Klinke F, Bosse U, Muller KM. Tumour regression in non-small-cell lung cancer following neoadjuvant therapy. Histological assessment. J Cancer Res Clin Oncol 1997;123:469–77.
45. Mandard AM, Dalibard F, Mandard JC, Marnay J, Henry-Amar M, Petiot JF, et al. Pathologic assessment of tumor regression after preoperative chemoradiotherapy of esophageal carcinoma. Clinicopathologic correlations. Cancer 1994;73:2680–6.
46. Melo S, Villanueva A, Moutinho C, Davalos V, Spizzo R, Ivan C, et al. Small molecule enoxacin is a cancer-specific growth inhibitor that acts by enhancing TAR RNA-binding protein 2-mediated microRNA processing. Proc Natl Acad Sci U S A 2011;108:4394–9.
47. Dunton CJ. New options for the treatment of advanced ovarian cancer. Semin Oncol 1997;24:S5-2–S5-11.
48. Shield K, Ackland ML, Ahmed N, cRice GE. Multicellular spheroids in ovarian cancer metastases: biology and pathology. Gynecol Oncol 2009;113:143–8.
49. Cannistra SA. Cancer of the ovary. N Engl J Med 2004;351:2519–29.

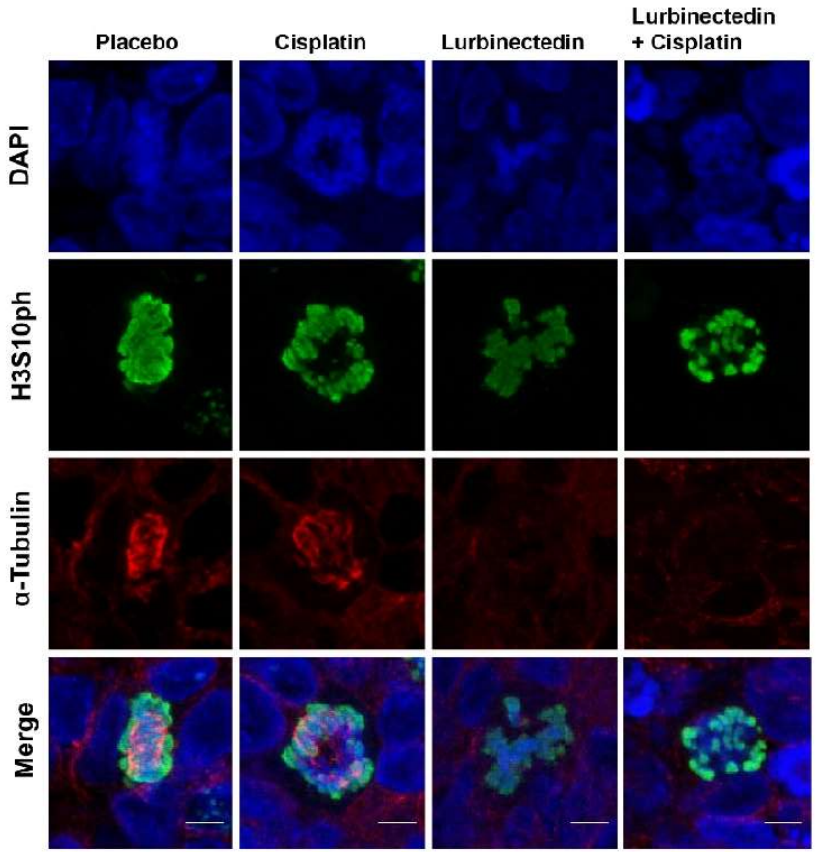

Supplementary Fig 1. Presence of aberrant mitotic figures in engrafted OVA1X tumors were analyzed by co-immunostaining with anti-H3S10ph (green staining), anti-α-tubulin (red staining).Chromosomes were labeled with DAPI in the blue channel. Treatment doses were: i) lurbinectedin (0.18 mg/kg); ii) cisplatin (3.5 mg/kg); and, iii) lurbinectedin plus cisplatin (0.18+3.5 mg/kg). Scale bar is 10 μm.

Supplementary Table 1 Extensive histopathologic tumor regression criteria analyses in post-chemotherapy engrafted OVA1X tumor.

	Mice	Fibrosis	Necrosis	Inflammation	Foamy macrophages	Calcification	Hemosiderin	Foreign-body giant cells	Giant tumor cells	Pattern of tumor infiltration [b]	Chemotherapy response based on histopathologic features [c]
Short-term response [a]											
Placebo	1	2+	2+	1+	0	0	0	0	1+	1+	*NHR*
	2	1+	3+	1+	0	0	0	0	1+	1+	*NHR*
	3	2+	1+	1+	0	0	1+	0	2+	1+	*NHR*
	4	0	3+	0	0	0	0	0	1+	1+	*NHR*
Cisplatin	5	3+	0	1+	0	0	0	0	0	3+	*MHR*
	6	1+	0	3+	0	0	0	0	0	3+	*MHR*
	7	3+	0	2+	0	0	1+	0	3+	2+	*MHR*
	8	3+	0	2+	0	0	2+	0	2+	3+	*MHR*
Lurbinectedin	9	2+	0	2+	0	0	2+	0	3+	3+	*MHR*
	10	2+	1+	2+	0	0	1+	0	3+	3+	*MHR*
	11	1+	0	1+	0	0	2+	0	3+	3+	*MHR*
	12	3+	0	2+	0	0	1+	0	3+	2+	*MHR*
	13	3+	0	2+	0	0	0	0	3+	2+	*MHR*
Lurbinectedin+cisplatin	14	3+	3+	2+	0	0	1+	0	3+	1+	*GHR*
	15	3+	2+	3+	0	0	1+	0	2+	3+	*GHR*
	16	3+	0	2+	0	0	3+	0	3+	3+	*GHR*
	17	3+	0	2+	0	0	2+	0	3+	3+	*CHR*
	18	3+	0	1+	2+	0	2+	0	3+	3+	*GHR*
	19	3+	0	2+	2+	0	2+	0	3+	3+	*GHR*

[a] For short-term response animals were sacrificed at day 21 of treatment.

[b] Pattern and extent of tumor infiltration was classified as following: 1+, macroscopic large confluent tumor mass(es); 2+, multiple small tumor foci; 3+, scattered solitary tumor cells or complete absence of residual tumor. While for the remaining regression criteria were graded as following. 0/1+, no or only minimally presence of the regression criterion within the specimen; 2+, focal occurrence of the respective regression criterion; 3+, widespread occurrence of the respective regression criterion.

[c] Three histopathologic response categories were defined based on the number of regression criteria: *NHR*, no histopathologic response (≤ 1 regresion criteria [3+] present); *MHR*, moderate (2 regression criteria [3+] present), and *GHR*, good histopathologic response (≥3 regression criteria [3+] present).

ARTICLE 2:

Piulats, J.M.; **Vidal, A.**; García-Rodríguez, F.J.; Muñoz, C.; Nadal, M.; Moutinho, C.; Martínez-Iniesta, M.; Mora, J.; Figueras, A.; Guinó, E.; Padullés, L.; Aytés, À.; Mollevi, D.G.; Puertas, S.; Martínez-Fernández, C.; Castillo, W.; Juliachs, M.; Moreno, V.; Muñoz, P.; Stefanovic, M.; Pujana, M.A.; Condom, E.; Esteller, M.; Germà-LLuch, J.R.; Capella, G.; Farré, L.; Morales, A.; Viñals, F.; Garcia Del Muro, X.; Cerón, J.; Villanueva, A. Orthoxenografts of testicular germ cell tumors demonstrate genomic changes associated with cisplatin resistance and identify PDMP as a re-sensitizing agent. Clinical Cancer Research 2018; 24: 3755 - 3766.

RESUM

Objectius:

1. Generació i caracterització clínico-patològica de models *PDOX/Orthoxenografts* de Tumors Germinals Testiculars de Cèl·lules Germinals (TTCG).
2. Evolució *in vivo* d'alguns d'aquests models preclínics de TTCGs com a models de resistència adquirida al tractament amb el cisplatí. Utilització d'aquests models preclínics per a identificació, i posterior validació en una sèrie clínica retrospectiva de tumors metastàtics, d'alteracions genètiques pronòstiques associades amb l'adquisició de resistència al cisplatí.
3. Identificació en els models preclínics de TTCGs i CEOs i del cuc *C. elegans* dels gens rellevants associats amb l'adquisició de resistència al cisplatí i validació preclínica d'una teràpia resensibilitzant en tumors refractaris.

Introducció: Investigar la base genètica de la resistència al cisplatí, ja que l'eficàcia de la quimioteràpia basada en cisplatí en el tractament de diferents càncers sovint es veu compromesa per la resistència intrínseca o adquirida de les cèl·lules tumorals als fàrmacs.

Disseny experimental: Es van generar 14 *orthoxenografts* trasplantant tumors testiculars de cèl·lules germinals (TTCG) no seminomatosos humans en ratolins,

mantenint les característiques del tumor primari en termes de genotip, fenotip i sensibilitat al cisplatí. Es van avaluar les alteracions cromosòmiques i genètiques en orthoxenografts sensibles al cisplatí i les seves parelles que havien desenvolupat resistència al cisplatí en ratolins atímics.

Resultats: Les anàlisis d'hibridació genòmica comparada de quatre parelles de xenoempelts van identificar reordenaments cromosòmics recurrents en tres dels tumors cisplatí resistents, mostrant guanys a la regió 9q32-q33.1. Es va trobar una correlació clínica entre la presència de guanys a 9q32-q33.1 en tumors de pacients refractaris al cisplatí i una pitjor supervivència global en tumors de cèl·lules germinals metastàtics. Es va estudiar el perfil d'expressió dels 60 gens situats en aquesta regió. *POLE3* i *AKNA* van ser els dos únics gens desregulats en tumors resistents que contenien el guany a 9q32-q33.1. A més a més, altres quatre gens (*GCS*, *ZNF883*, *CTR1* i *FLJ31713*) estaven desregulats en els cinc tumors resistents independentment de l'amplificació de 9q32-q33.1. Les RT-PCR en tumors i les anàlisis funcionals en *Caenorhabditis elegans* (*C. elegans*) van indicar que la influència en la resistència al cisplatí dels gens localitzats a 9q32-q33.1 podia estar causada per una regulació a l'alça o a la baixa d'aquests gens. Amb aquests resultats es va centrar l'estudi en la glucosilceramida sintasa (GCS) per demostrar que l'inhibidor de GCS DL-treo-PDMP resensibilitzava al platí els *orthoxenografts* generats resistents al cisplatí.

Translational Cancer Mechanisms and Therapy

Clinical Cancer Research

Orthoxenografts of Testicular Germ Cell Tumors Demonstrate Genomic Changes Associated with Cisplatin Resistance and Identify PDMP as a Resensitizing Agent

Josep M. Piulats[1,2], August Vidal[3,4], Francisco J. García-Rodríguez[1,8], Clara Muñoz[1], Marga Nadal[1], Catia Moutinho[5], María Martínez-Iniesta[1], Josefina Mora[6], Agnés Figueras[1], Elisabet Guinó[7], Laura Padullés[1], Àlvaro Aytés[1], David G. Molleví[1], Sara Puertas[1], Carmen Martínez-Fernández[8], Wilmar Castillo[1], Merce Juliachs[1], Victor Moreno[7], Purificación Muñoz[5], Milica Stefanovic[9], Miguel A. Pujana[1], Enric Condom[3], Manel Esteller[5], Josep R. Germà[2], Gabriel Capella[1], Lourdes Farré[1,10,11], Albert Morales[7], Francesc Viñals[1,12], Xavier García-del-Muro[2], Julián Cerón[8,13], and Alberto Villanueva[1,13,4]

Abstract

Purpose: To investigate the genetic basis of cisplatin resistance as efficacy of cisplatin-based chemotherapy in the treatment of distinct malignancies is often hampered by intrinsic or acquired drug resistance of tumor cells.

Experimental Design: We produced 14 orthoxenograft transplanting human nonseminomatous testicular germ cell tumors (TGCT) in mice, keeping the primary tumor features in terms of genotype, phenotype, and sensitivity to cisplatin. Chromosomal and genetic alterations were evaluated in matched cisplatin-sensitive and their counterpart orthoxenografts that developed resistance to cisplatin in nude mice.

Results: Comparative genomic hybridization analyses of four matched orthoxenografts identified recurrent chromosomal rearrangements across cisplatin-resistant tumors in three of them, showing gains at 9q32-q33.1 region. We found a clinical correlation between the presence of 9q32-q33.1 gains in cisplatin-refractory patients and poorer overall survival (OS) in metastatic germ cell tumors. We studied the expression profile of the 60 genes located at that genomic region. *POLE3* and *AKNA* were the only two genes deregulated in resistant tumors harboring the 9q32-q33.1 gain. Moreover, other four genes (*GCS, ZNF883, CTR1,* and *FLJ31713*) were deregulated in all five resistant tumors independently of the 9q32-q33.1 amplification. RT-PCRs in tumors and functional analyses in *Caenorhabditis elegans* (*C. elegans*) indicate that the influence of 9q32-q33.1 genes in cisplatin resistance can be driven by either up- or down-regulation. We focused on glucosylceramide synthase (GCS) to demonstrate that the GCS inhibitor DL-threo-PDMP resensitizes cisplatin-resistant germline-derived orthoxenografts to cisplatin.

Conclusions: Orthoxenografts can be used preclinically not only to test the efficiency of drugs but also to identify prognosis markers and gene alterations acting as drivers of the acquired cisplatin resistance. *Clin Cancer Res; 24(15); 3755–66. ©2018 AACR.*

[1]Program Against Cancer Therapeutic Resistance (ProCURE), Catalan Institute of Oncology (ICO), Bellvitge Institute for Biomedical Research (IDIBELL), Oncobell Program, L'Hospitalet del Llobregat, Barcelona, Catalonia, Spain. [2]Department of Medical Oncology, Catalan Institute of Oncology (IDIBELL), Barcelona, Spain. [3]Department of Pathology, Hospital Universitari de Bellvitge (IDIBELL), CIBERONC, Barcelona, Spain. [4]Xenopat S.L., Business Bioincubator, Bellvitge Health Science Campus, L'Hospitalet de Llobregat, Barcelona, Spain. [5]Cancer Epigenetics and Cell Biology Program (PEBC), Catalan Institute of Oncology (IDIBELL), Barcelona, Spain. [6]Department of Biochemistry, Hospital de Sant Pau, Barcelona, Spain. [7]Bioinformatic Unit, Catalan Institute of Oncology (IDIBELL), Barcelona, Spain. [8]Modelling Human Diseases in *C. elegans*. Genes, Disease and Therapy Program (IDIBELL), Barcelona, Spain. [9]Department of Cell Death and Proliferation, Instituto de Investigaciones Biomédicas de Barcelona (IIBB-CSIC), IDIBAPS, L'Hospitalet de Llobregat, Barcelona, Catalonia, Spain. [10]Laboratory of Experimental Pathology (LAPEX), Gonçalo Moniz Research Center, Oswaldo Cruz Foundation (CPQGM/FIOCRUZ), Salvador, Bahia, Brazil. [11]Institute of Science and Technology of Tropical Diseases (INCT/DT), Salvador, Brazil. [12]Departament de Ciencies Fisiologiques II, Universitat de Barcelona, L'Hospitalet de Llobregat, Barcelona, Spain. [13]C. elegans Core Facilty-IDIBELL, Barcelona, Spain.

Note: Supplementary data for this article are available at Clinical Cancer Research Online (http://clincancerres.aacrjournals.org/).

J.M. Piulats and A. Vidal contributed equally to this article.

Corresponding Authors: Alberto Villanueva, Catalan Institute of Oncology (ICO/IDIBELL), Hospital Duran i Reynals, 3a planta - Gran Via de l'Hospitalet, 199, L'Hospitalet de Llobregat, Barcelona 08908, Spain. Phone: 349-3260-7952; Fax: 349-3260-7466; E-mail: avillanueva@iconcologia.net; and Julián Cerón, Bellvitge Institute for Biomedical Research (IDIBELL),Hospital Duran i Reynals, 3a planta - Gran Via de l'Hospitalet, 199, L'Hospitalet de Llobregat, Barcelona 08907, Spain. Phone: 349-3260-7287; jceron@idibell.cat.

doi: 10.1158/1078-0432.CCR-17-1898

Translational Relevance

Cisplatin-based cytotoxic chemotherapy is the mainstay of the treatment of several types of neoplasias. The acquired resistance is a major clinical limitation for patient's survival. Orthoxenografts are the most advanced *ex vivo* platforms to investigate the efficiency of drugs in a personalized manner, but in this study, we also demonstrated other valuable tools to identify prognosis markers and novel resensitizing therapeutic approaches for the treatment of cisplatin-refractory tumors. As proof-of-principle, in this study we validate our approach demonstrating that presence of the 9q32-q33.1 gain is associated with poor risk defined by shorter overall survival (OS) and that genetic or pharmacologic inhibition of glucosylceramide synthase (GCS) activity is efficient to resensitize testicular and epithelial ovarian tumors refractory to cisplatin.

Introduction

Testicular germ cell tumors (TGCT) of adolescent and young adults are the most common malignancy in young men (1–3). They can be classified as seminomas (SE; originated in epithelium of the seminiferous tubules), which represent around 40% of cases, and nonseminomas (NSE; 60%). Seminomas are radio- and chemo-sensitive tumors highly curable at all stages. With the exception of teratomas, NSEs are also highly sensitive to cisplatin-based chemotherapy and, when combined with surgery, patients achieve high cure rates (4). In contrast with most advanced solid tumors, approximately 80%–90% of metastatic TGCTs will achieve complete cure after standard doses of cisplatin (CDDP) chemotherapy (4). Nevertheless, 10%–15% of patients die due to cisplatin refractoriness and the absence of alternative effective resensitizing therapies (5–7). Such high success in treating advanced testicular cancer has limited the number of studies addressing the treatment failure in refractory patients (8, 9).

In TGCTs, cisplatin resistance has been attributed to diverse cellular mechanisms (10–12), although the molecular details underlying treatment failure in refractory patients remains obscure (13–17). Patient-derived orthotopic xenografts, named PDOX or orthoxenografts, are relevant preclinical animal models that phenocopy human tumor properties (18,19). We have previously used TGCT orthoxenografts to explore novel therapeutic approaches for refractory TGCTs (20, 21). In this study, the genetic basis of acquired cisplatin resistance was investigated by comparative genomic hybridization (CGH) in a collection of matched cisplatin-sensitive and -resistant NSE tumors that were implanted orthotopically in nude mice. We studied genome amplifications and further investigated the 9q32-q33.1 region to identify cisplatin resistance–related genes. We found a clinical correlation between the presence of the 9q32-q33.1 gain and poor risk defined by shorter overall survival (OS). We also found gene expression alterations within the 9q32-q33.1 region that were associated with cisplatin resistance but not necessarily with the 9q32-q33.1 gain. Finally, we used a drug to inhibit one of the recurrently upregulated genes in cisplatin-refractory tumors, the glucosylceramide synthase (GCS), and observed that tumors were resensitized allowing the maintenance of the cisplatin-based therapy.

Materials and Methods

Human primary TGCT implantation and perpetuation in nude mice

To generate the collection of TGCT orthoxenografts, fresh surgical specimens of 62 human GCTs were implanted in nude mice. Twenty-two tumors were classified as pure SEs and 40 as NSE (21 as pure and 19 as mixed tumors containing different proportions of SE and NSE components). From the 40 NSEs, 14 tumors were perpetuated (35%), 10 derived from pure NSEs [three choriocarcinomas (CH), four embryonal carcinomas (EC), three yolk sac tumors (YS)], and four from mixed primary tumors. Five orthoxenografts were derived from several extragonadal tumor locations, and in four cases from patients treated previously with cisplatin-based chemotherapy (Supplementary Table S1). None of the 22 implanted pure gonadal seminomas (SE) grew in nude mice. Of the mixed tumors, comprising both SE and NSE components, only the NSEs grew in mice. Orthotopic implantation procedure of human tumors was performed as previously reported by our group (21) and briefly described in the Supplementary Data. IHC characterization is also described in the Supplementary Data. All patients gave written consent to participate in the study. The Institutional Ethics Committees approved the study protocol, and the animal experimental design was approved by the IDIBELL animal facility committee (AAALAC – Unit 1155). All experiments were performed in accordance with the guidelines for Ethical Conduct in the Care and Use of Animals as stated in The International Guiding Principles for Biomedical Research Involving Animals, developed by the Council for International Organizations of Medical Sciences.

Generation in mice of refractory engrafted NSEs to cisplatin treatment

Five selected engrafted tumors, TGT1X, TGT12X, TGT21XB, TGT34X and TGT38X, from patients without prior exposure to cisplatin, were allowed to grow until intraabdominal palpable masses were noted. Animals were administered with cisplatin intravenously at a dose of 2 mg/kg for 3 consecutive weeks (days 0, 7, and 14; cycle #1 of treatment). Post-cisplatin relapse, tumors were harvested, prepared as described previously and engrafted in new animals. This process was repeated up to five times by treating tumor-bearing mice with stepwise increasing doses of cisplatin: cycle #2, 3 mg/kg; cycle #3, 3.5 mg/kg; cycle #4, 4 mg/kg; and cycle #5, 5 mg/kg, as we described for ovarian tumors (22). When mice were treated at doses higher than 3.5 mg/kg, the signs of cisplatin-induced toxicity were ameliorated by administration of saline containing 5% glucose for 2 days. Dynamic CDDP responses were evaluated after assessing β-hCG and/or AFP serum levels, as described in Supplementary Data.

Analysis of point mutations and genomic imbalances

The presence of point mutations in a panel of selected cancer-related genes and microsatellite instability (MSI) were compared between sensitive and resistant paired orthoxenografts. Procedures are described in detail in the Supplementary Data.

Whole-genome analysis by NimbleGen CGH arrays

The CGH oligonucleotide array was carried out by NimbleGen Systems, Inc., at their facility in Wisconsin. Array design descriptions were: 2006-07-27_HG18_WG_CGH, single array CGH design for whole-human genome (hg18; NCBI Build 36).

Methods of DNA labeling array construction, hybridization, array normalization, and data analysis have been described in detail by Seltzer and colleagues (23).

Patients

Eighty-eight consecutive patients diagnosed with metastatic germ cell tumors and treated at the Institut Català d'Oncologia (Barcelona, Spain) between 1989 and 2004 were initially included in this study. Thirteen cases were not evaluated because of the lack of paraffin-embedded tissue blocks. Patient demographics and clinical characteristics of the 75 patients finally evaluated are listed in Supplementary Table S3. Sixty-three patients (84%) had NSE tumors and 12 (16%) had SE tumors. Four patients presented with mediastinal extragonadal disease. Sixty percent of the patients were classified as having a good prognosis, 19% as having an intermediate prognosis, and 21% as being of poor prognosis according to the IGCCCG categorization. Twenty-four patients were considered resistant, defined by progression or relapse despite adequate first-line chemotherapy treatment. Cases with mature teratoma only in the resected postchemotherapy mass and without posterior tumor relapse were considered sensitive. Tumor samples from primary tumors and/or resected metastases obtained before chemotherapy were included in a newly generated tissue microarray (TMA), as described previously (24). FISH analysis was described in Supplementary Material.

Quantitative gene and miRNA analysis

Total RNA was extracted using TRIzol (Invitrogen), following the manufacturer's instructions, and reverse-transcribed to cDNA. Quantitative RNA and miRNA analyses were performed as described in the Supplementary Material.

Cell culture, transfection and *in vitro* gene overexpression, and shRNAi knockdown experiments

The human NSE cell lines SuSaS (of teratocarcinoma origin) and its matched SuSaR ("R" for CDDP-resistant derived cell line) were grown for different experiments as described previously (25). For overexpression experiments, SuSaS cells were transfected with plasmid pCMV6-XL5-GCS containing the whole GCS human cDNA from OriGene (SC118052). Knockdown experiments were realized in SuSaR with four predesigned short hairpin RNAs (shRNA) for the human GCS gene from Qiagen (KH02376P) that were transfected with the jetPrime transfection kit (Polyplus), following manufacturer's instructions. GCS expression levels were analyzed by Western blot analysis at 24, 48, 72, and 96 hours posttransfection by anti-GCS (1/1,000; Protein-Tech) using anti-β-actin-HRP antibody as a control (1/20,000; Sigma-Aldrich). The chosen time to perform the experiments was 48 hours.

In vitro determination of drug resistance assays

Cisplatin (1 mg/mL) dissolved in NaCl (TEVA) and DL-threo-PDMP (Sigma-Aldrich) in DMSO at a final concentration of 59 mmol/L were assessed. Cell viability was determined by MTT assay. Briefly, 1×10^3 cells were plated onto 96-well plates, after 4 hours of transfection, fresh medium was added and cells were treated for 48 hours with different drugs concentration ranged from 0 to 20 μg/mL doses. MTT was added at a final concentration of 0.1% and after 2.5 hours of incubation (37°C, 5% CO_2) metabolic product formazan was dissolved in DMSO and the absorbance measured at 570 nm. Prism Software was used to calculate half maximal inhibitory concentration (IC_{50}) of the drugs.

Determination of GCS activity

Tumor samples were homogenized in lysis buffer (Tris-HCl 10 mmol/L, EDTA 1 mmol/L, and 0.1% Triton X-100 at pH 7.4) and centrifuged at 600 × *g* for 5 minutes. GCS activity was determined from NBD-C6-ceramide and UDP-glucose, the conversion product separated by TLC with chloroform/methanol/32% ammonia (70:30:5, v/v), and quantified by densitometry (Préférence/DVS, Sebia) as described previously (26). Briefly, for each assay, 200 μg of protein extract was suspended in reaction buffer (5 mmol/L $MgCl_2$, 5 mmol/L $MnCl_2$, and 1 mmol/L EDTA in 50 mmol/L HEPES, pH 7.2) and the substrate mixture containing 10 μmol/L NBD-C6-ceramide and 250 μmol/L UDP-glucose. After a 30-minute incubation at 37°C, reactions were terminated by adding 2.5 mL of chloroform/methanol (2:1, v/v), the samples were centrifuged (1,000 × *g*, 5 minutes), the lower phases dried under nitrogen, and subjected to TLC by using chloroform/methanol/32% ammonia (70:30:5, v/v) as the mobile phase.

Evaluation of *in vivo* responses of cisplatin-refractory orthoxenografts to treatment with DL-threo-PMDP

Tumors were implanted in mouse testicle and when homogeneous tumor sizes were detected, animals were randomized to four treatment groups ($n = 6$–8 mice/group): (i) vehicle; (ii) cisplatin (3.5 mg/kg); (iii) DL-threo-PDMP(D-threo-1-phenyl-2-decanoylamino-3-morpholino-1-propanol hydrochloride; Santa Cruz Biotechnology), 50 mg/kg dissolved in 5% of Tween 80%–0.85% NaCl; and (iv) DL-threo-PDMP+cisplatin (50 mg/kg+ 3.5 mg/kg). Cisplatin was intravenously administered once a week for three consecutive weeks (days 0, 7, and 14), while DL-threo-PDMP was administered daily by intraperitoneal injection over the 21-day period and mice were sacrificed on day 22 of treatment. In combined treatments, PDMP was administered one hour before cisplatin treatment. Ovarian orthoxenograft 17 model (OVA17X) was generated from a cisplatin-sensitive human serous epithelial ovarian tumor by orthotopic implantation (in the mouse ovary) in nude mice, as described previously (22). Cisplatin-resistant ovarian orthoxenograft 17 (OVA17XR) was derived from OVA17X by iterative treatment cycles with increasing doses of cisplatin, as described above for TGCT tumors. For the *in vivo* treatment with DL-threo-PMDP, OVA17XR was grown and implanted in the mouse ovary of several animals. When homogeneous tumor sizes were detected, they were randomized to four treatment groups ($n = 6$ mice/group) and treated as described previously.

Statistical analysis

For the clinicopathologic features, *P* values were calculated using the χ^2 test. Survival curves were estimated using the Kaplan–Meier method, and differences between individual curves were evaluated by multivariate Cox proportional hazards regression modeling. Analyses were adjusted for pathologic diagnostic classification. HRs and 95% confidence intervals (CI) were calculated. Likelihood ratio tests were used to assess the prognostic value of genomic amplification of 9q32-q33.1 by FISH in the TMA of metastatic GCTs. Values of $P < 0.05$ were considered significant.

Results

Establisment of orthoxenografts of TGCT NSE tumors

To study cisplatin resistance in TGCTs, our laboratory has compiled a valuable collection ($n = 14$) of both cisplatin-sensitive and -refractory TGCT NSE orthoxenografts (Supplementary Table S1). These orthoxenografts grew on mouse testicles as a big solid mass, displaying a strong correlation with their corresponding primary tumors in terms of histological appearance and expression of cellular markers (Fig. 1A and B). These tumors were kept stable throughout serial passages and, as occurring in patients, the secreted beta subunit of human chorionic gonadotropin (β-hCG) and/or alpha-fetoprotein (AFP) were detected in mouse serum as surrogate markers of tumor growth (Supplementary Table S1; refs. 27, 28).

Orthoxenografts reproduce in mice some of the patterns of dissemination observed in humans with the presence of retroperitoneal lymph nodes, lungs, and liver metastasis. Rare brain metastases were not detected in mice. Distant from what happens in humans in two tumors, we have detected the presence of peritoneal implants (Supplementary Table S1).

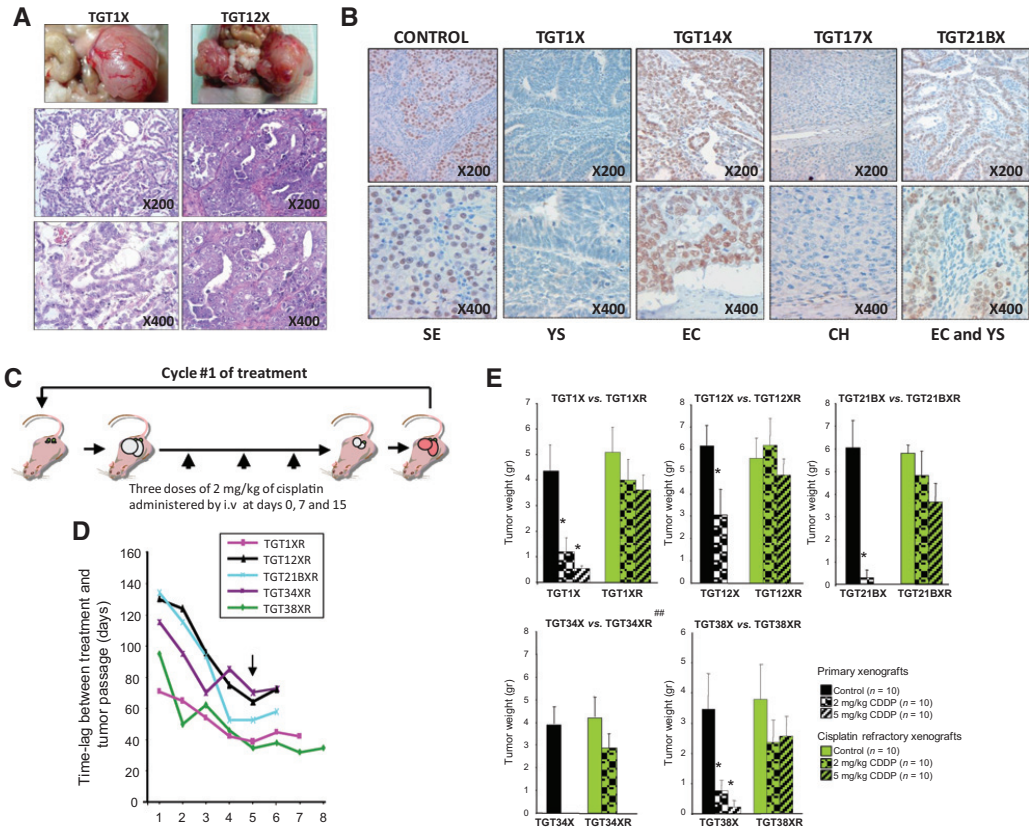

Figure 1.

Generation of TGCT orthoxenografts and development of paired cisplatin-refractory tumors. **A,** Macroscopic appearance and hematoxylin and eosin (H&E) staining of mice with orthoxenografts (left, TGT1X pure yolk sac, right, TGT12X pure embryonal carcinoma). **B,** OCT4 protein immunostaining. High levels of nuclear staining were only identified in TGT14X, pure embryonal carcinoma (EC) and TGT21BX, mixed EC and yolk sac tumor (YS). Absence of protein expression was noted in TGT1X, pure YS and TGT17X, pure choriocarcinoma (CH). Seminoma (SE) was used as a positive control. **C,** Generation of engrafted tumors refractory to cisplatin treatment combines: (i) five cycles of repetitive cisplatin treatments (one cycle: 3 doses of cisplatin administered by intravenous injection for three consecutive weeks, on days 0, 7, and 14) each cycle performed in diferent animals and (ii) doses of cisplatin were increased after each cycle of treatment ranging from 2 mg/kg (first cycle) to 5 (fifth cycle). **D,** The time lag between tumor-treatment and tumor-regrowth decreased as the different treatment cycles occurred. Tumors at cycle #5 of treatment (arrow) were used to assess the response to chemotherapy. **E,** Comparative short-term cisplatin response assays for paired nontreated versus cisplatin-resistant tumor. Mice were treated with low (2 mg/kg) and high (5 mg/kg) doses of cisplatin. TGT21BX and TGT34X showed a complete response at high doses. $^{\#\#}$, for paired TGT34X versus TGT34XR, only the response to the low dose was assessed (*, $P < 0.05$).

Orthoxenografts of NSE recapitulate the responses to cisplatin treatment in humans

We studied the pattern of responses to chemotherapy for nine orthoxenografts. Mice were treated with low (2 mg/kg) and high (5 mg/kg) doses of cisplatin, and their short- and long-term responses were evaluated. All tumors had a good short-term response to low doses of cisplatin, as indicated by a significant reduction in tumor weight in 8 cases and complete response in the tumor TGT21BX (Supplementary Fig. S1). A good correlation between tumor weight and reduction or absence of serum β-hCG and/or AFP levels was found, supporting its use as a dynamic surrogate marker of treatment efficacy. Differences among tumor weight and serum markers observed in TGT21AX after treatment can be explained by the predominance of a teratoma with a few microscopic islands of viable cells (Supplementary Fig. S1C). Administration of higher doses of cisplatin (5 mg/kg) was associated with a better response in all cases (Supplementary Fig. S1). In addition, there was a complete response in tumor TGT21AX (Supplementary Fig. S1C).

To investigate long-term cisplatin responses, a subgroup of the treated mice was kept alive postchemotherapy until tumor regrowth was observed. Tumors regrew in 8 of 9 cases, over a period of 15 to 135 days, independently of the cisplatin dose in most instances (Supplementary Fig. S1). In TGT39X, both treatments yielded a long and sustained response, as was confirmed by constant levels of AFP over a latency period of 90 days (Supplementary Fig. S1A). Histologic analysis of relapsed masses demonstrated the presence of a viable tumor in most cases, and the maintenance of the tumor heterogeneity, observed in mixed nontreated tumors (Supplementary Fig. S2). As observed in patients, cisplatin induced increasing teratoma differentiation in TGT21AX (Supplementary Figs. S1C, bottom S2).

Development of matched models of cisplatin refractoriness

To investigate cisplatin resistance against the same genetic background (sensitive vs. resistant), we developed several cisplatin-refractory tumor models. Thus, from this collection of 14 tumors, to develop this study, we selected 5 that were not exposed to cisplatin before implantation. This subset includes a YS (TGT1X), two embryonal carcinomas (TGT12X and TGT34X), a choriocarcinoma (TGT38X), and a mixed tumor (TGT21BX; Supplementary Table S1). Through five iterative cycles of treatment in different mice, and applying increasing doses of cisplatin through the cycles, we generated orthoxenografts with acquired resistance *in vivo* (named TGT1XR, TGT12XR, TGT21BXR, TGT34XR, and TGT38XR; Fig. 1C). During the process of resistance acquisition, a progressive shortened time lag between tumor treatment and tumor regrowth was noted, and the mice to mice passage time stabilized after five cycles of treatment in all cases (Fig. 1D). To evaluate the resistance to cisplatin in these transplanted tumors, paired short-term response assays between untreated (TGTX) and resistant (TGTXR) tumors at cycle #5 were performed (Fig. 1E). High levels of resistance were observed in all tumors at both low (2 mg/kg) and high (5 mg/kg) cisplatin doses. Finally, supporting the experimental value of this collection of paired sensitive/resistant orthoxenografts, we observed similar histologic pattern between original and cisplatin-resistant tumors (Supplementary Fig. S2).

Recurrent chromosomal imbalances were associated with acquired cisplatin resistance

In the DNA, cisplatin induces interstrand crosslinks and monoadducts that cause mutations and genomic instability (11, 29). Many of these alterations on the cisplatin-exposed DNA cannot be repaired and cause cellular lethality, but some may be selected and promote the cellular resistance to cisplatin. Thus, we investigated in paired TGCT orthoxenografts (sensitive vs. resistant) with the same genetic background whether the acquisition of cisplatin resistance was associated with the selection of specific genomic imbalances or mutations in a panel of selected genes. First, we did not find mutations in a subset of cancer-related genes including *K-ras*, *b-raf*, *PI3KCA*, *EGFR*, *c-Kit*, *PDGFRα* and *β*, *p15*, *p16*, and *SMAD4* or changes in the MSI status in resistant engrafted tumors. Then, we investigated chromosomal rearrangements, using array-based CGH, in four paired untreated parental engrafted tumors and their resistant counterparts (TGT1XR was later tested for 9q32-q33.1 amplification only). Few recurrent genomic changes were consistently detected in distinct resistant tumors when compared with their paired sensitive orthoxenograft (Fig. 2A). Particularly, gains at 9q were found in three of four cases, 9q32-q33.1 being the smallest common gain (5.1 M bp containing 60 genes) between three resistant tumors (Fig. 2B). In addition, gains at 15q23-q24.1 and 15q26.3 were identified in two tumors, and the loss of the Xp22.33 region was identified in three of four tumors (Supplementary Fig. S3). All these four genomic regions are hotspots to search for genes involved in the acquired resistance to cisplatin. In this study, we focused our attention on studying the 9q32-q33.1 region.

Amplification at 9q32-q33.1 is associated with an increased risk of death in advanced TGCT patients

To evaluate the clinical relevance of our results in orthoxenografts, gains at 9q32-q33.1 were studied by FISH in a human TMA including series of tumors from 75 patients with metastatic TGCTs (63 NSEs and 12 SEs) homogeneously treated with cisplatin-based chemotherapy in our hospital (Fig. 2C; Supplementary Table S2). Amplification at 9q32-q33.1 was identified in 18 of 75 (24%) cases, including 16 NSEs (5 CEs, 2 CHs, 1 YS, 2 TEs, and 6 mixed tumors) and two pure SEs (Table 1). Analysis of OS showed that amplification at the 9q32-q33.1 region was associated with a 2.79-fold greater risk of death in patients with metastatic GCTs ($P = 0.036$; HR = 2.79; 95% CI = 1.11–7.0; Table 1 and Fig. 2D). A higher risk of death associated to this genetic amplification was revealed when considering only patients with NSE ($n = 63$; $P = 0.026$; HR = 3.03; 95% CI = 1.18–7.76), but there was no difference in those with SE ($P = 0.54$; Table 1). OS subgroup analyses in NSE patients (presence of amplification vs. WT) showed a trend for good and intermediate risk groups alone; the relationship was statistically significant when we analyzed the two groups together ($P = 0.014$; HR = 5.16; 95% CI = 1.47–18.12; Table 1). This genetic amplification was also associated with shorter progression-free survival (PFS; $P = 0.043$; HR = 2.46; 95% CI = 1.07–5.63; Table 1; Fig. 2D) and such correlation was significant even when the NSE group alone was analyzed ($P = 0.024$, HR = 2.8, 95% CI = 1.19–6.57).

Moreover, there was a trend for tumors harboring the 9q32-q33.1 amplification to have a worse cisplatin response (Supplementary Table S3). Fifty percent of tumors with the

A

Tumor	Histology of resistant tumor [b]	Chromosome region [c]	Status	Scores [a]	Region	Size (Mbp)	Number of genes [d]
TGT12R	EC	9q21.11-q33.3	gain	+ 0.31	67.950 K - 123.690 K	55.7	502
		15q23-q24.1	gain	+ 0.36	69.690 K - 71.430 K	1.74	26
		15q26.3	gain	+ 0.37	97.770 K - 98.310 K	0.54	6
		Xp22.33	loss	- 0.29	30 K - 2.730 K	2.70	25
TGT21BR	YS, EC and CH	5p15.33-p15.2	gain	+ 0.30	90 K - 15.090 K	15.0	94
		9q21.11-q33.3	gain	+ 0.39	70.170 K - 123.690 K	53.5	461
		15q23-q24.1	gain	+ 0.39	69.690 K - 71.370 K	1.68	25
		15q24.3	gain	+ 0.30	74.970 K - 75.750 K	0.78	9
		15q26.3	gain	+ 0.41	97.830 K - 98.310 K	0.48	6
		Chromosome 21	gain	+ 0.28	0 K - 47.000 K	47	386
		Xp22.33	loss	- 0.45	30 K - 2.730 K	2.70	25
		Xp22.2	loss	- 0.42	9.510 K - 9.870 K	0.36	4
TGT34R	EC	No changes					
TGT38R	CH	9q32-q33.1	gain	+ 0.35	112.950 K - 118.050 K	5.10	60
		16p11.2-p11.1	gain	+ 0.34	34.350 K - 34.590 K	0.24	11
		20q13.13-q13.2	gain	+ 0.25	49.050 K- 49.770 K	0.72	5
		Xp22.23	loss	- 0.41	30 K - 2.730 K	2.70	25

[a] NimbleGen microarray data processed at 60 kbp average window. All the chromosomal gains or losses had a $\log_2$ score ≥0.30 or ≤0.30. No microarray data were available for TGT1R, a pure YS.
[b] Tumor histology: YS, yolk sac tumor, EC, embryonal carcinoma, CH, choriocarcinoma.
[c] Genomic changes were consistently detected in chemoresistant tumors at cycles #3 and #5 of chemotherapy.
[d] Location of genes in each region was based on build 36.3 from NCI.

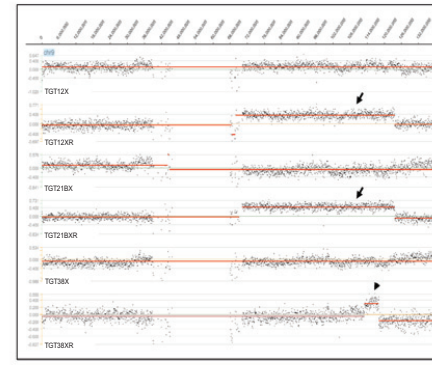

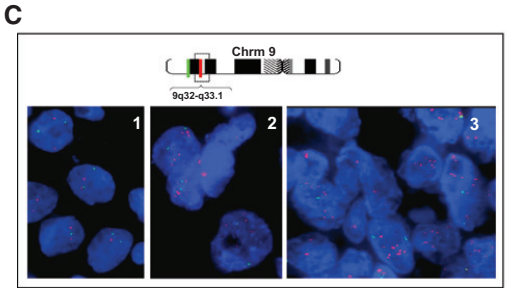

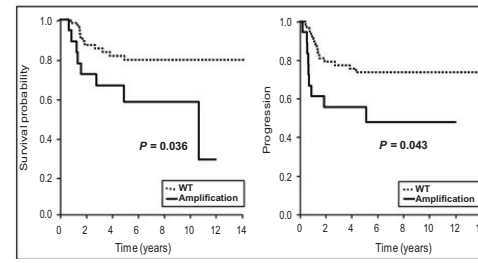

Figure 2.
Recurrent gains at 9q in refractory tumors. **A,** Chromosomal rearrangements related to acquired cisplatin resistance were identified when compared with four paired untreated parental engrafted tumors and their resistant counterparts. Whole-genome mapping was performed by oligonucleotide array CGH analysis (60 kbp window averaging) and visually depicted with the SignalMap graphical interface tool from Nimblegen Systems. **B,** The 9q21.11-q33.3 gain region (arrow) was identified in TGT12XR and TGT21BXR, while in tumor TGT38XR, there was a smaller overlapping region of 5.1 Mbp at 9q32-q33.1 (arrowhead). **C,** Representative FISH analyses of the copy number of 9q32-q33.1 in human metastatic CGT samples contained in the TMA. Interphase FISH with RP11-582I20 (red) and RP11-616C16 (green) probes. Panel 1: absence of amplification characterized by two red and two green signals in all interphase nuclei. Panels 2 and 3: amplification of the region. **D,** Kaplan–Meier plots by status of 9q32-q33.1 gains. Left, OS; right, PFS. *P* values are those from multivariate Cox proportional hazards regression models, controlling for the pathologic diagnostic classification.

amplification (9/18) were considered resistant to first-line chemotherapy compared with 26.3% (15/57) of tumors without it ($P = 0.060$). Up to 27.8% of tumors with the 9q32-q33.1 amplification did not achieve a tumor marker complete response or progressed during first-line treatment ($P = 0.007$; Supplementary Table S4).

Identification of 9q32-q33.1 genes whose expression is associated with tumor response to cisplatin

Next, to identify which genes within 9q32-q33.1 region could be related to cisplatin resistance, we performed quantitative PCR (qPCR) to study the expression levels of 60 genes and two miRNAs in the five paired sensitive/resistant engrafted tumors (Fig. 3A). In order to better represent our study of resistant tumors without the 9q32-q33.1 amplification, we included the pair TGT1X/TGT1XR in the gene expression profiling of this region to get a panel of three with and two without the 9q32-q33.1 gain. By qPCR, we found that 37 9q32-q33.1 genes, and the two miRNAs, were expressed in these five TGCTs (Fig. 3A and B). From these gene expression analyses, we observed that only two genes, *POLE3* and *AKNA*, were differently regulated in relation to the presence or absence of 9q32-q33.1 amplification. Interestingly, *POLE3* was upregulated in resistant tumors with 9q32-q33.1 gains, but downregulated in the two others without this genetic alteration. *AKNA* was downregulated in resistant tumors with 9q32-q33.1 gains, but not altered in the other two tumors without this alteration. Moreover, these results also indicate that a chromosomal gain does not necessarily mean gain of functions. Moreover, another five genes [*UGCG* (also known as *GCS*), *ZNF883*, *CTR1*, *ATP6V1G1*, and *FLJ31713*] were consistently up- or downregulated in all five resistant tumors independently of the 9q32-q33.1 amplification.

Table 1. Analysis of 9q32-q33.1 amplification in metastatic germ cell tumors

		Overall survival		Progression-free survival	
	N (%)	HR (95% CI)	*P*	HR (95% CI)	*P*
Chromosome copy number at 9q31-q32.1 ($n = 75$)					
WT	57 (76)	1	0.036[a]	1	0.043[a]
Amplification	18 (24)	2.79 (1.11–7.0)		2.46 (1.07–5.63)	
Stratified analysis					
Pathologic classification					
Nonseminoma ($n = 63$)					
WT	47 (74.6)	1	0.026[a]	1	0.024[a]
Amplification	16 (25.4)	3.03 (1.18–7.76)		2.8 (1.19–6.57)	
Seminoma ($n = 12$)					
WT	10 (83.3)	1 (0–Inf)	0.54	1 (0–Inf)	0.38
Amplification	2 (16.7)	0		0	
IGCCCG classification					
NSE with good risk ($n = 33$)					
WT	27 (81.8)	1	0.096	1	0.22
Amplification	6 (18.2)	5.89 (0.82–42.52)		3.29 (0.55–19.71)	
NSE with intermediate risk ($n = 14$)					
WT	10 (71.4)	1	0.15	1	0.28
Amplification	4 (28.6)	3.41 (0.68–17.02)		2.33 (0.52–10.44)	
NSE with poor risk ($n = 16$)					
WT	10 (62.5)	1	0.88	1	0.30
Amplification	6 (37.5)	0.9 (0.21–3.79)		2 (0.55–7.21)	
Grouping NSE according to good and intermediate risk ($n = 47$)					
WT	37 (78.7)	1	0.014 [a]	1	
Amplification	10 (21.3)	5.16 (1.47–18.12)		3.28 (1.03–10.37)	0.056

Abbreviation: WT, no amplification at 9q32-33.1.
[a]*P* values are from multivariate Cox models adjusted for pathological diagnostic classification.

Therefore, we found that gene expression changes at the 9q32-q33.1 region in resistant tumors were not necessarily correlated with the presence of the amplification, suggesting the coexistence of other mechanisms modifying gene expression that confer resistance to cisplatin.

The influence of genetic changes on resistant tumors is complex and multifactorial as reflected by the fact that the functional network (obtained from the web-based tool STRING) for 34 genes differentially expressed in these resistant tumors was rather poor (30), indicating a low functional relation between these genes. Importantly, the six genes showing deregulation in resistant tumors do not show any functional link (Supplementary Fig. S4).

Some gene functions involved in cisplatin response are conserved in *C. elegans*

We wondered whether the 9q32-q33.1 genes deregulated in resistant tumors were acting in the same manner in the response to cisplatin. Cisplatin has a broad mode of action being also toxic to eukaryotic cells of model organisms as *Caenorhabditis elegans* (*C. elegans*; ref. 31). We found that three of the five genes deregulated in resistant tumors (*GCS*, *CTR1*, and *ATP6V1G1*) were conserved in *C. elegans*. Through an automated toxicity assay, we found that *vha*-10/ATP6V1G1(RNAi) animals were sensitive to cisplatin (Supplementary Fig. S5). *GCS* present three paralogs in *C. elegans* and we needed to inactivate two of them at the time to produce sensitivity to cisplatin. On the contrary, worms treated with CTR1/F27C1.2(RNAi) were resistant to cisplatin exposure, as expected from the inactivation of the cooper transporter that is involved in cellular intake of cisplatin (Supplementary Fig. S5).

We conclude that 9q32-q33.1 genes deregulated in the resistant tumors can either be up- or downregulated, and provide either resistance or sensitivity to cisplatin. Moreover, the mechanisms of response seem to be conserved through evolution rather than be specific of human cells or tumors.

DL-threo-PDMP, a competitive inhibitor of GCS, resensitizes refractory TGCT and EOC orthoxenografts to cisplatin

As a proof-of-concept of our approach to search novel therapeutic strategies for overcoming cisplatin resistance, we decided to dig into the therapeutic value of one of these genes/proteins at the preclinical level. *GCS* was chosen on the grounds that: (i) displays increased mRNA expression in all cisplatin refractory orthoxenografts and (ii) there are specific inhibitors for GCS available, some of which are currently in clinical use for other pathologies (32, 33). First, NSE testicular germ cell line SuSaS and its paired cisplatin-resistant SuSaR were used as cellular models to corroborate the functional relationship among GCS expression/activity and cisplatin resistance in TGCTs. Significant differences among protein levels of GCS were observed between both cell lines, being more abundant in resistant cells (Fig. 4A, top). Transfected SuSaS cells overexpressing GCS (Fig. 4A, bottom) displayed a significant cisplatin-resistant increase (5-fold; Fig. 4B), while shRNAi knockdown of the endogenous GSC gene (70% of inhibition) in SuSaR cells correlates with a partial (57.6%) cisplatin resensitization (Fig. 4B). Likewise, the treatment of SuSaR cells with the specific GCS inhibitor DL-threo-PDMP (PDMP) mimics this cisplatin sensitization (44.8%; Fig. 4C). Combined cisplatin + PDMP treatment produces a significant increase in the intracellular levels of ceramide (Fig. 4D). Thus, we demonstrated that impaired GCS expression/activity *in vitro* resensitizes a cisplatin-resistant NSE cell line newly to cisplatin treatment.

Interestingly, cisplatin-refractory engrafted tumors exhibited an increase in GCS activity (Fig. 4D). Then, we treated TGT1XR and TGT38XR daily for 21 days with PDMP. As a single-agent, PDMP did not produce a significant response with respect to the vehicle-treated animals, and no significant

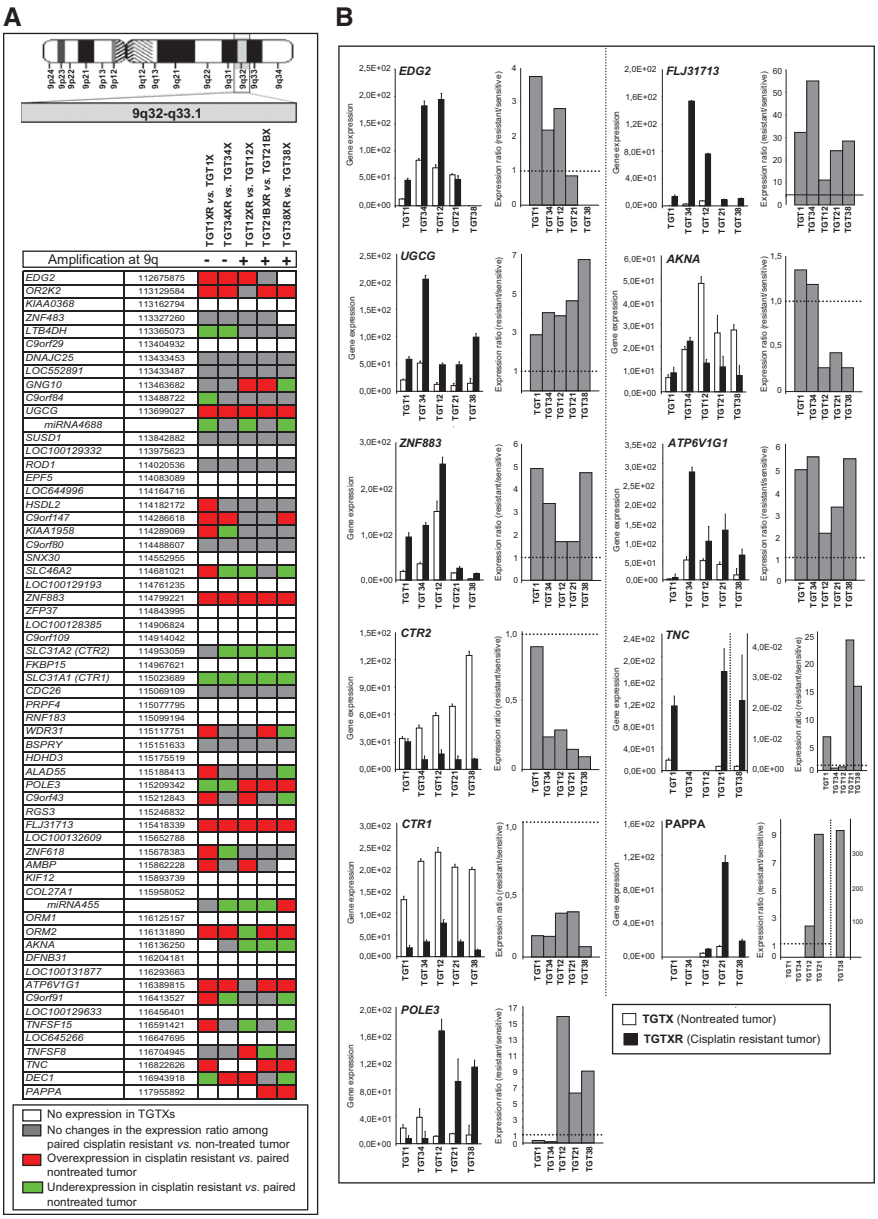

Figure 3.

Differential profiling expression patterns of the 60 genes and two miRNAs annotated on 9q32-q33.1 region determined by qPCR. **A,** Results are presented as changes in the expression levels in cisplatin-refractory tumors relative to the untreated tumors, grouped by 9q32-q33.1 gain status. No expression changes (in gray), underexpression in resistant tumors (in green), overexpression in resistant tumors (in red), and lack of expression in engrafted tumors (in white). **B,** Graphs showing qPCR experiments for relevant genes. For each gene, normalized gene expression (left graph), and the expression ratio among refractory versus sensitive tumors (right graph) are shown. Reactions were performed in triplicate and all data were normalized with endogenous control gene (β-actin).

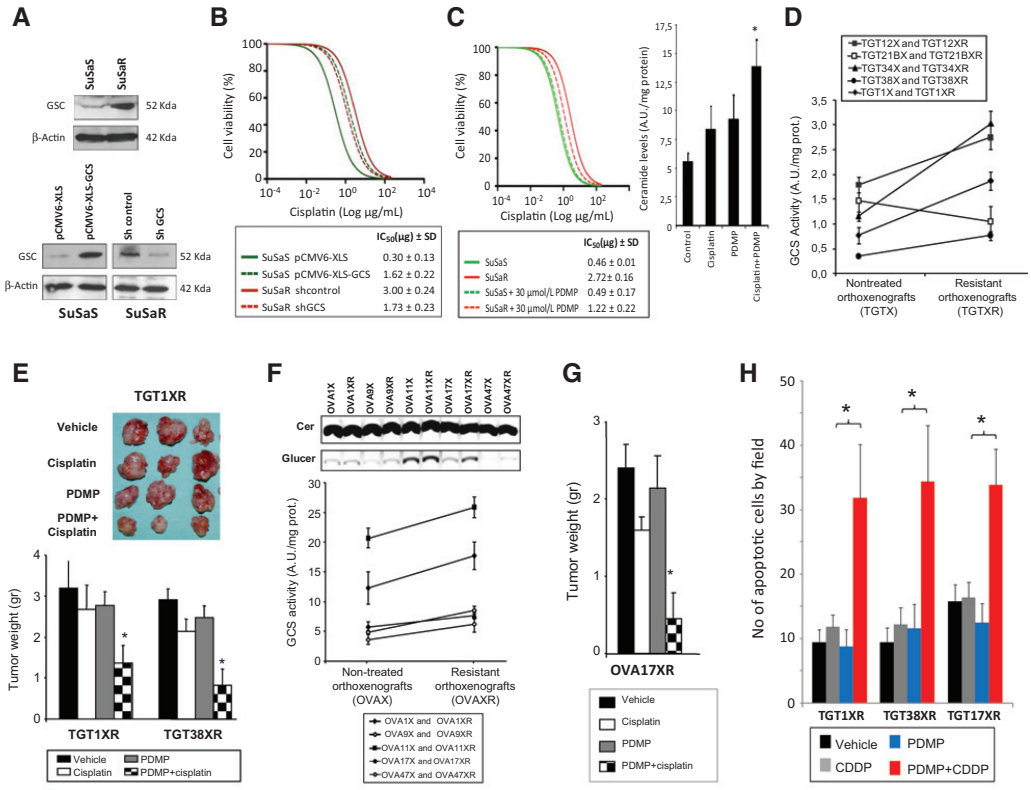

Figure 4.

GCS activity and cisplatin resensitization by DL-threo-PDMP (PDMP) in cisplatin-resistant cell lines and orthoxenografts. **A,** Differential protein expression levels of GCS in SuSaS and paired SuSaR determined by Western blot analysis (left) and GCS transient overexpression in SuSaS cells after transfection with pCMV6-GCS and shRNAi knockdown in SuSaR cells with a mix of four predesigned shRNAs for the human GCS (right). **B,** Cisplatin response of SuSaS cells overexpressing GCS and SuSaR cells with GCS silenced. Each curve represents the average of values from at least three independent experiments and cell proliferation was measured by MTT assay. **C,** Dose–response curves for SuSaS and SuSaR treated with cisplatin and with 30 μmol/L of PDMP [IC_{50} (μmol/L):SuSaS (29.93 ± 0.006)] and SuSaR (28.73 ± 0.054; left). Generation of ceramide was determined in SuSaR cells after treatment with cisplatin, PDMP and for combined cisplatin + PDMP (right). **D,** Activity of GCS in five paired sensitive versus refractory engrafted TGCTs. **E,** Responses of cisplatin-refractory engrafted TGT1XR and TGT38XR tumors to treatment with the GCS inhibitor DL-threo-PMDP. **F,** GCS activity was also determined in six paired sensitive versus refractory orthoxenografts of EOC. Increased levels of glucosylceramide were detected in 5 of 6 resistant cases. **G,** Response of cisplatin-refractory engrafted OVA17XR orthoxenograft (serous tumor) treated with the GCS inhibitor DL-threo-PDMP. **H,** Apoptosis was evaluated by immunostaining of caspase 3 in paraffin sections of residual tumor masses on day 21 of single cisplatin, PDMP, and combined cisplatin + treatments of TGT1XR, TGT38XR, and OVA17XR tumors (22). TGTX, untreated TGCT; TGTXR, cisplatin-refractory TGCT; OVAX, epithelial ovarian tumor; OVAXR, cisplatin-refractory epithelial ovarian tumor (*, $P < 0.05$).

differences were observed among individual PDMP and cisplatin treatments (Fig. 4E). Nevertheless, both tumors experienced significant tumor weight reductions (TGT38XR, 73.5% and TGT1XR, 42.8%) for combined PDMP + cisplatin treatment (Fig. 4E).

Finally, we asked whether the identified association among GCS and cisplatin resistance happens in other tumors commonly treated with cisplatin. Thus, GCS expression/activity was also determined in a panel of five paired cases of sensitive and cisplatin-resistant orthoxenografts of epithelial ovarian cancer (EOC) generated in our lab following the same described approach (22). In 4 of 5 (83.3%) serous tumors, a median increase of 52.5% ± 9.4% GCS activity was observed in the resistant orthoxenografts with respect to its paired sensitive tumors (Fig. 4F). Furthermore, PDMP treatment of OVA17XR, having high levels of GCS activity, has a cisplatin resensitizing effect (Fig. 4G; tumor weight reduction of 76.5% in combined cisplatin + PDMP treatment).

Together, the GCS inhibitor PDMP resensitizes cisplatin-refractory orthoxenografts to cisplatin treatment, providing a promising therapeutic opportunity for treatment of refractory cases; being a strong preclinical rationale for further clinical trials.

PDMP-induced tumor response is mediated by proapoptotic features in germ cell tumors and ovarian cancer

Next, we investigated whether tumor response mechanisms induced by PDMP associated with proapoptotic induction features. Thus, apoptotic drug induction was assessed in TGT1XR, TGT38XR, and OVA17XR by immunodetection in paraffin-embedded tissues of caspase-3, an early and specific apoptotic marker. In the three orthoxenografts, no significant differences for the proapoptotic induced effect were observed for the single treatments with respect to vehicle group (Fig. 4H). Whereas, for combined PDMP + cisplatin treatment, significant increase in the apoptosis levels was observed in the three tumors respect to cisplatin group (TGT1XR 2.7-fold, $P = 0.0016$; TGT38XR 2.81-fold, $P = 0.0011$; and for OVA17XR 2.06-fold, $P = 0.0002$).

Discussion

Establishment of advanced preclinical models of phenocopying patients' primary tumor features in terms of phenotype, genotype, and response to chemotherapy is a basic step on the way to identifying novel therapeutic targets and for testing antitumoral treatments. Here, we report the generation of an important collection of NSE TGCTs engrafted orthotopically in nude mice, keeping features of primary tumors including sensitivity to cisplatin. In our study, we have used five of those original tumors and their corresponding orthoxenografts that developed cisplatin resistance *in vivo*. Our methodology to induce cisplatin-resistant tumors includes exposure to an increasing concentration of cisplatin through five cycles. Such cisplatin treatment does not occur in the clinic, but in our hands was previously very efficient to generate cisplatin-resistant orthotopic tumors derived from EOC (22). Engrafting patient tumor tissues orthotopically into immunodeficient mice (termed "orthoxenografts or PDOX") are state-of-the-art preclinical models that may contribute to reduce the high rate of failure in translating preclinical results to patients. Among the orthoxenografts used in this study, we previously reported TGT1X, TGT38X, and also its paired resistant TGT38XR as tools to support the preclinical value of sunitinib and lapatinib in TGCT treatments (20, 21, 34). Likewise, other orthoxenografts of EOC and lung cancer have been used to evaluate potential patients' treatments (22, 35, 36).

In 1998, Rao and colleagues provided the first evidence of chromosomal amplification associated with cisplatin resistance by comparing unpaired GCTs obtained from relapse-free patients with chemotherapy-resistant tumors (37). Differently, our study compared resistant and sensitive tumors with the same genetic background and we identified fewer recurrent genomic changes across the different refractory tumors. Still, both studies found amplifications in similar regions at chromosomes 9 and 15. Other studies have identified distinct chromosomal imbalances upon cisplatin exposure suggesting that gains and losses of chromosomal regions are genome instability events whose specific influence in cisplatin resistance acquisition needs to be unraveled. Our study suggests that these genomic imbalances do not have a common impact on gene activities but are hotspots to find genes involved in the response to cisplatin. Thus, *GCS* and *CTR*-1/-2 genes are both deregulated in distinct manner (upregulated and downregulated, respectively) in all five resistant tumors independently of the 9q32-q33.1, indicating that these genes are major drivers of resistance to cisplatin and therefore genomic imbalance of their loci would favor tumor grow in presence of cisplatin. However, we still found a modest clinical correlation between the presence of 9q32-q33.1 gains in tumors and a poor risk defined by shorter OS. Here, we demonstrate that the presence of the 9q32-q33.1 amplification is associated with increased risk of progression and death in one of the largest cohort of patients with metastatic GCTs, of whom 32% are truly refractory to cisplatin treatment. Thus, determining the presence of this amplification can be especially helpful in the good/intermediate prognostic groups and may allow clinicians to include them under more aggressive protocols, or to offer alternative drug treatments. Although it is a single retrospective analysis, it is important to highlight its relevance given the difficulty to obtain representative TGCT series that include patients with a poor prognosis, and refractory tumors.

Regarding specific alterations in gene expression, few genes have been associated with cisplatin resistance in TGCT. Thus, low incidence of mutations in *KRAS*, *AKT1*, *PIK3CA*, and *HRAS* were exclusively identified in resistant GCTs cases, while *FGFR3* mutations occurred with equal frequency in both sensitive and resistant cases (14). Controversy exists about the presence of the b-raf (V600E) mutation in some refractory NSE (14, 38). The whole exome sequence of 42 TGCTs (including SE an NSE, but only some were refractory tumors) pointed few recurrent genetic changes identifying mutations in the XRCC2, which is a gene strongly implicated in defining cisplatin resistance (39). Recently, also by exome sequencing, TP53 pathway alterations including MDM2 amplifications have been described exclusively in patients with cisplatin-resistant tumors and they were particularly prevalent among primary mediastinal NSEs (17). Here we point to six genes within the 9q32-q33.1 region, two of them being (*POLE3* and *AKNA*) specifically deregulated in resistant tumors carrying the 9q32-q33.1 gain. POLE3 is a subunit of the DNA polymerase epsilon that binds DNA in a sequence-independent manner and is part of the CHRAC chromatic-remodeling complex (40). *AKNA* encodes an AT-hook transcription factor (41). The role of these two DNA-binding proteins in response to cisplatin should be studied in the future, but its distinct deregulation in cisplatin-refractory tumors (*POLE3* is upregulated, whereas *AKNA* is downregulated) indicate that their mechanisms of action in response to cisplatin exposure may be different. One explanation for the distinct types of deregulation of genes in 9q32-q33.1 is the frequent amplification of one parental chromosome (of part of it) with loss of the other parental chromosome that led to loss-of-heterozygosity (LOH) in GCTs, but not in other tumor types (42).

Other four genes displayed a deregulated expression in cisplatin-resistant orthoxenografts but such deregulation was not associated with the presence of the 9q32-q33.1 gain. One of them is CTR1, which encodes a copper transporter that has previously been associated to cellular mechanisms of resistance to cisplatin (33, 34). ZNF883 encodes a zinc finger protein that may be involved in transcriptional regulation and FLJ31713 is an uncharacterized protein. Finally, we experimentally confirmed the fourth gene, the *GCS*, as a target to resensitize tumors refractory to cisplatin.

Targeting GCS, due to its central role in the glycosphingolipid synthesis pathway, has emerged as a novel approach for treating metabolic diseases such as Gaucher, Niemann–Pick, and diabetes. In this context, several GCS inhibitors are in

clinical use or under development, including miglustat, PDMP, and EXEL-0346 among others (43–45). Recently, it has been reported that GCS inhibition improved sorafenib effectiveness *in vitro* and *in vivo* in experimental hepatocellular carcinoma, recovering drug sensitivity of sorafenib-resistant tumors in mice (46). Thus, the therapeutic value of GCS inhibitors as tool to resensitize cell to drugs may not be only restricted to cisplatin.

We have demonstrated the relevance of GCS activity as a biologic mechanism that mediates tumor cell protection against cisplatin exposure, and they denoted the significance of sphingolipid metabolism through cisplatin-induced tumor cell death. Thus, we hypothesize that PDMP or other GCS inhibitors, blocking the conversion of ceramide to glucosylceramide, should open an important therapeutic window in patients with refractory tumors by exploring the influence of ceramide pools in cisplatin-induced cell-death. Our preclinical results in advanced refractory cisplatin orthoxenografts of both GCTs and EOCs tumor models demonstrate that PDMP resensitizes to cisplatin treatment, providing a firm preclinical rationale of drug repositioning and for developing further clinical trials in the field. Interestingly, the association among GCS activity and cisplatin resistance has recently been reported also for head and neck cancer (47), pointing to a broader usage of GCS inhibitors to treat tumors refractory to cisplatin. Given the rather unspecific mechanisms of action of cisplatin, we believe that strategies to resensitize cisplatin-resistant TGCT orthoxenografts may help to improve the treatment of other tumors types that are unsuccessfully treated with cisplatin (8).

In summary, we report the generation of cisplatin-refractory orthoxenografts of germ cell tumors as preclinical models and demonstrate that this preclinical platform have a great potential to better design future trials for the treatment of patients with cisplatin-resistant/refractory tumors.

Disclosure of Potential Conflicts of Interest

A. Vidal has ownership interests (including patents) at Xenopat S.L. L. Padulles is an employee of Almirall SA. A. Villanueva has ownership interests (including patents) at Xenopat S.L. No potential conflicts of interest were disclosed by the other authors.

Authors' Contributions

Conception and design: J.M. Piulats, A. Vidal, M. Nadal, J.R. Germà, X. García-del-Muro, J. Cerón, A. Villanueva

Development of methodology: J.M. Piulats, A. Vidal, F.J. García-Rodríguez, M. Nadal, À. Aytés, S. Puertas, W. Castillo, P. Muñoz, M. Esteller, G. Capella, L. Farré, J. Cerón, A. Villanueva

Acquisition of data (provided animals, acquired and managed patients, provided facilities, etc.): J.M. Piulats, A. Vidal, C. Muñoz, M. Martínez-Iniesta, L. Padullés, M. Juliachs, V. Moreno, M. Stefanovic, E. Condom, M. Esteller, J.R. Germà, G. Capella, L. Farré, A. Morales, X. García-del-Muro, A. Villanueva

Analysis and interpretation of data (e.g., statistical analysis, biostatistics, computational analysis): J.M. Piulats, A. Vidal, F.J. García-Rodríguez, C. Muñoz, M. Nadal, C. Moutinho, A. Figueras, V. Moreno, M.A. Pujana, J.R. Germà, L. Farré, A. Morales, A. Villanueva

Writing, review, and/or revision of the manuscript: J.M. Piulats, A. Vidal, F.J. García-Rodríguez, C. Moutinho, D.G. Molleví, V. Moreno, J.R. Germà, L. Farré, F. Viñals, X. García-del-Muro, J. Cerón, A. Villanueva

Administrative, technical, or material support (i.e., reporting or organizing data, constructing databases): J.M. Piulats, A. Vidal, M. Martínez-Iniesta, L. Farré

Study supervision: J.M. Piulats, A. Vidal, J.R. Germà, X. García-del-Muro, J. Cerón, A. Villanueva

Acknowledgments

Several authors are grateful recipients of predoctoral fellowships: J.M. Piulats from the AECC and F.J. García-Rodríguez from the Instituto de Salud Carlos III (ISCIII). This study was supported by grants from the Spanish Ministry of Economy and Competitiveness (SAF2002-02265 and FIS: BFU2007-67123; PI10-0222, PI13-01339, and PI16/01898, to A. Villanueva; PI15-00895, to J. Cerón; SAF2013-46063R, to F. Viñals; PI030264, to X. García-del-Muro), Fundació La Marató TV3 (051430, to F. Viñals and X. García-del-Muro), Generalitat de Catalunya (2014SGR364, to A. Villanueva and F. Viñals; FIS09/0059, to A. Morales), cofunded by FEDER funds/European Regional Development Fund (ERDF) — a way to Build Europe. A. Villanueva received a BAE11/00073 grant. We thank the staff of the Animal Core Facility of IDIBELL for mouse care and maintenance.

The costs of publication of this article were defrayed in part by the payment of page charges. This article must therefore be hereby marked *advertisement* in accordance with 18 U.S.C. Section 1734 solely to indicate this fact.

Received July 5, 2017; revised November 22, 2017; accepted March 23, 2018; published first April 4, 2018.

References

1. Bray F, Ferlay J, Devesa SS, McGlynn KA, Møller H. Interpreting the international trends in testicular seminoma and nonseminoma incidence. Nat Clin Pract Urol 2006;3:532–43.
2. Ferlay J, Soerjomataram I, Dikshit R, Eser S, Mathers C, Rebelo M, et al. Cancer incidence and mortality worldwide: sources, methods and major patterns in GLOBOCAN 2012. Int J Cancer 2015;136:E359–86.
3. Ruf CG, Isbarn H, Wagner W, Fisch M, Matthies C, Dieckmann K-P. Changes in epidemiologic features of testicular germ cell cancer: age at diagnosis and relative frequency of seminoma are constantly and significantly increasing. Urol Oncol 2014;32:33.e1–6.
4. Beyer J, Albers P, Altena R, Aparicio J, Bokemeyer C, Busch J, et al. Maintaining success, reducing treatment burden, focusing on survivorship: highlights from the third European consensus conference on diagnosis and treatment of germ-cell cancer. Ann Oncol 2013;24:878–88.
5. Funt SA, Feldman DR, Bosl GJ. The management of advanced germ cell tumors in 2016: the Memorial Sloan Kettering approach. Oncology 2016;30:653–64.
6. Lorch A, Neubauer A, Hackenthal M, Dieing A, Hartmann JT, Rick O, et al. High-dose chemotherapy (HDCT) as second-salvage treatment in patients with multiple relapsed or refractory germ-cell tumors. Ann Oncol 2010;21:820–5.
7. Kollmannsberger C, Nichols C, Bokemeyer C. Recent advances in management of patients with platinum-refractory testicular germ cell tumors. Cancer 2006;106:1217–26.
8. Varmus H, Harlow E. Science funding: provocative questions in cancer research. Nature 2012;481:436–7.
9. Koychev D, Oechsle K, Bokemeyer C, Honecker F. Treatment of patients with relapsed and/or cisplatin-refractory metastatic germ cell tumours: an update. Int J Androl 2011;34:e266–73.
10. Houldsworth J, Korkola JE, Bosl GJ, Chaganti RS. Biology and genetics of adult male germ cell tumors. J Clin Oncol 2006;24:5512–8.
11. Galluzzi L, Vitale I, Michels J, Brenner C, Szabadkai G, Harel-Bellan A, et al. Systems biology of cisplatin resistance: past, present and future. Cell Death Dis 2014;5:e1257.
12. Shen D-W, Pouliot LM, Hall MD, Gottesman MM. Cisplatin resistance: a cellular self-defense mechanism resulting from multiple epigenetic and genetic changes. Pharmacol Rev 2012;64:706–21.
13. Honecker F, Wermann H, Mayer F, Gillis AJ, Stoop H, Van Gurp RJ, et al. Microsatellite instability, mismatch repair deficiency, and BRAF

mutation in treatment-resistant germ cell tumors. J Clin Oncol 2009;27:2129–36.
14. Feldman DR, Iyer G, Van Alstine L, Patil S, Al-Ahmadie H, Reuter VE, et al. Presence of somatic mutations within PIK3CA, AKT, RAS, and FGFR3 but not BRAF in cisplatin-resistant germ cell tumors. Clin Cancer Res 2014;20:3712–20.
15. Juliachs M, Muñoz C, Moutinho CA, Vidal A, Condom E, Esteller M, et al. The PDGFRβ-AKT pathway contributes to CDDP-acquired resistance in testicular germ cell tumors. Clin Cancer Res 2014;20:658–67.
16. Koster R, van Vugt MA, Timmer-Bosscha H, Gietema JA, de Jong S. Unravelling mechanisms of cisplatin sensitivity and resistance in testicular cancer. Expert Rev Mol Med 2013;15:e12.
17. Bagrodia A, Lee BH, Lee W, Cha EK, Sfakianos JP, Iyer G, et al. Genetic determinants of cisplatin resistance in patients with advanced germ cell tumors. J Clin Oncol 2016;34:4000–7.
18. Hidalgo M, Amant F, Biankin AV, Budinská E, Byrne AT, Caldas C, et al. Patient-derived xenograft models: an emerging platform for translational cancer research. Cancer Discov 2014;4:998–1013.
19. Byrne AT, Alférez DG, Amant F, Annibali D, Arribas J, Biankin AV, et al. Interrogating open issues in cancer precision medicine with patient-derived xenografts. Nat Rev Cancer 2017;17:254–68.
20. Juliachs M, Castillo-Ávila W, Vidal A, Piulats JM, Garcia Del Muro X, Condom E, et al. ErbBs inhibition by lapatinib blocks tumor growth in an orthotopic model of human testicular germ cell tumor. Int J Cancer 2013;133:235–46.
21. Castillo-Avila W, Piulats JM, Garcia Del Muro X, Vidal A, Condom E, Casanovas O, et al. Sunitinib inhibits tumor growth and synergizes with cisplatin in orthotopic models of cisplatin-sensitive and cisplatin-resistant human testicular germ cell tumors. Clin Cancer Res 2009;15:3384–95.
22. Vidal A, Muñoz C, Guillen M, Moreto J, Puertas S, Martinez-Iniesta M, et al. Lurbinectedin (PM01183), a New DNA minor groove binder, inhibits growth of orthotopic primary graft of cisplatin- resistant epithelial ovarian cancer. Clin Cancer Res 2012;18:5399–411.
23. Selzer RR, Richmond TA, Pofahl NJ, Green RD, Eis PS, Nair P, et al. Analysis of chromosome breakpoints in neuroblastoma at sub-kilobase resolution using fine-tiling oligonucleotide array CGH. Genes Chromosomes Cancer 2005;44:305–19.
24. Grande L, Bretones G, Rosa-Garrido M, Garrido-Martin EM, Hernandez T, Fraile S, et al. Transcription factors Sp1 and p73 control the expression of the proapoptotic protein NOXA in the response of testicular embryonal carcinoma cells to cisplatin. J Biol Chem 2012;287:26495–505.
25. Hogan B, Fellous M, Avner P, Jacob F. Isolation of a human teratoma cell line which expresses F9 antigen. Nature 1977;270:515–8.
26. Morales A, París R, Villanueva A, Llacuna L, García-Ruiz C, Fernández-Checa JC. Pharmacological inhibition or small interfering RNA targeting acid ceramidase sensitizes hepatoma cells to chemotherapy and reduces tumor growth *in vivo*. Oncogene 2007;26:905–16.
27. Fléchon A, Culine S, Théodore C, Droz J-P. Pattern of relapse after first line treatment of advanced stage germ-cell tumors. Eur Urol 2005;48:957–64.
28. Albers P, Albrecht W, Algaba F, Bokemeyer C, Cohn-Cedermark G, Horwich A, et al. Guidelines on testicular cancer. Eur Urol 2005;48:885–94.
29. Lemaire MA, Schwartz A, Rahmouni AR, Leng M. Interstrand cross-links are preferentially formed at the d(GC) sites in the reaction between cis-diamminedichloroplatinum (II) and DNA. Proc Natl Acad Sci U S A 1991;88:1982–5.
30. Szklarczyk D, Morris JH, Cook H, Kuhn M, Wyder S, Simonovic M, et al. The STRING database in 2017: quality-controlled protein–protein association networks, made broadly accessible. Nucleic Acids Res 2017;45:D362–9.
31. Hemmingsson O, Kao G, Still M, Naredi P. ASNA-1 activity modulates sensitivity to cisplatin. Cancer Res 2010;70:10321–8.
32. Patterson MC, Vecchio D, Prady H, Abel L, Wraith JE. Miglustat for treatment of Niemann-Pick C disease: a randomised controlled study. Lancet Neurol 2007;6:765–72.
33. Bennett LL, Mohan D. Gaucher disease and its treatment options. Ann Pharmacother 2013;47:1182–93.
34. Juliachs M, Vidal A, Garcia Del Muro X, Piulats JM, Condom E, Casanovas O, et al. Effectivity of pazopanib treatment in orthotopic models of human testicular germ cell tumors. BMC Cancer 2013;13:382.
35. Alsina-Sanchis E, Figueras A, Lahiguera Á, Vidal A, Casanovas O, Graupera M, et al. The TGFβ pathway stimulates ovarian cancer cell proliferation by increasing IGF1R levels. Int J Cancer 2016;139:1894–903.
36. Ambrogio C, Gómez-López G, Falcone M, Vidal A, Nadal E, Crosetto N, et al. Combined inhibition of DDR1 and Notch signaling is a therapeutic strategy for KRAS-driven lung adenocarcinoma. Nat Med 2016;22:270–7.
37. Rao PH, Houldsworth J, Palanisamy N, Murty VV, Reuter VE, Motzer RJ, et al. Chromosomal amplification is associated with cisplatin resistance of human male germ cell tumors. Cancer Res 1998;58:4260–3.
38. Honecker F, Wermann H, Mayer F, Gillis AJ, Stoop H, van Gurp RJ, et al. Microsatellite instability, mismatch repair deficiency, and BRAF mutation in treatment-resistant germ cell tumors. J Clin Oncol 2009;27:2129–36.
39. Litchfield K, Levy M, Huddart RA, Shipley J, Turnbull C. The genomic landscape of testicular germ cell tumours: from susceptibility to treatment. Nat Rev Urol 2016;13:409–19.
40. Kukimoto I, Elderkin S, Grimaldi M, Oelgeschlä T, Varga-Weisz PD. The histone-fold protein complex CHRAC-15/17 enhances nucleosome sliding and assembly mediated by ACF. Mol Cell 2004;13:265–77.
41. Siddiqa A, Sims-Mourtada JC, Guzman-Rojas L, Rangel R, Guret C, Madrid-Marina V, et al. Regulation of CD40 and CD40 ligand by the AT-hook transcription factor AKNA. Nature 2001;410:383–7.
42. Taylor-Weiner A, Zack T, O 'donnell E, Guerriero JL, Bernard B, Reddy A, et al. Genomic evolution and chemoresistance in germ-cell tumours. Nature 2016;540:114–8.
43. Richards S, Larson CJ, Koltun ES, Hanel A, Chan V, Nachtigall J, et al. Discovery and characterization of an inhibitor of glucosylceramide synthase. J Med Chem 2012;55:4322–35.
44. Huang W-C, Tsai C-C, Chen C-L, Chen T-Y, Chen Y-P, Lin Y-S, et al. Glucosylceramide synthase inhibitor PDMP sensitizes chronic myeloid leukemia T315I mutant to Bcr-Abl inhibitor and cooperatively induces glycogen synthase kinase-3-regulated apoptosis. FASEB J 2011;25:3661–73.
45. Yu T, Li J, Qiu Y, Sun H. 1-Phenyl-2-decanoylamino-3-morpholino-1-propanol (PDMP) facilitates curcumin-induced melanoma cell apoptosis by enhancing ceramide accumulation, JNK activation, and inhibiting PI3K/AKT activation. Mol Cell Biochem 2012;361:47–54.
46. Stefanovic M, Tutusaus A, Martinez-Nieto GA, Bárcena C, de Gregorio E, Moutinho C, et al. Targeting glucosylceramide synthase upregulation reverts sorafenib resistance in experimental hepatocellular carcinoma. Oncotarget 2016;7:8253–67.
47. Roh J-L, Kim EH, Park JY, Kim JW. Inhibition of glucosylceramide synthase sensitizes head and neck cancer to cisplatin. Mol Cancer Ther 2015;14:1907–15.

SUPPLEMENTARY DATA

Orthoxenografts of testicular germ cell tumors uncover genomic changes associated to cisplatin resistance and identify PDMP as a re-sensitizing agent

Josep M. Piulats [1,2&], August Vidal [3,12&], Francisco J García-Rodríguez [1], Clara Muñoz [1], Marga Nadal [1], Catia Moutinho [4], María Martínez-Iniesta [1], Josefina Mora [5], Agnés Figueras [1], Elisabet Guinó [6], Laura Padullés [1], Àlvaro Aytés [1], David G. Molleví [1], Sara Puertas [1], Carmen Martínez-Fernández[8], Wilmar Castillo [1], Merce Juliachs [1], Victor Moreno [6], Purificación Muñoz [4], Milica Stefanovic [7], Miguel A. Pujana [1], Enric Condom [3], Manel Esteller [4], Josep R. Germà [2], Gabriel Capella [1], Lourdes Farré [1,10], Albert Morales [7], Francesc Viñals [1,9], Xavier García-del-Muro [2], Julián Cerón [8,11] and Alberto Villanueva [1,11,12].

1. Program Against Cancer Therapeutic Resistance (ProCURE), Catalan Institute of Oncology (ICO), Bellvitge Institute for Biomedical Research (IDIBELL), L'Hospitalet del Llobregat, Barcelona 08908, Catalonia, Spain.
2. Department of Medical Oncology, Catalan Institute of Oncology – IDIBELL.
3. Department of Pathology, Hospital Universitari de Bellvitge – IDIBELL. CIBERONC.
4. Cancer Epigenetics and Cell Biology Program (PEBC), Catalan Institute of Oncology –IDIBELL
5. Department of Biochemistry, Hospital de Sant Pau, 08025 Barcelona, Spain.
6. Bioinformatic Unit, Catalan Institute of Oncology – IDIBELL.
7. Department of Cell Death and Proliferation, Instituto de Investigaciones Biomédicas de Barcelona (IIBB-CSIC), IDIBAPS, Barcelona, Catalonia, Spain.
8. Modelling Human Diseases in *C. elegans*. Genes, Disease and Therapy Program – IDIBELL.
9. Departament de Ciències Fisiològiques II, Universitat de Barcelona, Avda Feixa Llarga S/N 08907 L'Hospitalet de Llobregat, Barcelona, Spain.
10. Laboratory of Experimental Pathology (LAPEX), Gonçalo Moniz Research Center, Oswaldo Cruz Foundation (CPQGM/FIOCRUZ), Salvador, Bahia, Brazil; National Institute of Science and Technology of Tropical Diseases (INCT/DT), Salvador, Brazil.
11. *C. elegans* Core Facilty-IDIBELL.
12. Xenopat S.L., Business Bioincubator, Bellvitge Health Science Campus, 08907 L'Hospitalet de Llobregat, Barcelona, Spain.

SUPPLEMENTARY METHODS

Generation process of orthoxenografts of testicular germ cell tumors in nude mice

Primary tumor samples were obtained after surgical resection at Hospital Universitari de Bellvitge, Barcelona (Spain) and placed at room temperature in DMEM medium supplemented with 10% fetal bovine serum and penicillin/streptomycin. Fresh surgical specimens of human GCTs were implanted in nude mice. Animals were housed in a

sterile environment, cages and water were autoclaved and bedding and food was γ-ray sterilized. Tumors were implanted in the testis of five-week old male *nu/nu Swiss mice* (Charles River, France) weighting 18-22 g. After anesthesia by isofluorane inhalation, a median laparatomy was performed and the testes were mobilized. Tumor pieces were anchored to the testis surface with prolene 7.0 sutures. After implantation, mice were inspected twice a week, and if no tumor growth was apparent, mice were sacrificed six months after implantation. Serial tumor passaging was performed in two to five animals. Time lags varied for each tumor, depending upon their growth kinetics (**Table S1**). Four orthoxenografts were derived from patients previously treated with cisplatin-based chemotherapy.

Immunohistochemistry characterization of xenografted tumors

Tissues taken for histological studies were fixed in 10% buffered formalin and 3-µm slices of paraffin-embedded tissues were used for immunohistochemistry (IHQ) studies. Monoclonal primary antibody for OCT3/4 was diluted 1:300 (Santa Cruz) Reactions were visualized using the EnVision anti-mouse antibody system, and developed using the DAB-Plus Kit (Dako, Copenhagen, Denmark). Slides were counterstained with Harry's modified hematoxylin.

Determination of mouse serum levels of tumor markers

Serum concentrations of alpha-fetoprotein (AFP) and the β-subunit of human chorionic gonadotropin (β-hCG) concentrations were measured as subrogate tumor growth markers in the serum of nude mice using commercially available two-site enzyme chemiluminometric assays automated on the Immulite® 2000 analyzer (1,2).

Primary response of engrafted NSEs to cisplatin treatments

Small fragments of engrafted tumors were reimplanted in the testicles of 30 nude mice, as described above. When palpable intra-abdominal masses and increased levels of serum tumor marks had both been detected, usually 7–30 days after implantation, mice were randomized into three groups: (i) control group (n = 10), treated with vehicle; (ii) low-dose treatment group (n = 20) (2 mg/kg of cisplatin); and (iii) high-dose treatment group (n = 20) (5 mg/kg of cisplatin). Each treatment group was randomly divided into a *short-term response group* (n = 10), defined by tumor weight at the time of sacrifice of the control group, and a *long-term response group* (n = 10), defined by recurrent tumor mass regrowth post-chemotherapy. Cisplatin was intravenously administered (i.v.) once a week for three consecutive weeks (days 0, 7 and 14). Animals were sacrificed seven days after the final dose (day 21) to examine their short-term response.

Genetic characterization of engrafted NSE tumors

DNA was extracted following standard phenol-chloroform protocols, while total RNA was extracted using TRIZOL reagent following the manufacturers' instructions (Invitrogen). Nude mouse tissues were included in all PCR experiments to avoid mouse DNA and RNA contamination.

Mutations in *TP53* (exons 4-10); K-*ras* (codon 12 and 13), *b-raf* (exons 11 and 15), *EGFR* (exons 18, 19, 20 and 21), c-*Kit* (exons 9, 11, 13 and 17), *PDGFRα* (exons 12 and 14), *PDGFRβ* (exon 12) and *PI3KCA* (exons 9 and 20) were analyzed. All exons were amplified in independent PCR reactions using human intronic primers to avoid amplification of mouse DNA. PCR reactions were carried out using 100-200 ng of genomic DNA in a mixture containing PCR buffer, 100 mM deoxynucleotide

triphosphates, 0.5 μM of each primer and 1 unit of Taq DNA polymerase (Invitrogen). RNA was reverse-transcribed to cDNA using pd$(N)_6$ and the M-MLV retrotranscriptase kit (Invitrogen) and the entire coding *Smad*4 region was analyzed in five overlapping reactions. Primer sequences and PCR conditions are available on request. The presence of gene mutations was detected by direct sequence and/or single-strand chain polymorphism (SSCP). Homozygous deletions or microdeletions in *p15*, *p16* and *Smad4* were evaluated in agarose gels and were defined by the absence of PCR product in three independent experiments.

Genetic instability (MSI) was analyzed using Bethesda's set of five microsatellite markers (D2S123, BAT25, BAT26, D5S346 and BAT40).

FISH analysis

FISH was done by standard methods. We used the UCSC genome browser to select three bacterial artificial chromosomes (BACs) from the K32 BAC library (kindly provided by Dr L. Pérez-Jurado). BAC RP11-582I20 is contained in the amplified 9q32-9q33.1 region while RP11-616C16 flanks it at its distal end. FISH results were analyzed under an Olympus BX60 microscope and images were captured with a Cytovision (Applied Imaging) workstation. One hundred non-overlapping nuclei were scored for each sample.

Quantification of gene and miRNA expression

Total RNA was extracted using Trizol (Invitrogen, San Diego, CA), following the manufacturer's instructions, and reverse-transcribed to cDNA. Quantitative RNA and miRNA analyses was performed as described. Quantitative real-time RT-PCR analyses

were performed using the Light-Cycler 2.0 Roche System and LightCycler FastStart DNA Master SyBR Green I kit (Roche). All the primers were designed specifically to amplify human RNA. Primer sequences and PCR conditions are available on request. Experiments were performed in triplicate using three independent RT reactions. Gene expression was normalized with respect to β-actin.

For miRNA, RNA samples were DNase-treated with Turbo DNA-free (Ambion, Austin, TX), and determined as described (3). Reactions were performed in triplicate and incubated in an Applied Biosystems 7900HT Fast Real-Time PCR system in 384-well plates. All data were normalized with endogenous controls: PPIA, HPRT1 and RPLPO. The relative miRNA levels were calculated using the formula $2^{-\Delta\Delta Ct}$ (4).

C. elegans RNAi and cisplatin-response assays

The *C. elegans* N2 strain (wild type), and the *rrf-3 (pk1436)* and *cgt-1 (ok1045)* mutant strains were provided by the Caenorhabditis Genetic Centre (CGC). The bacterial RNAi clones used were obtained from the ORFeome-based RNAi library (5) or the JA library (6). For adult survival assays, RNAi by feeding was performed on synchronized worms (7) that were cultured in NGM plates containing 50 µg/ml ampicillin, 12.5 µg/ml Tetracycline and 3 mM IPTG. Then, at the young-adult stage, animals were transferred to a 96-well plate. Each well contained S-medium with the corresponding RNAi clone plus 50µg/ml ampicillin, 12.5 µg/ml Tetracycline 3 mM IPTG. Cisplatin (Sigma 15663-27-1) dissolved in water was added to each well to reach the indicated concentration. Lethality was scored as absence of movement that was recorded by an automated tracking system (wmicrotracker) that registers numbers of bins per hour (8). Cisplatin-induced toxicity was evaluated by measuring worm locomotor activity over a 24-h

period. All assays were performed at 20ºC, tracking 20 worms per well each time in each of four replicates.

SUPPLEMENTARY BIBLIOGRAPHY

1. Mora J, Gascón N, Tabernero JM, Germà JR, González F. Alpha-fetoprotein-concanavalin A binding as a marker to discriminate between germ cell tumours and liver diseases. Eur J Cancer. 1995;31A:2239–42.
2. Mora J, Gascón N, Tabernero JM, Rodríguez-Espinosa J, González-Sastre F. Different hCG assays to measure ectopic hCG secretion in bladder carcinoma patients. Br J Cancer. 1996;74:1081–4.
3. Davalos V, Moutinho C, Villanueva A, Boque R, Silva P, Carneiro F, et al. Dynamic epigenetic regulation of the microRNA-200 family mediates epithelial and mesenchymal transitions in human tumorigenesis. Oncogene. 2012;31:2062–74.
4. Livak KJ, Schmittgen TD. Analysis of relative gene expression data using real-time quantitative PCR and the 2(-Delta Delta C(T)) Method. Methods. 2001;25:402–8.
5. Rual J-F, Ceron J, Koreth J, Hao T, Nicot A-S, Hirozane-Kishikawa T, et al. Toward improving Caenorhabditis elegans phenome mapping with an ORFeome-based RNAi library. Genome Res. 2004;14:2162–8.
6. Kamath RS, Fraser AG, Dong Y, Poulin G, Durbin R, Gotta M, et al. Systematic functional analysis of the Caenorhabditis elegans genome using RNAi. Nature. 2003;421:231–7.
7. Porta-de-la-Riva M, Fontrodona L, Villanueva A, Cerón J. Basic Caenorhabditis elegans methods: synchronization and observation. J Vis Exp [Internet]. 2012 [cited 2017 Nov 15];e4019. Available from: http://www.jove.com/video/4019/

8. Simonetta SH, Golombek DA. An automated tracking system for Caenorhabditis elegans locomotor behavior and circadian studies application. J Neurosci Methods. 2007;161:273–80.

9. Szklarczyk D, Morris JH, Cook H, Kuhn M, Wyder S, Simonovic M, et al. The STRING database in 2017: quality-controlled protein–protein association networks, made broadly accessible. Nucleic Acids Res. 2017;45:D362–9.

Supplementary Table S1 Summary of characteristics of primary nonseminoma (NSE) tumors growing as xenografts in nude mice.

Human Primary Tumor					Orthoxenografts						
Primary tumor location	**Tumor**	**Histology** [a]	**Stage** [b]	**Patient's response to CDDP**	**Patient's CDDP treatment previous to biopsy**	**Histology**	**Xenograft perpetuated** [c]		**Time-lag between passages (days)** [d]	**Mouse serum markers** [e]	**Pattern of distal dissemination** [f]
							Orthotopic growth	**Subcutaneous growth**			
Testicle	**TGT1X** [J]	YS	Stage I	Not treated	No	YS	Yes	No	69 ± 17	AFP	Lung [g, h1]
	TGT11X	YS, EC, CH, TE	Stage I	Not treated	No	YS, EC, CH	Yes	No	ND	ND	ND
	TGT12X	EC	Good risk	Sensitive	No	EC	Yes	No	97 ± 25	β-hCG, AFP	None
	TGT14X	EC SE	Stage I	Not treated	No	EC	Yes	No	56 ± 17	β-hCG	Peritoneal implants [j, h2] Lymph node affection [j, h4]
	TGT21AX	YS, EC, CH, TE, SE	Stage I	Not treated	No	YS, EC, CH	Yes	Yes	49 ± 11	β-hCG, AFP	None
	TGT21BX	YS, EC, CH, TE, SE	Stage I	Not treated	No	YS, EC, CH	Yes	Yes	64 ± 14	β-hCG, AFP	None
	TGT34X	EC	Poor risk	Sensitive	No	EC	Yes	No	51 ± 8	β-hCG, AFP	Lymph node affection [j,h4]
	TGT38X [k]	CH	Poor risk	Sensitive	No	CH	Yes	No	20 ± 6	β-hCG	Lung [g, h1]
	TGT40X	YS, TE	Stage I	Not treated	No	YS	Yes	No	42 ± 8	AFP	None
Lymph node	TGT39X	YS, EC, TE	Poor risk	Sensitive	No	YS, EC	Yes	No	59 ± 13	β-hCG, AFP	Liver [j, h3] Peritoneal implants [g,h2]
	TGT41X	CH	Poor risk	Refractory	Yes	CH	Yes	No	18 ± 4	β-hCG	ND
	TGT44X [k]	YS, TE	Poor risk	Refractory	Yes	YS	Yes	No	50 ± 8	AFP	ND
Lung metastasis	TGT17X [k]	CH	Poor risk	Refractory	Yes	CH	Yes	No	24 ± 5	β-hCG	Lung [g ,h1]
Brain metastasis	TGT42X	EC	Poor risk	Refractory	Yes	EC	Yes	No	62 ± 10	β-hCG, AFP	ND

[a] Tumor histology: YS, yolk sac; EC, embryonal carcinoma; CH, choriocarcinoma; TE, teratoma; SE, seminoma.
[b] Stage at first diagnosis (Tumor localized in testicle referred as stage I; Stage II to IV classified following the International Germ Cell Cancer Collaborative Group (IGCCCG) classification).
[c] Primary tumor was simultaneously implanted in the testicles and subcutaneous tissues of nude mice. The tumor was considered perpetuated after at least six consecutive passages in nude mice.
[d] Time-lag between passages was calculated on the basis of the first six passages, for a median of 15 mice implanted with each tumor.
[e] Levels of alpha-fetoprotein (AFP) and/or β-subunit of human chorionic gonadotropin (β-hCG) were analyzed as tumor growth markers in the nude mouse serum.
[f] Presence of peritoneal implants has not been described in patients with TGCTs and probably their presence in some animals is a consequence of the methodology used in the implantation of tumors in mouse.
[g] Synchronous lung micrometastases were detected when nude mice were sacrificed.
[j] Liver macrometastases, peritoneal implants and lymph node affection were observed when nude mice were sacrificed.
[h] Orchiectomy was performed to confirm the dissemination patterns when palpable intra-abdominal masses were detected in 5 to 10 mice for each tumor. Animals were sacrificed 6-8 months after surgery, or when they lost weight: [h1], metachronic lung metastasis; [h2], metachronic peritoneal implants; [h3], metachronic liver metastases; [h4], metachronic lymph node.
[k] Xenografted tumors TGT38X and TGT44X characteristics were previously described [20,21,32].
None, absence of metastasis; ND, not determined.
Tumors used in this study are labeled in bold

Supplementary Table S2. Clinicopathological characteristics of patients, by response to cisplatin.

Characteristic	Sensitive (N = 51)		Resistant (N = 24)	
	No.	%	No.	%
Age, years				
Median	27.9		28.1	
Range	(16 – 56)		(15 - 53)	
Histology				
Seminoma	10	19.6	2	8.3
Nonseminoma	41	80.4	22	91.7
Localization				
Testis	51	100	20	83.3
Mediastinum	0	0	4	16.7
IGCCCG stage at diagnosis of metastasis [a]				
Good	38	74.5	7	29.2
Intermediate	7	13.7	7	29.2
Poor	6	11.8	10	41.7
First line of chemotherapy treatment [b]				
EP	9	17.6	2	8.3
BEP	33	64.7	12	50.0
Taxol-BEP	2	3.9	1	4.2
BOMP/EPI	7	13.7	9	37.5
Response to first line of chemotherapy treatment [c]				
Good response (CR, PR-)	51	100	16	66.7
Poor response (PR+, SD, PD)	0	0	8	33.3
Late relapse[d]				
Non	0		22	91.7
Yes	0		2	8.3

[a] IGCCCG International Germ Cell Cancer Collaborative Group.

[b] EP, etoposide/cisplatin; BEP, bleomycin/etoposide/cisplatin; BOMP/EPI, bleomycin/vincristine/methotrexate/ cisplatin-etoposide/cisplatin/ifosfamide.

[c] CR, complete remission characterized by tumor mass reduction by CT scan and negative valor of serum tumor marks; PR-, partial remission characterized by normalization of CT scan and negative valor of serum tumor markers; PR+, partial remission characterized by reduction of tumor mass by CT scan and positive valor of serum tumor markers; SD, stable disease; PD, progressive disease).

[d] Relapse >24 months after first diagnosis.

Supplementary Table S3. Tumors with amplification at 9q32-q33.1 in metastatic GCTs.

Patient	Histology [a]	Status of 9q32-q33.1 [b]	Cisplatin response
# 1	CE	High amplification	Resistant
#2	CE	High amplification	Sensitive
	CE	Low amplification	
	CE	NA	
#3	SE	NA	Resistant
	CE	High amplification	
#4	YS	High amplification	Resistant
	CE	High amplification	
	CH	High amplification	
	SE	High amplification	
#5	SE	High amplification	Sensitive
	CH	High amplification	
	TE	Low amplification	
#6	CH	Low amplification	Resistant
#7	CH	High amplification	Resistant
	CH	Low amplification	
#8	CE	Low amplification	Resistant
	YS	NA	
	TE	High amplification	
#9	SE	High amplification	Sensitive
#10	CE	High amplification	Sensitive
#11	YS	Low amplification	Resistant
#12	SE	Low amplification	
#13	TE	Low amplification	Resistant
#14	TE	Low amplification	Sensitive
#15	CE	High amplification	Sensitive
	CE	NA	
#16	CE	Low amplification	Sensitive
#17	CE	High amplification	Sensitive
	CE	NA	
	TE/CE	NA	
	CH	NA	
#18	CE	Low amplification	Resistant
	TE	Low amplification	

[a]Tumor histology: YS, yolk sac; EC, embryonal carcinoma; CH, choriocarcinoma; TE, teratoma; SE, seminoma.
[b] Low (4 or 5 signals) and high (>5 signals). NA, none amplified.

Supplementary Table S4. Patients classified with respect to 9q32-q33.1 amplification status.

	9q32-q33.1 status [e]				
	Non-amplification (N = 57)		Amplification (N = 18)		
	Number	%	Number	%	*P*
Age, years					0.25
Median	27.6		29.1		
Range	(15 - 56)		(16 - 53)		
Histology					0.52
Seminoma	10	17.5	2	11.1	
Nonseminoma	47	82.5	16	88.9	
Localization					0.96
Testis	54	94.7	17	94.4	
Mediastinum	3	5.3	1	5.6	
IGCCCG stage at diagnosis of metastasis [a]					0.26
Good	37	64.9	8	44.4	
Intermediate	10	17.5	4	22.2	
Poor	10	17.5	6	33.3	
First line of chemotherapy treatment [b]					0.83
EP	9	15.8	2	11.1	
BEP	35	61.4	10	55.6	
Taxol-BEP	2	3.5	1	5.6	
BOMP/EPI	11	19.3	5	27.8	
Response to first line of chemotherapy treatment [c]					0.007
Good response (CR, PR-)	54	94.7	13	72.2	
Poor response (PR+, SD, PD)	3	5.3	5	27.8	
Sensitivity to cisplatin [d]					0.060
Sensitive	42	73.7	9	50.0	
Resistant	15	26.3	9	50.0	

[a] IGCCCG International Germ Cell Cancer Collaborative Group.

[b] EP, etoposide/cisplatin; BEP, bleomycin/etoposide/cisplatin; BOMP/EPI, bleomycin/vincristine/methotrexate/ cisplatin-etoposide/cisplatin/ifosfamide

[c] CR, complete remission characterized by tumor mass reduction by CT scan and negative value of serum tumor marks; PR-, partial remission characterized by normalization of CT scan and negative value of serum tumor markers; PR+, partial remission characterized by reduction of tumor mass by CT scan and positive value of serum tumor markers; SD, stable disease; PD, progressive disease.

[d] Patients who achieved durable complete response with first-line cisplatin-based chemotherapy were considered sensitive. Patients who had either a poor response or relapsed after first-line chemotherapy were considered resistant to cisplatin.

[e] Amplification at 9q determined by FISH using two different probes (see *Material and Methods*).

SUPPLEMENTARY FIGURE LEGENDS

Supplementary Fig. 1. Short- and long-term CDDP responses at low (2 mg/kg) and high (5 mg/kg) doses of CDDP were characterized in xenografted tumors. (A) TGT1X, a pure YS; TGT12X and TGT14X, two pure ECs, and TG39X, a mixed tumor with EC and YS components. Dynamic curves of CDDP treatments show a sustained response, characterized by levels of AFP that were maintained for 90 days (TGT39X, right panel). Dynamic CDDP response curves were generated by serial AFP and β-hCG determinations in the serum of control (saline-treated) and drug-treated mice in both types of responses and for 2 and 5 mg/kg doses of CDDP. (B) and (C) Characterization of differential CDDP responses of TGT21AX and TGT21BX, two tumors obtained from the same patient. A complete short- and long-term response was obtained at high doses for both tumors. (C) H&E analyses of relapsed masses in long-term response (2 mg/kg) of TGT21AX, showed the presence of a teratoma (TE), characterized by the absence of tumor serum markers.

Supplementary Fig. 2. Comparative histological analysis of original non-treated orthoxenografts and their pairs with acquired resistance to CDDP after five cycles of treatment in mice. All tumors maintained the same histological appearance, and unlike untreated tumors, higher levels of fibrosis and necrosis were observed. **TGT21AX differentiated to a growing teratoma after the first cycle of CDDP treatment, and did not regrow after mouse reimplantation.

Supplementary Fig. 3. Representative recurrent imbalanced regions in different orthoxenografts with acquired CDDP resistance. (A) Gains at 15q23-q24.1 and 15q26.3 were identified in TGT12XR and TGT21BXR. (B) Loss of the Xp22.33 region happens in TGT12XR, TGT21XR and TGT38XR. Whole-genome mapping was performed by oligonucleotide array CGH analysis (60 kbp window averaging) visually depicted with the SignalMap graphical interface tool from Nimblegen Systems. Arrows indicate regions of new gain/loss in resistant tumors.

Supplementary Fig. 4. Physical and Functional interactions of proteins encoded by 9q32-q33.1 genes expressed in PDOXs of this study. UniProtKB/Swiss-Prot ID names

were loaded to the web-based tool STRING 10.5 (9). The resulting network contains 33 nodes and 4 edges, with a Protein-Protein Interaction (PPI) p-value of 0.221, which means that the network have significantly less interaction than expected. Blue line, Known interaction from curated databases; Pink line, Known interaction from curated databases; Green line, Text mining; and Black line, Co-expres “

Supplementary Fig 5. Impact of some RNAi clones on cisplatin toxicity in *Caenorhabditis elegans* adults

(A) Cisplatin induces a dose-dependent descrease in *C. elegans* adult locomotor activity. Locomotor activity is represented as percentage of variation respect to initial activity of a worm population growing in liquid media. Since cisplatin cause sterility, animals that were not expose to cisplatin show an increase in the movement due to the presence of newborn larvae. (B) To score the effect of RNAi clones in cisplatin toxicity, we plotted the percentage of locomotor activity after 24 hours of exposure to cisplatin. Animals exposed at 500µg/µl keep about 30-35% of their initial locomotor activity. (C) Different response of worms fed with some RNAi clones exposed to 500 µg/µl of cisplatin. Inactivation of *vha-10(RNAi)* and *F27C1.2(RNAi)* cause sensitivity and resistance to cisplatin respectively. *cgt-1* and *cgt-3* are functionally redundant and double inactivation (*cgt-1* mutation plus *cgt-3*(RNAi)) is required to induce sensitivity to cisplatin. RNAi against F27C1.2 was started at L1 stage whereas *vha-10(RNAi) and cgt-3(RNAi)* was initiated at L3 stage. RNAi against the Copper-transporter encoding gene F27C1.2 was performed on the RNAi sensitive background *rrf-3(pk1426). ***p<0,001, **p<0,01, *p<0,05* compared to control, $^{++}$ *p<0,01* compared to *cgt-1(ok1045)* and *cgt-3(RNAi)* ^^^ *p<0,001* compared to *rrf-3(pk1426)* by Student’s t-test.

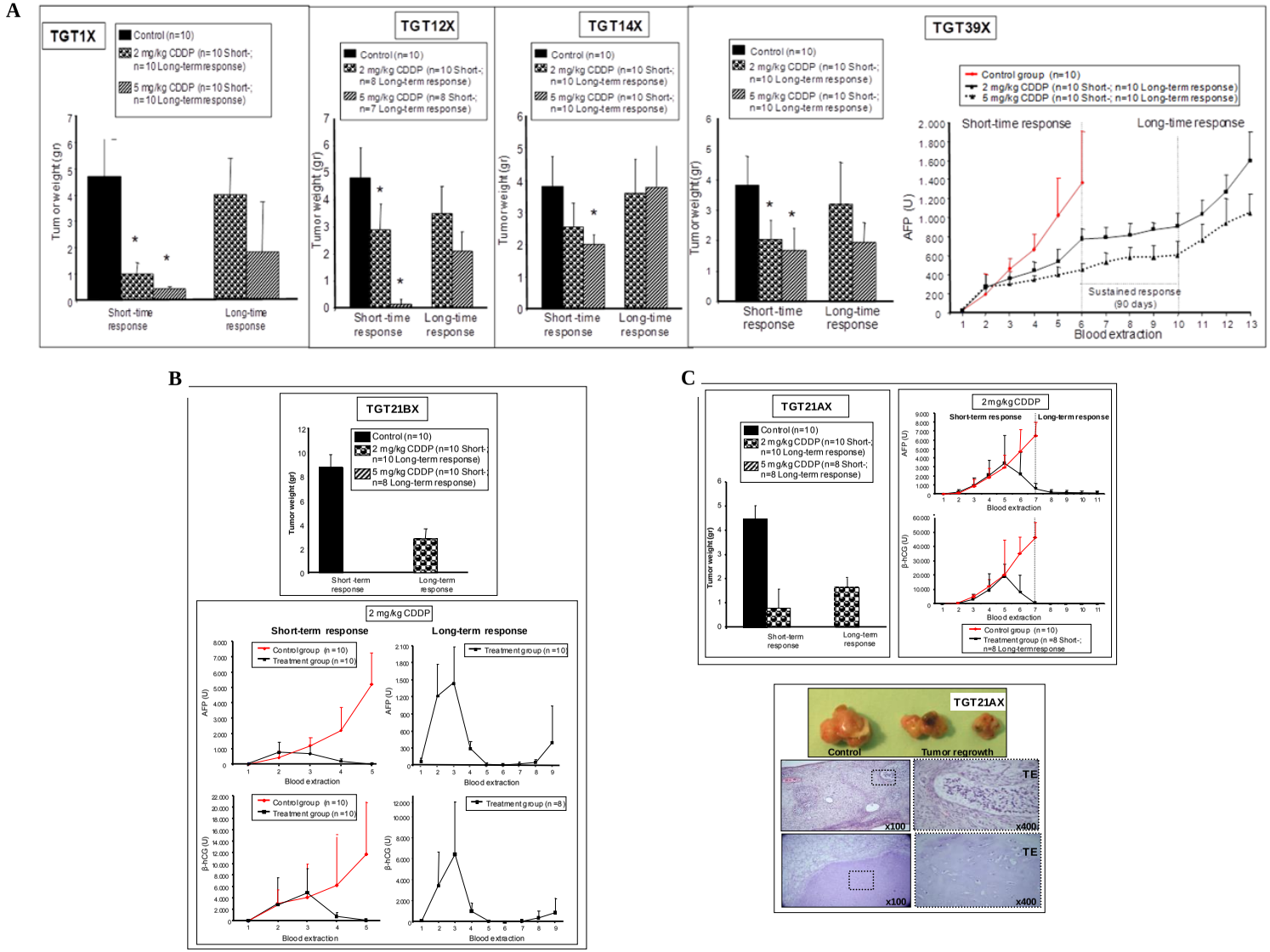

Supplementary Fig. 1. Short- and long-term CDDP responses at low (2 mg/kg) and high (5 mg/kg) doses of CDDP were characterized in xenografted tumors. (A) TGT1X, a pure YS; TGT12X and TGT14X, two pure ECs, and TG39X, a mixed tumor with EC and YS components. Dynamic curves of CDDP treatments show a sustained response, characterized by levels of AFP that were maintained for 90 days (TGT39X, right panel). Dynamic CDDP response curves were generated by serial AFP and β-hCG determinations in the serum of control (saline-treated) and drug-treated mice in both types of responses and for 2 and 5 mg/kg doses of CDDP. (B) and (C) Characterization of differential CDDP responses of TGT21AX and TGT21BX, two tumors obtained from the same patient. A complete short- and long-term response was obtained at high doses for both tumors. H&E analyses of relapsed masses in long-term response (2 mg/kg) of TGT21AX, showed the presence of a teratoma (TE), characterized by the absence of tumor serum markers.

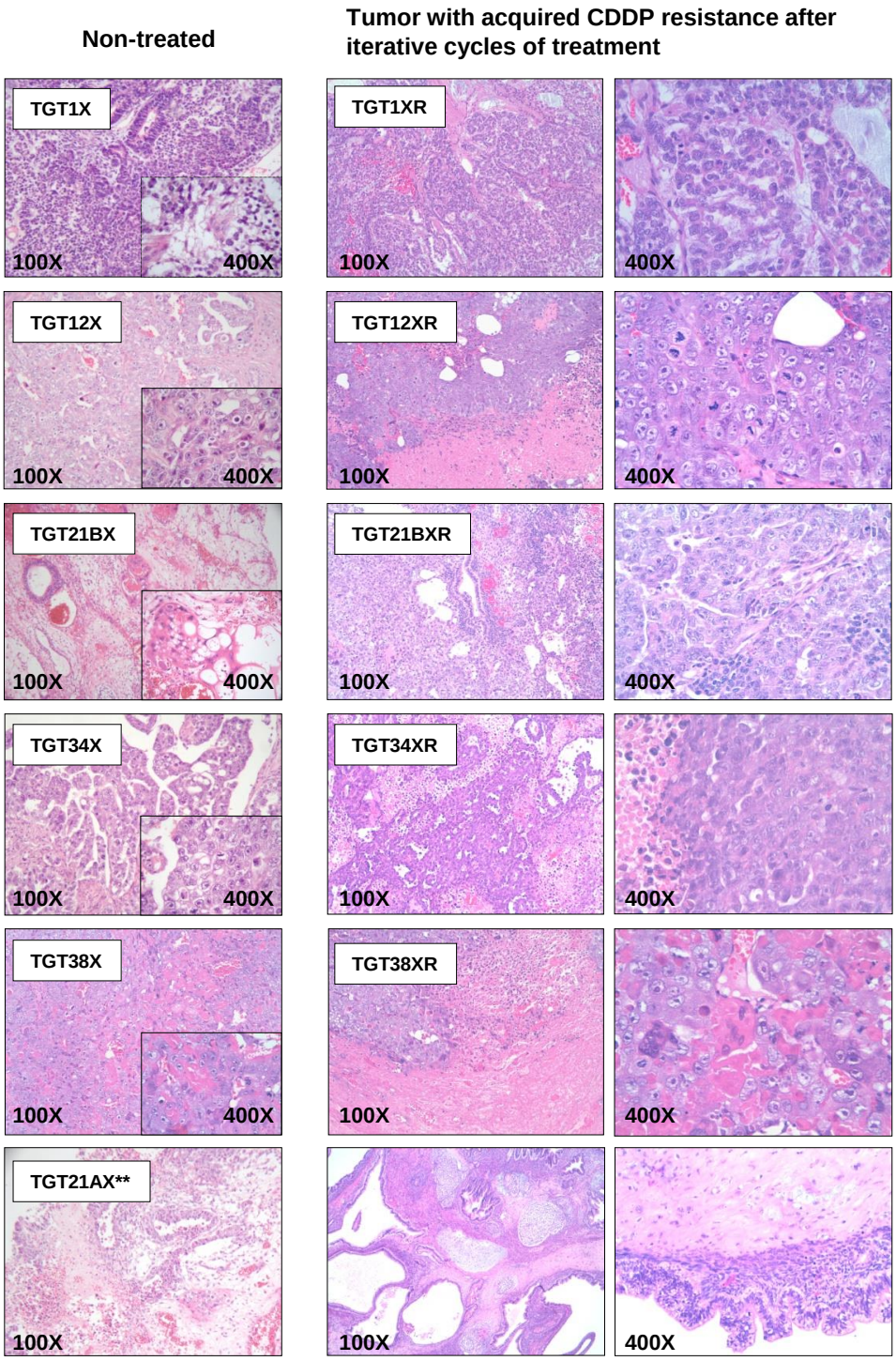

Supplementary Fig. 2. Comparative histological analysis of original non-treated orthoxenografts and their pairs with acquired resistance to CDDP after five cycles of treatment in mice. All tumors maintained the same histological appearance, and unlike untreated tumors, higher levels of fibrosis and necrosis were observed. **TGT21AX differentiated to a growing teratoma after the first cycle of CDDP treatment, and did not regrow after mouse reimplantation.

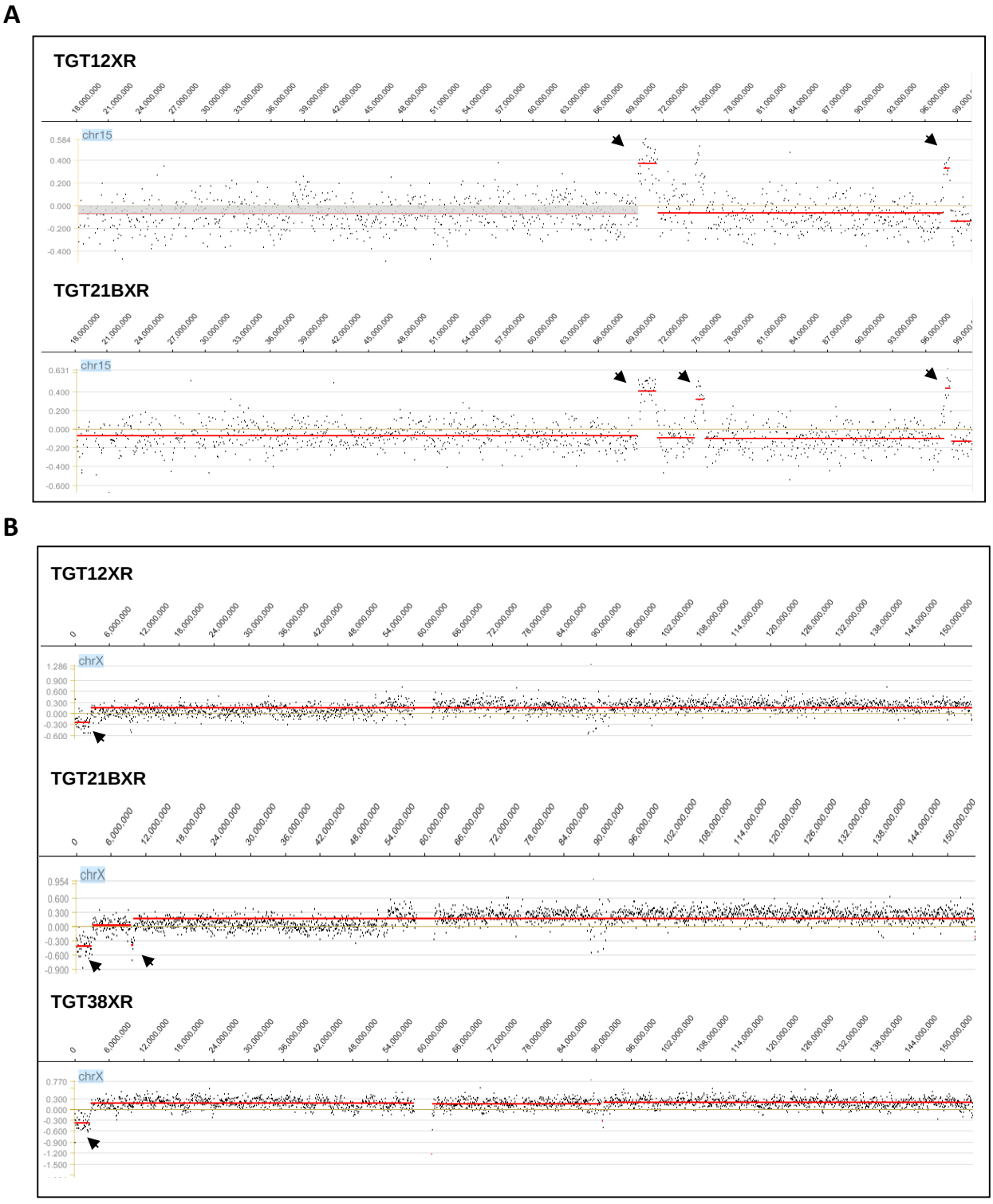

Supplementary Fig. 3. Representative recurrent imbalanced regions in different orthoxenografts with acquired CDDP resistance. (A) Gains at 15q23-q24.1 and 15q26.3 were identified in TGT12XR and TGT21BXR. (B) Loss of the Xp22.33 region happens in TGT12XR, TGT21XR and TGT38XR. Whole-genome mapping was performed by oligonucleotide array CGH analysis (60 kbp window averaging) visually depicted with the SignalMap graphical interface tool from Nimblegen Systems. Arrows indicate regions of new gain/loss in resistant tumors.

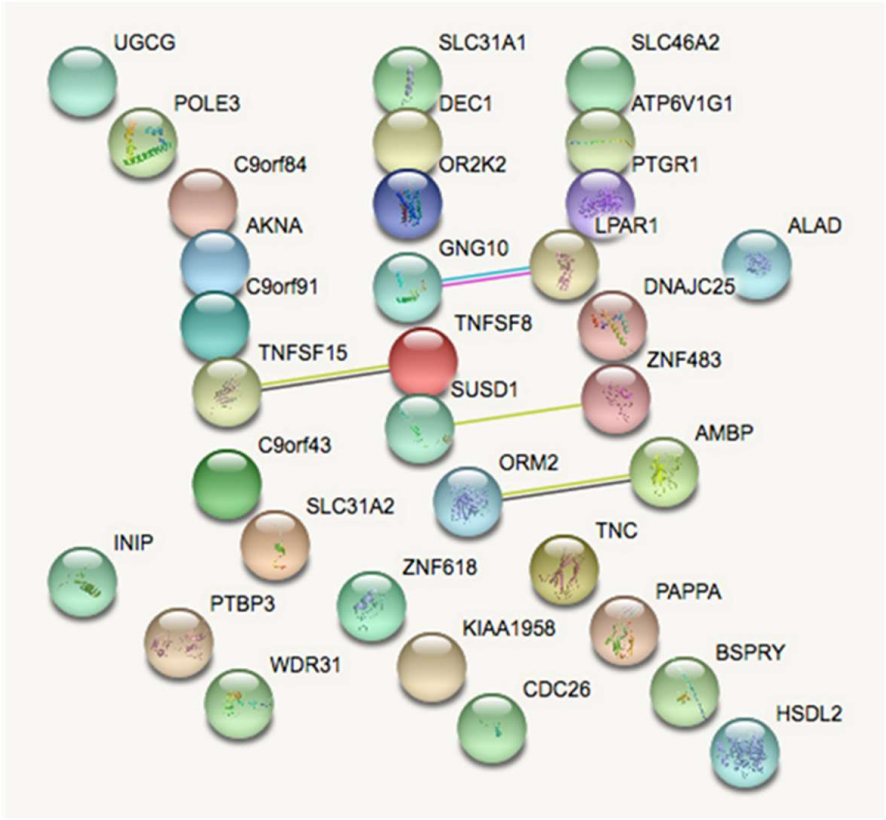

Supplementary Fig. 4. Physical and functional interactions of proteins encoded by 9q32-q33.1 genes expressed in PDOXs of this study. UniProtKB/Swiss-Prot ID names were loaded to the web-based tool STRING 10.5 [30]. The resulting network contains 33 nodes and 4 edges, with a Protein-Protein Interaction (PPI) p-value of 0.221, which means that the network have significantly less interaction than expected. Blue line, Known interaction from curated databases; Pink line, Known interaction from curated databases; Green line, Text mining; and Black line, Co-expres.

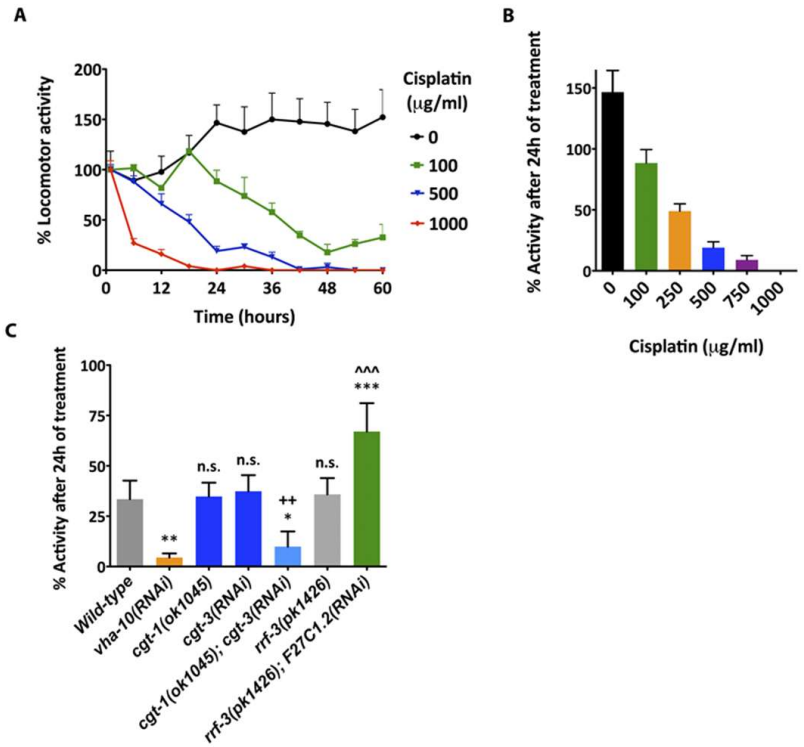

Supplementary Fig 5. Impact of some RNAi clones on cisplatin toxicity in *Caenorhabditis elegans* adults. (A) Cisplatin induces a dose-dependent descrease in *C. elegans* adult locomotor activity. Locomotor activity is represented as percentage of variation respect to initial activity of a worm population growing in liquid media. Since cisplatin cause sterility, animals that were not expose to cisplatin show an increase in the movement due to the presence of newborn larvae. (B) To score the effect of RNAi clones in cisplatin toxicity, we plotted the percentage of locomotor activity after 24 hours of exposure to cisplatin. Animals exposed at 500 µg/µl keep about 30-35% of their initial locomotor activity. (C) Different response of worms fed with some RNAi clones exposed to 500 µg/µl of cisplatin. Inactivation of *vha-10(RNAi)* and *F27C1.2(RNAi)* cause sensitivity and resistance to cisplatin respectively. *cgt-1* and *cgt-3* are functionally redundant and double inactivation (*cgt-1* mutation plus *cgt-3*(RNAi)) is required to induce sensitivity to cisplatin. RNAi against F27C1.2 was started at L1 stage whereas *vha-10(RNAi) and cgt-3(RNAi)* was initiated at L3 stage. RNAi against the Copper-transporter encoding gene F27C1.2 was performed on the RNAi sensitive background *rrf-3(pk1426)*. ***$p<0,001$, **$p<0,01$, *$p<0,05$ compared to control, $^{++}$ $p<0,01$ compared to *cgt-1(ok1045)* and *cgt-3(RNAi)* ^^^ $p<0,001$ compared to *rrf-3(pk1426)* by Student's t-test.

ARTICLE 3:

Ambrogio, C.; Carmona, F.J.; **Vidal, A.**; Falcone, M.; Nieto, P.; Romero, O.A.; Puertas, S.; Vizoso, M.; Nadal, E.; Poggio, T.; Sánchez-Céspedes, M.; Esteller, M.; Mulero, F.; Voena, C.; Chiarle, R.; Barbacid, M.; Santamaria,D.; Villanueva, A. Modeling lung cancer evolution and preclinical response by orthotopic mouse allografts. Cancer Research 2014; 74: 5978 – 5988.

RESUM

Objectiu:

1. Generació i caracterització d'al·loempelts ortotòpics (*orthoallografts*) mitjançant la implantació en el pulmó de ratolins immunodeprimits dels tumors pulmonars generats en el model K-Ras$^{lox/LSLG12Vgeo}$ i el model EML4-ALK de ratolins modificats genèticament.

Introducció: L'evolució del càncer de pulmó és un procés encara poc conegut degut a la manca d'estudis versàtils longitudinals *in vivo*. És fonamental arribar a establir models animals de carcinoma de pulmó no cèl·lula petita que siguin capaços de recapitular fidelment la malaltia humana per a millorar el coneixement d'aquest procés.

Disseny experimental: Mitjançant la generació d'*orthoallografts* de carcinoma de pulmó no cèl·lula petita (CPNCP) murí i les seves corresponents línies cel·lulars primàries aparellades proporcionem una detallada descripció *in vivo* del procés de malignització que depèn del temps. Així, en aquest treball hem desenvolupat un enfocament versàtil i reproduïble que supera importants desavantatges que presenten els models animals preexistents de CPNCP generats en GEMM (ratolins modificats genèticament), en particular aquells que estan associats tant amb la baixa heterogeneïtat histològica com la capacitat de generar metàstasis espontànies. Aquesta metodologia es basa en la implantació ortotòpica seqüencial al pulmó de ratolins immunodeficients de petits fragments sòlids dels tumors CPNCP murins generats en GEMM.

Resultats: Amb aquest enfocament, hem generat una ortoal·lobanc de CPNCP, és a dir una col·lecció d'adenocarcinomes pulmonars murins passats en sèrie al

llarg del temps en ratolins immunodeficients, així com una col·lecció de línies cel·lulars aparellades derivades d'aquests tumors crescuts en els ratolins immunodeficients. En aquest models hem reproduint la natura estocàstica del desenvolupament del càncer de pulmó identificant l'adquisició de potencial de disseminació metastàsica, la selecció de mutacions co-*drivers,* així com l'aparició d'heterogeneïtat intratumoral.

Conclusions: Aquesta aproximació combina la robustesa dels models de càncer en ratolins modificats genèticament amb la flexibilitat de la metodologia de la implantació ortotòpica dels tumors murins en ratolins immunodeficients . Aquesta eina s'ha aplicat per a l'avaluació pre-clínica de diferents aproximacions terapèutiques. A més, aquest sistema es pot implementar per a millorar el disseny de futurs tractaments per a pacients amb carcinoma de pulmó no cèl·lula petita (CPNCP).

Integrated Systems and Technologies

Cancer Research

Modeling Lung Cancer Evolution and Preclinical Response by Orthotopic Mouse Allografts

Chiara Ambrogio[1], Francisco J. Carmona[2], August Vidal[3], Mattia Falcone[4], Patricia Nieto[1], Octavio A. Romero[2], Sara Puertas[5], Miguel Vizoso[5], Ernest Nadal[6], Teresa Poggio[7], Montserrat Sánchez-Céspedes[2], Manel Esteller[2,8,9], Francisca Mulero[10], Claudia Voena[7], Roberto Chiarle[7,11], Mariano Barbacid[1], David Santamaría[1], and Alberto Villanueva[5,12]

Abstract

Cancer evolution is a process that is still poorly understood because of the lack of versatile *in vivo* longitudinal studies. By generating murine non–small cell lung cancer (NSCLC) orthoallobanks and paired primary cell lines, we provide a detailed description of an *in vivo*, time-dependent cancer malignization process. We identify the acquisition of metastatic dissemination potential, the selection of co-driver mutations, and the appearance of naturally occurring intratumor heterogeneity, thus recapitulating the stochastic nature of human cancer development. This approach combines the robustness of genetically engineered cancer models with the flexibility of allograft methodology. We have applied this tool for the preclinical evaluation of therapeutic approaches. This system can be implemented to improve the design of future treatments for patients with NSCLC. *Cancer Res; 74(21); 5978–88. ©2014 AACR.*

Introduction

Lung cancer is the leading cause of cancer death worldwide. Non–small cell lung cancer (NSCLC) accounts for about 85% of cases, with a 5-year survival rate below 15% (1). To improve control over this devastating disease, a variety of *in vivo* preclinical models have been used during the last decade. Among those, subcutaneous xenografts of human NSCLC cell lines have been extensively applied for drug sensitivity assays (2). Alternatively, intrapulmonary delivery of human cell lines in nude mice has provided a more clinically relevant system to study NSCLC biology (3). However, these methodologies still present some disadvantages. In particular, it is troublesome to obtain a single intraparenchymatous lung tumor that mimics the clinical situation and allows longitudinal follow-up. Indeed, localized intrapulmonary disease accounts for the majority of patients with NSCLC and is the basis of further tumor progression. In parallel, genetically engineered mouse models (GEMM) have become indispensable tools for our understanding of the mechanisms that contribute to tumor development as well as for treatment design and target validation demands. However, GEMM lung tumors induced by a single initiating oncogene are predominantly early-stage lesions, display limited histologic variation, and metastasize rather infrequently (4).

In sum, there is an urgent necessity to establish suitable animal models of NSCLC that faithfully recapitulate every salient aspect of the human disease. Here, we report a versatile and reproducible approach that circumvents important disadvantages of preexisting animal models of NSCLC, in particular those associated with low histologic heterogeneity and lack of spontaneous metastasis. This methodology is based on sequential orthotopic implantation of small solid fragments from an individual murine primary tumor into recipient mice. With this approach, we have generated an NSCLC orthoallobank: a comprehensive archived collection of serially passaged murine lung adenocarcinomas together with paired cell lines. This methodology enables full recapitulation of human NSCLC histopathologic features, including selection of mutations in

[1]Experimental Oncology, Molecular Oncology Programme, Centro Nacional de Investigaciones Oncológicas (CNIO), Madrid, Spain. [2]Cancer Epigenetics and Biology Program (PEBC), Bellvitge Biomedical Research Institute (IDIBELL), Barcelona, Spain. [3]Department of Pathology, Hospital Universitari de Bellvitge, Barcelona, Spain. [4]Department of Genetics, Biology and Biochemistry, Molecular Biotechnology Center, University of Torino, Torino, Italy. [5]Translational Research Laboratory, Catalan Institute of Oncology, Bellvitge Biomedical Research Institute (IDIBELL), Barcelona, Spain. [6]Department of Medical Oncology, Catalan Institute of Oncology, Bellvitge Biomedical Research Institute (IDIBELL), Barcelona, Spain. [7]Department of Molecular Biotechnology and Health Sciences, Center for Experimental Research and Medical Studies (CERMS), University of Torino, Torino, Italy. [8]Department of Physiological Sciences II, School of Medicine, University of Barcelona, Barcelona, Catalonia, Spain. [9]Institucio Catalana de Recerca i Estudis Avançats (ICREA), Barcelona, Catalonia, Spain. [10]Molecular Imaging Unit, Biotechnology Programme, Centro Nacional de Investigaciones Oncológicas (CNIO), Madrid, Spain. [11]Department of Pathology, Harvard Medical School, Boston Children's Hospital, Boston, Massachusetts. [12]XenOPAT S.L., Business Bioincubator, Bellvitge Health Science Campus, Barcelona, Spain.

Note: Supplementary data for this article are available at Cancer Research Online (http://cancerres.aacrjournals.org/).

C. Ambrogio and F.J. Carmona contributed equally to this article.

Corresponding Authors: David Santamaría, Experimental Oncology, Molecular Oncology Programme, Centro Nacional de Investigaciones Oncológicas (CNIO), Madrid 28029, Spain. Phone: 34917328015; Fax: 3491328000; E-mail: dsantamaria@cnio.es; and Alberto Villanueva, Translational Research Laboratory, Catalan Institute of Oncology, Bellvitge Biomedical Research Institute (IDIBELL), Barcelona 08907, Spain. E-mail: avillanueva@iconcologia.net

doi: 10.1158/0008-5472.CAN-14-1606

relevant tumor suppressors together with metastatic dissemination. Our method offers a powerful tool to study the poorly characterized progression toward full-blown metastatic adenocarcinomas present at the time of diagnose in human patients. Moreover, it provides a rapid and standardized platform for the preclinical evaluation of therapeutic treatments *in vivo*.

Materials and Methods

Animals

The *K-Ras*$^{lox/LSLG12Vgeo}$; *RER1*$^{ert/ert}$ strain has been previously described (5). Lung tumors were induced by intraperitoneal injection of 4-hydroxitamoxifen as previously described (5). EML4-ALK mice will be reported elsewhere (Voena and colleagues, manuscript submitted). In brief, a cDNA fragment encoding EML4-ALK (variant 1) was ligated to the surfactant protein-C (SP-C) promoter as well as to a polyadenylation signal. The expression cassette was injected into pronuclear stage embryos of FVB/N mice. The presence of the transgene was examined by PCR analysis after extraction of DNA from the tail of founder animals. RT-PCR analysis was performed to detect EML4-ALK mRNA to confirm the lung-specific expression of the transgene. Crl:NU-*Foxn1*^{nu} mice were purchased from Charles River. All animal experiments were approved by the Ethical Committee of CNIO and IDIBELL and performed in accordance with the guidelines for Ethical Conduct in the Care and Use of Animals as stated in The International Guiding Principles for Biomedical Research Involving Animals, developed by the Council for International Organizations of Medical Sciences (CIOMS).

Orthotopic implantation in Crl:NU-*Foxn1*^{nu} mice

Primary tumors from inducible *K-Ras*$^{lox/LSLG12Vgeo}$ or EML4-ALK mice were aseptically isolated and placed at room temperature in DMEM supplemented with 10% FBS plus 50 U/mL penicillin and 50 mg/mL streptomycin. Within 12 hours from surgical resection, tumors were implanted in Crl:NU-*Foxn1*^{nu} mice following previously reported procedures (3). Briefly, mice were anesthetized with a continuous flow of 1% to 3% isoflurane/oxygen mixture (2 L/min) and subjected to right thoracotomy. Mice were situated in left lateral decubitus position, and a small transverse skin incision (~5–8 mm) was made in the right chest wall. Chest muscles were separated by a sharp dissection and costal and intercostals muscles were exposed. An intercostal incision of 2 to 4 mm on the third or fourth rib on the chest wall was made and a small tumor piece of 2 to 4 mm^3 was introduced into the chest cavity. The tumor specimen was deposited following two alternative surgical procedures: (i) tumor specimens were deposited between the second and the third lung lobule and (ii) for the chemotherapeutic approach, tumor specimens were anchored to the lung surface with Prolene 7.0 suture. Next, the chest wall incision was closed with surgery staples, and finally chest muscles and skin were closed. Mice were inspected twice a week and monitored for the presence of breathing problems. On average, implanted lung tumours were harvested at humane endpoint, cut into small fragments, and serially transplanted into two to three new animals. These engrafted tumors (named orthoallografts) were also cryopreserved as 2 to 4 mm^3 pieces in a solution of 90% FBS and 10% dimethyl sulfoxide and stored in liquid nitrogen for subsequent future implantations. In addition, a fresh small piece was used to derive matched cell lines *in vitro* when appropriate (see below).

In vivo drug treatments

K-Ras$^{lox/LSLG12Vgeo}$ orthoallografts were implanted in Crl:NU-*Foxn1*^{nu} mice and randomly allocated into the treatment groups. Mice were intravenously treated at days 7, 12, and 17 (cisplatin, 3 mg/kg; paclitaxel, 20 mg/kg) and sacrificed at day 22 postimplantation.

EML4-ALK orthoallografts were implanted in Crl:NU-*Foxn1*^{nu} mice and randomly allocated into the treatment groups. Crizotinib (100 mg/kg) was administered daily by oral gavage starting on day 60 postimplantation and continued during 10 days. Upon completion of both treatments, hematoxylin and eosin (H&E)-stained lung sections were blindly assessed by a pathologist. Crizotinib (PF-02341066) was a kind gift from Pfizer Inc.

Micro PET-CT imaging and analysis

Images were acquired using eXplore Vista PET-CT (GE Healthcare). Mice were injected with 15MBq of ^{18}F-FDG into the lateral tail vein in a volume of 100 μL. During imaging, mice were anesthetized with a continuous flow of 1% to 3% isoflurane/oxygen mixture (2 L/min). Forty-five minutes after radiotracer injection, micro-CT images were acquired at 400 projections and collected in one full rotation of the gantry in approximately 10 minutes. Micro PET scans were performed at 20 minutes per bed. CT images were reconstructed using filtered back projection with a Shepp–Logan filter and PET images with 3D OSEM reconstruction algorithm. ^{18}F-FDG (2[^{18}F]fluoro-2-deoxy-D-glucose) PET-CT images were analyzed using Amide Medical Image Data Examiner (AMIDE) software for evaluation of tumor ^{18}F-FDG uptake. ^{18}F-FDG uptake is indicated as maximal standardized uptake value (SUV Max), and was calculated by drawing a 3-dimensional (3D) region of interest (ROI) over the tumor applying the formula SUV = ROI radioactivity concentration (MBq/cc)/injected dose (MBq)/mice body weight (g).

Generation of murine K-Ras^{G12V} NSCLC cell lines and single-cell clones

Freshly collected lung tumor tissues coming from *K-Ras*$^{lox/LSLG12Vgeo}$ and EML4-ALK orthotopic implants were minced with sterile scalpels. Single cells and clumps were transferred to cell culture plates and maintained in DMEM supplemented with 10% FBS plus 50 U/mL penicillin and 50 mg/mL streptomycin under standard culture conditions. When cell colonies with epithelial cell morphology were observed, cells were trypsinized and expanded. For the single-cell colony generation, cells were diluted with culture medium to obtain a concentration of approximately 1 cell/100μL and seeded in 96-well plates (100μL/well). After 12 hours, each well was carefully examined by bright-field microscopy. Wells containing single cells with epithelial

morphology were marked, and the culture medium in such wells was changed every 3 days. Expanded cell populations derived from these colonies were subjected to further characterization. When appropriate, doxorubicin (Sigma-Aldrich) was used at 5 μg/mL.

For X-Gal staining, cultured cells were fixed with 0.2% glutaraldehyde for 15 minutes and incubated in X-Gal staining solution (0.1 mol/L phosphate buffer, 2 mmol/L $MgCl_2$, 5 mmol/L potassium ferrocyanide, and 5 mmol/L potassium ferricyanide containing 1 mg/mL X-Gal [5-bromo-4-chloro-3-indolyl-β-D-galactosidase]) for 12 to 16 hours at 37°C.

Quantitative RT-PCR

Total cellular RNA (1 μg), extracted by RNeasy Mini Kit (QIAGEN), was reverse-transcribed by random primers using SuperScript Double-Stranded cDNA Synthesis Kit (Invitrogen), and the reverse transcription reaction (1 μL) was then subjected to PCR amplification using FastStart Universal SYBR Green Master (Roche). PCR signals were recorded on a StepOnePlus Real-time PCR System (Applied Biosystems) and analyzed using the StepOne version 2.2 software (Applied Biosystems). Primer sets were the following:

(i) Cytokeratin 13 Fw: TCGTGACTGGCATCTGAAAC
Cytokeratin 13 Rev: AGGATGATCCGGTTGTTGTC

(ii) Cytokeratin 19 Fw: GGGGGTTCAGTACGCATTGG
Cytokeratin 19 Rev: GAGGACGAGGTCACGAAGC

(iii) Vimentin Fw: CGGCTGCGAGAGAAATTGC
Vimentin Rev: CCACTTTCCGTTCAAGGTCAAG

(iv) E-cadherin Fw: TTTTCGGAAGACTCCCGATTCA
E-cadherin Rev: AGCTTGTGGAGCTTTAGATGC

(v) N-cadherin Fw: CTGATAGCCCGGTTTCACTTG
N-cadherin Rev: CAGGCTTTGATCCCTCTGGA

Western blotting

About 25 μg of protein extracts obtained from cell lysates was separated on SDS-PAGE (Bio-Rad), transferred to a nitrocellulose membrane, and blotted with primary antibodies raised against p53 (Cell Signaling Technology), p21 (Santa Cruz Biotechnology), and GAPDH (Sigma).

Tumorigenicity assays

Cells (1×10^6) were resuspended in 200 μL of sterile PBS and then inoculated by tail vein injection into Crl:NU-*Foxn1*^{nu} mice of 6 to 10 weeks of age. Animals were euthanized at different time points postinoculation, and whole lungs or individual lung tumors were collected.

Histopathology

For routine histologic study, lung lobes were fixed in 10% buffered formalin (Sigma) and embedded in paraffin. Paraffin sections (5 μm thick) were then processed for either H&E staining or immunohistochemistry. Images were acquired with a LEICA DM4000B microscope equipped with LEICA DC500 digital camera. Antibodies used for immunostaining included those raised against cleaved caspase-3 (R&D Systems), cytokeratin-7, and thyroid transcription factor 1 (Abcam).

Results

Establishment and validation of an orthoallobank of murine NSCLC by orthotopic implantation in Crl:NU-*Foxn1*^{nu} mice

To develop orthotopic lung cancer implants, we took advantage of the inducible *K-Ras*^{G12V} model that was engineered as a silent knock-in mutation preceded by a floxed transcription stop cassette (Lox-Stop-Lox or LSL). Activation of the *K-Ras*^{LSLG12Vgeo} allele is achieved upon Cre recombinase–mediated excision of the stop cassette, resulting in the development of NSCLC (6). To generate a more aggressive model, we used the *K-Ras*$^{lox/LSLG12Vgeo}$ strain that includes a floxed version of the *K-Ras* wild-type allele. In this compound strain, delivery of the Cre recombinase results in expression of the oncogenic mutation together with the concomitant ablation of the wild-type copy of *K-Ras* (5). With this approach, we recapitulated the recurrent LOH event as found in 50% of human lung tumors with K-Ras activating mutations (7).

A total of 46 primary NSCLC tumors were isolated from four *K-Ras*$^{lox/LSLG12Vgeo}$ mice upon appearance of breathing difficulties (on average 11 months subsequent to oncogene induction). These primary lesions displayed limited histologic heterogeneity and were mainly classified as solid or papillary adenocarcinomas (Supplementary Table S1). All tumors were individually implanted in the right parieto-pleural lung region of Crl:NU-*Foxn1*^{nu} mice (hereafter nude mice) following a surgical procedure that can be easily implemented in any standard animal facility. Twenty-seven (~60%) implanted tumors successfully engrafted and were able to grow as orthotopic implants through a period of time ranging from 98 to 150 days from implantation to humane endpoint (Supplementary Table S1). We observed that papillary primary tumors engrafted more efficiently (82%) when compared with solid tumors (50%). In 12 cases (26%), tumors did not grow through a follow-up period of 6 months, whereas the remaining seven animals had to be prematurely euthanized because of postoperative complications.

Passage #1 implants were used to perform consecutive mouse-to-mouse serial transplantations, resulting in faster tumor growth and consequently shorter lifespan (Supplementary Table S1). At the humane endpoint of every passage, all tumors were harvested and cryopreserved to create a comprehensive NSCLC orthoallobank. In addition, we embedded in paraffin and snap froze all implants upon conclusion of every passage to generate an inclusive archive of samples for future analysis. To check the viability of cryopreserved samples, we thawed and orthotopically reimplanted four different second-passage orthoallografts (*oag-9*, *oag-12*, *oag-21*, and *oag-22*) chosen to represent the three most frequent histologic subtypes (papillary, acinar, and solid; Supplementary Table S2). Importantly, these tumors not only successfully engrafted but also displayed median passage duration and histologic features indistinguishable from paired samples implanted without the cryopreservation step. Next, to test its suitability as a practical tool for the validation of preclinical treatments, we assessed whether the evolution of implanted tumors could be followed-up by standard imaging technology. To this end, we analyzed a

cohort of animals orthotopically implanted with cryopreserved tumors by PET following injection of ^{18}F-FDG. Tumor-specific FDG-PET signal was readily measurable upon implantation and increased during the course of the experiment becoming detectable in other lung lobules (Fig. 1A and B). This was further documented by post-mortem histopathologic analysis (Fig. 1C).

Finally, to prove whether this methodology could be extended to other driver oncogenes found in human NSCLC, we implanted murine primary lung tumors derived from EML4-ALK transgenic mice (Voena and colleagues, manuscript submitted; see Materials and Methods). Eleven tumors were orthotopically implanted in nude mice, resulting in four successful engraftments (36%). The observed frequency of engraftment increased to 77% when the procedure was replicated with EML4-ALK; p53$^{-/-}$ primary tumors (Supplementary Table S3). All these lesions were also subjected to sequential passages (up to passage #3) and cryopreserved. This indicates that the methodology described above can be potentially extended to primary tumors from virtually any alternative GEMM.

NSCLC orthoallografts faithfully recapitulate human disease including histologic heterogeneity and progressive malignization over time

In humans, invasive adenocarcinoma represents 60% to 70% of all surgically resected lung cancer cases. According to the predominant histologic pattern, adenocarcinomas can be further classified in differentiated (comprising lepidic, acinar, papillary, and micropapillary) and undifferentiated/solid subtypes (8). However, lung tumors in K-Ras mutant mice display much lower complexity than human NSCLC. Indeed, the heterogeneity of human disease is poorly represented in primary tumors from *K-Ras*$^{lox/LSLG12Vgeo}$ mice, which predominantly display a differentiated pattern (Supplementary Table S1; see also ref. 9). In sharp contrast, orthoallografts obtained after a single passage in nude mice closely reproduced the diverse histologic appearance of human NSCLC. Unlike what we observed in the originating primary tumors, the most representative histologic subtypes found in human cancers appeared with variable frequency in the orthoallograft collection (Supplementary Fig. S1 and Supplementary Table S2).

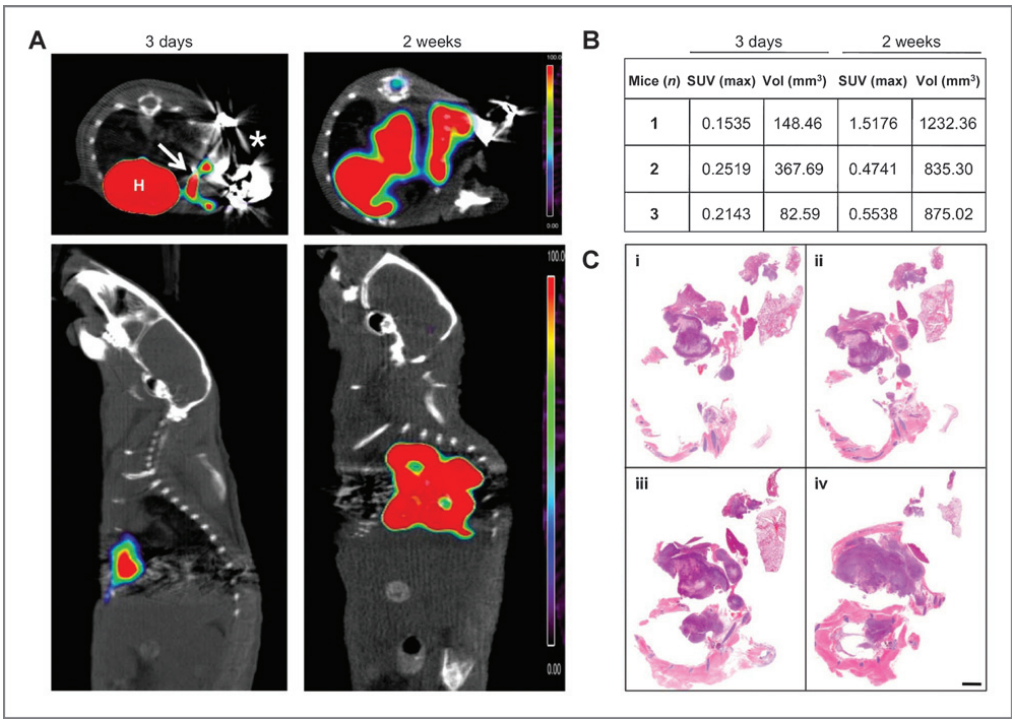

Figure 1. Follow-up of orthoallograft implants by ^{18}F-FDG PET-CT imaging. A, representative axial (top) and sagittal (bottom) projections of FDG-PET scans performed at the indicated time points following implantation of a passage #2 cryopreserved orthoallograft. Proper tumor FDG-PET signal upon tumor implantation is indicated by an arrow. Corollary postsurgery processes such as wound healing did not interfere with the detection of the tumor-specific FDG-PET signal. Asterisks mark atypical CT artifacts due to the presence of surgery staples. H, heart. B, quantification of both ^{18}F-FDG uptake (SUV Max) and tumor volume was assessed at the indicated time points in three animals receiving independent cryopreserved tumor implants. C, H&E-stained sections from one representative animal sacrificed following FDG-PET analysis at the 2 weeks' time point. The nonadjacent sections shown (i–iv) represent distally spaced regions along the anteroposterior axis. Scale bar, 2 mm.

We next asked whether the serial passaging of NSCLC orthoallografts could reveal a tendency to acquire increased malignancy over time. This is an important aspect, as the initial stages of malignization are difficult to be approached in humans. To this end, a group of representative primary tumors ($n = 6$) including predominant differentiated and undifferentiated histologic subtypes were passed mouse-to-mouse in the course of up to four sequential passages (Supplementary Table S4). As an initial evidence of increased malignancy, we first examined whether orthoallografts may have accumulated mutations with prognostic value. We focused our search to the tumor suppressor genes *p53* and *Lkb1* (also known as *Stk11*), as both present the highest frequency of co-occurrence with *K-Ras* activating mutations in advanced human NSCLC (10). While we failed to detect changes in the most frequently mutated *p53* exons (exons 4, 6, and 7), on average, 10% of the tumor cells in two of the 13 orthoallografts analyzed presented aberrations in the *Lkb1* gene, a frequently mutated gene in human NSCLC (11). We detected one nonsynonymous mutation (D162G) and one deletion (E354Δ) affecting the Lkb1 protein kinase and C-terminal regulatory domains, respectively (Fig. 2A). These regions concentrate most Lkb1 cancer–related mutations in humans (11). Importantly, Lkb1 aberrations were not identified in the originating passage #1 implants (Fig. 2A). Furthermore, the expression of the tumor suppressor p16 was decreased in late-passage samples, thus resembling the loss of p16 in human NSCLC progression (Fig. 2B; ref. 12). Finally, it has been proposed that expression of embryonic stem cell (ESC) markers correlates with undifferentiated NSCLC and is associated with worse prognosis (13). We took advantage of an RT-PCR array to measure the expression changes of a collection of established ESC markers during the orthotopic sequential transplantation (data not shown). *Klf4*, *Oct4*, *c-Myc*, *CD24*, and *Lgr6* displayed a higher expression fold change in late- versus early-passage implants in a cohort of paired samples ($n = 8$; Fig. 2B).

We further collected other evidences that suggested an evolution toward a more malignant phenotype during the serial passaging of orthoallografts. First, we observed that the period from tumor implantation to humane endpoint was progressively shortened along the serial transplantation procedure. Yet, beyond passage #3, this period remained constant

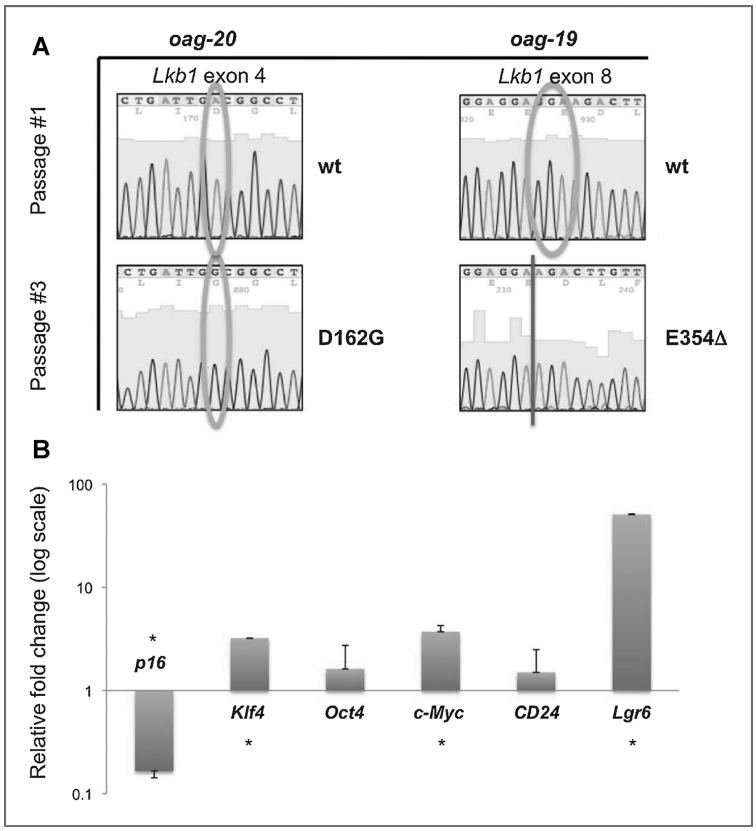

Figure 2. Identification of Lkb1 mutations and p16 silencing in late-passage orthoallografts. A, chromatograms obtained upon sequencing of passage #1 (top) and #3 (bottom) of the orthoallograft implants *oag-19* and *oag-20*. The resulting amino acid changes are indicated. Mutation analysis was carried out by sequencing of individual PCR products. Both D162G and E354Δ mutations were found in approximately 10% of the sequences. B, quantification of the relative expression levels by qRT-PCR of the indicated genes in late passage implants. For normalization purposes, the expression levels of all analyzed transcripts in passage #1 implants were considered as 1. *, $P < 0.01$.

(Fig. 3A). In all cases and irrespectively of passage duration, when the initial implant predominantly displayed solid features, we did not observe major histologic changes through passages being the engrafted tumor histologically stable (data not shown). In contrast, those implants that initially showed a predominant differentiated pattern eventually displayed an increase in the incidence of the solid subtype (Fig. 3B). Importantly, despite of the increment of undifferentiated components, these tumors maintained some degree of histologic heterogeneity as also observed in human biopsies (Supplementary Table S3).

Notably, in addition to their close histologic resemblance to human NSCLC, orthoallografts displayed metastatic potential as early as passage #1. This is in sharp contrast to K-Ras mutant GEMM models that lack metastatic capacity unless additional genetic modifications are included (4). As mentioned above and akin to human disease, the engrafted implants frequently invade neighboring lung lobules and disseminate to various locations forming macroscopic implants in the diaphragm, ribs, chest cavity, lymph nodes, and liver (Fig. 3C). Furthermore, careful histopathologic scrutiny of brain and liver sections, two of the main metastatic target tissues of primary human NSCLC, revealed the presence of micrometastasis in 7 of 21 (33%) implant-bearing animals (Fig. 3D and Supplementary Table S5).

Murine NSCLC cell lines generated from primary and metastatic tumors are p53-proficient

Thus far, it has been unfeasible to efficiently establish murine NSCLC cell lines that are p53-proficient. This is particularly relevant, as 50% of human NSCLC cases retain a wild-type p53 (14). In an attempt to establish such primary cell lines, orthotopic implants were resected and mechanically disaggregated immediately after passage #1 and maintained in culture under standard conditions. Following this approach, a panel of 35 murine K-Ras^{G12V} lung cancer (mKLC) cell lines was successfully derived from their corresponding orthoallografts. The process of cell line generation occurred with similar efficiency irrespectively of the predominant histologic subtype. Yet, the paired metastatic cell lines predominantly originate from solid orthoallografts (Supplementary Table S6). To assess whether these cell lines retained metastatic dissemination potential, a cohort of mice received a cell line derived from a diaphragmatic implant via tail vein injection. As expected because of the inoculation route, all animals developed pulmonary nodules. Remarkably, the injected animals also developed macroscopic tumors in various tissues such as lymph nodes, bone, liver, adrenal gland, ovary, skin, and salivary gland, thereby resembling the metastatic pattern reported in human patients with NSCLC (Fig. 4 and data not shown).

Next, four mKLC lines were further characterized *in vitro*. To confirm expression of K-Ras^{G12V} and the absence of stromal contaminants, we took advantage of the surrogate marker β-geo, inserted as a bicistronic transcript at the 3′–untranslated region (UTR) of the *K-Ras* locus (6). As expected, all cell lines displayed strong X-Gal staining, indicative of K-Ras^{G12V} expression (Supplementary Fig. S2A). Although all cell lines showed a characteristic morphology evocative of an epithelial origin, we nevertheless assessed by RT-PCR the expression of prototypical epithelial markers such as cytokeratin 13, cytokeratin 19, and E-cadherin along with the mesenchymal markers vimentin and N-cadherin. All tested mKLC cell lines

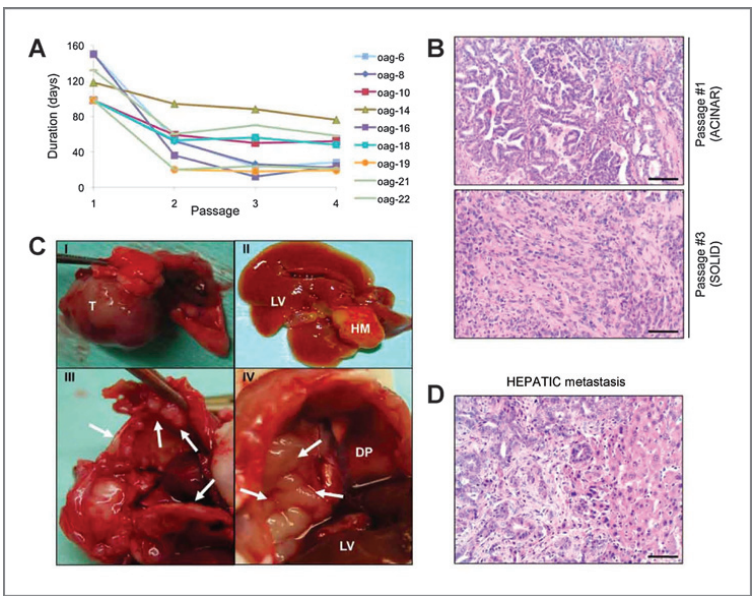

Figure 3. Orthoallografts acquire aggressive histopathology features and metastatic capacity upon sequential passaging. A, evolution of the passage duration along four sequential transplants of nine independent NSCLC orthoallografts. B, H&E staining of a representative case of a differentiated adenocarcinoma at passage #1 (top) evolving to a solid subtype upon completion of passage #3 (bottom). C, macroscopic aspect of an engrafted orthoallograft upon completion of passage #1 (I) together with metastatic liver lesion (II), invasion of neighboring ribs (III) and diaphragm (IV). D, representative images of an H&E-stained liver metastasis detected in recipient nude mice at endpoint of passage #1. DP, diaphragm; HM, hepatic metastasis; LV, liver; T, implanted tumor. Arrows, tumor nodes invading neighboring tissues. Scale bars, 100 μm.

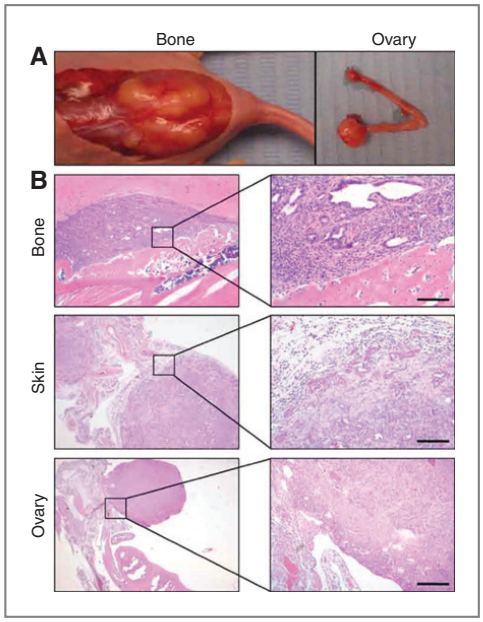

Figure 4. Cell lines derived from spontaneous metastasis display wide dissemination potential *in vivo*. A, macroscopic aspect of bone (left) and ovary (right) from a recipient nude mice 25 days after tail vein inoculation with 10^6 mKLC cells derived from a diaphragmatic implant. B, H&E staining of bone (top), skin (middle), and ovary (bottom) showing distal dissemination of the metastatic cell line upon tail vein injection. Right, higher magnification images of selected areas. Scale bars, 100 μm (top) and 200 μm (middle and low).

expressed these epithelial markers (Supplementary Fig. S2B). Interestingly, we also observed increased levels of vimentin and N-cadherin when compared with primary tumors, suggesting the acquisition of a mesenchymal-like phenotype as previously reported for other epithelial cancer cell lines *in vitro* (15).

p53 is known to be stabilized in response to DNA damage and other stress signals, resulting in the induction of several downstream targets that mediate a variety of cellular responses such as cell-cycle arrest or apoptosis (16). To assess p53 functionality, we exposed the mKLC lines to the genotoxic agent doxorubicin. This treatment resulted in clear p53 stabilization together with an induction of the p53 transcriptional target p21, indicating that mKLC cell lines derived by an orthoallograft procedure can be efficiently established preserving a functional p53 response (Supplementary Fig. S2C).

Cell-autonomous determination of NSCLC histologic heterogeneity

Considering that undifferentiated histopathologic subtypes are associated with poor prognosis in human patients with NSCLC (17), we set out to assess the capacity of our mKLC cell lines to fully reconstitute tumor heterogeneity *in vivo*. To this end, we used grafting by tail vein injection to favor lung colonization and performed a time course study to investigate tumor progression. Injection of 1×10^6 cells resulted in tumor formation that recapitulated the histologic heterogeneity as well as time-dependent evolution observed in the orthoallografted tumors. Whereas early stages (12 days) were characterized by small nodules of tumor cells with focal acinar differentiation, tumor progression invariably resulted in the appearance of adenocarcinomas with predominant solid features at humane endpoint (25 days; Supplementary Fig. S3). Importantly, the presence of a variable contribution of other histologic subtypes was also identified in a cell line–dependent manner (data not shown). We next aimed to assess whether this histologic heterogeneity, also observed in the majority of orthotopic implants as well as in human disease, was the result of a mosaic composition of cells of different nature or instead a reflection of inherent cellular plasticity *in vivo*. To this end, we generated single-cell clones starting from mKLC mass cultures and injected them via tail vein into recipient mice. Remarkably, single-cell clones were able to generate lung lesions displaying different histologic subtypes with variable composition depending on the individual clone (Supplementary Fig. S4).

Orthotopic implants as a model for preclinical evaluation of therapeutic intervention

We next wanted to assess whether the orthotopic implants could be used to anticipate therapeutic response in the clinic. To this end, we subjected nude mice implanted with K-Ras^{G12V} orthoallografts to the current standard of care for patients with NSCLC consisting of cisplatin-based chemotherapy (cisplatin plus paclitaxel). As shown in Fig. 5A, the cohort receiving chemotherapy showed a reduction in tumor burden when compared with those receiving vehicle alone. This was accompanied by the appearance of abnormal nuclei in the majority of cells, displaying enlarged, irregular, or multinucleated morphology (Fig. 5B). Overall, this response and the resulting histopathologic changes recapitulate the clinical outcome observed in patients with NSCLC subjected to this chemotherapeutic regime (18, 19).

Next, we aimed to extend our approach to a targeted therapy currently used in clinical practice with patients with NSCLC. Because there are no targeted treatments available for K-Ras mutant tumors, we studied the EML4-ALK model for which a crizotinib-based therapy is already in use in the clinic. Patients with NSCLC harboring an EML4-ALK inversion show an initial response accompanied by substantial tumor regression but this is inevitably followed by the acquisition of resistance (20). Interestingly, mice carrying EML4-ALK implants displayed a substantial tumor burden reduction when subjected to crizotinib treatment (Fig. 5C), with viable tumor areas scattered among necrotic and fibrotic tissue that may be responsible for future relapse (Fig. 5D and Supplementary Table S7).

Discussion

We describe a novel and reproducible methodology based on sequential orthotopic implantation of primary tumors in recipient mice that circumvents most of the disadvantages

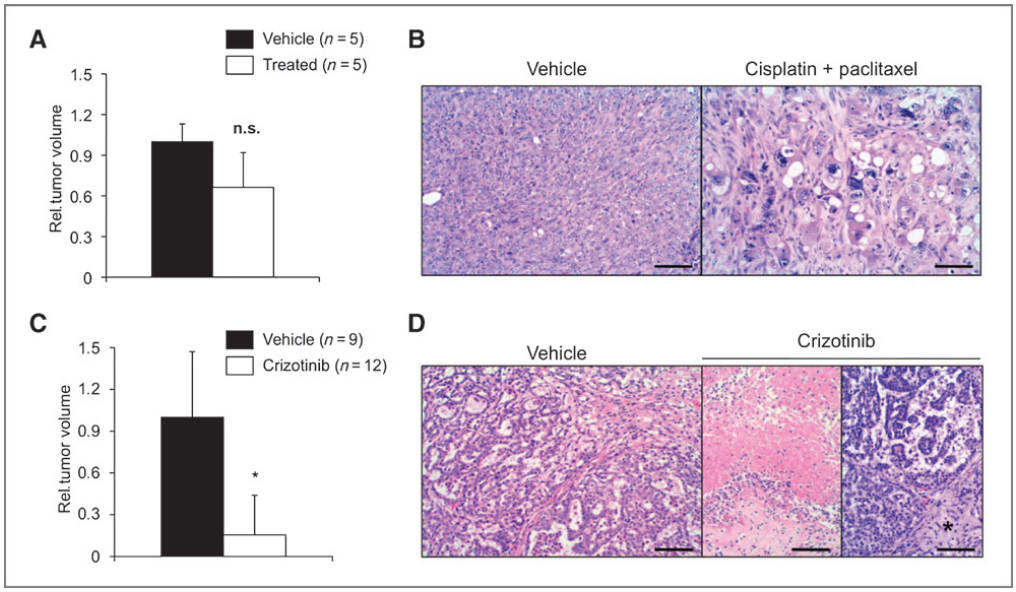

Figure 5. Orthoallografts as preclinical models for therapeutic assessment and target validation *in vivo*. A, nude mice implanted with K-Ras^{G12V} orthotopic tumors were treated three times during a 10-day period starting 7 days after implantation either with vehicle only (solid column) or subjected to the standard chemotherapy for patients with NSCLC (cisplatin plus paclitaxel, empty column). Tumor burden was quantified at endpoint ($n = 5$; error bars, mean ± SD). B, H&E staining of sections from K-Ras^{G12V} orthotopic tumors showing a vehicle-treated sample (left) and nuclei with prototypical aberrant morphology following chemotherapy (right). C, nude mice implanted with EML4-ALK orthotopic tumors were treated daily for 2 weeks starting 60 days after implantation either with vehicle only (solid column) or with crizotinib. Tumor burden was quantified at endpoint ($n = 9$–12; error bars, mean ± SD). D, H&E staining of sections from EML4-ALK orthotopic tumors showing a vehicle-treated sample (left) and two representative tumor areas showing a predominant necrotic response (middle) or viable tumor cells in a fibrotic context (right) following crizotinib therapy. *,a fibrotic area adjacent to tumor cells. Scale bars, 100 μm. *, $P < 0.05$; n.s., not significant.

associated with murine models of NSCLC such as the presence of low histologic heterogeneity and lack of spontaneous metastasis. With this approach, we have been able to document cancer evolution toward an increased malignant phenotype. This time-dependent evolutionary trend had been previously postulated for the progression of human NSCLC but lacked formal experimental evidence. In our model, the progressive acquisition of malignant traits is supported by several observations:

1. Serial passaging results in increased local invasion together with acquisition of distant metastatic potential displaying the same dissemination tropism observed in humans.
2. Similarly to advanced human NSCLC, serial passaging results in the acquisition of tumor-promoting mutations as well as loss of expression of relevant tumor suppressor genes. These alterations were not found in the original primary lesions, suggesting that they are progressively enriched as a consequence of fitness advantage and selective pressure.
3. Marked intratumor heterogeneity is generated by NSCLC cell lines originating form single cells and evolves over time toward an increase in more undifferentiated histologic subtypes that resemble those associated with poor prognosis in humans.
4. Both K-Ras^{G12V}- and EML4-ALK–driven implants are responsive to chemotherapy and crizotinib, respectively, but invariably display viable tumor cells posttreatment.
5. Serial transplantation allowed for the first time the generation of p53-proficient murine NSCLC primary cell lines.

The orthoallobank is a powerful tool to allow a comprehensive study of NSCLC evolution (Fig. 6). Our approach is well suited for the study of tumor features from a cell-autonomous perspective such as target validation exercises (both genetically and pharmacologically based), appearance of resistance mechanisms, and the contribution of stromal components. However, it is now accepted that the immune system plays both host-protective and tumor-promoting functions that influence various important aspects from tumor onset to metastatic dissemination (21, 22). In this context, the lack of a functional adaptive immune response represents an obvious limitation. The implementation of this technology in syngeneic mice is ongoing and will facilitate

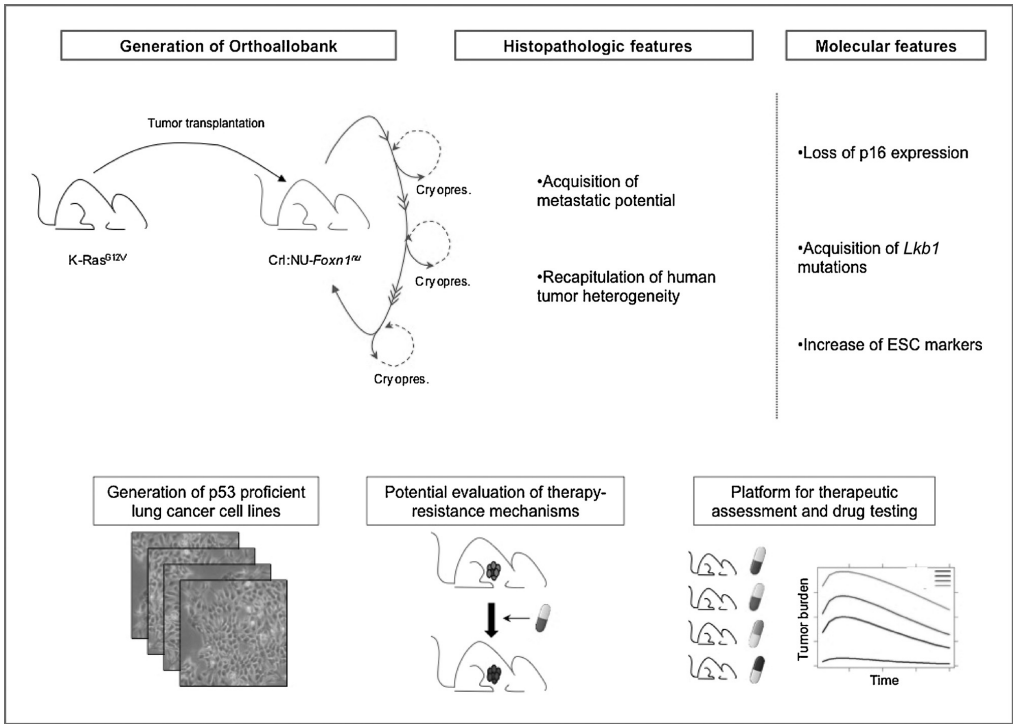

Figure 6. Graphical abstract. Schematic representation of the main findings and applications of the murine orthoallobank procedure.

the analysis of the immune system contribution, resulting in a more comprehensive approach (data not shown). The collection of archived samples may be used to characterize by deep sequencing technologies the order of genomic events that eventually lead to the establishment of aggressive NSCLC. This is particularly relevant, as in humans, many of the co-driver mutations that trigger or influence the progression of the disease remain poorly defined. They appear with variable frequency and are often difficult to set apart from the substantial number of passenger mutations. Because there is no fitness advantage associated with passenger mutations, their accumulation during tumor development is largely proportional to time (23). Because of the relatively short period from implantation to malignization, this orthotopic allograft approach may diminish the chances to accumulate passenger mutations. Instead, those that play a relevant role during tumor development will be selected for, thus facilitating their identification. Indeed, we have identified mutations in the tumor suppressor gene *Lkb1* identical to those previously reported in human NSCLC. Among those, the D162 mutation has been shown to be important for the structural integrity of human LKB1, and mutations affecting this residue have been reported in Peutz–Jeghers syndrome and other types of cancer (24). Therefore, this methodology will yield the causal and temporal relationships between specific genotypic aberrations acquired during multistage carcinogenesis and the resulting lung cancer phenotype. For instance, our results suggest that mutations affecting p53 arise later than those in Lkb1 or p16 silencing in K-Ras^{G12V}–driven NSCLC. Interestingly, unlike the originating primary tumor models, the serial transplantation of both K-Ras^{G12V} and EML4-ALK implants results in the acquisition of metastatic potential. Thus, this approach offers an invaluable platform to potentially characterize the metastatic dissemination process *in vivo* as well as the mutations, gene expression variations, or epigenetic changes responsible for the acquisition of the invasive capacity.

Likewise, the orthoallobank is a versatile and rapid platform for the preclinical assessment of therapeutic regimes including those dealing with the appearance of resistance mechanisms. K-Ras^{G12V}- and EML4-ALK–driven implants respond to chemotherapy and crizotinib, respectively, and display histopathologic features that could facilitate the understanding of the clinical outcome in patients subjected to similar regimes. While this response is comparable to that observed in primary murine tumors (20, 25), the orthotopic approach is substantially faster, reproducible, and homogenous, thus resulting in a

more reliable and straightforward alternative. Furthermore, selected tumors from the archived orthoallobank that carry particular sets of co-driver mutations could be treated simultaneously to assess potential differences in the therapeutic response that may depend on, or be influenced by, a particular genetic composition. Also, proteomic profiling of plasma samples could potentially be applied for the identification of predictive biomarkers of treatment efficacy (26).

In sum, we show a new systematic approach to study the evolution of cancer that provides a powerful strategy not only to tease out the molecular events that stimulate NSCLC progression but also to identify novel therapeutic strategies to fight this devastating disease.

Disclosure of Potential Conflicts of Interest

A. Villanueva is founder of the Spin-off of XenOPAT S.L. No potential conflicts of interest were disclosed by the other authors.

Authors' Contributions

Conception and design: C. Ambrogio, F.J. Carmona, A. Vidal, M. Barbacid, D. Santamaría, A. Villanueva

Development of methodology: C. Ambrogio, F.J. Carmona, A. Vidal, O.A. Romero, T. Poggio, M. Sánchez-Céspedes, M. Esteller, F. Mulero, C. Voena, D. Santamaría, A. Villanueva

Acquisition of data (provided animals, acquired and managed patients, provided facilities, etc.): C. Ambrogio, F.J. Carmona, A. Vidal, M. Falcone, P. Nieto, O.A. Romero, S. Puertas, M. Vizoso, M. Sánchez-Céspedes, M. Esteller, R. Chiarle, M. Barbacid, A. Villanueva

Analysis and interpretation of data (e.g., statistical analysis, biostatistics, computational analysis): C. Ambrogio, F.J. Carmona, A. Vidal, S. Puertas, M. Esteller, F. Mulero, R. Chiarle, D. Santamaría, A. Villanueva

Writing, review, and/or revision of the manuscript: C. Ambrogio, F.J. Carmona, A. Vidal, S. Puertas, E. Nadal, F. Mulero, R. Chiarle, D. Santamaría, A. Villanueva

Administrative, technical, or material support (i.e., reporting or organizing data, constructing databases): A. Vidal, M. Vizoso

Study supervision: C. Ambrogio, F.J. Carmona, M. Barbacid, D. Santamaría, A. Villanueva

Acknowledgments

The authors thank Samuele Marro, Maria Luigia De Bonis, and Manuel Serrano for critical reading of the article.

Grant Support

This work was supported by grants from the European Research Council (ERC-AG/250297-RAS AHEAD), EU-Framework Programme (LSHG-CT-2007-037665/CHEMORES, HEALTH-F2-2010-259770/LUNGTARGET, and HEALTH-2010-260791/EUROCANPLAT- FORM), Spanish Ministry of Economy and Competitiveness (SAF2011-30173), and Autonomous Community of Madrid (S2011/BDM-2470/ONCOCYCLE) to M. Barbacid; European Research Council (ERC-StG-2009-242965-LUNELY), Associazione Italiana per la Ricerca sul Cancro (AIRC) grant IG-12023, and Association for International Cancer Research (AICR) grant 12-0216 (R. Chiarle); Fondo de Investigaciones Sanitarias (PI10-0222, PI13-01339), INNPACTO (ORALBEADS-IPT-2011-0754-900000), and Generalitat de Catalunya (2005SGR00727) to A. Villanueva. E. Nadal was supported by a Juan Rodés contract (JR13/0002) from the Carlos III Institute of Health. C. Ambrogio is the recipient of a postdoctoral fellowship from the Spanish Association Against Cancer (AECC).

The costs of publication of this article were defrayed in part by the payment of page charges. This article must therefore be hereby marked *advertisement* in accordance with 18 U.S.C. Section 1734 solely to indicate this fact.

Received May 29, 2014; revised August 18, 2014; accepted August 25, 2014; published OnlineFirst September 12, 2014.

References

1. World Health Organization (WHO). World Cancer Report 2008 [Internet]. Lyon, France: IARC Press; 2008. p. 512. Available from: http://www.who.int/cancer/publications/world_cancer_report2008/en/.
2. Gazdar AF, Girard L, Lockwood WW, Lam WL, Minna JD. Lung cancer cell lines as tools for biomedical discovery and research. J Natl Cancer Inst 2010;102:1310–21.
3. Onn A, Isobe T, Itasaka S, Wu W, O'Reilly MS, Ki Hong W, et al. Development of an orthotopic model to study the biology and therapy of primary human lung cancer in nude mice. Clin Cancer Res [Internet] 2003;9:5532–9. Available from: http://www.ncbi.nlm.nih.gov/pubmed/14654533.
4. Kwon M, Berns A. Mouse models for lung cancer. Mol Oncol [Internet] 2013;7:165–77. Available from: http://www.ncbi.nlm.nih.gov/pubmed/23481268.
5. Puyol M, Martín A, Dubus P, Mulero F, Pizcueta P, Khan G, et al. A synthetic lethal interaction between K-Ras oncogenes and Cdk4 unveils a therapeutic strategy for non–small cell lung carcinoma. Cancer Cell 2010;18:63–73.
6. Guerra C, Mijimolle N, Dhawahir A, Dubus P, Barradas M, Serrano M, et al. Tumor induction by an endogenous K-ras oncogene is highly dependent on cellular context. Cancer Cell 2003;4:111–20.
7. Li J, Zhang Z, Dai Z, Plass C, Morrison C, Wang Y, et al. LOH of chromosome 12p correlates with Kras2 mutation in non–small cell lung cancer. Oncogene 2003;22:1243–6.
8. Travis WD, Brambilla E, Noguchi M, Nicholson AG, Geisinger KR, Yatabe Y, et al. International association for the study of lung cancer/American thoracic society/European respiratory society international multidisciplinary classification of lung adenocarcinoma. J Thorac Oncol 2011;6:244–85.
9. Jackson EL, Olive KP, Tuveson DA, Bronson R, Crowley D, Brown M, et al. The differential effects of mutant p53 alleles on advanced murine lung cancer. Cancer Res 2005;65:10280–8.
10. Ding L, Getz G, Wheeler DA, Mardis ER, McLellan MD, Cibulskis K, et al. Somatic mutations affect key pathways in lung adenocarcinoma. Nature 2008;455:1069–75.
11. Sanchez-Cespedes M. A role for LKB1 gene in human cancer beyond the Peutz-Jeghers syndrome. Oncogene 2007;26:7825–32.
12. Merlo A, Herman JG, Mao L, Lee DJ, Gabrielson E, Burger PC, et al. 5′ CpG island methylation is associated with transcriptional silencing of the tumour suppressor p16/CDKN2/MTS1 in human cancers. Nat Med 1995;1:686–92.
13. Hassan KA, Chen G, Kalemkerian GP, Wicha MS, Beer DG. An embryonic stem cell-like signature identifies poorly differentiated lung adenocarcinoma but not squamous cell carcinoma. Clin Cancer Res [Internet] 2009;15:6386–90. Available from: http://www.ncbi.nlm.nih.gov/pubmed/19808871.
14. Chiba I, Takahashi T, Nau MM, D'Amico D, Curiel DT, Mitsudomi T, et al. Mutations in the p53 gene are frequent in primary, resected non–small cell lung cancer. Lung Cancer Study Group. Oncogene 1990;5:1603–10.
15. Kalluri R, Weinberg RA. The basics of epithelial-mesenchymal transition. J Clin Invest 2009;119:1420–8.
16. Kruse JP, Gu W. Modes of p53 regulation. Cell 2009;137:609–22.
17. Bryant CM, Albertus DL, Kim S, Chen G, Brambilla C, Guedj M, et al. Clinically relevant characterization of lung adenocarcinoma subtypes based on cellular pathways: an international validation study. PLoS One 2010;5:e11712.
18. Schiller JH, Harrington D, Belani CP, Langer C, Sandler A, Krook J, et al. Comparison of four chemotherapy regimens for advanced non–small-cell lung cancer. N Engl J Med [Internet] 2002;346:92–8. Available from: http://www.ncbi.nlm.nih.gov/entrez/query.fcgi?cmd=Retrieve&db=PubMed&dopt=Citation&list_uids=11784875\nfile://cdhb.local/dfsgeneral/CHC12homelink/DavidG3/Documents/Epapers/Schiller.

19. Yamane Y, Ishii G, Goto K, Kojima M, Nakao M, Shimada Y, et al. A novel histopathological evaluation method predicting the outcome of non–small cell lung cancer treated by neoadjuvant therapy: the prognostic importance of the area of residual tumor. J Thorac Oncol 2010;5:49–55.
20. Chen Z, Akbay E, Mikse O, Tupper T, Cheng K, Wang Y, et al. Co-clinical trials demonstrate superiority of crizotinib to chemotherapy in ALK-rearranged non–small cell lung cancer and predict strategies to overcome resistance. Clin Cancer Res 2014;20:1204–11.
21. Bindea G, Mlecnik B, Fridman WH, Pagès F, Galon J. Natural immunity to cancer in humans. Curr Opin Immunol 2010;22:215–22.
22. Schreiber RD, Old LJ, Smyth MJ. Cancer immunoediting: integrating immunity's roles in cancer suppression and promotion. Science 2011;331:1565–70.
23. Bozic I, Antal T, Ohtsuki H, Carter H, Kim D, Chen S, et al. Accumulation of driver and passenger mutations during tumor progression. Proc Natl Acad Sci U S A 2010;107:18545–50.
24. Zeqiraj E, Filippi BM, Deak M, Alessi DR, van Aalten DMF. Structure of the LKB1-STRAD-MO25 complex reveals an allosteric mechanism of kinase activation. Science 2009;326:1707–11.
25. Oliver TG, Mercer KL, Sayles LC, Burke JR, Mendus D, Lovejoy KS, et al. Chronic cisplatin treatment promotes enhanced damage repair and tumor progression in a mouse model of lung cancer. Genes Dev 2010;24:837–52.
26. Taguchi A, Politi K, Pitteri SJ, Lockwood WW, Faça VM, Kelly-Spratt K, et al. Lung cancer signatures in plasma based on proteome profiling of mouse tumor models. Cancer Cell 2011;20:289–99.

Table S1. K-Ras^{G12V} tumors serially transplanted in Crl:NU-*Foxn1*^{nu} mice and paired derived cell lines.

Tumor	Tumor size [a]	Histological classification of primary K-Ras^{G12V} tumors	Duration of first tumor passage (days)	Median duration of second and third passages [d]	Orthoa-llograft name	Cell line derived
1	+++	Papillary predominant ADC	118	94	*oag-1*	-
2	+++		98	ni	*oag-2*	-
3	+++		118	dead	*oag-3*	-
4	+++		118	dead	*oag-4*	-
5	+++		150	91	*oag-5*	-
6	+++		150	40	*oag-6*	Y[e, f]
7	+++		150	91	*oag-7*	-
8	+		dead [b]	-	-	-
9	+++	Micropapillary predominant ADC	98	24	*oag-8*	Y[e]
10	+++		98	- [c]	*oag-9*	-
11	+++		- [c]	-	-	-
12	+++		98	54	*oag-10*	Y[e, f]
13	+++		45	52	*oag-11*	Y
14	+	Solid predominant ADC	150	91	*oag-12*	-
15	+	Acinar predominant ADC	118	ni	*oag-13*	-
16	+	Micropapillary predominant ADC	118	58	*oag-14*	-
17	+++	Solid predominant ADC	118	ni	*oag-15*	-
18	+++		- [c]	-	-	-
19	+	Solid predominant ADC	- [c]	-	-	-
20	+		- [c]	-	.	-
21	+		- [c]	-	-	-
22	++	Acinar predominant ADC	dead [b]	-	-	-
23	++		150	39	*oag-16*	-
24	+++	Solid predominant ADC	118	ni	*oag-17*	-
25	+	Solid predominant ADC [g]	98	74	*oag-18*	-
26	+		dead [b]	-	-	-
27	+	Micropapillary predominant ADC	98	30	*oag-19*	Y[e, f]
28	+	Papillary predominant ADC [g]	98	37	*oag-20*	Y[e]
29	+++	Solid predominant ADC	98	22	*oag-21*	Y[e, f]
30	+++		- [c]	-	-	-
31	+++		132	46	*oag-22*	Y[e, f]
32	+		- [c]	-	-	-
33	+	Solid predominant ADC	dead [b]	-	-	-
34	+	Micropapillary predominant ADC	98	- [c]	*oag-23*	-
35	+++	Solid predominant ADC [g]	dead [b]	-	-	-
36	+++		98	94	*oag-24*	Y
37	+++		- [c]	-	-	-
38	+	Solid predominant ADC	150	- [c]	*oag-25*	-
39	+		- [c]	-	-	-
40	++	Micropapillary predominant ADC	98	- [c]	*oag-26*	-
41	++	Papillary predominant ADC [g]	98	88	*oag-27*	Y
42	+		- [c]	-	-	-
43	+		- [c]	-	-	-
44	+		dead [b]	-	-	-
45	+		dead [b]	-	-	-
46	+		- [c]	-	-	-

[a] size of K-Ras^{G12V} primary tumors before implantation: +, <2 mm^3 size; ++, 2 to 4 mm^3 size; +++,(> 4 mm^3 size).
[b] dead as a consequence of the surgery procedure
[c] unsuccessful engraftment
[d] median duration of tumor passage #2 and #3; [e] cell line derived from more than one passage
[f] cell line derived from metastatic implant
[g] presence of signet ring cells
ADC, Adenocarcinoma
ni: not re-implanted after passage #1

Table S2. Semiquantitative assessment of the percentages of histologic components in passage #1 engrafted tumors.

Orthoallograft	Histological classification of engrafted tumors	Semiquantitative histologic components					
		Lepidic	Acinar	Papillary	Micropapillary	Solid	Spindle
oag-1	Papillary predominant adenocarcinoma	0	15	70	10	5	0
oag-2	Acinar predominant adenocarcinoma [a]	0	50	0	5	15	30
oag-3	Acinar predominant adenocarcinoma	0	60	15	15	0	10
oag-4	Acinar predominant adenocarcinoma	0	50	0	40	0	10
oag-5	Acinar predominant adenocarcinoma	0	100	0	0	0	0
oag-6	Micropapillary predominant adenocarcinoma	0	10	5	80	5	0
oag-7	Acinar predominant adenocarcinoma	0	50	40	5	5	0
oag-8	Acinar predominant adenocarcinoma [b]	0	50	30	20	0	0
oag-9	Solid predominant adenocarcinoma	0	30	0	0	70	0
oag-10	Micropapillary predominant adenocarcinoma	0	10	0	90	0	0
oag-11	Papillary predominant adenocarcinoma	0	30	40	0	30	0
oag-12	Acinar predominant adenocarcinoma	0	95	0	5	0	0
oag-13	Acinar predominant adenocarcinoma	0	50	20	0	30	0
oag-14	Solid predominant adenocarcinoma [a]	0	0	0	0	100	0
oag-15	Acinar predominant adenocarcinoma	5	95	0	0	0	0
oag-16	Papillary predominant adenocarcinoma	0	10	60	30	0	0
oag-17	Solid predominant adenocarcinoma	0	0	10	90	0	0
oag-18	Solid predominant adenocarcinoma [a]	0	5	5	90	0	0
oag-19	Solid predominant adenocarcinoma	0	5	0	0	80	15
oag-20	Micropapillary predominant adenocarcinoma [a]	0	5	0	90	5	0
oag-21	Acinar predominant adenocarcinoma [a,b]	0	40	0	0	30	30
oag-22	Acinar predominant adenocarcinoma	0	55	5	0	40	0
oag-23	Acinar predominant adenocarcinoma [a]	0	50	10	0	0	40
oag-24	Solid poorly differentiated adenocarcinoma with spindle cell features	0	0	0	0	0	100
oag-25	Acinar predominant adenocarcinoma	0	90	0	5	5	0
oag-26	Solid predominant adenocarcinoma [b]	0	0	0	0	100	0
oag-27	Micropapillary predominant adenocarcinoma [a]	0	35	0	40	0	25

[a] Presence of signet ring cells

[b] Lymph-node affection or presence of diaphragmatic invasion

Table S3. EML4-ALK tumors orthotopically implanted in Crl:NU-*Foxn1*^{nu} mice.

Number of nude mice implanted	Histological classification of engrafted EML4-ALK tumors	Semiquantitative histologic components [a]				Serial passage		
		Acinar	Papillary	Micropapillary	Solid	#1	#2	#3
	Tg EML4-ALK ; p53 -/-							
1	Predominant papillary adenocarcinoma	40	60	0	0	70	32	29
2	Predominant papillary adenocarcinoma	0	100	0	0	85	47	35
3	No engraftment							
4	Predominant papillary adenocarcinoma	0	100	0	0	103	28	25
5	Predominant solid adenocarcinoma	20	0	0	80	103	42	45
6	No engraftment					-		
7	No engraftment					-		
8	Predominant papillary adenocarcinoma	0	80	0	20	76	69	54
9	Predominant papillary adenocarcinoma	0	80	0	20	103	28	35
10	Predominant papillary adenocarcinoma	0	60	0	40	103	28	35
11	Predominant acinar adenocarcinoma	80	0	10	10	103	28	21
12	Predominant solid adenocarcinoma	0	0	0	100	50	60	35
	Tg EML4-ALK ; p53 +/+							
13	No engraftment					-		
14	No engraftment					-		
15	Predominant papillary adenocarcinoma	20	80	0	0	115	109	91
16	No engraftment					-		
17	No engraftment					-		
18	No engraftment					-		
19	Predominant papillary adenocarcinoma	0	100	0	0	103	82	96
20	No engraftment					-		
21	Predominant solid adenocarcinoma	0	0	0	100	103	92	76
22	Predominant solid adenocarcinoma	0	0	0	100	103	83	dead
23	No engraftment					-		

[a] Lepidic and sarcomatoid components were not identified.

Table S4. Histologic progression of orthoallografts upon sequential mice-to-mice passages.

Orthoallograft	Passage	Histological classification of engrafted tumors	Histological subtypes					
			Lepidic	Acinar	Papillary	Micropapillary	Solid	Spindle
oag-8	#1	Acinar predominant adenocarcinoma	0	50	5	5	40	0
	#2	Solid predominant adenocarcinoma	0	30	0	0	70	0
	#3 [a]	Solid predominant adenocarcinoma	0	0	0	0	70	30
	#3 [a]	Solid predominant adenocarcinoma	0	20	0	0	70	10
	#3 [a]	Solid predominant adenocarcinoma	0	5	0	0	75	20
oag-10	#1	Micropapillary predominant adenocarcinoma	0	10	0	90	0	0
	#3 [a]	Solid predominant adenocarcinoma	0	30	10	0	60	0
	#3 [a]	Acinar predominant adenocarcinoma	0	50	40	10	0	0
oag-14	#1	Solid predominant adenocarcinoma [b]	0	0	0	0	100	0
	#3	Solid predominant adenocarcinoma [b]	0	30	0	10	60	0
oag-19	#1	Solid predominant adenocarcinoma	0	5	0	0	80	15
	#2	Solid predominant adenocarcinoma	0	15	0	0	85	0
	#3	Solid predominant adenocarcinoma	0	5	0	5	85	5
	#4	Solid predominant adenocarcinoma	0	5	0	0	95	0
oag-21	#1	Acinar predominant adenocarcinoma	0	40	0	0	30	30
	#2	Adenocarcinoma with predominant spindle cell features	0	20	0	0	30	50
	#3	Solid predominant adenocarcinoma	0	25	0	5	70	0
	#4	Solid predominant adenocarcinoma	0	10	0	0	90	0
oag-22	#1	Acinar predominant adenocarcinoma	0	55	5	0	40	0
	#2	Acinar predominant adenocarcinoma	0	50	30	0	20	0
	#3	Acinar predominant adenocarcinoma	0	60	15	0	25	0

[a] Independent tumors derived from same passage implant.

[b] Presence of signet ring cells

Table S5. Presence of distal metastasis in animals implanted with the indicated orthoallografts.

Lung orthoallograft	Presence of metastasis
oag-1	-
oag-2	-
oag-3	-
oag-4	-
oag-5	-
oag-6	-
oag-7	-
oag-8	Liver
oag-9	-
oag-10	Liver; Brain
oag-11	-
oag-12	-
oag-13	-
oag-14	Liver
oag-15	-
oag-16	-
oag-17	-
oag-18	Liver
oag-19	Liver, Brain
oag-20	-
oag-21	Liver
oag-22	-
oag-23	-
oag-24	-
oag-25	-
oag-26	-
oag-27	Liver

Table S6. Summary of primary cell lines obtained from the indicated orthoallograft implants.

Orthoallograft	Passage	Predominant histology of orthoallografts	Derived cell line	Paired metastatic derived cell line
oag-6	#2	Micropapillary predominant adenocarcinoma	mKLC1.7B	-
	#3	Micropapillary predominant adenocarcinoma	mKLC1.7C	-
oag-8	#1	Acinar predominant adenocarcinoma	mKLC2.1A	-
	#2	Solid predominant adenocarcinoma	mKLC2.1B	-
	#3	Solid predominant adenocarcinoma	mKLC2.1C	mKLC2.1C-DI
				mKLC2.1C-RI
				mKLC2.1C-HI
				mKLC2.1C-MD
oag-10	#1	Micropapillary predominant adenocarcinoma	mKLC2.4A	-
	#2	Micropapillary predominant adenocarcinoma	mKLC2.4B	mKLC2.4B-HM
oag-11	#1	Papillary predominant adenocarcinoma	mKLC2.5A	-
oag-19	#1	Solid predominant adenocarcinoma	mKLC4.1A	mKLC5A-DI
	#3	Solid predominant adenocarcinoma	mKLC4.1C	mKLC5C-DI
oag-20	#2	Micropapillary predominant adenocarcinoma	mKLC4.2B	-
	#3	Solid predominant adenocarcinoma	mKLC4.2C	-
oag-21	#1	Acinar predominant adenocarcinoma	mKLC4.3A	mKLC7A-DI
	#2	Adenocarcinoma with predominant spindle cell features	mKLC4.3B	mKLC7B-DI
	#3	Solid predominant adenocarcinoma	mKLC4.3C	-
	#4	Solid predominant adenocarcinoma	mKLC4.3D	mKLC4.3D-DI
				mKLC4.3D-RI
				mKLC4.3D-HI
				mKLC4.3D-MD
oag-22	#2	Acinar predominant adenocarcinoma	mKLC4.5B	-
	#3	Acinar predominant adenocarcinoma	mKLC4.5C	mKLC4.5C-DI1
				mKLC4.5C-DI2
oag-24	#1	Solid poorly differentiated adenocarcinoma with spindle cell features	mKLC1.4A	-
oag-27	#1	Micropapillary predominant adenocarcinoma	mKLC2.5A	-

-DI, diaphragmatic implants; -RI, rib implants; -HI, heart implants; MD, mediastinic lymph-node; -HM, hepatic metastasis.

Table S7. Histopathological characterization of EML4-ALK implants after crizotinib treatment.

	Mice	Tumor histology	% of tumor cells	% of fibrosis	% of necrosis	Foamy macrophages	Inflammation	Hemosiderin	Tumor viable post-treatment
Cohort 1									
Placebo	1	Micropapillary	100	0	0	No	No	No	Yes
	2	Micropapillary	100	0	0	No	No	No	Yes
	3	Micropapillary	90	10	0	No	No	No	Yes
	4	Micropapillary	100	0	0	No	No	No	Yes
	5	Micropapillary	85	15	0	No	No	No	Yes
Crizotinib	1	Micropapillary	90	10	0	No	Yes	No	Yes
	2	Micropapillary	95	5	0	Yes	Yes	Yes	Yes
	3	Micropapillary	30	70	0	Yes	Yes	Yes	Yes
	4	Micropapillary	0	100	0	Yes	Yes	Yes	No
	5	Micropapillary	100	0	0	No	No	No	Yes
	6	Micropapillary	90	10	0	Yes	Yes	No	Yes
Cohort 2									
Placebo	1	Micropapillary/Acinar	80	20	0	Yes	Yes	No	Yes
	2	Micropapillary/Acinar	95	5	0	Yes	Yes	No	Yes
	3	Micropapillary/Acinar	95	5	0	Yes	Yes	Yes	Yes
	4	Micropapillary/Acinar	80	20	0	Yes	Yes	No	Yes
Crizotinib	1	Micropapillary/Acinar	50	50	0	Yes	Yes	Yes	Yes
	2	Micropapillary/Acinar	50	50	0	Yes	Yes	Yes	Yes
	3	Micropapillary/Acinar	40	50	10	Yes	Yes	Yes	Yes
	4	Micropapillary/Acinar	0	60	40	Yes	Yes	Yes	Yes
	5	Acinar	20	20	60	Yes	Yes	Yes	Yes
	6	Acinar	20	20	60	Yes	Yes	Yes	Yes

Supplementary Materials

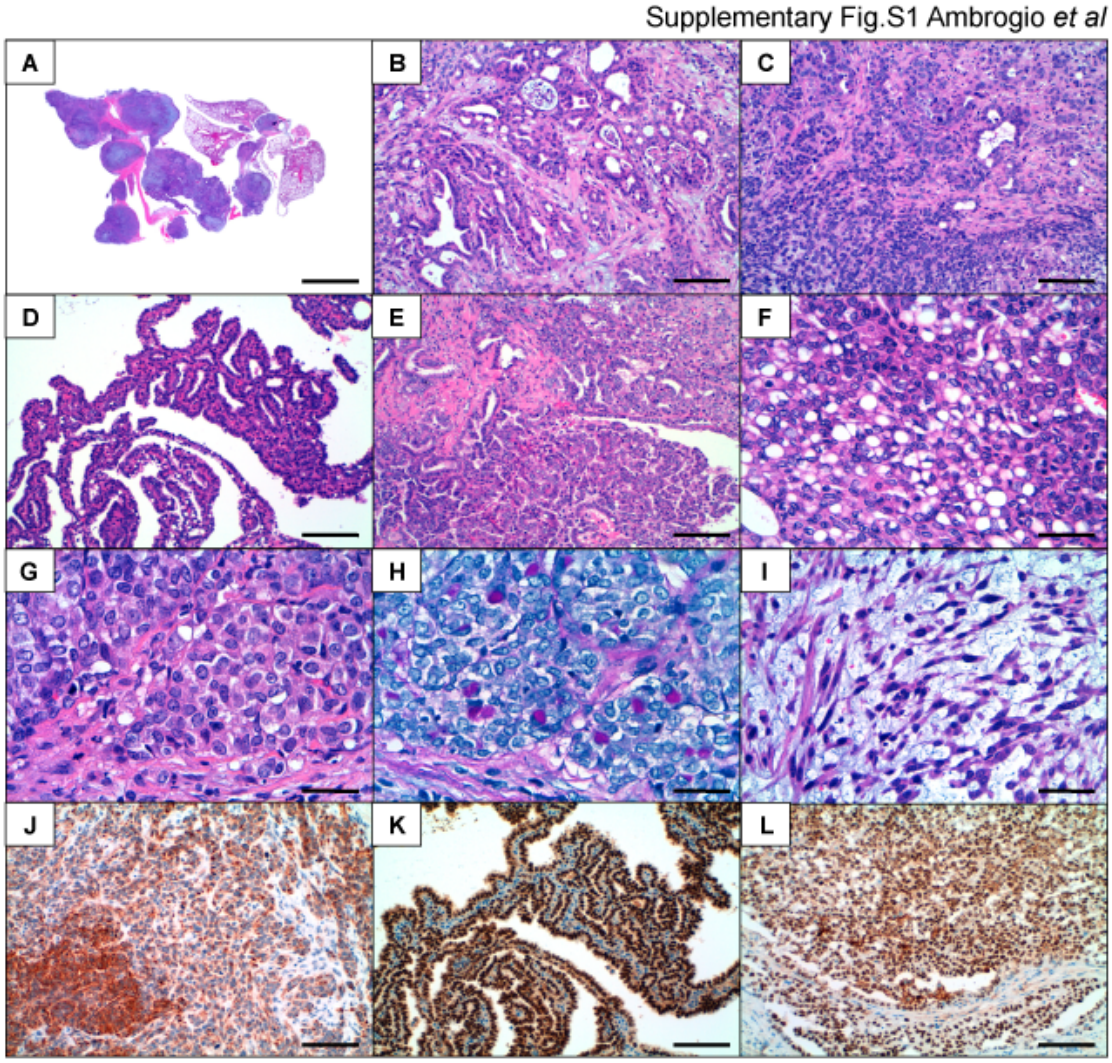

Fig. S1. Common histological subtypes of NSCLC orthoallografts.

Passage #1 orthoallografts derived from *K-Ras*$^{lox/LSLG12V}$; RERT$^{ert/ert}$ primary tumors after implantation into recipient nude mice. Engrafted tumors reproduce the major histological subtypes of human invasive lung adenocarcinoma. **A)** H&E staining of a representative engrafted tumor that shows invasion of the host lung. **B)** Acinar

adenocarcinoma consists of round to oval-shaped malignant glands invading a fibrous stroma. **C)** Papillary adenocarcinoma with contribution of solid adenocarcinoma. **D)** Pure papillary adenocarcinoma. **E)** Adenocarcinoma with areas of acinar and micropapillary subtypes. **F**) Adenocarcinoma with signet ring cell features. **G)** Solid adenocarcinoma with mucin component. **H)** Diastase-periodic acid Schiff (DPAS) staining to highlight the intracytoplasmatic mucin droplets in solid adenocarcinoma. **I)** Poorly differentiated adenocarcinoma with spindle cell features and sarcomatoid appearance. **J)** Cytokeratin 7 immunohistochemical staining in predominant solid adenocarcinoma with acinar component. **K)** Thyroid transcription factor-1 (TTF-1) immunohistochemical staining in papillary adenocarcinoma. **L)** TTF1 immunohistochemical staining in solid adenocarcinoma. Scale bars 100 µm except panel A (1 mm) and G, H, I (50 µm).

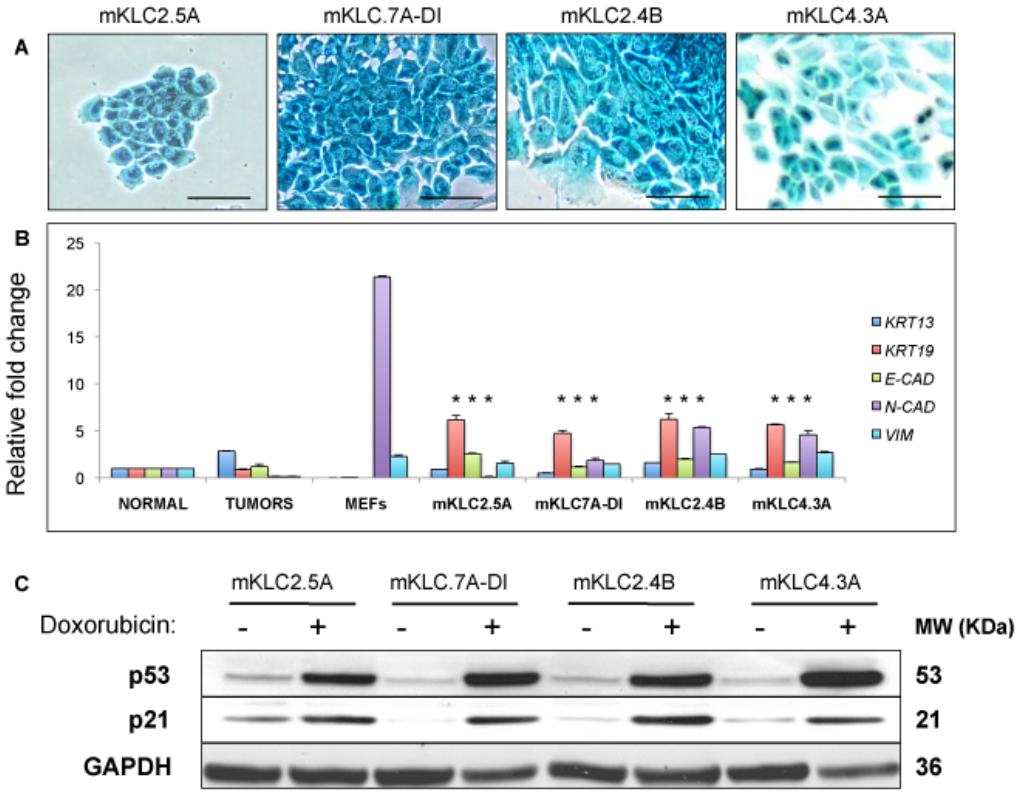

Fig. S2. *In vitro* characterization of primary cell lines derived from NSCLC orthoallografts.

A) Detection of K-Ras^{G12V} expression (based on its surrogate marker ß-Geo) by X-Gal staining in the indicated primary mKLC cell lines. Scale bar: 40 microns. **B)** qRT-PCR of the cytokeratins 13 and 19, N- and E-cadherin and vimentin in the indicated mKLC cell lines. Samples from murine normal lung, *K-Ras*$^{lox/LSLG12Vgeo}$ NSCLC primary tumors and mouse embryonic fibroblasts (MEFs) were assessed in parallel for comparative purposes. **C)** Western blot analysis of p53 and p21 in lysates prepared from the indicated mKLC cell lines in the presence or absence of doxorubicin. GAPDH is shown as a loading control. * indicates p-value < 0.01.

Supplementary Fig.S3 Ambrogio *et al*

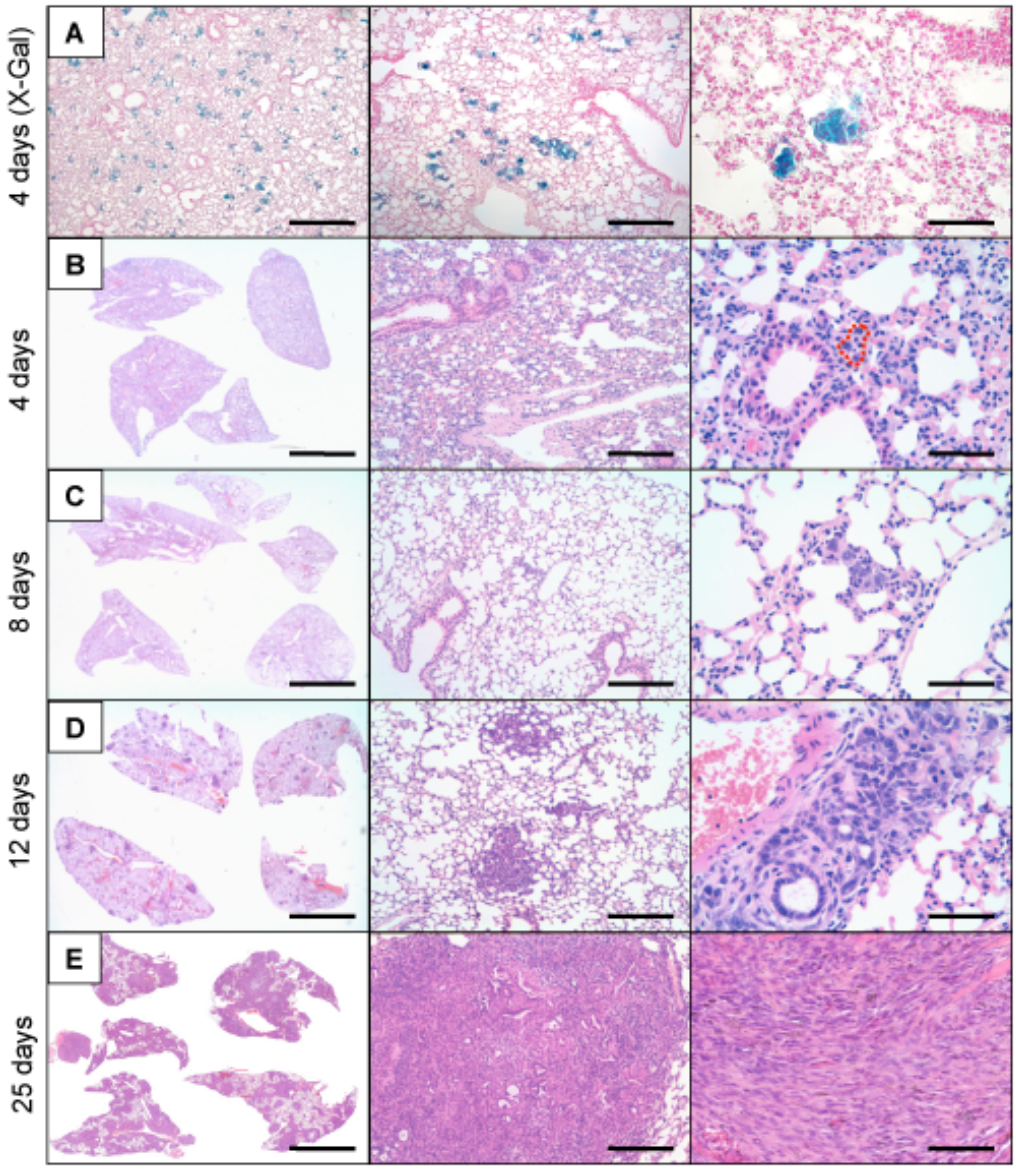

Fig. S3. Lung colonization and tumor formation upon reintroduction of mKLC cell lines.

A cohort of recipient nude mice (n=3 per time point) was inoculated with 10^6 mKLC cells (3 independent cell lines) via tail vein injection. Lung tissue was collected at 4, 8, 12, and 25 days post-injection and tissue sections stained with H&E **A)** X-Gal staining of lung sections after 4 days to facilitate detection of mKLC cells. **B)** Small clusters of tumor cells (marked by a red dashed line) were observed after 4 days. **C)** Presence of clusters of scattered atypical cells identified after 8 days. **D)** Small nodules of tumor cells with focal acinar differentiation observed at 12 days post-injection. **E)** Confluent tumor nodules including both acinar and solid components observed at humane end point (25 days after injection). Images of increasing magnification are shown from left to right, scale bars: left column 2 mm (except upper panel 400 µm), middle column 200 µm, right column 100 µm.

Supplementary Fig.S4 Ambrogio *et al*

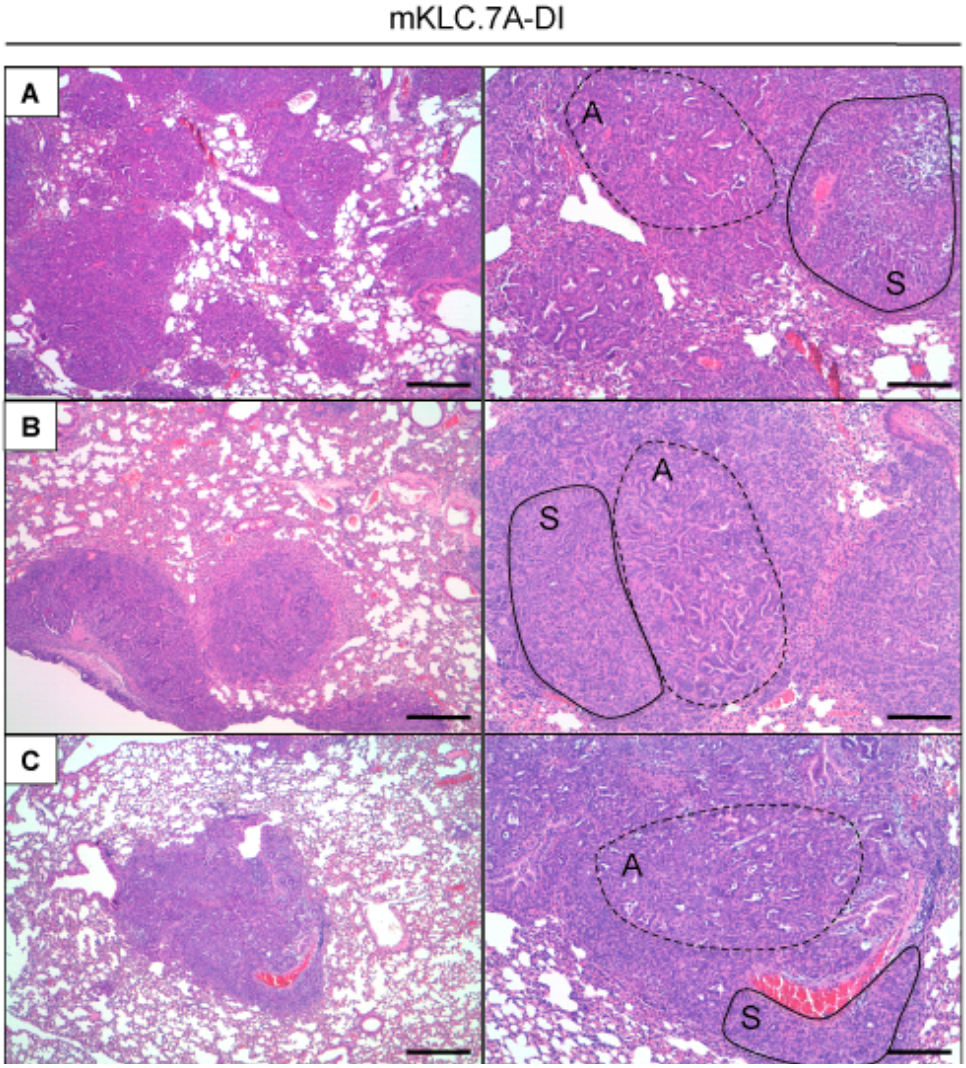

Fig. S4. Inoculation of mKLC single cell clones gives rise to NSCLC heterogeneity *in vivo.*

Representative H&E staining of lung tumors developed following tail vein injection of three independent cell lines **(A-C)** derived upon single cell cloning of mKLC.7A-DI. The presence of mixed solid (S) and acinar (A) histopathological component is indicated in the right panels. Scale bars 400 μm (left panels), 200 μm (right panels).

Supplementary Figure Legend

Figure S1. Common histological subtypes of NSCLC orthoallografts.
Passage #1 orthoallografts derived from *K-Ras*$^{lox/LSLG12V}$; RERT$^{ert/ert}$ primary tumors after implantation into recipient nude mice. Engrafted tumors reproduce the major histological subtypes of human invasive lung adenocarcinoma. **A)** H&E staining of a representative engrafted tumor that shows invasion of the host lung. **B)** Acinar adenocarcinoma consists of round to oval-shaped malignant glands invading a fibrous stroma. **C)** Papillary adenocarcinoma with contribution of solid adenocarcinoma. **D)** Pure papillary adenocarcinoma. **E)** Adenocarcinoma with areas of acinar and micropapillary subtypes. **F**) Adenocarcinoma with signet ring cell features. **G)** Solid adenocarcinoma with mucin component. **H)** Diastase-periodic acid Schiff (DPAS) staining to highlight the intracytoplasmatic mucin droplets in solid adenocarcinoma. **I)** Poorly differentiated adenocarcinoma with spindle cell features and sarcomatoid appearance. **J)** Cytokeratin 7 immunohistochemical staining in predominant solid adenocarcinoma with acinar component. **K)** Thyroid transcription factor-1 (TTF-1) immunohistochemical staining in papillary adenocarcinoma. **L)** TTF1 immunohistochemical staining in solid adenocarcinoma. Scale bars 100 μm except panel A (1 mm) and G, H, I (50 μm).

Figure S2. *In vitro* characterization of primary cell lines derived from NSCLC orthoallografts.
A) Detection of K-Ras^{G12V} expression (based on its surrogate marker ß-Geo) by X-Gal staining in the indicated primary mKLC cell lines. Scale bar: 40 microns. **B)** qRT-PCR of the cytokeratins 13 and 19, N- and E-cadherin and vimentin in the indicated mKLC cell lines. Samples from murine normal lung, *K-Ras*$^{lox/LSLG12Vgeo}$ NSCLC primary tumors and mouse embryonic fibroblasts (MEFs) were assessed in parallel for comparative purposes. **C)** Western blot analysis of p53 and p21 in lysates prepared from the indicated mKLC cell lines in the presence or absence of doxorubicin. GAPDH is shown as a loading control. * indicates p-value < 0.01.

Figure S3. Lung colonization and tumor formation upon reintroduction of mKLC cell lines.

A cohort of recipient nude mice (n=3 per time point) was inoculated with 10_6 mKLC cells (3 independent cell lines) via tail vein injection. Lung tissue was collected at 4, 8, 12, and 25 days post-injection and tissue sections stained with H&E **A)** X-Gal staining of lung sections after 4 days to facilitate detection of mKLC cells. **B)** Small clusters of tumor cells (marked by a red dashed line) were observed after 4 days. **C)** Presence of clusters of scattered atypical cells identified after 8 days. **D)** Small nodules of tumor cells with focal acinar differentiation observed at 12 days post-injection. **E)** Confluent tumor nodules including both acinar and solid components observed at humane end point (25 days after injection). Images of increasing magnification are shown from left to right, scale bars: left column 2 mm (except upper panel 400 µm), middle column 200 µm, right column 100 µm.

Figure S4. Inoculation of mKLC single cell clones gives rise to NSCLC heterogeneity *in vivo*.

Representative H&E staining of lung tumors developed following tail vein injection of three independent cell lines **(A-C)** derived upon single cell cloning of mKLC.7A-DI. The presence of mixed solid (S) and acinar (A) histopathological component is indicated in the right panels. Scale bars 400 µm (left panels), 200 µm (right panels).

ARTICLE 4:

Devis-Jauregui, L*; **Vidal, A.***; Plata-Peña, L.*; Santacana, M.; García-Mulero, S.; Bonifaci, N.; Noguera-Delgado, E.; Ruiz, N.; Gil, M.; Dorca, E.; Llobet, F.J.; Coll-Iglesias, L.; Gassner, K.; Martinez-Iniesta, M.; Rodriguez-Barrueco, R.; Barahona, M.; Marti, L.; Viñals, F.; Ponce, J.; Sanz-Pamplona, R.; Piulats, J.M.; Vivancos, A.; Matias-Guiu, X.; Villanueva, A.; Llobet-Navas, D. Generation and Integrated Analysis of Advanced Patient-Derived Orthoxenograft Models (PDOX) for the Rational Assessment of Targeted Therapies in Endometrial Cancer. Advanced Science 2023; 10: 2204211.

RESUM

Objectius:

1. Generació i caracterització clinicopatològica de models PDOX/Orthoxenografts de carcinoma endometrioide d'endometri.
2. Utilització dels PDOX de carcinoma endometrioide d'endometri per a dissenyar de manera racional una teràpia dirigida a partir de la caracterització transcriptòmica i del perfil mutacional d'aquests models.

Introducció: El maneig clínic del càncer d'endometri (CE) es veu limitat per la reduïda disponibilitat de tractaments de segona línia així como de biomarcadors moleculars que ens permetin predir la recurrència. Aquestes limitacions han dificultat el tractament d'aquestes pacients i les taxes de supervivència no han millorat en les darreres quatre dècades.

Disseny experimental: L'aparició d'estudis coordinats com *The Cancer Genome Atlas Uterine Corpus Endometrial Carcinoma* (TCGA_UCEC) ha solucionat parcialment aquest problema, però la manca de bons models experimentals encara representa un coll d'ampolla que impedeix que els estudis translacionals es puguin traduir en la millora del tractament de les pacients amb CE. En aquest context, es presenta el primer estudi que reporta la generació d'una col·lecció de models murins *orthoxenograft* derivats de pacients amb CE de tipus

endometrioide (PDOX). Aquests models ens han de permetre superar aquestes limitacions experimentals, obrint el camí cap a una medicina de precisió d'última generació en CE.

Resultats: La col·lecció de 15 tumors primaris i PDOX derivats i perpetuats en ratolins s'ha caracteritzat extensivament mitjançant un enfocament integratiu basat en transcriptòmica, perfils mutacionals i anàlisi morfològica. Els tumors de CE implantats en l'úter de ratolins (implantació ortotòpica) conserven les principals característiques moleculars i morfològiques dels tumors originals de les pacients. Com a prova de concepte, en un dels PDOX que té la mutació $HER2^{R678Q}$ hem avaluat el potencial terapèutic del trastuzumab, un inhibidor del receptor 2 del factor de creixement epidèrmic humà (HER2) amb un interès creixent en CE.

Conclusions: Les nostres dades indiquen que els models PDOX derivats de càncer d'endometri de pacients representen eines adequades per a millorar recerca del càncer d'endometri en els propers anys.

RESEARCH ARTICLE

ADVANCED SCIENCE Open Access

www.advancedscience.com

Generation and Integrated Analysis of Advanced Patient-Derived Orthoxenograft Models (PDOX) for the Rational Assessment of Targeted Therapies in Endometrial Cancer

Laura Devis-Jauregui, August Vidal, Laura Plata-Peña, Maria Santacana, Sandra García-Mulero, Nuria Bonifaci, Eulàlia Noguera-Delgado, Nuria Ruiz, Marta Gil, Eduard Dorca, Francisco J. Llobet, Laura Coll-Iglesias, Katja Gassner, Maria Martinez-Iniesta, Ruth Rodriguez-Barrueco, Marc Barahona, Lola Marti, Francesc Viñals, Jordi Ponce, Rebeca Sanz-Pamplona, Josep M. Piulats, Ana Vivancos, Xavier Matias-Guiu, Alberto Villanueva,* and David Llobet-Navas**

Clinical management of endometrial cancer (EC) is handicapped by the limited availability of second line treatments and bona fide molecular biomarkers to predict recurrence. These limitations have hampered the treatment of these patients, whose survival rates have not improved over the last four decades. The advent of coordinated studies such as The Cancer Genome Atlas Uterine Corpus Endometrial Carcinoma (TCGA_UCEC) has partially solved this issue, but the lack of proper experimental systems still represents a bottleneck that precludes translational studies from successful clinical testing in EC patients. Within this context, the first study reporting the generation of a collection of endometrioid-EC-patient-derived orthoxenograft (PDOX) mouse models is presented that is believed to overcome these experimental constraints and pave the way toward state-of-the-art precision medicine in EC. The collection of primary tumors and derived PDOXs is characterized through an integrative approach based on transcriptomics, mutational profiles, and morphological analysis; and it is demonstrated that EC tumors engrafted in the mouse uterus retain the main molecular and morphological features from analogous tumor donors. Finally, the molecular properties of these tumors are harnessed to assess the therapeutic potential of trastuzumab, a human epidermal growth factor receptor 2 (HER2) inhibitor with growing interest in EC, using patient-derived organotypic multicellular tumor spheroids and in vivo experiments.

1. Introduction

Epidemiological data from cancer registry programs indicate that, between 1975 and 2014, 5-year survival rates have improved for the most common cancers except for cervix and endometrial cancer, greatly evidencing the need to find more efficient therapeutic options for these patients.[1] Endometrial cancer (EC) is the most common gynecological cancer in developed countries, standing as the 4th most frequent and the 6th most deadliest type of tumor in women in the Unites States.[2] Not surprisingly, the number of new cases and deaths for EC in 2020 worldwide were estimated as 417 367 and 97 370, respectively,[3] and current trends indicate that EC incidence and death rates are further increasing in part due to the rise of predisposing risk factors, especially those related to metabolic syndrome such as obesity.[2,4,5]

In general, the prognosis and clinical course for most EC patients is favorable. Accordingly, the majority of them (≈75%) present localized early disease symptomatology, such as vaginal bleeding or

The ORCID identification number(s) for the author(s) of this article can be found under https://doi.org/10.1002/advs.202204211

DOI: 10.1002/advs.202204211

L. Devis-Jauregui, L. Plata-Peña, E. Noguera-Delgado, F. J. Llobet, L. Coll-Iglesias, K. Gassner, R. Rodriguez-Barrueco, X. Matias-Guiu, D. Llobet-Navas
Molecular Mechanisms and Experimental Therapy in Oncology-Oncobell Program
Bellvitge Biomedical Research Institute (IDIBELL)
L'Hospitalet de Llobregat
Barcelona 08908, Spain
E-mail: xmatias@bellvitgehospital.cat dllobet@idibell.cat

discharge, which favors early stage diagnosis and curative surgery leading to 5-year overall survival rates of 80–95%. Nevertheless, around 15–20% of EC patients will experience tumor recurrence, largely impacting treatment options and patient survival.[6,7] Adjuvant therapeutic options for recurred, as well as for advanced or metastatic, EC patients are very limited and encompass the delivery of standard chemotherapy, mainly platinum or paclitaxel. However, treatment resistance is unfortunately common and only 10–15% of all EC patients will benefit from it.[8] This is worsened by the limited availability of established second line treatments, validated patient selection protocols, and licensed targeted drugs for EC.[9] Consequently, the prognosis of patients with recurred or metastatic EC is still poor with median survival rates of less than one year and median progression free survival rates of four months.[10] Altogether, these data indicate that EC patients presenting refractory or systemic disease represent nowadays a therapeutic challenge, which is aggravated by the limited response rates associated to current adjuvant chemotherapy.

In the last years, patient-derived xenograft (PDX) models have emerged as powerful tools in cancer research.[11–13] PDX models have been revealed as extraordinary accurate preclinical models with a high predictive drug-response value[14] by outperforming regular in vitro cell line models and cell-line-derived xenografts because of their ability to retain, among others, essential tumor traits from the original tissue donor such as tumor heterogeneity, molecular fingerprints (genetic and transcriptomic), tissue architecture, spatial distribution, and cell-to-cell interactions. Not surprisingly, a high correlation between PDX and patient response has been observed when PDXs were included in clinical or coclinical trials,[11,15,16] offering the potential to increase the success rate of compound approval after assessment in patient clinical trials. Altogether, this analytical strategy has become an innovative resource to fine-tune treatment decisions in the future and to accelerate drug development and personalized medicine by complementing pathology and molecular analysis.

Herein, we expand our knowledge on the therapeutic potential and value of this experimental system by generating and profiling a collection of patient-derived orthoxenografts (PDOXs) from 15 endometrioid endometrial cancer patients. We provide evidence that EC tissue orthotopic engraftment in mice retains most of the histological, genetic, and transcriptomic features of patient donors. Moreover, by leveraging this information, we have assessed the therapeutic utility of trastuzumab (a human epidermal growth factor receptor 2, HER2 inhibitor) in HER2-mutated tumors, collectively demonstrating the relevance of PDOX models to explore new therapeutic avenues for EC patients. Finally, we also show that PDOXs are dynamic entities and that, as such, can exhibit intriguing evolutionary features such as dedifferentiation as they progress in vivo.

A. Vidal, N. Ruiz, E. Dorca, X. Matias-Guiu
Department of Pathology
University Hospital of Bellvitge
Bellvitge Biomedical Research Institute (IDIBELL)
L'Hospitalet de Llobregat
Barcelona 08908, Spain

M. Santacana, X. Matias-Guiu
Scientific and Technical Service of Immunohistochemistry
Lleida Institute for Biomedical Research Dr. Pifarré Foundation
IRBLleida
Hospital Universitari Arnau de Vilanova
Lleida 25198, Spain

M. Santacana, X. Matias-Guiu
Department of Pathology
Universitat de Lleida/Institut de Recerca Biomèdica de Lleida/Hospital Universitari Arnau de Vilanova
Lleida 25198, Spain

S. García-Mulero, R. Sanz-Pamplona
Unit of Biomarkers and Susceptibility
Oncology Data Analytics Program (ODAP)
Catalan Institute of Oncology (ICO)
Oncobell Program
Bellvitge Biomedical Research Institute (IDIBELL) and CIBERESP
L'Hospitalet de Llobregat
Barcelona 08908, Spain

N. Bonifaci, X. Matias-Guiu
Department of Basic Sciences
Universitat de Lleida/Institut de Recerca Biomèdica de Lleida
Edifici Biomedicina I, Lab 2.4, Lleida 25198, Spain

N. Bonifaci, K. Gassner, J. M. Piulats, X. Matias-Guiu, D. Llobet-Navas
Centro de Investigación Biomédica en Red de Cáncer (CIBERONC)
Instituto de Salud Carlos III
(ISCIII)
Madrid 28029, Spain

M. Gil, J. M. Piulats
Catalan Institute of Oncology (ICO)
Bellvitge Biomedical Research Institute (IDIBELL)
L'Hospitalet de Llobregat Barcelona
Barcelona 08908, Spain

M. Martinez-Iniesta, F. Viñals, A. Villanueva
Chemoresistance and Predictive Factors Group
Program Against Cancer Therapeutic Resistance (ProCURE)
Catalan Institute of Oncology (ICO)
Bellvitge Biomedical Research Institute (IDIBELL)
L'Hospitalet de Llobregat
Barcelona 08908, Spain
E-mail: avillanueva@iconcologia.net

R. Rodriguez-Barrueco
Anatomy Unit
Department of Pathology and Experimental Therapy
School of Medicine
University of Barcelona (UB)
L'Hospitalet de Llobregat
Barcelona 08907, Spain

M. Barahona, L. Marti, J. Ponce
Department of Gynaecology
University Hospital of Bellvitge
Bellvitge Biomedical Research Institute (IDIBELL)
L'Hospitalet de Llobregat
Barcelona 08908, Spain

F. Viñals
Department of Physiological Sciences
School of Medicine
University of Barcelona (UB)
L'Hospitalet de Llobregat
Barcelona 08907, Spain

A. Vivancos
Cancer Genomics Group
Vall d'Hebron Institute of Oncology (VHIO)
Barcelona 08035, Spain

A. Villanueva
Xenopat S.L.
Parc Cientific de Barcelona (PCB)
Barcelona 08028, Spain

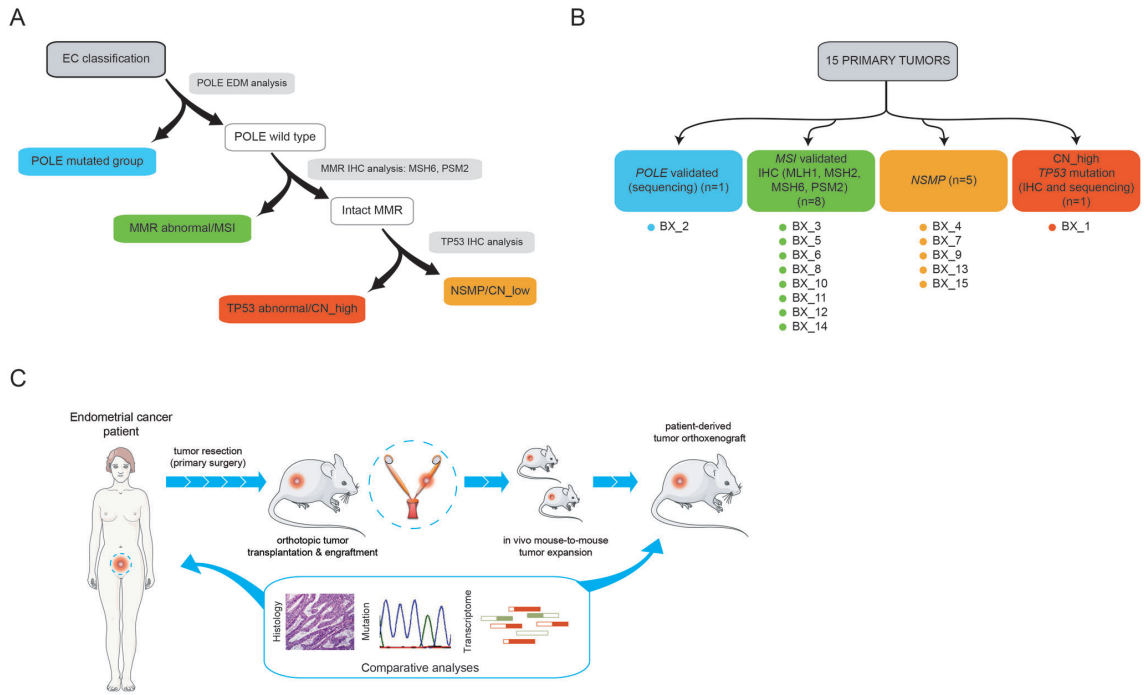

Figure 1. Initial patient sample analysis, characterization, and strategy used for PDOX generation. A) Schematic overview of standard procedures during EC sample pathologic assessment. In a first triage, samples are assessed for the presence of POLE exonuclease domain mutations (EDM) at exons 9 and 13 by targeted DNA sequencing. Wild type POLE EC samples are then analyzed by immunohistochemistry to assess the levels of mismatch repair genes (MMR) as a diagnostic surrogate of the MSI molecular subtype. MMR proficient tumors are then subjected to an analysis by immunohistochemistry of *TP53* protein levels. As in the case of MMR genes, high levels of *TP53* are used as a nonperfect surrogate marker of *TP53*-mutated EC and CN-high tumors. Tumors that do not fall into any category are collectively called NSMP (nonspecific molecular profile, low copy number, microsatellite stable (MSS)). B) Schematic overview of the TCGA_UCEC-based molecular classification of primary tumors used in this study. C) Establishment of PDOX models for preclinical treatment in endometrial cancer overview. Resected fragments of endometrial cancer tumor were orthotopically injected into athymic mice uteruses. To test the reproducibility of patient features in the mouse model, primary tumors and established PDOXs were characterized by immunohistochemistry, RNA-seq, and mutational analyses. Parts of the Figure 1c were drawn by using pictures from Servier Medical Art. Servier Medical Art by Servier is licensed under a Creative Commons Attribution 3.0 Unported License (https://creativecommons.org/licenses/by/3.0/).

2. Results

2.1. Patient Description and Establishment of PDOXs

In our study, we prospectively recruited 15 patients diagnosed with EC of endometrioid morphology, the most frequent EC histological subtype, who underwent primary surgical resection at the Hospital Universitari de Bellvitge/Bellvitge Hospital (HUB) (Tables S1 and S2, Supporting Information). Detailed histological analysis determined that 14 patients (93.3%) presented endometroid endometrial cancer (EEC) with the exception of 1 patient (6.7%) who presented a mixed endometroid–serous carcinoma (90% endometrioid; 10% serous). Most patients were diagnosed at stage I (12/15; 80%) and presented well or moderately differentiated tumors (10/15; 66.7%). Seven patients (46.7%) did not receive any additional treatment after primary surgery and 7/15 patients (46.7%) were treated with brachytherapy +/− radiotherapy. Two patients (13.3%) presented recurrence and 1 of these patients died of the disease (6.7%). Median follow-up time was 59.27 months (47.30–71.23 months). Among the two patients who suffered recurrence, patient 5 (biopsy BX5) was diagnosed at stage IB of the disease with grade 3 (G3) EEC and, in addition to surgery, received a combination of radiotherapy and brachytherapy as adjuvant treatment. Patient 9 (BX9) was diagnosed at stage IA G1 and did not receive adjuvant treatment. Following the HUB standard pathological analysis based on morphological features and TCGA molecular EC biomarkers (**Figure 1**A), primary tumors were classified into polymerase epsilon mutated (POLE-mutated), tumors presenting microsatellite instability (MSI), nonspecific molecular profile; low copy number or microsatellite stable (MSS) (NSMP), and *TP53*-mutated (serous-like, high copy number) (Figure 1B).

To generate the PDOX models, nonnecrotic tissue fragments from EC resected tumors were stored in supplemented medium and immediately implanted into recipient uteruses of immunodeficient mouse females in order to preserve cell viability (Figure 1C). Tumor growth was monitored twice per week with an engraftment average time (engraftment to early passage P1 tumors) of 102.47 days (84.57–120.36). Once the PDOX models were established, we performed histological,

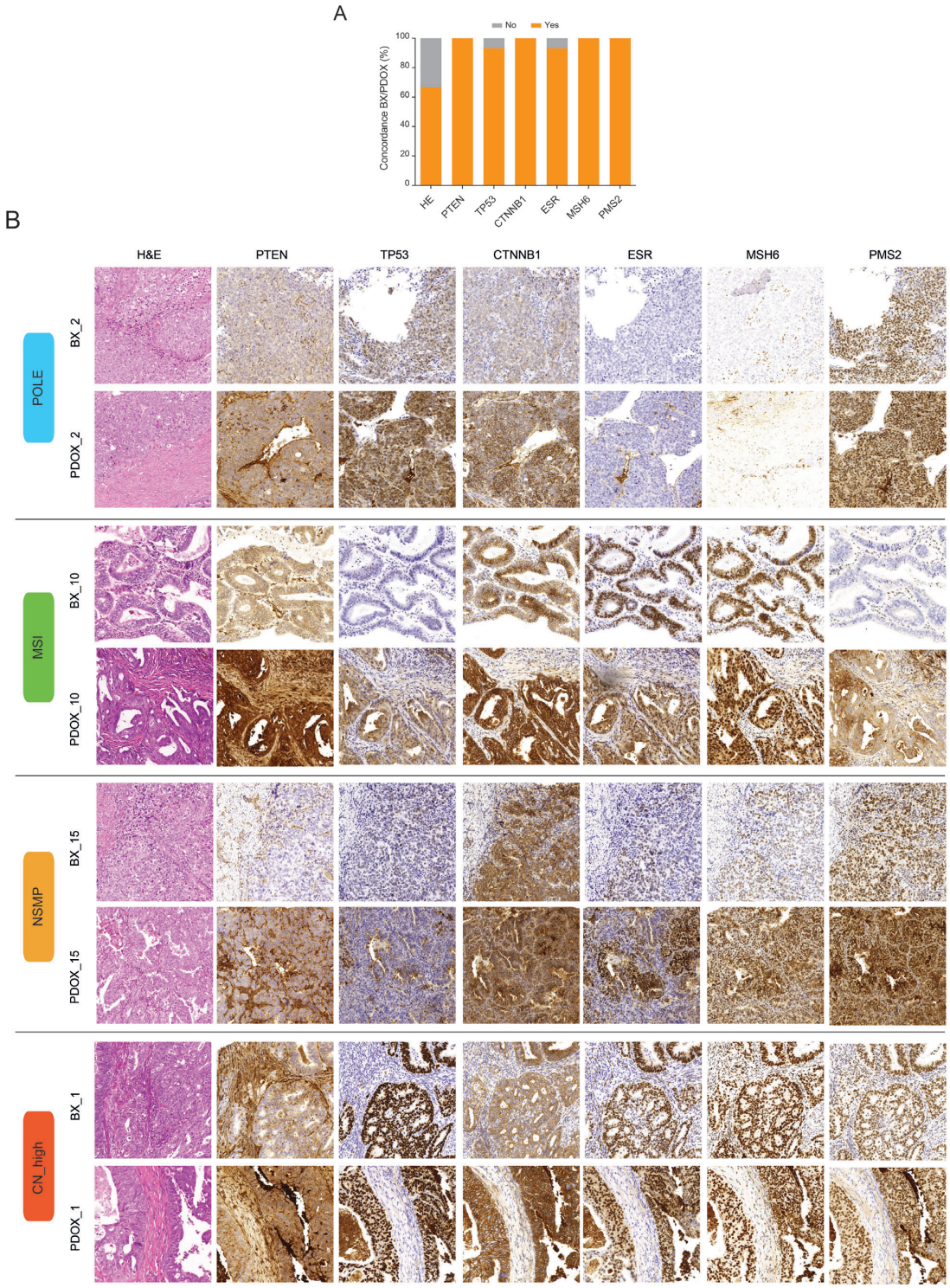

mutational, and genome-wide transcriptional analyses between the primary tissue and the tumors from the mouse avatar at P1 to assess their main morphological, genetic, and transcriptomic characteristics.

2.2. PDOX Models Retain the Main Histological and Molecular Features of Primary Tumors

Hematoxylin eosin (HE) staining, as well as phosphatase and tensin homolog (*PTEN*), *TP53*, *CTNNB1*, estrogen receptor (*ESR*), mutS homolog 6 (*MSH6*), *PMS2* immunostainings were performed in both primary tumors and PDOXs. Overall, PDOXs presented a high degree of concordance at histological level (≈70% with their primary tumors) and molecular biomarker expression (**Figure 2**A,B and Figures S1 and S2 and Table S3 (Supporting Information)). Full concordance was detected in *PTEN*, nuclear *CTNNB1*, *MSH6*, and *PMS2* immunostainings between BXs and PDOXs. *ESR* and *TP53* showed a good correlation (93.33%) between BXs and PDOXs. In the case of *TP53*, and in line with our initial assessment (Figure 1B), BX1 and its derived PDOX1 presented an abnormal staining by immunohistochemistry (a surrogate of the copy number high, CN_high molecular EC subgroup) and were therefore classified within the *TP53*-mutated (serous-like, high copy number) group. Of note, 2 PDOX models (PDOX7 and PDOX13) displayed differences in the expression of certain molecular biomarkers compared to their primary tumor (BX). This is evidenced in PDOX7 by an increase in tumor grade from G1 to G3 with undifferentiated tumor areas and a concomitant loss in *ESR* expression (**Figure 3**A). This result is in agreement with the histologic difference observed in this model (G3 and presence of undifferentiated tumor areas) (Table S3, Supporting Information). On the other hand, PDOX13 presented de novo serous carcinoma areas, as observed in the HE, characterized by an abnormal *TP53*, *p16*, and *IMP2* stainings that were not observed in the initial tumor biopsy (Figure 3B,C).

2.3. Transcriptomic Characterization of Tumors and PDOX Models

To further explore the molecular similarity between PDOX and primary tumors, we analyzed their transcriptional landscape by RNA_sequencing. After curated filtering of reads from mouse origin (please see the Experimental Section for further technical details), a high degree of resemblance at transcriptional level was correlated across the 15 paired samples (BX and PDOX) (Spearman's $\rho = 0.89–0.95$) (**Figure 4**A and Figure S3 (Supporting Information)). We also performed differential expression analysis to identify differentially expressed genes (DEGs) between primary tumors and PDOXs (Figure 4B). Interestingly, we found 1146 downregulated and 10 upregulated genes in PDOXs compared with the corresponding primary samples (Table S4, Supporting Information), reflecting potential biological differences between both tissues. In this line, unbiased gene set enrichment analysis (GSEA) analysis[17] using the archived gene ontology biological process (Figure 4C) and hallmark gene annotations (Figure 4D), revealed that genes with enriched expression in primary tumors were mostly associated with human tumor microenvironment (e.g., genes involved in transplant rejection alloimmune response, immune cell differentiation and activation, etc.), which is consistent with the profound changes in the human tumor-associated stroma (cancer-associated fibroblasts, immune cells, extracellular matrix, endothelial cells, etc.) and its replacement by the murine stromal components commonly seen in mouse xenografts.[12] To support this, we inferred changes in the human infiltrating stromal compartment by employing the microenvironment cell populations-counter (MCP-counter) method, which has one of the highest specificities in quantifying the absolute abundance of multiple stromal cell compartments from transcriptomic data[18] (Figure 4E). As expected, we identified significant changes in immune and stromal infiltrates across the 15 BX and PDOX samples, including a decrease in human T cells and cytotoxic lymphocytes, and a reduction in human endothelial cells and fibroblasts in the PDOXs with respect to BXs which, collectively, indicate that human stromal cells are progressively being replaced by murine cells upon engraftment in the mouse uterus. This was also supported by our gene set variation analysis (GSVA)[19] of the fibroblastic and endothelial content when using gene expression from mouse and human origin in PDOX samples (Figure 4F) which, collectively, evidence a significant enrichment in mouse stromal cells within the human orthoxenograft. Altogether, our results indicate that PDOX tumors exhibit not only a notable retention in histological and biomarker features, but also an excellent correlation with BX samples at transcriptomic level. Also, consistent with previous observations, our data point at important changes in the tumor microenvironment.

2.4. Mutational Profiling of Primary Tumors and PDOX Models for the Rational Assessment of Targeted Therapies

Our data indicate that PDOXs could be harnessed to explore novel precision medicine compounds in EC based on distinctive BX–PDOX tumor molecular fingerprints. To this end, we resolved to identify relevant BX analogous actionable or predictive treatment response mutations in our PDOXs. Hence, we performed DNA targeted next generation sequencing in EC and PDOX tumors using a comprehensive cancer gene panel that includes 57 cancer-associated genes (Table S5, Supporting Information). A total of 68 and 85 mutations were detected in primary tumors and in PDOXs, respectively (Table S6, Supporting Information). Noteworthy, PDOXs 1, 3, 4, 6, 7, 8, 9, 10, 12, and 13 presented a slight increase in the number of mutations compared to

Figure 2. Morphological and immunohistochemical correlation between primary tumors (BXs) and PDOXs. A) Percentage of cases displaying consistent positive correlations between paired BX–PDOX after morphologic analysis by hematoxylin and eosin (HE) and after immunohistochemical detection of canonical EC biomarkers (*PTEN*, *TP53*, *CTNNB1*, *ESR*, *MSH6*, and *PMS2*). B) Representative examples of fully correlated BX–PDOX pairs. Images illustrate HE stainings and detection by immunohistochemistry of *PTEN*, *TP53*, *CTNNB1*, *ESR*, *MSH6*, and *PMS2* between BX and PDOX. BX1 (CN-high), BX2 (POLE-mutated), BX10 (MSI), and BX15 (MSS).

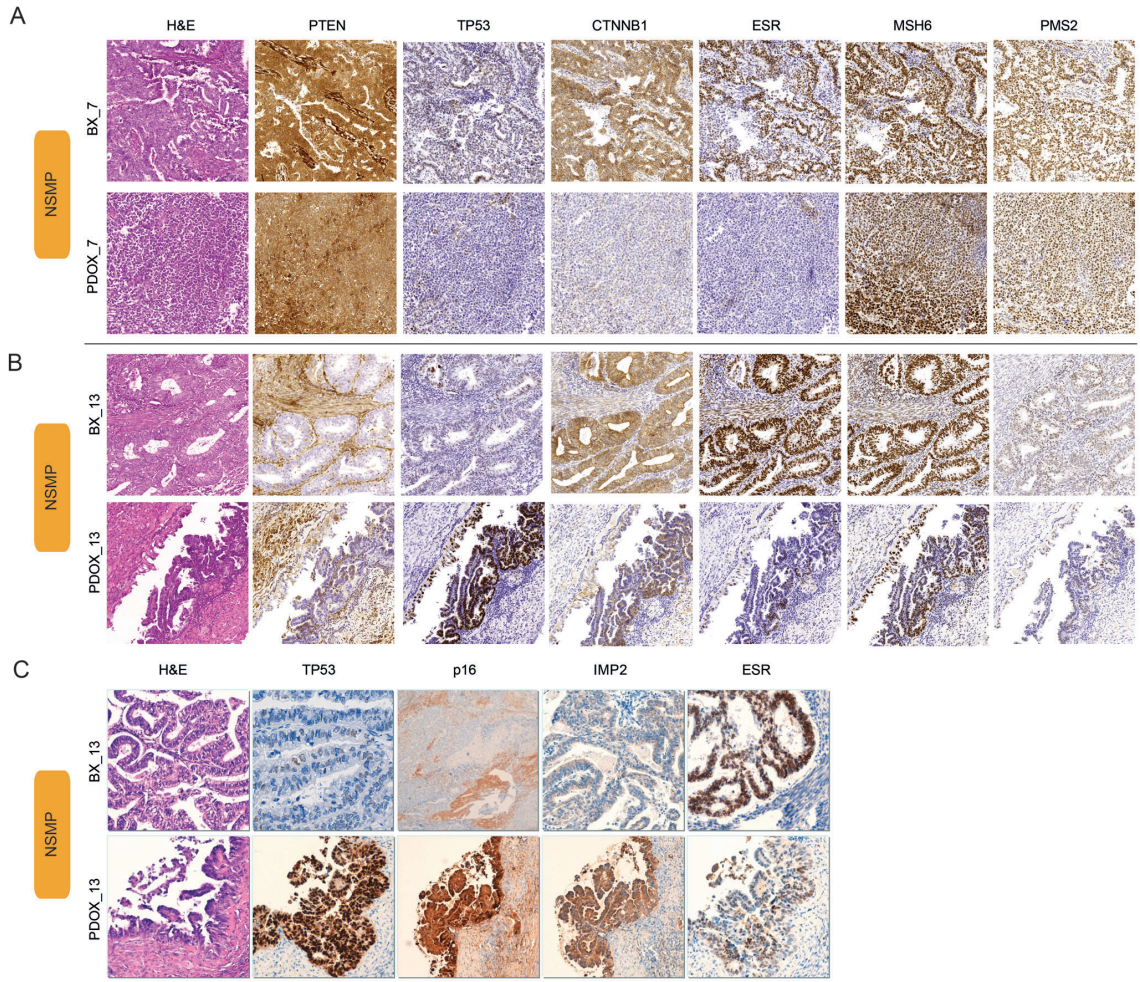

Figure 3. Detection of immunohistochemical differences between primary tumors (BXs) and PDOXs. Representative images presenting two PDOX cases displaying immunohistochemical tumor features that were not detected in the original primary tumor: A) pair BX7–PDOX7 and B) pair BX13–PDOX13. Images show a differential *ESR* expression in PDOX7, while PDOX13 presented areas of serous carcinoma and abnormal *TP53* overexpression that were not observed in the primary tumor. C) HE and immunostaining images for *TP53*, *p16*, *IMP2*, and *ESR* in PDOX13.

their original primary tumor (**Figure 5**A). Common and fully concordant mutations shared by primary and PDOX cases ($n = 48$), representing the 70.59% and 56.47% of all mutations found in primary tumors and PDOX, respectively, encompassed several of the most relevant genes involved in EC development and progression, including *PTEN*, *PIK3CA*, *TP53*, and *KRAS* (Figure 5B). Importantly, full coincidental mutations were also found in other genes with a less clear role in the development and/or progression of EC but with potential therapeutic interest (e.g., fibroblast growth factor receptor 1 (*FGFR1*), erb-b2 receptor tyrosine kinase 2 (*ERBB2*), etc.). Altogether, these data suggest that PDOXs are able to retain the majority of assessed mutations (>50%) detected in primary tumors and that this information could be leveraged to assess personalized treatments.

2.5. Evaluation of Trastuzumab as a Potential Precision Medicine Agent for Endometrioid Endometrial Cancer

Based on all the aforementioned, we focused on *ERBB2* for further analysis. *ERBB2* (hereafter termed HER2) is a membrane tyrosine kinase receptor that belongs to a family of four receptors (HER1–4) involved in cell growth, survival, and proliferation.[20,21] HER2 is a well-known oncogene, and it is found overexpressed in multiple types of tumors owing to, mainly, copy number alteration (CNA) events (amplifications).[22] In EC, although the reported frequencies are variable, it is well established that HER2 is also found amplified and/or overexpressed in tumors with high grade histology (≈10–80%),[22] and that this genetic alteration is frequently associated to *TP53*

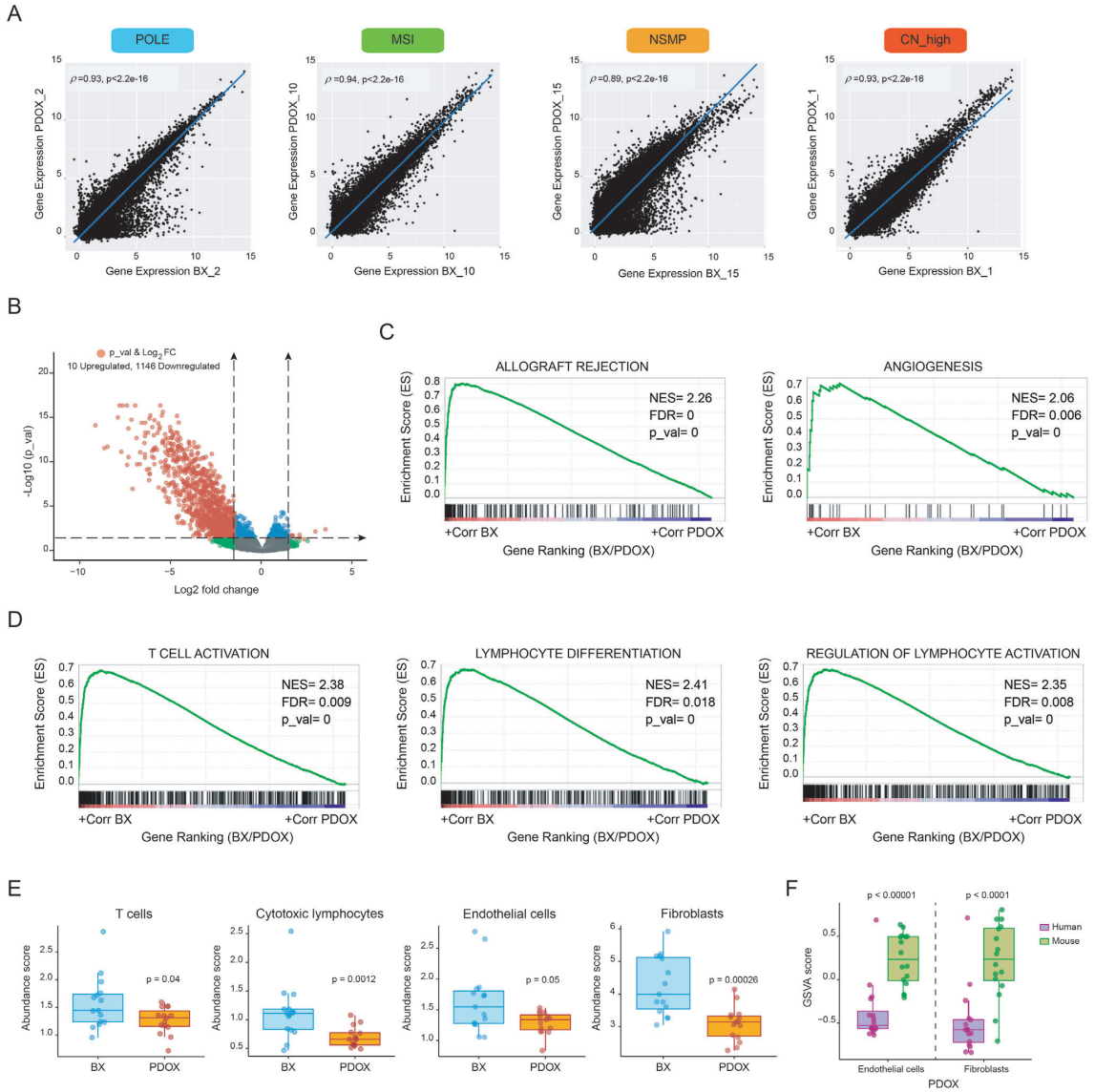

Figure 4. Transcriptomic analysis of BX and PDOX tumor pairs. A) Total RNA sequencing for the 15 pairs of BX/PDOX tumors was conducted and computationally analyzed. BX and PDOX pairs correlated extremely well at transcriptomic level. Spearman's correlation (rho) ρ values and p values indicate the strength and significance of the correlations, respectively. B) Volcano plot depicting differentially expressed genes between PDOXs and primary tumors (p value < 0.05 and logFC > abs(1.5)). A total of 1146 genes were significantly reduced and only 10 were significantly increased in the PDOX samples. C) Significantly enriched gene annotations by GSEA from gene ontology biological pathways (GO) and D) hallmarks indicative of progressive changes in the human tumor microenvironment. E) Transcriptional inference of stroma and immune infiltrates using the MCP-counter reveals a decrease in the abundance of representative signatures of human T cells, cytotoxic lymphocytes, endothelial cells, and fibroblasts in the PDOX. F) GSVA analysis of the representation in fibroblastic and endothelial gene annotations from mouse and human specific reads.

mutations.[23] Importantly, HER2 mutations have also been found in EC, albeit with lower frequency (≈2–3%).[22] Despite the clinical relevance of HER2 amplification/overexpression and mutational status in EC is still a matter of intense debate, HER2 has attracted attention as a putative therapeutic target. Indeed, not only the inhibition of HER2 has shown potent anticancer effects in vitro and in vivo, alone or in combination,[24,25] but also has demonstrated encouraging results in clinical trials. It must be noted, however, that with the exception of few studies that encompass a reduced number of EC patients

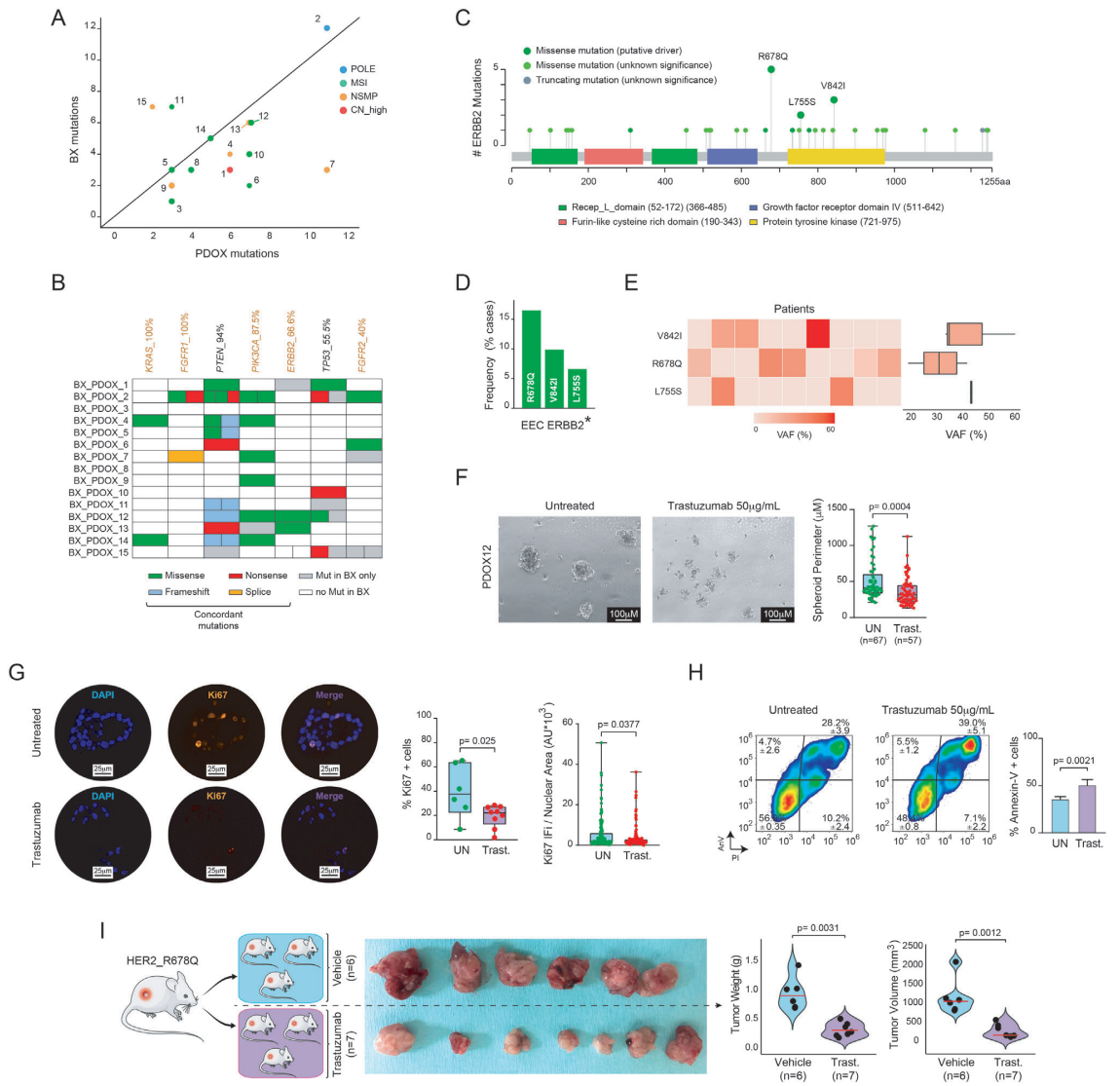

Figure 5. Mutational characterization of BX and PDOXs and effects of trastuzumab in vivo. A) Dot plot representing the correlation between the number of mutations in primary tumors and PDOXs. B) Schematic representation of common somatic mutations for several EC-relevant genes between primary tumors (BX) and their respective PDOX. Gene mutations are ranked from left to right according to percentage of mutations presenting concordance in relation to all mutations for a given gene in BX (i.e., percentage of mutations for a given gene that are maintained in PDOX models). Missense, frameshift, and nonsense mutations were detected. Genes highlighted in orange represent druggable genes. C) Lollipop plot and analysis of the HER2 mutational landscape in endometrioid EC. Analysis has been performed on HER2-mutated tumors (n = 31), using the TCGA_ucec dataset. D) Bar graph showing that *ERBB2*^{R678Q} mutations account for >15% of HER2 mutations in EC. E) Heatmap and boxplots depicting the variant allele frequency (VAF) for the three most frequent HER2 mutations in EC: V842I, R678Q, and L755S. F) Generation of tumor spheroids. Left, bright field representative analysis of untreated and trastuzumab-treated *ERBB2*^{R678Q} spheres after 24 h. Right, quantification of spheroid perimeters. Statistical significance was determined by paired Student's t-test. G) Analysis of *Ki67* expression levels by immunofluorescence (IF) in untreated and trastuzumab-treated spheroids after 24 h. Left, representative IF images. Right, quantification of percentage of *Ki67*-positive cells and alternative quantification after normalizing *Ki67* intensity (arbitrary units) to nuclear area, as previously reported.[76] H) Analysis of Annexin-V staining by flow cytometry on untreated and 24 h treated spheroids with trastuzumab. I) In vivo assessment of trastuzumab anticancer effects on PDOX12, *ERBB2*^{R678Q}-mutated, mouse model. Females were treated twice per week with 4 µg kg^{-1} of trastuzumab i.p. for a period for four weeks. Quantification of tumor weight and volume was performed at the end of the experiment. Statistical significance in in vivo experimentation was assessed by the Mann–Whitney test. Parts of the Figure 5I were drawn by using pictures from Servier Medical Art. Servier Medical Art by Servier is licensed under a Creative Commons Attribution 3.0 Unported License (https://creativecommons.org/licenses/by/3.0/).

with HER2 mutations,[26–28] most of the existing clinical trials assessing anti-HER2 agents in EC are conducted on patients presenting amplified or overexpressed *ERBB2*. For instance, existing evidence from the NCT01367002 study indicates that combination of trastuzumab (an anti-HER2 antibody) with adjuvant paclitaxel–carboplatin increases progression-free survival rates when compared to the same combination without trastuzumab in advanced/recurrent endometrial cancer patients with HER overexpression.[29,30] More recently, results from the Targeted Agent Profiling and Utilization Registry study (NCT02693535) also demonstrate the therapeutic benefit of the combination of trastuzumab with pertuzumab mostly in amplified/overexpressed *ERBB2*/*ERBB3* uterine tumors.[26] In this scenario, we decided to explore the potential use of our PDOX models to test novel therapeutic strategies by assessing the anticancer efficacy of trastuzumab in HER2-mutated tumors. To address this, we selected the PDOX12, which harbors a BX12 matched HER2 mutation at the juxtamembrane domain of HER2 ($HER2^{R678Q}$). $HER2^{R678Q}$ represents a suitable experimental context, since this mutation has been reported as the most recurrent *ERBB2* juxtamembrane domain mutation after massive exome sequencing analysis from ≈111 000 cancer patients, representing ≈400 cancer types, including endometrial cancer.[31] Importantly, $HER2^{R678Q}$ is regarded as a hotspot mutation[32,33] (https://www.cancerhotspots.org) and a driver oncogenic event that confers gain of function features by increasing HER2 phosphorylation and downstream signaling in bladder cancer and breast epithelial cells, where it accelerates acinar structure formation and cell survival.[31,34] Finally, $HER2^{R678Q}$ has been shown to confer sensitivity to trastuzumab in vitro.[31,35] In agreement, our analysis of the HER2 mutational landscape across >10 000 tumors using the cBioportal platform[36] confirmed that $HER2^{R678Q}$ is one of the most prevalent mutations in cancer (Figure S4A, Supporting Information). Importantly, when we categorized $ERBB2^{R678Q}$ mutations according to tumor type, we found that >30% of $ERBB2^{R678Q}$ mutations cluster in the endometrial cancer type (Figure S4B, Supporting Information). Collectively, our data indicate not only that $ERBB2^{R678Q}$ is one of the most frequent *ERBB2* mutations in cancer globally, but also indicate for the first time that $ERBB2^{R678Q}$ is particularly enriched in endometrial cancer. Additional analysis using the TCGA_uterine corpus endometrial cancer (ucec) dataset further demonstrates that this mutation is the most frequent in endometrioid EC among all *ERBB2* mutations (Figure 5C–E).

Next, to explore the effects of trastuzumab, we initially assessed its activity using ex vivo patient-derived organotypic multicellular tumor spheroids.[37] Despite tumor spheroids do not fully mimic the 3D conditions of living organs (e.g., vascularization, tissue-tissue interfaces, mechanical pressures or tumor microenvironment),[38] they are more informative than traditional 2D cell cultures as tumor spheroids more closely recapitulate certain tissular architecture features (e.g., cell to cell interactions), and physiological properties of analogous in vivo tumors.[39] Hence, spheroids from BX12 were generated and exposed to trastuzumab following previously reported experimental conditions.[40] As hypothesized, trastuzumab impinged a dramatic effect on cell fitness, characterized by a reduction in tumor spheroid perimeter (Figure 5F) and decreased expression of the cell proliferation marker *Ki67* (Figure 5G). Interestingly, treatment with trastuzumab also triggered a notable cytotoxic effect, as measured by apoptosis induction (Figure 5H). On the basis of these lines of evidence, we resolved to assess the antitumor effect of trastuzumab in vivo using the $ERBB2^{R678Q}$-mutated PDOX12. To this end, the colony of immunosuppressed mouse females harboring engrafted BX12 tumors in the uterus was expanded and animals were randomized before treatment. As shown in Figure 5I, treatment with trastuzumab significantly delayed tumor growth, as evidenced by a remarkable reduction in tumor weight and volume. Altogether, our data demonstrate not only that PDOXs derived from primary EC biopsies maintain essential morphologic and molecular features, but that its genetic profiling can reveal unexpected tumor vulnerabilities that can be used to advance personalized treatments in endometrial cancer.

3. Discussion

Prior to 1930s–1940s, uterine cervix and uterine corpus cancers were considered a single epidemiological entity (i.e., uterine cancer) that constituted the major cause of biased cancer-related deaths against women in comparison to men.[41] The implementation of screenings for the early detection of cervix cancer reduced uterine cancer death rates by 80% and represents to date one of the major achievements in cancer prevention. Unfortunately, in the case of endometrial (or uterine corpus) cancer, the technological advances accomplished in the cancer arena (e.g., robotic surgery, imaging, or pathological analysis) have been complemented with a scarce increase in therapeutic opportunities, especially in the area of precision medicine or targeted therapies.

Up to present, Bokhman's dualistic model is the most widely used strategy to classify EC and one of the pillars aiding treatment decisions.[42] The model is based on clinical and pathological features and broadly classifies ECs into type I or endometroid (EEC) and type II or nonendometroid (NEEC) tumors. Type I tumors are low grade, estrogen-dependent tumors that predominate in pre- or perimenopausal women and represent ≈75% of all diagnosed ECs. On the other hand, type II ECs are estrogen-independent tumors that mainly develop in older women and present a poor clinical outcome. They include mostly serous and clear cell histological subtypes.[43] Currently, the mainstay approach guiding treatment decisions in endometrial cancer is based on histological risk criteria that include histological subtype, grade, lymphovascular invasion, and tumor stage,[4] being the International Federation of Gynecology and Obstetrics (FIGO) staging the single strongest prognostic parameter for EC patients. However, these assessments are often challenging and the difficulties that pathologists sometimes encounter to reach a consensus in the analysis and interpretation of these criteria has hindered the development of standardized guidelines to avoid patient under- or overtreatment. In this line, the discovery in 2013 by the TCGA consortia of a new classification based on molecular profiling of EC has shed light onto the different genomic subtypes of EC, offering the potential to improve EC patient stratification postsurgery by supporting expert gynecopathologist analyses.[44] Importantly, the European Society of Gynaecological Oncology (ESGO), the European SocieTy for Radiotherapy and Oncology (ESTRO), and the European Society of Pathology (ESP) ESGO-ESTRO-ESP guidelines, which represent the main reference on

evidence-based recommendations for the improvement of care for women with EC, have incorporated the molecular classification as an essential pilar on EC diagnosis and treatment.[45] Moreover, the TCGA_UCEC molecular classification has provided abundant genetic and epigenetic information with the potential to improve tailored treatments. Results of this study show that unsupervised hierarchical clustering of somatic copy number alterations (SNCAs) and exome sequence analysis categorized EC tumors in four groups: group-1 or POLE-ultramutated (EEC with mutations in POLE, showing high mutation rates, with low SNCA and associated with good prognosis), group-2 or MSI (EEC with microsatellite instability (hypermutated) and low SNCA), and group-3 (EEC exhibiting microsatellite stability and amplification of 1q) showing similar progression-free survival rates. Finally, group-4 (serous carcinomas (NEEC) and 12% of EEC, particularly grade 3 tumors) is characterized by presenting high SNCA, *TP53* mutations, and worse prognosis. One of the most interesting results is the identification of molecular similarities between group-4 and high grade serous ovarian carcinomas and basal-like breast tumors, outlining a potential shared treatment strategy.

Current treatments for EC patients do not substantially differ from those that have been implemented for decades, and little advances have been achieved in this underfunded and often overlooked area of research.[46] In fact, it is commonly accepted that traditional chemotherapeutic regimes are less effective in EC when compared with cancers of other organs, greatly emphasizing the urgent need to identify new molecular targets and treatment options. The discovery and emergence of the TCGA_ucec-based genomic information is thus expected to hasten the discovery of new molecular targets and strategies to combat EC in the future. Some of the most promising targeted therapies currently being assessed include those that involve the inhibition of the phosphatidylinositol-3-kinase(*PI3K)*–mammalian target of rapamycin (*mTOR),* PI3K-mTOR pathway, *FGFR2,* or *RAS*–mitogen activated protein kinase (*MAPK)* while, most recently, immunotherapy has become the primary approach in many trials.[9] In this line, the approval in May 2017 by the U.S. Food and Drug Administration (FDA) of pembrolizumab for the treatment of refractory microsatellite (MS) instable-high/mismatch-repair (MMR)-deficient EC,[47] the approval in 2019 of pembrolizumab combined with lenvatinib for the treatment of progressed MMR proficient/MS stable EC,[48] and the recent approval of dostarlimab for the treatment of advanced MSI endometrial cancer[49,50] have significantly improved the clinical management of this disease. However, despite our knowledge of EC has increased considerably over the last decade, EC treatment still lags far behind other types of malignancies in the area of precision medicine. The lack of proper experimental model systems at the preclinical triage still represents a major impediment precluding success of anticancer drug assessment in clinical trials. Consequently, the future implementation of novel, more efficient and less toxic treatment options in EC must stem from accelerated and improved transferability success of "from bench to bedside" studies, one of the major bottlenecks that hamper therapeutic compound approval. In this line, despite several novel therapies are supported by conventional in vitro/in vivo preclinical evidences, the efficacy to translate these findings into the clinic has remained extremely low[51,52] and successful drugs in preclinical testing often fail upon reaching phase III clinical trials.[53] Accordingly, only 5% of compounds with validated preclinical anticancer properties are approved by the FDA for clinical implementation.[54] The reasons behind these low success rates could lie in the inability of commonly established preclinical models to recapitulate the complexity of a patient tumor,[52] the discrepancies observed, over time and with increased cell passaging, between the primary tumor and its derived cell line,[55] or the limited value of conventional cell lines to predict treatment response.[52]

In a recent pilot study from our laboratory, we reported the anticancer properties of the autophagy inhibitor chloroquine combined with sorafenib in three PDOX EC models.[56] The robustness of the assay combined with an evident translational potential prompted us to further characterize this experimental system by expanding this methodology to the most frequent EC molecular subtypes and by interrogating primary tumor-PDOX resemblance through genetic and transcriptomic approaches. To achieve this and to overcome all the aforementioned experimental limitations, we have expanded our knowledge on EC by generating direct orthotopic xenograft models from 15 EC patients. Although the generation of panels of >10 subcutaneous and/or subrenal EC PDX have been described in the recent years,[57–61] to the best of our knowledge, no other attempts to systematically implant and profile at a genome-wide scale matched primary tumor and orthotopically inserted primary-derived EC tissue in mice have been reported. Importantly, we provide abundant data demonstrating that implantation and engraftment of primary EC tissue in the mouse uterus can regenerate the human tumor in mice. In this regard, it is well recognized that the site of implantation (heterotopic vs orthotopic) can influence not only tumor growth, desmoplasia, vascularization, stromal infiltration, and response to antineoplastic treatments but also dramatically affect the metastatic behavior, being heterotopic PDX less able to better recapitulate the tumor progression observed in cancer patients.[62–66] Altogether, our experimental system aims at mirroring as close as possible the patient's tumor by preserving the natural setting of the disease through an orthotopic implantation.

Our data indicate that PDOX tumors recapitulate the main morphological, molecular, and transcriptomic features of the primary tumor, can be expanded in recipient mice (avatars), and can be used to explore the therapeutic potential of targeted therapeutic compounds. Accordingly, in this study, we performed a successful in vivo analysis using trastuzumab, an inhibitor of HER2 with growing interest in EC clinical management,[26,29,30] after the identification of an actionable mutation ($ERBB2^{R678Q}$) in the primary and the corresponding PDOX tumor. Interestingly, we have also found not only that $ERBB2^{R678Q}$ represents the main missense mutation in endometrioid EC but also that it can be targeted in PDOX tumors which, to the best of our knowledge, constitutes the first demonstration that this mutation can be pharmacologically tackled in vivo. However, it must be noted that other relevant endometrial cancer related genes (e.g., AT-rich interaction domain 1A, *ARID1A*) were not included in our gene panel, which represents a limitation in our study. Thus, our data demonstrate that the retention of essential morphologic, genetic, and transcriptomic tumor traits within the PDOX models can be harnessed to tailor patient treatment in real time and maximize therapeutic benefit. Importantly, this system could potentially be also

used to anticipate and predict tumor progression when included in coclinical trials.

Finally, our data also demonstrate that tumors engrafted in vivo may present features that can differ from the original tumor biopsy, as demonstrated by the detection of increased histological grade (e.g., PDOX3), or the progression into more aggressive histological types (such as *TP53*-positive serous carcinoma in the case of PDOX13, or undifferentiated carcinoma as seen in PDOX7). While many factors may contribute to these differences,[67–69] it seems clear that, in light of our findings, the orthotopic perpetuation of EC in mice may allow certain PDOX the opportunity to progress "in vivo" long after surgical resection. Strikingly, these observations maintain the parallelism with what can be seen in patients, since transformation of a preexisting endometrioid carcinoma into these aggressive histological types is a well-recognized phenomenon and examples of mixed endometrioid–serous carcinomas[70] or dedifferentiated carcinomas (endometrioid carcinomas with undifferentiated carcinoma)[71] have been previously reported. Interestingly, recent data obtained by microdissection followed by DNA sequencing have demonstrated that, in the cases presenting a morphologic merge between these different tumor entities, the aggressive histological type results from the progression of the endometrioid component.[70,72–75] Hence, our study shows not only that PDOX tumors may recapitulate the morphologic, immunohistochemical, and molecular features of the primary tumor, but also that it may provide a dynamic "in vivo" model to deepen unresolved questions in EC progression from a biological and mechanistic point of view.

Altogether, while these observations warrant additional studies in the PDX arena, our data indicate that EC-patient-derived PDOX models unambiguously represent suitable tools to enhance endometrial cancer research in the forthcoming years.

4. Experimental Section

Establishment of PDOX in Mice and Treatment: Primary sample collection and tumor engraftment were approved by the IDIBELL Committee for Animal Experimentation (CEIC Bellvitge Hospital approval reference number PR047/18). Endometrioid endometrial tumors were obtained at the HUB/Bellvitge Hospital and the Catalan Institute of Oncology between 2010 and 2015. Ethical and legal protection guidelines of human subjects, including informed consent from the patient to implant the tumor in mice, were strictly followed and conducted according to the procedure 9111, assigned to AlbertoVillanueva, which was approved by the Generalitat de Catalunya. Selected nonnecrotic tissue fragments (2–3 mm^3) from resected tumors were placed in supplemented Dulbecco's modified Eagle medium (DMEM) (10% fetal bovine serum, FBS, and penicillin/streptomycin) at room temperature. Six week old Hsd:Athymic Nude-*Foxn1*^{nu} mouse females were subjected to a lateral laparotomy (n = 2 to 4) under isofluorane-induced anesthesia. Animal uteri were exposed and then, primary tumor resected pieces were anchored using prolene 7.0 sutures. Finally, the abdominal incision was closed with surgery staples. Tumor growth was monitored by careful inspection and abdominal palpation twice per week, for the generation of PDOX cohort and during in vivo treatments and harvested when the tumor reached a certain volume (≈300–500 mm^3).[56] Thereafter, small fragments of the tumor were transplanted into 2 to 4 new mice. For subsequent implantation, engrafted tumors at early mouse passages (#1–3) were cut in 6–8 mm^3 fragments and stored in liquid nitrogen in FBS–10% dimethyl sulfoxide. Animals were housed in a sterile environment, cages and water were autoclaved, and bedding and food were γ-ray sterilized. For tumor characterization, i.e., immunohistochemical analysis and molecular studies, early passage 1 (P1) tumors were selected. For trastuzumab treatment in vivo, engrafted tumors at early mouse passage 2 (P2) were used. Females orthotopically harboring the *ERBB2*-mutated BX12 tumor were randomized and treated with 4 µg kg^{-1} of intraperitoneally (i.p.) injected trastuzumab for 4 weeks, twice per week. Total time elapsed for the in vivo experimentation was 85 days, 55 days between tumor engraftment until treatment, and 30 days of trastuzumab experimentation. A control group of females (n = 5) harboring *ERBB2*-mutated BX12 was used as surrogate controls to indirectly estimate tumor growth of the experimental cohort. All animals were culled, and tumors were resected in parallel the same day. Trastuzumab was purchased from the HUB pharmacy service.

Generation and Analysis of Patient-Derived Organotypic Multicellular Tumor Spheroids: Tumor samples were collected in DMEM (Gibco, 11965-092) and transported to the laboratory at 4 °C. Samples were transferred to a 10 cm tissue culture dish and minced into small pieces (2 mm or smaller) with a sterile scalpel. Fragments were collected in a tube with 20 mL of sterile phosphate-buffered saline (PBS) and centrifuged at 200 *g* for 5 min. After that, minced samples were resuspended in DMEM supplemented with Liberase DH (Roche, 05401054) at 0.28 u mL^{-1} and digested for 1–2 h at 37 °C. Sample aliquots were observed every 20 min under optical microscopy to check for small cell aggregates. After digestion, samples were centrifuged at 200 *g* for 5 min, after which pellets were resuspended in 20 mL of PBS. Thereafter, samples were filtered through a 100 µm cell strainer and the filtrate was transferred to a 50 mL tube. Samples were finally centrifuged at 200 *g* for 5 min and the pellet containing spheroids was cultured in 6-well ultralow attachment plates with Mammocult human medium kit (StemCell Technologies, 05620) supplemented with 4 µg mL^{-1} of heparin (StemCell Technologies, 7980) and 0.48 µg mL^{-1} of hydrocortisone solution (StemCell Technologies, 07925) at 37 °C and 5% CO_2. After 10 days in culture, spheroids were collected, and media was removed after centrifugation at 100 *g* for 5 min. Fresh media containing 50 µg mL^{-1} of trastuzumab (Selleckchem, A2007) was added and the spheroids were kept in 6-well ultralow attachment plate during 24 h at 37 °C and 5% CO_2.

To analyze cell viability by flow cytometry, tumor spheroids were disaggregated after incubating with 200 µL of TrypLE Express (Gibco, 12604-013) at 37 °C for 20–30 min. Samples were then brought to single cell suspensions by gentle pipetting, after which they were washed with PBS and resuspended in 500 µL of binding buffer (BD Biosciences, 556454) with 5 µL fluorescein-isothiocyanate-conjugated Annexin V (Immunostep S.L., ANXVDY-200T) and 5 µL propidium iodide (PI) staining solution (BD Biosciences, 51-66211E). Cells were incubated on ice for 30 min and analyzed using the FlowJo and Kaluza softwares. To estimate spheroid perimeters, 10× spheroid images were captured on an Olympus IX70 inverted microscope. Perimeters were then measured using the ImageJ software. To perform *Ki67* immunofluorescent stainings, spheroids were embedded in Histogel (Life Technologies S.A., HG-4000-012) and fixed in 4% paraformaldehyde (Life Technologies S.A., 28908) overnight at room temperature. After that, spheroids were embedded in paraffin and the immunofluorescence staining was performed as follows: first, paraffin sections were dewaxed and rehydrated to carry out an antigen retrieval with citrate buffer at pH = 6 on a DeCloaking chamber. For the immunodetection, samples were washed with tris-buffered saline (TBS) 3 times for 5 min, blocked with TBS + 0.5% triton + 3% donkey serum for 1 h at room temperature, and finally incubated with 1:100 purified mouse anti-*Ki67* (BD Pharmigen, 550609) for 48 h at 4 °C. A goat anti-mouse immunoglobulin G (IgG, (H+L)) Alexa Fluor 568 (TermoFisher Scientific, A-11004) was used as secondary antibody. Nuclei were stained with 4',6-diamidino-2-phenylindole (DAPI) (Invitrogen, D21490). Differences in *Ki67* expression by immunofluorescence were conducted as previously reported:[76] nuclear DAPI stainings were used to estimate nuclei dimensions using ImageJ on images captured on a Nikon Eclipse 80i vertical fluorescence microscope. Then, the ImageJ ROI Manager tool was used to measure the *Ki67* fluorescence intensity after which the intensity of *Ki67* staining per nuclei was normalized to its respective area. Alternatively, overlaid DAPI–*Ki67* images were used to calculate the percentage of *Ki67*-positive nuclei.

Statistical significances for all experimental procedures involving tumor spheroids were determined by Student's *t*-test.

Primary Tissue Analysis: Immunohistochemical studies: tissue blocks were sectioned at thickness of 3 µm, dried for 1 h at 65 °C before pretreatment procedure of deparaffinization, rehydration, and epitope retrieval in the Pretreatment Module, PT-LINK (Agilent Technologies-DAKO, Santa Clara, CA, USA) at 95 °C for 20 min in 50× Tris/EDTA (ethylenediaminetetraacetic acid) buffer, pH 9. Before staining the sections, endogenous peroxidase was blocked. The antibodies used were against *P53* (ready to use, clone DO-7), *β-catenin* (ready to use, clone *β-catenin-1*), *PTEN* (1:100 dilution, clone 6H2.1), *ESR* (ready to use, clone 1D5), *MSH6* (ready to use, clone EP49), *PMS2* (ready to use, clone EP51 from Agilent Technologies-DAKO, Santa Clara, CA, USA), *IMP2* (1:100 dilution, clone EPR6741 from Abcam, Cambridge, MA), and *p16* (clone E6H4, Roche Diagnostics). After incubation, the reaction was visualized with the EnVision FLEX Detection Kit for *P53*, *ER*, *MSH6 PMS2*, *IMP2*, and *p16* or EnVision FLEX+ Mouse/Rabbit Linker Detection Kit (Agilent Technologies-DAKO, Santa Clara, CA, USA) for *PTEN* and *β-catenin*, using diaminobenzidine chromogen as a substrate. Slides were counterstained with hematoxylin. Immunoexpression was graded semiquantitatively by considering the percentage and the intensity of the staining. Histological scores (Hs) from two independent pathologists were obtained from each sample, encompassing values from 0 (no immunoreaction) to 300 (maximum immunoreactivity). The score was obtained by applying the following formula, Hs = 1*x* (% light staining) + 2*x* (% moderate staining) + 3*x* (% strong staining), as previously reported.[77] Identification of POLE-mutated tumors: POLE mutation status was determined after the identification of pathogenic mutations in the POLE exonuclease domain (exons 9–14) by Sanger sequencing and analysis with the SeqStudio genetic analyzer (Applied Biosystems).

DNA Extraction and Amplicon Seq VHIO-Card: DNA extraction was performed from 5 × 10 µm sliced sections of formalin-fixed paraffin-embedded (FFPE) material using the Maxwell FFPE Tissue LEV DNA Purification Kit. Tumor area content was evaluated by a pathologist. A minimum tumor content was set to 20%, in order to allow detection of 5% minimum allele frequency mutations. An initial multiplex-polymerase chain reaction with a proofreading polymerase was performed on samples using a panel of over 800 primer pairs targeting frequent mutations in oncogenes plus several tumor suppressors, totaling 57 genes (Table S4, Supporting Information). Indexed libraries were pooled and loaded onto a HiSeq instrument and sequencing performed (2 × 100). Initial alignment was performed with Burrows-Wheeler Aligner (BWA) after primer sequence clipping and variant calling performed with the GATK Unified Genotyper and VarScan2 followed by ANNOVAR annotation. Somatic single nucleotide polymorphisms (SNPs) were filtered out with dbSNP and 1000 genome datasets (minor allele frequency MAF > 0.05). All detected variants were manually checked.

RNA Extraction: Total RNA was isolated from primary tumors (BX) and PDOX tumors from mice using the RNeasy Micro kit (Qiagen, 74004) according to the manufacturer instructions. Total RNA concentration was determined on a Thermo Scientific NanoDrop 2000c UV–vis Spectrophotometer (Thermo Scientific, Wilmington, DE). RNA integrity number was assessed using an Agilent 2100 Bioanalyzer to determine the quality of RNA.

RNA-Seq: RNA_sequencing data that support the findings of this study were deposited in the Gene Expression Omnibus (https://www.ncbi.nlm.nih.gov/geo/) under accession number GSE214657. Stranded 2 × 75 bp single end polyA capture messenger RNA (mRNA) sequencing was performed on a NextSeq500 Illumina sequencing platform at Newcastle University Genomics Core Facility (https://www.ncl.ac.uk/gcf/). Raw files were merged, and quality control assessed by FastQC analysis (https://www.bioinformatics.babraham.ac.uk/projects/fastqc/). Trimmomatic software[78] was used to trim Illumina adaptors and bad quality reads. Then, reads were mapped over human reference transcriptome (hg19/GRCh38) with STAR.[79] An annotation file in general transfer format (GTF) (downloaded from the UCSC Table Browser, using RefSeq genes table)[80] including 23 687 genes and 41 970 transcript isoforms was used for the indexing step. Samples from xenografts were aligned against mouse transcriptome (mm10/GRCm38), previously indexed. R package XenofilteR[81] was used for deconvolution of mouse and human reads on xenografts samples. XenofilteR is an accurate method developed to remove sequence reads of mouse origin from human sequences in DNA and RNA-seq data with high sensitivity results. After removal of the mouse-derived reads, aligned sequences were quantified with RNA-Seq by Expectation-Maximization software (RSEM),[82] and gene expression matrix was extracted as transcripts per million and then transformed to log2 scale. Finally, not expressed genes were removed and an adjustment for reduction of the batch effect was performed with ComBat function from R package sva.

DEG and Functional Analysis: To identify enrichment in specific cellular functions and pathways, a GSEA[17] was performed comparing "Primary Tumor" samples versus "Xenografts–PDOXs" samples. GSEA performs a functional enrichment analysis under different conditions by nonparametric test of equality of distributions. Hallmarks collection from MsigDB was interrogated, including a total of 50 gene sets that summarized the most representative biological states and processes. A differential Expression Analysis was performed to identify DEGs between primary tumors and PDOXs. A linear model was fitted using the R package Limma,[83] and a list of DEG with p-value < 0.05 and logFC > abs(1.5) was extracted.

Stromal Cell Infiltration Analysis: The R package MCP-counter[18] was used to quantify infiltration of nine cell types, including T and B lymphocytes, natural killer (NK) cells, monocytic lineage cells, myeloid dendritic cells, neutrophils, endothelial cells, and fibroblasts. Comparisons of cell types between groups were performed using nonparametric Mann–Whitney test, and differences were considered significant when $p < 0.05$. In order to infer the specie originating the tumor microenvironment cells (human or mouse) in the PDOX samples, four MCP-counter gene sets (T cells, cytotoxic lymphocytes, endothelial cells, and fibroblasts) were selected. Then, gene set variation analysis from R package "GSVA" was performed using those gene profiles to obtain the enrichment scores.[19] GSVA was performed both over the human expression matrix and the mouse expression matrix. The resulting scores were compared by the Mann–Whitney test.

Supporting Information

Supporting Information is available from the Wiley Online Library or from the author.

Acknowledgements

L.D.-J., A.V., and L.P.-P. contributed equally to this work. This study was funded by the JGW Patterson Foundation through the Project No. 30015.088/25of17/PA/IXS (D.L.-N.), the Asociación Española contra el Cáncer Scientific Foundation (FC-AECC) through the Project Nos. LABAE19004LLOB (D.L.-N.), GCTRA1804MATI (X.M.-G.), and IDEAS098VILL-IDEAS16 (A.V.), by the Instituto de Salud Carlos III (ISCIII) through the Project Nos. CP17/00063 (D.L.-N.), PI18/00795 (D.L.-N.), PI21/00672 (D.L.-N.), PI16/01898 (A.V.), and PI19/01320 (A.V.) (cofounded by the European Regional Development Fund (ERDF) "a way to build Europe"), by the Generalitat de Catalunya through the Project No. 2014SGR364 (A.V.) and by the Fundació La Marató through the Project No. 201919-33 (X.M.-G.). D.L.-N. is recipient of a Miguel Servet scheme (Grant No. MS17/00063) (cofounded by the European Social Fund (ESF), "investing in your future"), Ministerio de Ciencia, Innovación y Universidades, Gobierno de España. L.D.-J. (Grant No. RyC-2021-034346-I) and R.R.-B. (RyC-2016-19671) are recipients of a Ramón y Cajal scheme. K.G. is recipient of a PFIS fellowship (Grant No. FI19/00188). The authors also want to thank the CERCA programme/Generalitat de Catalunya for institutional support.

Conflict of Interest

The authors declare no conflict of interest.

Author Contributions

X.M.-G., A.V., and D.L.-N. developed the project conception and designed the research. L.D.-J., R.S.-P., X.M.-G., A.V., and D.L.-N. prepared the paper. L.D.-J., A.V., L.P.-P., M.S., E.N.-D., F.J.L., L.C.-I., K.G., M.M.-I., R.R.-B., and F.V. conducted research (hands on conduct of the experiments and data collection). L.D.-J., S.G.-M., N.B., R.S.-P., and A.V. analyzed data and performed statistical analysis. A.V., N.R., M.G., E.D., M.B., L.M, J.P., J.M.P., and X.M.-G. coordinated human sample collection, clinical information, written consents, and intellectual content collection. All authors contributed to data interpretation and revised the paper.

Data Availability Statement

RNA_sequencing data that support the findings of this study have been deposited in the Gene Expression Omnibus (https://www.ncbi.nlm.nih.gov/geo/) under accession number GSE214657.

Keywords

endometrial cancer, HER2, patient-derived orthoxenografts, PDOX, targeted therapies

Received: July 22, 2022
Revised: October 18, 2022
Published online: November 14, 2022

[1] A. Jemal, E. M. Ward, C. J. Johnson, K. A. Cronin, J. Ma, A. B. Ryerson, A. Mariotto, A. J. Lake, R. Wilson, R. L. Sherman, R. N. Anderson, S. J. Henley, B. A. Kohler, L. Penberthy, E. J. Feuer, H. K. Weir, *J. Natl. Cancer Inst.* **2017**, *109*, djx030.
[2] R. L. Siegel, K. D. Miller, H. E. Fuchs, A. Jemal, *CA-Cancer J. Clin.* **2021**, *71*, 7.
[3] H. Sung, J. Ferlay, R. L. Siegel, M. Laversanne, I. Soerjomataram, A. Jemal, F. Bray, *CA-Cancer J. Clin.* **2021**, *71*, 209.
[4] N. Colombo, C. Creutzberg, F. Amant, T. Bosse, A. González-Martín, J. Ledermann, C. Marth, R. Nout, D. Querleu, M. R. Mirza, C. Sessa, M. Abal, O. Altundag, F. Amant, A. van Leeuwenhoek, S. Banerjee, T. Bosse, A. Casado, L. C. de Agustín, D. Cibula, N. Colombo, C. Creutzberg, J.-M. del Campo, G. Emons, F. Goffin, A. González-Martín, S. Greggi, C. Haie-Meder, D. Katsaros, V. Kesic, et al., *Ann. Oncol.* **2016**, *27*, 16.
[5] J. Lortet-Tieulent, J. Ferlay, F. Bray, A. Jemal, *J. Natl. Cancer Inst.* **2018**, *110*, 354.
[6] L. S. Bradford, J. A. Rauh-Hain, J. Schorge, M. J. Birrer, D. S. Dizon, *Am. J. Clin. Oncol.* **2015**, *38*, 206.
[7] C. L. Creutzberg, W. L. J. van Putten, P. C. Koper, M. L. M. Lybeert, J. J. Jobsen, C. C. Wárlám-Rodenhuis, K. A. J. De Winter, L. C. H. W. Lutgens, A. C. M. van den Bergh, E. van der Steen-Banasik, H. Beerman, M. van Lent, *Gynecol. Oncol.* **2003**, *89*, 201.
[8] S. Tangjitgamol, H. T. See, J. Kavanagh, *Int. J. Gynecol. Cancer* **2011**, *21*, 885.
[9] A. Oaknin, A. León-Castillo, D. Lorusso, *Curr. Opin. Oncol.* **2020**, *32*, 471.
[10] G. F. Fleming, *J. Clin. Oncol.* **2007**, *25*, 2983.
[11] Y. Koga, A. Ochiai, *Cells* **2019**, *8*, 418.
[12] M. Hidalgo, F. Amant, A. V. Biankin, E. Budinská, A. T. Byrne, C. Caldas, R. B. Clarke, S. de Jong, J. Jonkers, G. M. Mælandsmo, S. Roman-Roman, J. Seoane, L. Trusolino, A. Villanueva, *Cancer Discovery* **2014**, *4*, 998.
[13] X. Y. Woo, J. Giordano, A. Srivastava, Z.-M. Zhao, M. W. Lloyd, R. de Bruijn, Y.-S. Suh, R. Patidar, L. Chen, S. Scherer, M. H. Bailey, C.-H. Yang, E. Cortes-Sanchez, Y. Xi, J. Wang, J. Wickramasinghe, A. V. Kossenkov, V. W. Rebecca, H. Sun, R. J. Mashl, S. R. Davies, R. Jeon, C. Frech, J. Randjelovic, J. Rosains, F. Galimi, A. Bertotti, A. Lafferty, A. C. O'farrell, E. Modave, et al., *Nat. Genet.* **2021**, *53*, 86.
[14] I. Garrido-Laguna, M. Uson, N. V. Rajeshkumar, A. C. Tan, E. de Oliveira, C. Karikari, M. C. Villaroel, A. Salomon, G. Taylor, R. Sharma, R. H. Hruban, A. Maitra, D. Laheru, B. Rubio-Viqueira, A. Jimeno, M. Hidalgo, *Clin. Cancer Res.* **2011**, *17*, 5793.
[15] H. Gao, J. M. Korn, S. Ferretti, J. E. Monahan, Y. Wang, M. Singh, C. Zhang, C. Schnell, G. Yang, Y. Zhang, O. A. Balbin, S. Barbe, H. Cai, F. Casey, S. Chatterjee, D. Y. Chiang, S. Chuai, S. M. Cogan, S. D. Collins, E. Dammassa, N. Ebel, M. Embry, J. Green, A. Kauffmann, C. Kowal, R. J. Leary, J. Lehar, Y. Liang, A. Loo, E. Lorenzana, et al., *Nat. Med.* **2015**, *21*, 1318.
[16] M. Hidalgo, E. Bruckheimer, N. V. Rajeshkumar, I. Garrido-Laguna, E. De Oliveira, B. Rubio-Viqueira, S. Strawn, M. J. Wick, J. Martell, D. Sidransky, *Mol. Cancer Ther.* **2011**, *10*, 1311.
[17] A. Subramanian, P. Tamayo, V. K. Mootha, S. Mukherjee, B. L. Ebert, M. A. Gillette, A. Paulovich, S. L. Pomeroy, T. R. Golub, E. S. Lander, J. P. Mesirov, *Proc. Natl. Acad. Sci. USA* **2005**, *102*, 15545.
[18] E. Becht, N. A. Giraldo, L. Lacroix, B. Buttard, N. Elarouci, F. Petitprez, J. Selves, P. Laurent-Puig, C. Sautès-Fridman, W. H. Fridman, A. de Reyniès, *Genome Biol.* **2016**, *17*, 218.
[19] S. Hänzelmann, R. Castelo, J. Guinney, *BMC Bioinf.* **2013**, *14*, 7.
[20] N. E. Hynes, H. A. Lane, *Nat. Rev. Cancer* **2005**, *5*, 341.
[21] M. A. Lemmon, J. Schlessinger, *Cell* **2010**, *141*, 1117.
[22] D.-Y. Oh, Y.-J. Bang, *Nat. Rev. Clin. Oncol.* **2020**, *17*, 33.
[23] D. S. Ross, K. A. Devereaux, C. Jin, D. Y. Lin, Y. Zhang, A. Marra, V. Makker, B. Weigelt, L. H. Ellenson, M. H. Chui, C. Jin, D. Y. Lin, Y. Zhang, *Mod. Pathol.* **2021**, *35*, 962.
[24] J. Tymon-Rosario, E. Bonazzoli, S. Bellone, A. Manzano, S. Pelligra, A. Guglielmi, B. Gnutti, N. Nagarkatti, B. Zeybek, P. Manara, L. Zammataro, J. Harold, D. Mauricio, N. Buza, P. Hui, G. Altwerger, G. Menderes, E. Ratner, M. Clark, V. Andikyan, G. S. Huang, D.-A. Silasi, M. Azodi, P. E. Schwartz, A. D. Santin, *Gynecol. Oncol.* **2021**, *163*, 334.
[25] G. Yadav, D. M. Roque, S. Bellone, D. D. Manavella, T. M. P. Hartwich, M. Zipponi, J. Harold, J. Tymon-Rosario, L. Mutlu, G. Altwerger, G. Menderes, E. Ratner, N. Buza, P. Hui, G. S. Huang, V. Andikyan, M. Clark, M. Azodi, P. E. Schwartz, L. B. Alexandrov, A. D. Santin, *Gynecol. Oncol.* **2022**, *166*, 351.
[26] H. M. Ali-Ahmad, M. Rothe, P. K. Mangat, L. Garrett-Mayer, E. Ahn, J. Chan, M. L. Maitland, A. S. Balmanoukian, S. R. Patel, Z. Reese, C. W. Drescher, C. A. Leath, R. Li, A. M. Tsimberidou, R. L. Schilsky, *J. Clin. Oncol.* **2021**, *39*, 5508.
[27] D. M. Hyman, S. A. Piha-Paul, H. Won, J. Rodon, C. Saura, G. I. Shapiro, D. Juric, D. I. Quinn, V. Moreno, B. Doger, I. A. Mayer, V. Boni, E. Calvo, S. Loi, A. C. Lockhart, J. P. Erinjeri, M. Scaltriti, G. A. Ulaner, J. Patel, J. Tang, H. Beer, S. D. Selcuklu, A. J. Hanrahan, N. Bouvier, M. Melcer, R. Murali, A. M. Schram, L. M. Smyth, K. Jhaveri, B. T. Li, et al., *Nature* **2018**, *554*, 189.
[28] B. T. Li, F. Meric-Bernstam, S. D. Puvvada, J. Rowbottom, D. Jolliffe, M. Gustavson, A. Mendoza-Naranjo, *J. Clin. Oncol.* **2021**, *39*, TPS3162.
[29] A. N. Fader, D. M. Roque, E. Siegel, N. Buza, P. Hui, O. Abdelghany, S. Chambers, A. A. Secord, L. Havrilesky, D. M. O'malley, F. J. Backes, N. Nevadunsky, B. Edraki, D. Pikaart, W. Lowery, K. Elsahwi, P. Celano, S. Bellone, M. Azodi, B. Litkouhi, E. Ratner, D.-A. Silasi, P. E. Schwartz, A. D. Santin, *Clin. Cancer Res.* **2020**, *26*, 3928.
[30] A. N. Fader, D. M. Roque, E. Siegel, N. Buza, P. Hui, O. Abdelghany, S. K. Chambers, A. A. Secord, L. Havrilesky, D. M. O'malley, F. Backes, N. Nevadunsky, B. Edraki, D. Pikaart, W. Lowery, K. S. Elsahwi, P.

Celano, S. Bellone, M. Azodi, B. Litkouhi, E. Ratner, D.-A. Silasi, P. E. Schwartz, A. D. Santin, *J. Clin. Oncol.* **2018**, *36*, 2044.
[31] K. B. Pahuja, T. T. Nguyen, B. S. Jaiswal, K. Prabhash, T. M. Thaker, K. Senger, S. Chaudhuri, N. M. Kljavin, A. Antony, S. Phalke, P. Kumar, M. Mravic, E. W. Stawiski, D. Vargas, S. Durinck, R. Gupta, A. Khanna-Gupta, S. E. Trabucco, E. S. Sokol, R. J. Hartmaier, A. Singh, A. Chougule, V. Trivedi, A. Dutt, V. Patil, A. Joshi, V. Noronha, J. Ziai, S. D. Banavali, V. Ramprasad, et al., *Cancer Cell* **2018**, *34*, 792.
[32] M. T. Chang, T. S. Bhattarai, A. M. Schram, C. M. Bielski, M. T. A. Donoghue, P. Jonsson, D. Chakravarty, S. Phillips, C. Kandoth, A. Penson, A. Gorelick, T. Shamu, S. Patel, C. Harris, J. Gao, S. O. Sumer, R. Kundra, P. Razavi, B. T. Li, D. N. Reales, N. D. Socci, G. Jayakumaran, A. Zehir, R. Benayed, M. E. Arcila, S. Chandarlapaty, M. Ladanyi, N. Schultz, J. Baselga, M. F. Berger, et al., *Cancer Discovery* **2018**, *8*, 174.
[33] M. T. Chang, S. Asthana, S. P. Gao, B. H. Lee, J. S. Chapman, C. Kandoth, J. Gao, N. D. Socci, D. B. Solit, A. B. Olshen, N. Schultz, B. S. Taylor, *Nat. Biotechnol.* **2016**, *34*, 155.
[34] M. de Martino, D. Zhuang, T. Klatte, M. Rieken, M. Roupret, E. Xylinas, T. Clozel, M. Krzywinski, O. Elemento, S. F. Shariat, *Cancer Biol. Ther.* **2014**, *15*, 1239.
[35] M. Nagano, S. Kohsaka, T. Ueno, S. Kojima, K. Saka, H. Iwase, M. Kawazu, H. Mano, *Clin. Cancer Res.* **2018**, *24*, 5112.
[36] E. Cerami, J. Gao, U. Dogrusoz, B. E. Gross, S. O. Sumer, B. A. Aksoy, A. Jacobsen, C. J. Byrne, M. L. Heuer, E. Larsson, Y. Antipin, B. Reva, A. P. Goldberg, C. Sander, N. Schultz, *Cancer Discovery* **2012**, *2*, 401.
[37] E. Ivanova, M. Kuraguchi, M. Xu, A. J. Portell, L. Taus, I. Diala, A. S. Lalani, J. Choi, E. S. Chambers, S. Li, S. Liu, T. Chen, T. U. Barbie, G. R. Oxnard, J. J. Haworth, K.-K. Wong, S. E. Dahlberg, A. A. Aref, D. A. Barbie, M. Bahcall, C. P. Paweletz, P. A. Jänne, *Clin. Cancer Res.* **2020**, *26*, 2393.
[38] A. Sontheimer-Phelps, B. A. Hassell, D. E. Ingber, *Nat. Rev. Cancer* **2019**, *19*, 65.
[39] M. E. Katt, A. L. Placone, A. D. Wong, Z. S. Xu, P. C. Searson, *Front. Bioeng. Biotechnol.* **2016**, *4*, 12.
[40] C. E. Rodríguez, S. I. Reidel, E. D. Bal de Kier Joffé, M. A. Jasnis, G. L. Fiszman, *PLoS One* **2015**, *10*, e0137920.
[41] R. L. Siegel, K. D. Miller, A. Jemal, *CA-Cancer J. Clin.* **2015**, *65*, 5.
[42] J. V. Bokhman, *Gynecol. Oncol.* **1983**, *15*, 10.
[43] X. Matias-Guiu, J. Prat, *Histopathology* **2013**, *62*, 111.
[44] D. A. Levine, *Nature* **2013**, *497*, 67.
[45] N. Concin, X. Matias-Guiu, I. Vergote, D. Cibula, M. R. Mirza, S. Marnitz, J. Ledermann, T. Bosse, C. Chargari, A. Fagotti, C. Fotopoulou, A. Gonzalez Martin, S. Lax, D. Lorusso, C. Marth, P. Morice, R. A. Nout, D. Ofunding'donnell, D. Querleu, M. R. Raspollini, J. Sehouli, A. Sturdza, A. Taylor, A. Westermann, P. Wimberger, N. Colombo, F. Planchamp, C. L. Creutzberg, *Int. J. Gynecol. Cancer* **2021**, *31*, 12.
[46] J. N. Mcalpine, S. M. Temkin, H. J. Mackay, *Cancer* **2016**, *122*, 2787.
[47] Merck Sharp & Dohme Corp. Keytruda. Merck Sharp & Dohme Corp. , FDA pembrolizumab prescribing information, https://www.accessdata.fda.gov/drugsatfda_docs/label/2019/125514s065lbl.pdf (accessed: April 2019).
[48] U.S. Food and Drug Administration: Simultaneous review decisions for pembrolizumab plus lenvatinib in Australia, Canada, and the United States, http://www.fda.gov/drugs/resources-information-approved-drugs/si-multaneous-review-decisionspembrolizumab-plus-lenvatinib-australia-cana-da-and-us (accessed: October 2019).
[49] FDA approves immunotherapy for endometrial cancer with specific biomarker, news release, FDA, https://prn.to/3ngdVSL (accessed: April **2020**).
[50] FDA grants accelerated approval for GSK's Jemperli (dostarlimab-gxly) for women with recurrent or advanced dMMR endometrial cancer, news release, GlaxoSmithKline, https://bit.ly/3tIUqVj (accessed: April 2021).
[51] N. Eritja, A. Yeramian, B.-J. Chen, D. Llobet-Navas, E. Ortega, E. Colas, M. Abal, X. Dolcet, J. Reventos, X. Matias-Guiu, *Adv. Exp. Med. Biol.* **2017**, *943*, 149.
[52] J. I. Johnson, S. Decker, D. Zaharevitz, L. V. Rubinstein, J. M. Venditti, S. Schepartz, S. Kalyandrug, M. Christian, S. Arbuck, M. Hollingshead, E. A. Sausville, *Br. J. Cancer* **2001**, *84*, 1424.
[53] D. Annibali, E. Leucci, E. Hermans, F. Amant, *Methods Mol. Biol.* **2019**, *1862*, 217.
[54] L. Hutchinson, R. Kirk, *Nat. Rev. Clin. Oncol.* **2011**, *8*, 189.
[55] V. C. Daniel, L. Marchionni, J. S. Hierman, J. T. Rhodes, W. L. Devereux, C. M. Rudin, R. Yung, G. Parmigiani, M. Dorsch, C. D. Peacock, D. N. Watkins, *Cancer Res.* **2009**, *69*, 3364.
[56] N. Eritja, B.-J. Chen, R. Rodríguez-Barrueco, M. Santacana, S. Gatius, A. Vidal, M. D. Martí, J. Ponce, L. Bergadà, A. Yeramian, M. Encinas, J. Ribera, J. Reventós, J. Boyd, A. Villanueva, X. Matias-Guiu, X. Dolcet, D. Llobet-Navàs, *Autophagy* **2017**, *13*, 608.
[57] V. F. Bonazzi, O. Kondrashova, D. Smith, K. Nones, A. T. Sengal, R. Ju, L. M. Packer, L. T. Koufariotis, S. H. Kazakoff, A. L. Davidson, P. Ramarao-Milne, V. Lakis, F. Newell, R. Rogers, C. Davies, J. Nicklin, A. Garrett, N. Chetty, L. Perrin, J. V. Pearson, A.-M. Patch, N. Waddell, P. M. Pollock, *Genome Med.* **2022**, *14*, 3.
[58] J. Depreeuw, E. Hermans, S. Schrauwen, D. Annibali, L. Coenegrachts, D. Thomas, M. Luyckx, I. Gutierrez-Roelens, D. Debruyne, K. Konings, P. Moerman, I. Vergote, D. Lambrechts, F. Amant, *Gynecol. Oncol.* **2015**, *139*, 118.
[59] H.-Y. Shin, E.-J. Lee, W. Yang, H. S. Kim, D. Chung, H. Cho, J.-H. Kim, *Cancers* **2022**, *14*, 829.
[60] M. Zhu, N. Jia, Y. Nie, J. Chen, Y. Jiang, T. Lv, Y. Li, L. Yao, W. Feng, *Int. J. Gynecol. Cancer* **2018**, *28*, 1812.
[61] B. Villafranca-Magdalena, C. Masferrer-Ferragutcasas, C. Lopez-Gil, E. Coll-de la Rubia, M. Rebull, G. Parra, Á. García, A. Reques, S. Cabrera, E. Colas, A. Gil-Moreno, C. P. Moiola, *Int. J. Mol. Sci.* **2022**, *23*, 6266.
[62] L. Farre, I. Casanova, S. Guerrero, M. Trias, G. Capella, R. Mangues, *FASEB J.* **2002**, *16*, 975.
[63] D. J. Erstad, M. Sojoodi, M. S. Taylor, S. Ghoshal, A. A. Razavi, K. A. Graham-O'regan, N. Bardeesy, C. R. Ferrone, M. Lanuti, P. Caravan, K. K. Tanabe, B. C. Fuchs, *Dis. Models Mech.* **2018**, *11*, dmm034793.
[64] R. M. Hoffman, *Nat. Rev. Cancer* **2015**, *15*, 451.
[65] X. Y. Fu, J. M. Besterman, A. Monosov, R. M. Hoffman, *Proc. Natl. Acad. Sci. USA* **1991**, *88*, 9345.
[66] X. Fu, F. Guadagni, R. M. Hoffman, *Proc. Natl. Acad. Sci. USA* **1992**, *89*, 5645.
[67] U. Ben-David, R. Beroukhim, T. R. Golub, *Nat. Rev. Cancer* **2019**, *19*, 97.
[68] U. Ben-David, G. Ha, Y.-Y. Tseng, N. F. Greenwald, C. Oh, J. Shih, J. M. Mcfarland, B. Wong, J. S. Boehm, R. Beroukhim, T. R. Golub, *Nat. Genet.* **2017**, *49*, 1567.
[69] A. C. H. Hoge, M. Getz, A. Zimmer, M. Ko, L. Raz, R. Beroukhim, T. R. Golub, G. Ha, U. Ben-David, *npj Precis. Oncol.* **2022**, *6*, 30.
[70] L. Coenegrachts, D. A. Garcia-Dios, J. Depreeuw, M. Santacana, S. Gatius, M. Zikan, P. Moerman, L. Verbist, D. Lambrechts, X. Matias-Guiu, F. Amant, *Virchows Arch. Pathol. Anat. Physiol.* **2015**, *466*, 415.
[71] E. G. Silva, M. T. Deavers, D. C. Bodurka, A. Malpica, *Int. J. Gynecol. Pathol.* **2006**, *25*, 52.
[72] M. Köbel, B. Meng, L. N. Hoang, N. Almadani, X. Li, R. A. Soslow, C. B. Gilks, C.-H. Lee, *Am. J. Surg. Pathol.* **2016**, *40*, 166.
[73] C. Matrai, S. Motanagh, S. Mirabelli, L. Ma, B. He, E. Chapman-Davis, B. Kurtis, O. Elemento, J. M. Mosquera, L. H. Ellenson, *Am. J. Surg. Pathol.* **2020**, *44*, 1104.
[74] E. Kuhn, A. Ayhan, A. Bahadirli-Talbott, C. Zhao, I.-M. Shih, M. Shih Ie, *Am. J. Surg. Pathol.* **2014**, *38*, 660.
[75] J. M. Rosa-Rosa, S. Leskelä, E. Cristóbal-Lana, A. Santón, M. Á. López-García, G. Muñoz, B. Pérez-Mies, M. Biscuola, J. Prat, O. E. Esther, R.

A. Soslow, X. Matias-Guiu, J. Palacios, E. Cristobal-Lana, A. Santon, M. A. Lopez-Garcia, G. Munoz, *Mod. Pathol.* **2016**, *29*, 1390.
[76] C. C. Agley, C. P. Velloso, N. R. Lazarus, S. D. R. Harridge, *J. Histochem. Cytochem.* **2012**, *60*, 428.
[77] M. Santacana, O. Maiques, J. Valls, S. Gatius, A. I. Abó, M. Á. López-García, A. Mota, J. Reventós, G. Moreno-Bueno, J. Palacios, C. Bartosch, X. Dolcet, X. Matias-Guiu, *Hum. Pathol.* **2014**, *45*, 2394.
[78] A. M. Bolger, M. Lohse, B. Usadel, *Bioinformatics* **2014**, *30*, 2114.
[79] A. Dobin, C. A. Davis, F. Schlesinger, J. Drenkow, C. Zaleski, S. Jha, P. Batut, M. Chaisson, T. R. Gingeras, *Bioinformatics* **2013**, *29*, 15.
[80] K. D. Pruitt, T. Tatusova, D. R. Maglott, *Nucleic Acids Res.* **2007**, *35*, D61.
[81] R. J. C. Kluin, K. Kemper, T. Kuilman, J. R. de Ruiter, V. Iyer, J. V. Forment, P. Cornelissen-Steijger, I. de Rink, P. ter Brugge, J.-Y. Song, S. Klarenbeek, U. Mcdermott, J. Jonkers, A. Velds, D. J. Adams, D. S. Peeper, O. Krijgsman, *BMC Bioinf.* **2018**, *19*, 366.
[82] B. Li, C. N. Dewey, *BMC Bioinf.* **2011**, *12*, 323.
[83] M. E. Ritchie, B. Phipson, D. Wu, Y. Hu, C. W. Law, W. Shi, G. K. Smyth, *Nucleic Acids Res.* **2015**, *43*, e47.

SUPPORTING TABLES

Table S1: Patients characteristics

Age	(N=15)
Mean (±sd)	61.1 (±13.9)
Median	59
BMI	(N=15)
Mean (±sd)	30.3 (±5.1)
Median	31.5
Tumor type	(N=15)
Endometrioid	14 (93.3%)
Mixed (90% endometroid)	1 (6.7%)
Grade	(N=15)
1	6 (40%)
2	4 (26.7%)
3	5 (33.3%)
FIGO	(N=15)
IA	10 (66.7%)
IB	2 (13.3%)
II	2 (13.3%)
IIIC2	1 (6.7%)
Treatment	(N=15)
None	7 (46.7%)
BT	4 (26.7%)
BT+RT	3 (20.0%)
CT+RT	1 (6.7%)
Recurrence	(N=15)
No	13 (86.7%)
Yes	2 (13.3%)
Death	(N=15)
No	14 (93,3%)
Yes	1 (6,7%)
Follow-up	(N=15)

Mean months (CI)	59.27 (47.30-71.23)
PDOX growth time	(N=15)
Mean days (CI)	102.47 (84.57-120.36)

Table S2: Individual patient clinical parameters

Patient	Age	BMI	Treatment	Time-elapsed after primary tumor PDOX engraftment to first passage in mice
1	49	24	BT	128
2	50	34	BT	115
3	73	36	None	49
4	35	21	CT+RT	113
5	85	32.1	BT+RT	30
6	77	31	None	99
7	59	23.3	BT+RT	109
8	67	27.8	None	79
9	54	39	None	98
10	84	31.5	None	120
11	51	25	BT	90
12	61	33.8	BT+RT	152
13	58	30.9	None	96
14	59	34	None	113
15	54	31.7	BT	146

Table S3. Histologic characterization of primary tumors and PDOX

Case	TCGA	Histology		Grade		PTEN		TP53		CTNNB1 (nuclear)		ESR		MSH6		PMS2	
	BX	BX	PDOX	BX	PDOX	BX	PDOX	BX	PDOX	BX	PDOX	BX	PDOX	BX	PDOX	BX	PDOX
1	TP53	EEC	EEC	G2	G2	Loss	Loss	Abn	Abn	-	-	+	+	WT	WT	WT	WT
2	POLE	EEC	EEC	G3	G3	Loss	Loss	WT	WT	-	-	-	-	Loss	Loss	WT	WT
3	MSI	EEC	EEC	G1	G2	WT	WT	WT	WT	-	-	+	+	WT	WT	Loss	Loss
4	MSS	EEC	EEC	G3	G2	WT	WT	WT	WT	-	-	+	+	WT	WT	WT	WT
5	MSI	EEC	EEC	G3	G3	WT	WT	WT	WT	+	+	-	-	WT	WT	Loss	Loss
6	MSI	EEC	EEC	G2	G2	WT	WT	WT	WT	-	-	+	+	WT	WT	Loss	Loss
7	MSS	EEC	Undiff	G1	G3	WT	WT	WT	WT	-	-	+	-	WT	WT	WT	WT
8	MSI	EEC	EEC	G1	G1	Loss	Loss	WT	WT	-	-	+	+	WT	WT	Loss	Loss
9	MSS	EEC	EEC	G1	G1	Loss	Loss	WT	WT	+	+	+	+	WT	WT	WT	WT
10	MSI	EEC	EEC	G1	G1	WT	WT	WT	WT	-	-	+	+	WT	WT	Loss	Loss
11	MSI	Mixed	Mixed	G3	G3	Loss	Loss	WT	WT	-	-	+	+	WT	WT	Loss	Loss
12	MSI	EEC	EEC	G1	G1	Loss	Loss	WT	WT	-	-	+	+	WT	WT	Loss	Loss
13	MSS	EEC	Serous	G2	G2	Loss	Loss	WT	Abn	-	-	+	+	WT	WT	WT	WT
14	MSI	EEC	EEC	G2	G3	Loss	Loss	WT	WT	-	-	+	+	WT	WT	Loss	Loss
15	MSS	EEC	EEC	G3	G3	Loss	Loss	WT	WT	-	-	+	+	WT	WT	WT	WT

Table S4. Differentially expressed genes PDOX vs BX

Gene	logFC	AveExpr	t	P.Value	adj.P.Val	B statistic
C1QB	-7,814922925	1,868216456	-22,39080318	4,15916E-21	5,08307E-17	37,6826424
C1QA	-7,66019027	1,799580054	-21,66837235	1,11456E-20	5,08307E-17	36,76541243
TYROBP	-6,963280723	1,567376174	-21,64417598	1,15255E-20	5,08307E-17	36,73413673
C1QC	-7,412964263	1,598733799	-21,55820184	1,29864E-20	5,08307E-17	36,6227118
CLEC14A	-5,587954538	0,717256717	-21,46638945	1,47583E-20	5,08307E-17	36,50320678
SPI1	-5,444553187	0,707378125	-20,18458471	9,26759E-20	2,65995E-16	34,77743355
SLAMF8	-5,496187136	0,695962838	-19,3851532	3,06896E-19	6,68589E-16	33,64402193
FCER1G	-6,12959568	2,017399602	-19,37729833	3,10592E-19	6,68589E-16	33,63265678
ABI3	-4,66939749	0,295453738	-19,2351486	3,86008E-19	7,38604E-16	33,42619432
DCN	-7,912376879	2,860590238	-18,89782777	6,5013E-19	1,11959E-15	32,93021726
AIF1	-6,179118086	1,036547619	-18,6721115	9,25558E-19	1,449E-15	32,59350598
FCGR3A	-7,165966752	1,628361201	-18,41852404	1,38233E-18	1,98376E-15	32,21050324
MPEG1	-5,911680551	0,956197276	-18,29383127	1,68658E-18	2,23421E-15	32,02031775
APBB1IP	-4,580569852	0,182536593	-17,87256461	3,33081E-18	4,09713E-15	31,36854937
CD93	-6,414983117	1,236691756	-17,78718385	3,82956E-18	4,39659E-15	31,23468613
FCGR2A	-6,608132982	1,386464083	-17,74591951	4,09753E-18	4,41022E-15	31,1697741
CD2	-5,694804974	0,852421511	-17,58987979	5,29792E-18	5,36679E-15	30,92302868
SPARC	-9,141039395	4,207004753	-17,2772907	8,91442E-18	8,52863E-15	30,42254957
CYTH4	-5,048042807	0,600751332	-16,95232521	1,54376E-17	1,34053E-14	29,89333418
ELTD1	-5,61363943	0,814504256	-16,93232567	1,59726E-17	1,34053E-14	29,86046236
CSF1R	-6,023060225	1,249842964	-16,91873724	1,6347E-17	1,34053E-14	29,83810786
RGS1	-7,335967252	1,739307808	-16,68924523	2,42306E-17	1,89671E-14	29,45808693
SLA	-5,643033916	0,837008861	-16,5529819	3,06723E-17	2,29655E-14	29,23020781
CYYR1	-5,036357229	0,410430282	-16,28069082	4,93585E-17	3,54167E-14	28,76976765
FLI1	-4,980161875	0,56454293	-16,17588776	5,93768E-17	4,09011E-14	28,59072044
MS4A6A	-6,40371989	1,1169257	-16,00573571	8,03143E-17	5,27464E-14	28,29783731
GIMAP6	-4,7393148	0,407609434	-15,98933095	8,26985E-17	5,27464E-14	28,26945527
PLVAP	-6,255626616	1,920225786	-15,93044753	9,18724E-17	5,65048E-14	28,16736985
TMEM204	-4,644736136	0,426445028	-15,90771249	9,56887E-17	5,68226E-14	28,12786603
LCP2	-5,736803542	0,89674134	-15,86055586	1,04132E-16	5,97755E-14	28,04577042
MRVI1	-5,322397915	0,963304103	-15,64627091	1,53303E-16	8,51623E-14	27,67002284
CD3E	-4,892186917	0,737502524	-15,57963739	1,7304E-16	9,31223E-14	27,55227301
STAB1	-5,938827953	2,278400619	-15,46269602	2,14225E-16	1,09724E-13	27,34457073
ROBO4	-4,876452814	0,330478074	-15,45659621	2,16632E-16	1,09724E-13	27,33369976
COL15A1	-6,422871146	1,763815365	-15,32638371	2,75196E-16	1,35404E-13	27,10075767
CCR5	-4,57634218	0,180422757	-15,25280934	3,15254E-16	1,50805E-13	26,96839071
SASH3	-4,992300421	0,687620781	-15,05875286	4,52247E-16	2,1049E-13	26,61665211
GYPC	-4,94670184	0,466278541	-15,02978219	4,77424E-16	2,16361E-13	26,56381356
NDN	-4,942256415	0,476253756	-15,01282701	4,92822E-16	2,17612E-13	26,53284991
PDGFRB	-6,886855887	2,283122905	-14,99118579	5,13219E-16	2,20954E-13	26,49328592
GNLY	-5,179000123	0,504565816	-14,94023645	5,64736E-16	2,37203E-13	26,39995213
EVI2B	-5,300023245	0,661686826	-14,84456442	6,76307E-16	2,71133E-13	26,22396994
CD37	-4,487694842	0,157454344	-14,84401745	6,77006E-16	2,71133E-13	26,22296111
CXorf36	-4,683596467	0,234049901	-14,71652305	8,62048E-16	3,37394E-13	25,98696381
RAMP3	-5,455866508	0,814887089	-14,53805405	1,21222E-15	4,63901E-13	25,65375569
TREM2	-4,598552086	0,297242479	-14,51496872	1,26715E-15	4,74384E-13	25,61040931
CD247	-4,016658163	0,035744818	-14,41627501	1,53243E-15	5,6149E-13	25,42445796
LST1	-5,417246617	0,709925566	-14,32473763	1,82946E-15	6,56358E-13	25,25106065
DOK2	-3,744463153	-0,153983556	-14,2975389	1,92866E-15	6,77826E-13	25,19936539
LILRB4	-5,137129491	0,486844614	-14,21056925	2,28455E-15	7,86843E-13	25,03353112

ITGAX	-5,48024372	1,322660245	-14,19380007	2,36058E-15	7,97088E-13	25,00146144
PTPRC	-6,45268209	1,382046501	-14,17927669	2,42853E-15	8,04262E-13	24,97366199
RASAL3	-4,017620404	0,47345537	-14,16489507	2,49779E-15	8,11593E-13	24,94611133
HCK	-5,005590274	0,709010789	-14,09246755	2,87873E-15	9,18049E-13	24,80702065
CD84	-4,852444959	0,318474147	-14,01083357	3,38035E-15	1,05842E-12	24,64956224
LAIR1	-5,001141552	0,904185524	-13,97995127	3,59277E-15	1,10484E-12	24,58980462
IL16	-4,470612103	0,780129083	-13,8913048	4,28194E-15	1,29367E-12	24,41768799
TRAF3IP3	-3,982412551	-0,047550683	-13,7870555	5,26889E-15	1,56441E-12	24,21416135
VSIG4	-5,311579787	0,579069341	-13,74277986	5,75605E-15	1,68008E-12	24,12735488
TIGIT	-4,629314868	0,282714287	-13,70724077	6,18041E-15	1,77388E-12	24,05751831
DOCK2	-4,593025189	0,26203482	-13,67465597	6,59769E-15	1,8626E-12	23,99336242
FCGR1A	-4,914697064	0,349600199	-13,64229648	7,04074E-15	1,92877E-12	23,9295318
HOXD10	-4,608815104	0,385950336	-13,64121436	7,05608E-15	1,92877E-12	23,92739522
GIMAP1	-3,4874944	-0,309551203	-13,58779552	7,85719E-15	2,08384E-12	23,82175879
IGLL5	-8,478650234	2,321861191	-13,58727977	7,86537E-15	2,08384E-12	23,82073731
SPN	-3,729564621	-0,181237508	-13,57772615	8,01837E-15	2,09219E-12	23,80181031
LILRB2	-4,62087369	0,202688512	-13,54385484	8,58585E-15	2,20682E-12	23,73462323
ADORA3	-3,604059193	-0,14828729	-13,47470295	9,87595E-15	2,50108E-12	23,59704851
ARHGAP9	-4,482836457	0,6913504	-13,45693274	1,02385E-14	2,55533E-12	23,56160735
VWF	-5,849211507	2,882184865	-13,44949308	1,03944E-14	2,55716E-12	23,54675887
COL3A1	-8,647755135	4,456930782	-13,34925235	1,27479E-14	3,09199E-12	23,34607417
CD52	-5,943181402	1,217293922	-13,29549026	1,42289E-14	3,40328E-12	23,23796465
ARHGAP25	-4,648960956	0,926310079	-13,28269517	1,46067E-14	3,44578E-12	23,21218597
IKZF1	-4,410421333	0,522711158	-13,24487195	1,57848E-14	3,67338E-12	23,13587151
GIMAP7	-4,368013341	0,315045484	-13,19292101	1,75638E-14	4,03288E-12	23,03078147
NKG7	-4,972885178	0,447197582	-13,18270735	1,79371E-14	4,0644E-12	23,01008363
CNRIP1	-4,129165903	0,003003879	-13,17250146	1,83182E-14	4,09686E-12	22,9893894
HAVCR2	-5,003847329	0,878810438	-13,15379566	1,90385E-14	4,20336E-12	22,95142856
ANGPT2	-5,900526221	1,75635974	-13,14415673	1,94209E-14	4,23352E-12	22,93185177
FCGR2B	-5,169034647	0,47676899	-13,1040207	2,11E-14	4,54204E-12	22,85021813
PLEK	-5,76174741	1,129824181	-13,07080415	2,26019E-14	4,80527E-12	22,78251551
FLT1	-5,963811996	2,152036929	-13,05482921	2,33628E-14	4,90648E-12	22,74990898
GPR116	-5,000684407	1,111506685	-13,0156517	2,53422E-14	5,24557E-12	22,66981658
FPR3	-4,930021882	0,411104476	-13,01103197	2,55867E-14	5,24557E-12	22,66036033
ZEB2	-5,132420072	0,887809771	-13,00002066	2,61792E-14	5,30391E-12	22,63781087
C3AR1	-5,126822576	0,455662955	-12,94764529	2,91963E-14	5,8464E-12	22,53035823
FNDC1	-4,565656225	0,403478957	-12,90996727	3,15856E-14	6,25213E-12	22,45285777
GGT5	-4,33454745	0,750049659	-12,88937324	3,29754E-14	6,45305E-12	22,41042647
GPR4	-3,877871766	-0,145903675	-12,88074184	3,35763E-14	6,49683E-12	22,39262762
CD53	-6,037901657	1,842461847	-12,87123964	3,4251E-14	6,55373E-12	22,37302284
IL10RA	-4,689022902	1,17096223	-12,81250983	3,87407E-14	7,33136E-12	22,25161398
A2M	-7,722541104	3,972616434	-12,78768245	4,08162E-14	7,64017E-12	22,20016596
FGR	-4,851095032	0,630816439	-12,74251693	4,48892E-14	8,31222E-12	22,10638356
GZMA	-5,3202227	0,826330751	-12,73307596	4,57919E-14	8,38918E-12	22,0867493
CXCL9	-6,681974115	1,490395915	-12,71000549	4,80771E-14	8,71512E-12	22,03872491
FERMT3	-3,523580879	1,865521815	-12,64090522	5,56471E-14	9,98228E-12	21,89449999
IGSF6	-4,268014344	0,08070877	-12,51053769	7,34336E-14	1,30371E-11	21,62082755
NLRC3	-3,558224006	0,060574432	-12,49465931	7,59667E-14	1,33492E-11	21,58735409
APOC2	-4,86287055	0,528990322	-12,47998883	7,83868E-14	1,35553E-11	21,55639973
TESPA1	-2,76543485	-0,725030908	-12,47804211	7,87138E-14	1,35553E-11	21,55229022
CCL3	-5,202834279	0,562172132	-12,42435416	8,83056E-14	1,49774E-11	21,43877321
SFRP4	-6,431590506	1,545725076	-12,42221737	8,87113E-14	1,49774E-11	21,43424792
MYCT1	-3,830580752	-0,151060907	-12,35439334	1,02631E-13	1,71593E-11	21,2903197

CD27	-4,239336671	0,158549035	-12,3267838	1,08921E-13	1,80359E-11	21,23156822
TNFAIP8L2	-3,921301897	-0,147097384	-12,32088049	1,10317E-13	1,8093E-11	21,21899413
GMFG	-5,108151576	0,715626965	-12,28350711	1,19587E-13	1,94284E-11	21,13928911
AMICA1	-4,231808232	0,374251873	-12,25454325	1,27318E-13	2,04911E-11	21,07740027
NCKAP1L	-4,692905181	0,938864486	-12,22666414	1,35244E-13	2,15652E-11	21,01773132
FYB	-4,893387514	0,98972134	-12,15118114	1,59341E-13	2,51745E-11	20,85569354
ISLR	-6,035650956	2,545338612	-12,12443246	1,68901E-13	2,64423E-11	20,79810283
SAMD3	-3,086838379	-0,541515056	-12,07550287	1,87938E-13	2,91575E-11	20,69252525
COL6A3	-7,328289567	3,430832427	-12,05662211	1,9586E-13	3,01152E-11	20,65170546
LILRB3	-4,176036321	-0,019730172	-12,04292842	2,01819E-13	3,07568E-11	20,62207212
IL2RB	-4,528343545	1,013340625	-12,01969715	2,12356E-13	3,20788E-11	20,57174564
CXCR6	-4,307170052	0,076864474	-11,97446262	2,34522E-13	3,51192E-11	20,47355879
INMT	-3,258579073	-0,376877899	-11,96076323	2,41692E-13	3,56434E-11	20,443772
RGS5	-4,633747438	3,826987826	-11,95988004	2,42162E-13	3,56434E-11	20,44185085
LAPTM5	-6,42203236	3,724157134	-11,94918083	2,4793E-13	3,61831E-11	20,41856977
CD163	-5,940132615	0,973406238	-11,92826918	2,59612E-13	3,75696E-11	20,37302525
MMRN1	-4,255274808	0,134115259	-11,91768235	2,6574E-13	3,8136E-11	20,34994667
CARD11	-3,211026544	-0,296472951	-11,8801585	2,8868E-13	4,10856E-11	20,26803338
ITK	-4,120850039	-0,047323313	-11,87627665	2,91166E-13	4,10998E-11	20,25954927
NTM	-3,584182066	-0,114164657	-11,84646098	3,11008E-13	4,35436E-11	20,19432129
KLRK1	-4,231981835	0,079993649	-11,83342156	3,20116E-13	4,44574E-11	20,16575949
SIGLEC10	-4,421829043	0,103166188	-11,80807771	3,38608E-13	4,66493E-11	20,11018425
MYO1G	-3,41572415	0,117873146	-11,75818575	3,78277E-13	5,17008E-11	20,00054066
MS4A4A	-4,610229929	0,228394413	-11,75128161	3,8413E-13	5,19719E-11	19,98534308
IFFO1	-3,673719489	0,581508829	-11,74875314	3,86296E-13	5,19719E-11	19,97977583
GIMAP8	-4,039437563	0,372274734	-11,71031967	4,20815E-13	5,61771E-11	19,89505179
ITGAL	-4,63857996	1,188514212	-11,66630565	4,64252E-13	6,14073E-11	19,79779456
LILRB1	-3,737314085	0,063082122	-11,66354509	4,67125E-13	6,14073E-11	19,79168632
SLAMF7	-5,281770396	0,891770568	-11,63936778	4,93077E-13	6,43222E-11	19,73814823
CSF2RB	-4,627978573	0,238015192	-11,63603547	4,96768E-13	6,43222E-11	19,73076333
NID2	-4,833074577	0,722322599	-11,62766172	5,06169E-13	6,50503E-11	19,71219954
MS4A7	-4,883247561	0,392499873	-11,60171928	5,36466E-13	6,84332E-11	19,6546307
C1orf162	-3,664858686	1,20135071	-11,56886491	5,7752E-13	7,31284E-11	19,58159982
EMCN	-4,314929829	0,08149082	-11,52396229	6,38892E-13	8,03092E-11	19,48156316
CD86	-4,732927618	0,64365662	-11,51663087	6,49529E-13	8,10547E-11	19,46520518
HK3	-3,815060598	-0,009340655	-11,47203467	7,18263E-13	8,89871E-11	19,3655523
SLAMF6	-3,750392007	-0,191311585	-11,43082458	7,88398E-13	9,69786E-11	19,27323785
EVI2A	-5,339623214	0,670168608	-11,36794252	9,09203E-13	1,11026E-10	19,13195305
GIMAP4	-5,5616421	1,098532171	-11,36490654	9,15494E-13	1,11026E-10	19,1251188
OLFML2B	-4,70898361	1,571446235	-11,35360313	9,39311E-13	1,13118E-10	19,09966329
SH2D3C	-3,948405243	0,528721523	-11,2426213	1,20973E-12	1,44672E-10	18,8488485
SIGLEC9	-2,853873394	-0,639570892	-11,16023896	1,4611E-12	1,73528E-10	18,66162962
SRGN	-6,714019653	2,420742268	-11,12062908	1,60042E-12	1,88773E-10	18,57129786
THBS2	-5,913176652	1,469463165	-11,11297322	1,62888E-12	1,90822E-10	18,55381469
PRKCB	-3,859693536	-0,045931403	-11,09721498	1,6891E-12	1,9654E-10	18,51780449
SPARCL1	-6,854973046	2,903330912	-11,09399278	1,70169E-12	1,96676E-10	18,51043721
GPR65	-3,99912998	0,05086723	-11,04853621	1,88991E-12	2,16975E-10	18,40635956
IGJ	-7,400688599	1,963616011	-11,02298653	2,00494E-12	2,28656E-10	18,34774166
BIN2	-4,18294869	0,603575063	-10,98118737	2,20879E-12	2,50089E-10	18,2516578
CLEC2B	-5,303944767	1,173836468	-10,9786337	2,22191E-12	2,50089E-10	18,24578023
RUNX1T1	-3,514578639	-0,125848855	-10,92435519	2,5205E-12	2,81854E-10	18,12064805
CXCL12	-5,282811833	0,596253583	-10,91512452	2,57523E-12	2,86116E-10	18,09932924
IL21R	-3,520453397	-0,32461286	-10,89077892	2,72547E-12	3,0075E-10	18,04304752

GZMB	-5,139975282	0,736550237	-10,88820502	2,74187E-12	3,0075E-10	18,03709264
TNFRSF4	-2,788274219	-0,580214092	-10,88455056	2,76533E-12	3,01403E-10	18,02863631
MARCH1	-4,016623686	0,21074099	-10,75771396	3,72062E-12	4,02974E-10	17,73404359
CD3D	-4,48458665	0,461855493	-10,74339707	3,84785E-12	4,12937E-10	17,70065689
MSR1	-5,10281673	0,782813895	-10,74199152	3,86057E-12	4,12937E-10	17,69737769
C11orf96	-4,595153726	0,813965825	-10,7193392	4,07174E-12	4,31519E-10	17,64449301
CD48	-5,468936901	0,695223443	-10,71748625	4,08953E-12	4,31519E-10	17,64016405
LY86	-3,664807217	-0,275344725	-10,71541941	4,10946E-12	4,31519E-10	17,63533485
ALOX5AP	-5,200210363	0,869096822	-10,65807407	4,70408E-12	4,88073E-10	17,50111983
OLFML1	-4,021203003	0,26990168	-10,65801614	4,70473E-12	4,88073E-10	17,50098401
MYO1F	-4,039549504	1,628963933	-10,62426668	5,09519E-12	5,25415E-10	17,42178935
BTK	-3,779922924	0,067166933	-10,61994335	5,14755E-12	5,27654E-10	17,41163347
CCL4	-4,864107969	0,457891403	-10,57739567	5,69316E-12	5,8013E-10	17,31155222
EGFLAM	-3,764503463	0,173261078	-10,55601078	5,98939E-12	6,06725E-10	17,26115906
CLEC5A	-4,07970606	-0,016442489	-10,54497464	6,14838E-12	6,19189E-10	17,23512867
CLEC1A	-3,207508848	-0,210009607	-10,53870075	6,24069E-12	6,24831E-10	17,22032347
SULF1	-6,199735594	3,167045414	-10,51900809	6,53972E-12	6,50986E-10	17,17381837
SIRPG	-3,242091026	-0,343626254	-10,51250968	6,64159E-12	6,57326E-10	17,15846069
ZEB1	-4,24562681	1,706267938	-10,50740858	6,72269E-12	6,61551E-10	17,14640132
TEK	-4,155390403	0,166776535	-10,46260619	7,47994E-12	7,3142E-10	17,04033549
CLEC10A	-3,225750804	-0,494872931	-10,46049862	7,51764E-12	7,3142E-10	17,03533938
JAM3	-4,453439345	0,73412396	-10,43827022	7,92729E-12	7,66943E-10	16,98260942
COL5A1	-6,322382238	2,432825461	-10,428624	8,1121E-12	7,80438E-10	16,95970617
SIGLEC1	-4,20351705	0,322141298	-10,42624878	8,15828E-12	7,8052E-10	16,95406471
ADAMTS2	-5,296119701	1,247071415	-10,4081866	8,51834E-12	8,10466E-10	16,9111399
SLA2	-3,128620785	-0,262411933	-10,3602382	9,55512E-12	9,03471E-10	16,796978
HSPA7	-3,857742097	0,270929037	-10,35825036	9,60078E-12	9,03471E-10	16,79223842
RPL19P12	-2,843771315	1,121854586	-10,34268042	9,96629E-12	9,32769E-10	16,75509688
THBD	-4,216913071	0,634188802	-10,29347437	1,12177E-11	1,04422E-09	16,63750332
HAND2	-3,350555962	-0,432470352	-10,2770532	1,16702E-11	1,0763E-09	16,59818724
COX7A1	-3,781643124	0,067156788	-10,27644603	1,16873E-11	1,0763E-09	16,59673284
TAGAP	-3,951652228	0,133128558	-10,2722158	1,18071E-11	1,08154E-09	16,58659846
EXOC3L2	-2,619128911	-0,554551297	-10,25813274	1,22148E-11	1,10988E-09	16,55284225
KLRB1	-3,744555077	-0,235470794	-10,25709596	1,22454E-11	1,10988E-09	16,5503561
CYBB	-5,155146861	2,063661764	-10,2473436	1,25369E-11	1,12778E-09	16,52696333
PTPN7	-4,314827763	0,834992941	-10,24559848	1,25898E-11	1,12778E-09	16,522776
OR51E1	-2,994746267	-0,406229451	-10,24397383	1,26393E-11	1,12778E-09	16,51887735
CD8A	-4,607243577	1,59159468	-10,1862403	1,45322E-11	1,28999E-09	16,38010449
KCNMB1	-4,121464138	0,034963334	-10,17250302	1,50238E-11	1,32679E-09	16,34701834
WNT2	-4,757558123	1,290514149	-10,17014661	1,51098E-11	1,32758E-09	16,34134037
GPR183	-4,433634316	0,333089877	-10,16005903	1,54838E-11	1,35354E-09	16,31702511
PPP1R16B	-3,722124947	0,149227812	-10,11738926	1,71734E-11	1,49365E-09	16,21402132
DTX1	-3,255239176	-0,021988605	-10,10392706	1,77447E-11	1,53559E-09	16,18147292
PECAM1	-5,379243006	2,616952847	-10,10152774	1,78485E-11	1,53685E-09	16,17566936
MAGI2-AS3	-3,65070467	0,102182403	-10,09788197	1,80075E-11	1,54282E-09	16,16684936
ATP8B4	-3,077365307	0,02103526	-10,08849774	1,84234E-11	1,57064E-09	16,1441384
MRGPRF	-3,569299122	0,332786388	-10,03457681	2,10109E-11	1,77443E-09	16,01341288
NRXN2	-3,685556939	0,086081023	-10,03440147	2,10199E-11	1,77443E-09	16,01298717
WAS	-3,380386859	1,090503758	-10,02889612	2,13043E-11	1,78966E-09	15,9996178
IRF4	-3,271958314	-0,400018112	-10,01972783	2,17866E-11	1,8213E-09	15,97734418
ABCC9	-3,492789504	-0,251609511	-10,01311781	2,21413E-11	1,84201E-09	15,96127861
C3orf72	-3,353900168	-0,163183331	-9,993155594	2,32487E-11	1,92484E-09	15,91272491
MNDA	-4,216146871	0,000325103	-9,98933365	2,34671E-11	1,93362E-09	15,90342272

PCDH12	-3,546700074	0,034237479	-9,966025423	2,48452E-11	2,03742E-09	15,84665039
LSP1	-4,817914387	1,927639155	-9,960977267	2,51544E-11	2,04446E-09	15,83434482
CCR1	-3,805104746	0,87805979	-9,960748831	2,51684E-11	2,04446E-09	15,8337879
MYH11	-6,177888149	1,641745924	-9,916708512	2,804E-11	2,26703E-09	15,72628613
SIGLEC7	-2,699674688	-0,757910989	-9,912801502	2,83104E-11	2,27819E-09	15,71673651
THY1	-6,160316113	2,537175855	-9,893752638	2,96674E-11	2,37629E-09	15,67014722
TMEM119	-3,891483035	0,347954699	-9,877657098	3,08658E-11	2,46083E-09	15,63074286
HCST	-3,328686763	0,599052599	-9,848909069	3,31306E-11	2,62923E-09	15,56027609
NCF1	-3,594415094	0,232389395	-9,810247209	3,64469E-11	2,87652E-09	15,46533244
CD28	-3,186662041	-0,455792887	-9,808762493	3,65808E-11	2,87652E-09	15,46168233
GVINP1	-3,367514922	-0,243093667	-9,806563591	3,67801E-11	2,87904E-09	15,45627587
GAB3	-2,961984898	0,058032961	-9,781574199	3,91239E-11	3,04866E-09	15,3947883
FOXF1	-3,128555663	-0,439813021	-9,773471158	3,99162E-11	3,09639E-09	15,37483226
SAMSN1	-4,601610329	0,397139818	-9,742533816	4,30952E-11	3,32799E-09	15,29855857
CCL5	-5,123547936	2,4113772	-9,718199396	4,57766E-11	3,51928E-09	15,23847293
LOC100130231	-2,677148076	-0,769174295	-9,706340656	4,71445E-11	3,59279E-09	15,20916275
C16orf54	-2,813991081	-0,67472459	-9,706293304	4,71501E-11	3,59279E-09	15,20904568
FAM162B	-2,445244714	-0,862311888	-9,686165717	4,95683E-11	3,76042E-09	15,15925447
IL7R	-4,800806008	0,907512861	-9,63043819	5,69465E-11	4,30121E-09	15,02111109
TARP	-3,091182734	-0,562156966	-9,625319068	5,76782E-11	4,33745E-09	15,0084002
GIMAP1-GIMAP5	-3,646483373	-0,253478865	-9,620322353	5,84016E-11	4,37276E-09	14,99598984
ZNF683	-2,89682661	-0,659335028	-9,583811729	6,3977E-11	4,76947E-09	14,90520583
CETP	-2,324759223	-0,877725639	-9,546049156	7,0317E-11	5,21952E-09	14,81111935
OLR1	-4,062961302	0,00092936	-9,430836737	9,39212E-11	6,9417E-09	14,52287455
SELP	-2,980841027	-0,562877889	-9,417860534	9,7044E-11	7,14186E-09	14,49029775
HTR2B	-3,798028707	0,243759883	-9,401373243	1,01165E-10	7,41348E-09	14,44887362
SCIMP	-2,877641672	-0,550297194	-9,397774307	1,02088E-10	7,44942E-09	14,43982645
CD300LF	-3,314262727	-0,38037306	-9,373927764	1,08426E-10	7,8785E-09	14,3798359
GNG2	-4,426718919	0,887814068	-9,337494193	1,18894E-10	8,60284E-09	14,28803236
HNRNPKP3	-2,505125902	-0,855185382	-9,315968545	1,25558E-10	9,04701E-09	14,23370912
ZAP70	-3,409122524	0,437044831	-9,286751006	1,35218E-10	9,70245E-09	14,1598745
FCGR1B	-2,861566548	-0,608461733	-9,240985245	1,51898E-10	1,08541E-08	14,04399083
GIMAP5	-4,110729541	0,070802777	-9,213932095	1,62732E-10	1,15802E-08	13,97535718
COL6A2	-6,201470865	3,350693727	-9,205434643	1,66295E-10	1,1785E-08	13,95377894
FGF1	-3,367289765	0,509163549	-9,167396052	1,83246E-10	1,29331E-08	13,85706592
KIAA1755	-3,406654249	0,085929529	-9,159361921	1,87046E-10	1,31475E-08	13,83661436
KDR	-4,316053886	1,27277224	-9,130071054	2,01596E-10	1,41125E-08	13,76197882
HIC1	-3,44773281	0,177245276	-9,115733885	2,09133E-10	1,45809E-08	13,72540469
MRC1	-3,829150221	0,12575944	-9,109492143	2,12503E-10	1,47089E-08	13,70947341
BATF	-3,228284539	-0,033677813	-9,108141666	2,1324E-10	1,47089E-08	13,7060258
RASGRP2	-3,05647192	-0,312613463	-9,107607761	2,13532E-10	1,47089E-08	13,70466274
CD34	-4,330739302	2,250498487	-9,066206957	2,37454E-10	1,62916E-08	13,5988501
ZNF469	-3,151279368	-0,116339649	-9,059496792	2,41582E-10	1,6509E-08	13,58167863
BCL6B	-3,177294852	0,531193461	-9,036738259	2,56133E-10	1,74342E-08	13,52339431
SYNPO2	-4,878435453	1,799742126	-9,025466095	2,63668E-10	1,78765E-08	13,49450087
CD209	-2,790590072	-0,671212553	-9,020756019	2,66883E-10	1,80235E-08	13,48242272
NRIP2	-2,825638196	-0,694929235	-8,992057067	2,87356E-10	1,93303E-08	13,40876559
P2RY14	-3,270942497	-0,472277085	-8,971701557	3,02842E-10	2,02928E-08	13,35645585
APOE	-4,091510249	4,023385541	-8,94492084	3,24522E-10	2,16493E-08	13,28755071
CDH13	-4,160649274	0,12311391	-8,943332849	3,25856E-10	2,16493E-08	13,28346192
ECSCR	-3,625858231	0,563613636	-8,940699432	3,2808E-10	2,16493E-08	13,2766806
CTSW	-3,610712126	0,343141139	-8,940658958	3,28115E-10	2,16493E-08	13,27657637

MMP9	-5,259518313	1,461417678	-8,91334677	3,52125E-10	2,31448E-08	13,20619032
TRPC4	-2,679075883	-0,607653914	-8,909769252	3,554E-10	2,32186E-08	13,19696339
BHLHE22	-2,566951986	-0,82427234	-8,909178832	3,55944E-10	2,32186E-08	13,19544046
LOC100506776	-2,523675983	-0,777407016	-8,902993692	3,61688E-10	2,35043E-08	13,17948363
ACVRL1	-4,322885638	1,541375697	-8,899341286	3,65125E-10	2,36384E-08	13,17005854
LILRA6	-2,814115308	-0,700690679	-8,896759651	3,67574E-10	2,37078E-08	13,16339552
ACTA2	-5,00622035	4,375001807	-8,8705146	3,93443E-10	2,52817E-08	13,09560884
CD14	-4,276048504	2,735375729	-8,85992487	4,044E-10	2,58891E-08	13,06823152
LYL1	-2,624598284	-0,303988285	-8,844472612	4,20949E-10	2,68487E-08	13,02825665
CNTN4	-3,589092585	-0,31320204	-8,82248152	4,45699E-10	2,83224E-08	12,97131154
GPR171	-2,75118492	-0,732155873	-8,81868919	4,50114E-10	2,84979E-08	12,961485
CCR2	-3,134052669	-0,540721998	-8,817102281	4,51975E-10	2,85109E-08	12,9573725
PXDN	-4,852009063	1,917676537	-8,81239742	4,57539E-10	2,86714E-08	12,94517782
CD96	-3,745646063	0,935681104	-8,812135799	4,5785E-10	2,86714E-08	12,94449963
LILRB5	-2,466525595	-0,874485535	-8,802896009	4,68988E-10	2,92625E-08	12,92054192
GZMH	-3,812705092	-0,201395787	-8,784138865	4,92456E-10	3,06158E-08	12,87187225
MEF2C	-4,213283527	1,284223277	-8,762928262	5,2044E-10	3,22392E-08	12,81678077
HAPLN1	-5,038951989	1,072896652	-8,756917238	5,28661E-10	3,26311E-08	12,80115726
ITGA11	-4,082590154	0,405640051	-8,720966709	5,80672E-10	3,57134E-08	12,70761772
VIPR2	-2,812189517	-0,677249614	-8,701617088	6,10795E-10	3,74324E-08	12,65720192
CMKLR1	-3,5591721	0,474709472	-8,688016096	6,32917E-10	3,86506E-08	12,62173497
WISP1	-4,155772722	0,960637577	-8,684446546	6,38857E-10	3,88755E-08	12,61242274
CD7	-3,043501676	0,535412623	-8,658173215	6,84364E-10	4,1498E-08	12,5438298
LY96	-3,778940482	0,251401571	-8,655068766	6,89955E-10	4,16902E-08	12,53571893
NUDT10	-3,025065117	-0,566489341	-8,645309657	7,07835E-10	4,26211E-08	12,51021352
DIO2	-4,68967287	2,52160994	-8,631751653	7,33462E-10	4,40103E-08	12,47475911
TFEC	-3,455141562	-0,100729894	-8,626185213	7,44255E-10	4,45028E-08	12,46019585
MIR143HG	-3,960169892	0,403470486	-8,623238956	7,50033E-10	4,46932E-08	12,45248604
IL12RB1	-2,708067104	-0,557231068	-8,618113794	7,60194E-10	4,51424E-08	12,43907175
SLC2A3	-5,133722251	2,020165581	-8,61032728	7,759E-10	4,59167E-08	12,41868526
SIGLEC14	-2,863272628	-0,676112019	-8,567791497	8,67722E-10	5,11748E-08	12,30718008
HTRA3	-4,119295635	1,371357533	-8,563653445	8,77226E-10	5,15588E-08	12,2963199
SP140	-3,214903438	0,028742235	-8,561629028	8,81915E-10	5,1658E-08	12,29100607
RNASEK-C17orf49	-4,035932143	1,152313262	-8,559833497	8,86094E-10	5,17269E-08	12,2862926
HOXD9	-4,089784698	0,886396937	-8,558296479	8,89688E-10	5,17612E-08	12,28225742
F13A1	-4,794870079	1,442639601	-8,548880743	9,12029E-10	5,28824E-08	12,25753134
TBX21	-2,134671271	-0,907264549	-8,529076505	9,60904E-10	5,55293E-08	12,20548727
MFNG	-3,093561781	1,39531282	-8,516076456	9,9443E-10	5,72745E-08	12,17129659
ACAN	-3,216760484	-0,478943058	-8,509058369	1,01302E-09	5,81508E-08	12,15282967
NCF1C	-2,975925944	-0,352682446	-8,485442079	1,07822E-09	6,1688E-08	12,09064079
RCSD1	-4,11587971	0,868422156	-8,457344306	1,16139E-09	6,62264E-08	12,01655744
ABCG2	-3,148421491	-0,13152089	-8,449060504	1,18714E-09	6,74711E-08	11,99469681
ALDH1A2	-3,875206908	1,033267689	-8,432340738	1,24089E-09	7,0294E-08	11,95054725
MMP11	-3,869175331	5,829341996	-8,420664449	1,27989E-09	7,19594E-08	11,9196941
APOC1	-4,799226042	3,117208197	-8,420652138	1,27993E-09	7,19594E-08	11,91966156
ICOS	-2,752707077	-0,731394794	-8,419800219	1,28283E-09	7,19594E-08	11,91740978
AOAH	-3,088350271	0,02035977	-8,416219462	1,29506E-09	7,241E-08	11,90794419
CCL18	-4,272847029	0,127855778	-8,402345852	1,34361E-09	7,48812E-08	11,87125437
MMP12	-5,678432666	1,048759813	-8,388174209	1,39511E-09	7,75007E-08	11,83375106
UBASH3A	-2,114119885	-0,757986633	-8,36105799	1,49933E-09	8,30224E-08	11,76192046
IL2RA	-3,590111577	-0,24338657	-8,313673706	1,70086E-09	9,38786E-08	11,63617604
CD33	-2,733560254	-0,684269868	-8,312477893	1,70629E-09	9,38786E-08	11,63299902

LPL	-3,092016041	0,27315618	-8,299181448	1,76785E-09	9,69558E-08	11,59766102
FCGR1C	-3,603575038	-0,197209358	-8,280885409	1,85627E-09	1,01265E-07	11,54899915
CXCR3	-2,646550398	-0,602516262	-8,280500497	1,85818E-09	1,01265E-07	11,54797495
GUCY1A2	-3,7268095	0,614722915	-8,277664864	1,87229E-09	1,01712E-07	11,54042912
HBB	-5,367833292	0,666026895	-8,260574516	1,95971E-09	1,06126E-07	11,49492906
FOLR2	-3,223497584	-0,219542055	-8,239307843	2,07432E-09	1,11981E-07	11,43825908
LUM	-7,106702301	3,976245145	-8,235476159	2,09569E-09	1,12781E-07	11,42804264
OSCAR	-2,463651393	-0,140944361	-8,163610585	2,5406E-09	1,36298E-07	11,23608774
TIE1	-4,219908044	1,127561578	-8,158664297	2,57455E-09	1,3769E-07	11,22285245
MAGEH1	-3,683646827	0,606676096	-8,156159693	2,59191E-09	1,3819E-07	11,21614946
P2RY13	-3,283328087	-0,466084289	-8,130900935	2,77385E-09	1,47434E-07	11,14850694
PDGFRA	-4,61800076	1,831925364	-8,12392196	2,82637E-09	1,49763E-07	11,12980346
ACAP1	-3,208564532	1,152463088	-8,108217681	2,9483E-09	1,55433E-07	11,08769444
LYZ	-5,442084959	3,032029891	-8,107821505	2,95144E-09	1,55433E-07	11,08663175
MS4A14	-2,548077974	-0,833709346	-8,100763851	3,00802E-09	1,5793E-07	11,06769731
CSF3R	-4,336017714	0,623328253	-8,074474095	3,22868E-09	1,69E-07	10,99711271
HBA2	-4,34468438	0,751508497	-8,052592615	3,42486E-09	1,78726E-07	10,9382992
SLAMF1	-2,73890043	-0,683848188	-8,041723438	3,52677E-09	1,83488E-07	10,90906305
GSPT2	-2,563033361	-0,713357771	-8,032106668	3,61951E-09	1,87506E-07	10,88318365
KLHL6	-3,416581129	0,662864791	-8,03146653	3,62577E-09	1,87506E-07	10,88146059
EDNRB	-3,362632861	-0,290356567	-8,012131178	3,82014E-09	1,96966E-07	10,82939225
CD4	-4,734147497	2,351463728	-7,999293821	3,95502E-09	2,03311E-07	10,79479734
GZMK	-3,988364977	-0,045062519	-7,996881188	3,9809E-09	2,04033E-07	10,7882934
FLJ44635	-2,249140098	1,050184406	-7,992122436	4,03246E-09	2,06062E-07	10,77546276
CLEC4A	-3,096196996	0,122103721	-7,979606156	4,17133E-09	2,12528E-07	10,74170305
EXOC3L1	-2,150814916	-0,716788933	-7,969914188	4,2822E-09	2,17457E-07	10,71554826
GPR34	-3,18447152	-0,453667151	-7,968955852	4,29333E-09	2,17457E-07	10,71296148
ECM2	-3,491474114	-0,028165582	-7,966137788	4,32621E-09	2,1848E-07	10,70535418
FOXL2	-2,996462812	-0,251096747	-7,959111698	4,40931E-09	2,22026E-07	10,68638327
SEMA6B	-3,155002909	0,297543588	-7,952653066	4,48713E-09	2,25286E-07	10,66893929
SH2D1A	-3,582877271	-0,316309697	-7,943032476	4,60565E-09	2,30564E-07	10,64294595
MSC	-3,24652059	-0,341275962	-7,92975706	4,77444E-09	2,38321E-07	10,60705961
ESM1	-5,324939956	1,255335163	-7,927013279	4,81011E-09	2,39407E-07	10,59963994
PARP15	-2,370345504	-0,922575581	-7,913530472	4,98932E-09	2,47611E-07	10,56316695
ARHGDIB	-4,462266162	4,194715893	-7,908379667	5,05957E-09	2,50376E-07	10,54922753
CD6	-2,928063618	0,940439165	-7,893456749	5,26881E-09	2,59983E-07	10,50882435
CPXM1	-4,899706366	2,145237536	-7,891079444	5,30295E-09	2,6092E-07	10,50238545
CD248	-4,707177395	1,428840856	-7,857237862	5,814E-09	2,85251E-07	10,41065318
RGS18	-2,723060764	-0,746217951	-7,854659262	5,85494E-09	2,85937E-07	10,40365797
PVRIG	-2,434610432	-0,700202922	-7,854266778	5,86119E-09	2,85937E-07	10,40259317
LMOD1	-4,158518669	0,86306976	-7,812169618	6,57327E-09	3,19769E-07	10,28827942
GPR84	-2,893748541	-0,47172956	-7,797670975	6,83837E-09	3,31728E-07	10,24886055
KCNJ8	-3,373601737	0,266366946	-7,780757299	7,16139E-09	3,46422E-07	10,20284463
TRPV2	-3,407831617	0,807195485	-7,770988442	7,35498E-09	3,5479E-07	10,17625196
GIPC3	-2,569052181	-0,402514863	-7,767426198	7,42689E-09	3,57258E-07	10,16655209
ITM2A	-3,940888265	0,436216837	-7,750864248	7,77071E-09	3,72756E-07	10,12143514
HLA-G	-3,378640367	0,461082658	-7,730494304	8,21586E-09	3,93015E-07	10,06590114
CADPS	-2,856121492	-0,519054718	-7,701251248	8,90061E-09	4,24591E-07	9,986093005
CD300A	-4,035140611	1,086294027	-7,681407383	9,39803E-09	4,47081E-07	9,931880616
ASPN	-4,518031303	0,404014194	-7,679622314	9,44414E-09	4,48037E-07	9,927001694
IL2RG	-4,549249198	2,194596451	-7,671084715	9,66786E-09	4,57391E-07	9,903661846
EMR2	-3,254592594	0,394052774	-7,667885601	9,75307E-09	4,60158E-07	9,894914057
RNASE6	-3,180673108	1,176880349	-7,625848384	1,09463E-08	5,15043E-07	9,779857861

CCND2	-4,469397033	2,055180746	-7,602013738	1,16876E-08	5,48426E-07	9,71453361
SRPX2	-3,656233318	1,003350321	-7,591815533	1,20202E-08	5,62499E-07	9,686563635
TCEAL7	-3,168406333	-0,400521932	-7,571867574	1,26988E-08	5,92644E-07	9,631820018
DAB2	-4,707023576	2,05186807	-7,553711932	1,33502E-08	6,21361E-07	9,581956581
DLL4	-3,712760948	1,384995552	-7,54038228	1,38499E-08	6,42883E-07	9,545324183
HEPH	-3,965445498	1,599866853	-7,538384892	1,39264E-08	6,44697E-07	9,53983329
CTSK	-2,715361979	3,830915885	-7,524504368	1,44701E-08	6,68068E-07	9,501663076
LPXN	-1,588263633	3,240789623	-7,513404868	1,49203E-08	6,8701E-07	9,471125173
CCM2L	-2,721167605	-0,490700946	-7,510542003	1,50387E-08	6,90616E-07	9,463246417
FCGR2C	-3,068267334	-0,550800578	-7,499910194	1,54868E-08	7,09304E-07	9,43397926
ADAMTS4	-3,747918622	0,816708628	-7,498229647	1,55589E-08	7,10714E-07	9,429351932
FOXP3	-2,167521678	0,248112995	-7,472155791	1,67216E-08	7,61805E-07	9,357519006
PDE1B	-2,683759398	-0,631735098	-7,458524409	1,73642E-08	7,88993E-07	9,319935432
RFTN1	-3,953432207	2,069307153	-7,447838533	1,78854E-08	8,10537E-07	9,290458966
HSPA12B	-2,918513828	-0,283171588	-7,436566879	1,84524E-08	8,34037E-07	9,259353319
PYHIN1	-2,452195939	-0,814945742	-7,422382823	1,91919E-08	8,65191E-07	9,220191106
ELK2AP	-5,289296691	0,536900013	-7,414697821	1,9605E-08	8,81509E-07	9,198963797
ADAMDEC1	-4,021473042	-0,097011812	-7,402467339	2,02812E-08	9,09539E-07	9,165168078
FCN1	-2,644081612	-0,785707527	-7,397430019	2,05666E-08	9,1994E-07	9,151244135
NCF1B	-2,625021383	-0,558447633	-7,394378585	2,07414E-08	9,25357E-07	9,142808183
SIT1	-2,729178839	-0,527241253	-7,388314692	2,10933E-08	9,37196E-07	9,126041091
TMEM130	-2,48253781	-0,761597335	-7,387933867	2,11156E-08	9,37196E-07	9,124987952
TLR7	-2,679397532	-0,630299585	-7,382173607	2,14559E-08	9,4985E-07	9,109056584
PLCL1	-2,203945161	-0,587883513	-7,376811251	2,17776E-08	9,61622E-07	9,094222559
SGIP1	-3,321469358	0,209317746	-7,372306732	2,20517E-08	9,71233E-07	9,081759243
SLCO2B1	-4,191591211	1,365003672	-7,335597648	2,44197E-08	1,07278E-06	8,980111246
GNGT2	-2,180874263	-0,74189871	-7,296449299	2,72303E-08	1,19321E-06	8,871553993
LAMC3	-3,86859022	0,947549658	-7,279907658	2,85144E-08	1,24631E-06	8,825636909
MGP	-5,116295236	4,155588571	-7,259691722	3,01675E-08	1,31523E-06	8,769482466
RNASE2	-2,090824736	-1,062335965	-7,25034185	3,09646E-08	1,34657E-06	8,743496938
CRTAM	-2,346412902	-0,842641733	-7,246913626	3,12622E-08	1,35609E-06	8,733966859
OSM	-3,47106035	-0,232111261	-7,241480983	3,17397E-08	1,37334E-06	8,718862283
JAK3	-3,70155945	1,571388863	-7,233312377	3,24717E-08	1,40149E-06	8,696145185
DOCK10	-3,29379013	1,179404775	-7,228143044	3,29437E-08	1,41831E-06	8,681765659
CD80	-2,190616632	-0,896258544	-7,217450213	3,39423E-08	1,45766E-06	8,65201289
EDNRA	-3,89443414	1,18785897	-7,213610466	3,43084E-08	1,46971E-06	8,641326003
CXorf21	-2,284936645	-0,965280011	-7,184120693	3,72563E-08	1,59204E-06	8,559200163
ARHGEF6	-3,38850526	1,460440632	-7,170947944	3,86548E-08	1,64771E-06	8,522487552
LDB2	-3,988942083	1,293130419	-7,163775358	3,94385E-08	1,67696E-06	8,50249026
LRRN4CL	-2,927296367	0,245288684	-7,138900896	4,22835E-08	1,79351E-06	8,433100673
SHE	-2,508576102	-0,216703853	-7,1357276	4,26611E-08	1,80508E-06	8,424244122
DENND1C	-2,890713452	0,829227461	-7,124518326	4,40224E-08	1,85811E-06	8,392951607
PLXDC1	-4,125022387	1,150262925	-7,118529455	4,47677E-08	1,88495E-06	8,3762277
COLEC12	-2,922476656	0,322631668	-7,091531974	4,82895E-08	2,02828E-06	8,300794321
HPGDS	-2,256901922	-0,922399428	-7,087979305	4,87734E-08	2,04362E-06	8,290862631
ITGB2	-4,587997363	2,817937336	-7,083574459	4,93802E-08	2,06402E-06	8,27854696
CCL4L1	-3,175549691	-0,496569517	-7,068916558	5,14549E-08	2,14035E-06	8,23755107
CCL4L2	-3,175549691	-0,496569517	-7,068916558	5,14549E-08	2,14035E-06	8,23755107
SDS	-3,230830681	0,366486359	-7,062563759	5,23814E-08	2,17364E-06	8,219776932
TNFSF13B	-3,09672287	0,703550497	-7,034413132	5,66943E-08	2,34695E-06	8,140970054
VCAM1	-4,301370909	1,215404544	-7,029633614	5,74615E-08	2,37301E-06	8,127582546
LILRA1	-1,59355545	-1,310970608	-7,018033315	5,93676E-08	2,44106E-06	8,095081057
FAM78A	-2,531679238	0,737279738	-7,01788216	5,93928E-08	2,44106E-06	8,09465747

PTPRCAP	-2,685828919	1,741067607	-7,011956307	6,03915E-08	2,4762E-06	8,078049624
STX11	-2,818784759	-0,054592373	-7,002264444	6,20617E-08	2,53863E-06	8,050880118
PAMR1	-4,295706105	1,928421221	-6,974348437	6,71386E-08	2,7398E-06	7,972574005
SOX18	-2,522377836	-0,103253397	-6,970902201	6,77938E-08	2,75999E-06	7,96290216
GPR85	-1,83117263	-0,866967592	-6,965154049	6,89012E-08	2,79846E-06	7,946767598
SCML4	-1,83652191	-1,16667329	-6,957351265	7,04337E-08	2,85397E-06	7,924861066
C1QTNF7	-3,019887734	-0,597804466	-6,954837073	7,09348E-08	2,86753E-06	7,917801231
CACNA2D4	-2,515801534	-0,394923862	-6,932405501	7,55686E-08	3,04268E-06	7,854788332
HLA-DQA1	-5,20962391	3,283021378	-6,931974273	7,56607E-08	3,04268E-06	7,853576521
DYSF	-2,87105293	1,27367826	-6,931333134	7,57977E-08	3,04268E-06	7,851774801
ATP1B2	-2,474802945	-0,605315535	-6,907730939	8,10207E-08	3,24478E-06	7,785422722
LAG3	-2,995530945	1,301935494	-6,905021365	8,16432E-08	3,26213E-06	7,777802228
MEG3	-3,874463701	0,149403159	-6,90182823	8,23829E-08	3,28407E-06	7,76882092
CORO1A	-2,672698981	3,278445534	-6,899341406	8,29638E-08	3,29958E-06	7,761825628
NLRC4	-2,311010782	-0,879227959	-6,896797385	8,35623E-08	3,31573E-06	7,75466888
LY9	-2,492242262	-0,861627202	-6,892736518	8,45266E-08	3,34628E-06	7,74324382
TNFRSF1B	-3,573012295	2,805171594	-6,879154019	8,78348E-08	3,46928E-06	7,705019608
RHOJ	-3,360675106	1,218760764	-6,878185039	8,80758E-08	3,47083E-06	7,702292066
SPOCK2	-2,37484459	3,507190798	-6,875355291	8,87833E-08	3,49072E-06	7,694326257
CXCL13	-5,092680602	1,264452548	-6,871293205	8,9809E-08	3,52301E-06	7,682890169
COL5A2	-3,397445018	4,34231704	-6,859051593	9,29732E-08	3,63884E-06	7,64841743
GAPT	-2,364895003	-0,925300831	-6,849015491	9,56512E-08	3,73517E-06	7,620145841
ITIH3	-2,134128351	-0,894999516	-6,8414734	9,7715E-08	3,80713E-06	7,59889417
FGD2	-2,691893646	0,421506862	-6,824211871	1,0261E-07	3,98881E-06	7,550237393
LOC100132891	-2,712774553	-0,605993354	-6,809615602	1,06942E-07	4,14784E-06	7,509073782
PDCD1LG2	-2,679312444	-0,053114252	-6,801201109	1,09523E-07	4,2384E-06	7,485335556
NCF4	-3,809628739	1,022661503	-6,765069369	1,21341E-07	4,68522E-06	7,383337029
ARHGEF15	-3,133071817	0,55695613	-6,735702949	1,31891E-07	5,07963E-06	7,30035799
APLNR	-3,036341834	0,420184116	-6,73502487	1,32145E-07	5,07963E-06	7,298441157
AIM2	-2,822100375	-0,464443205	-6,721636112	1,37269E-07	5,26482E-06	7,260585493
LYVE1	-2,433499865	-0,890998401	-6,710158867	1,4182E-07	5,4273E-06	7,228123107
TMEM255B	-2,224367721	-0,814968569	-6,708110907	1,42648E-07	5,44688E-06	7,222329535
STAT4	-2,609624079	0,641321363	-6,697395922	1,47061E-07	5,60296E-06	7,192011998
SNX20	-2,249729514	-0,761280578	-6,691244128	1,49656E-07	5,68926E-06	7,174601714
ARHGAP15	-3,643541236	0,711647291	-6,689591278	1,50362E-07	5,70348E-06	7,169923453
SVEP1	-3,123259164	0,987667125	-6,687910555	1,51082E-07	5,71822E-06	7,165166081
ADORA2A	-2,473718386	1,00858187	-6,669002729	1,59433E-07	6,02105E-06	7,111631399
GRP	-2,40597247	-0,834749885	-6,666110457	1,60751E-07	6,05754E-06	7,103439924
AQP1	-3,208726205	3,182864431	-6,648372023	1,69078E-07	6,35742E-06	7,053187217
IL3RA	-2,806534646	0,485443106	-6,633443501	1,76424E-07	6,61915E-06	7,010876399
S100B	-3,082943529	-0,293064796	-6,631110336	1,776E-07	6,64882E-06	7,004262161
ZNF831	-1,935369438	-1,003612505	-6,617792364	1,84471E-07	6,87966E-06	6,966499522
FCN3	-2,474978989	-0,736134143	-6,617612527	1,84566E-07	6,87966E-06	6,96598951
RAC2	-4,554720046	2,029561126	-6,613005009	1,87006E-07	6,95557E-06	6,952921916
NLRP3	-2,375399542	-0,649891074	-6,611060218	1,88046E-07	6,97917E-06	6,94740573
MEI1	-2,445898089	-0,301532535	-6,607657358	1,89879E-07	7,03206E-06	6,937753219
POU2F2	-2,408294367	0,732265349	-6,606452373	1,90533E-07	7,04112E-06	6,934334969
MMP19	-3,326146102	0,77558807	-6,601438633	1,93276E-07	7,12722E-06	6,920111052
CD79B	-2,978770735	-0,099826635	-6,583953864	2,03161E-07	7,47572E-06	6,870492554
MZB1	-3,848851147	0,649673485	-6,57021039	2,11288E-07	7,75819E-06	6,831475544
HOPX	-4,141794936	2,074408741	-6,553871068	2,21379E-07	8,11141E-06	6,785071398
DARC	-3,494489171	-0,02587318	-6,549041511	2,24453E-07	8,20661E-06	6,771351674
SLC2A5	-2,817178033	0,821127366	-6,525730919	2,39912E-07	8,75322E-06	6,705108244

ENPP2	-4,310523604	2,472640132	-6,500454756	2,57891E-07	9,38932E-06	6,633236459
TNFSF8	-3,163036507	-0,069234491	-6,493089069	2,63383E-07	9,56901E-06	6,612284193
ABCA8	-2,922015726	-0,580035849	-6,485886517	2,68866E-07	9,74767E-06	6,591792426
LAT2	-2,9378371	1,514628391	-6,476986057	2,75802E-07	9,97813E-06	6,566465175
PPAPDC3	-2,040819424	-0,895612296	-6,47052957	2,80946E-07	1,01429E-05	6,54808921
CD1C	-2,446682867	-0,884406899	-6,461460064	2,88336E-07	1,0388E-05	6,522271598
ITGAM	-2,972278543	0,680237646	-6,43843441	3,07992E-07	1,10729E-05	6,45670163
ISM1	-3,319691067	1,465173846	-6,413450575	3,30853E-07	1,187E-05	6,385516697
LRRC25	-3,040790725	0,380034169	-6,412229582	3,32013E-07	1,18869E-05	6,382036778
EMILIN1	-3,958390382	1,721401078	-6,402163915	3,41735E-07	1,22096E-05	6,353345336
KIR2DL4	-1,689259621	-1,263118522	-6,383334268	3,607E-07	1,28605E-05	6,29965589
ADAM12	-3,111798222	0,028878531	-6,369562539	3,75239E-07	1,33512E-05	6,260374438
C1orf54	-2,746451767	1,751647316	-6,354236977	3,92116E-07	1,39229E-05	6,216647488
STMN2	-2,017842009	-0,916191178	-6,351122836	3,95637E-07	1,40191E-05	6,207760494
CCDC102B	-2,249178052	-0,380374932	-6,33929937	4,09302E-07	1,44735E-05	6,174014006
GJD3	-1,801385481	0,516547766	-6,318618949	4,34356E-07	1,5328E-05	6,114968412
PIK3R6	-2,264031795	-0,653077445	-6,317371927	4,35916E-07	1,53515E-05	6,111407196
PIEZO2	-1,899633427	-1,157931619	-6,28144913	4,83343E-07	1,6987E-05	6,008782006
LOC158376	-1,677715076	-1,192103797	-6,270835407	4,98327E-07	1,7478E-05	5,978446748
RAPGEF4	-2,094769218	0,585001605	-6,26336812	5,09149E-07	1,78213E-05	5,957100704
TAL1	-1,915243952	-0,911327607	-6,253417378	5,2394E-07	1,83018E-05	5,928650788
HBA1	-2,927777308	-0,314980958	-6,24740201	5,3309E-07	1,85837E-05	5,911449846
GREM1	-3,950239615	0,377429282	-6,244231055	5,37978E-07	1,87161E-05	5,902381734
TRAF1	-2,17208335	2,50249429	-6,24353139	5,39063E-07	1,87161E-05	5,900380801
HLA-DRB6	-3,935445948	2,161329638	-6,237004742	5,49288E-07	1,90328E-05	5,881714374
DCHS1	-2,824516287	2,216150082	-6,23499341	5,52478E-07	1,91049E-05	5,875961452
GRAP2	-1,88513326	-1,043548882	-6,226554239	5,66068E-07	1,95356E-05	5,851820985
CD244	-2,111309102	-0,769357098	-6,225298442	5,68119E-07	1,95672E-05	5,848228432
PCED1B-AS1	-2,407904955	-0,877767654	-6,211889444	5,9049E-07	2,02971E-05	5,809863291
RASGRP4	-1,822740334	-1,196378166	-6,20821852	5,96768E-07	2,0472E-05	5,799358644
PRF1	-3,631407653	0,548155574	-6,205734437	6,01055E-07	2,05621E-05	5,792249856
ZBTB46	-2,737732848	0,623991448	-6,205314182	6,01783E-07	2,05621E-05	5,791047167
RARRES2	-4,003034412	3,580234252	-6,199527457	6,11901E-07	2,08664E-05	5,774485779
CLMP	-2,648285375	-0,412166141	-6,197886193	6,14802E-07	2,09239E-05	5,76978824
PDCD1	-2,801971617	-0,098299756	-6,181482719	6,44566E-07	2,18936E-05	5,722831827
KLRC1	-2,021468232	-1,097014217	-6,18021636	6,46923E-07	2,19118E-05	5,719206218
PDPN	-3,965547207	1,160451418	-6,179829147	6,47646E-07	2,19118E-05	5,718097605
COL1A1	-3,353715926	7,197402238	-6,176478424	6,53932E-07	2,20811E-05	5,708503984
IL18RAP	-2,371333438	-0,473968105	-6,162194211	6,81429E-07	2,29645E-05	5,667600139
CD226	-2,086983059	-0,638278071	-6,147047568	7,11859E-07	2,39432E-05	5,6242162
HAAO	-2,547266214	-0,235425435	-6,144702077	7,16692E-07	2,40553E-05	5,617497152
CLIP3	-2,023866615	2,577344558	-6,144077631	7,17984E-07	2,40553E-05	5,615708281
SLC7A7	-3,207009696	1,666888571	-6,139778198	7,26946E-07	2,43082E-05	5,603391068
NOVA2	-1,830921679	-1,023274644	-6,135594922	7,35773E-07	2,45557E-05	5,591405819
FAP	-4,334173701	1,521727682	-6,134474422	7,38156E-07	2,45876E-05	5,58819541
PIK3CG	-2,683890222	-0,734775441	-6,121799516	7,65657E-07	2,54234E-05	5,551875876
PLA2G2D	-2,940083836	-0,568715041	-6,121553082	7,66201E-07	2,54234E-05	5,551169657
MEDAG	-2,681909551	-0,54689215	-6,119365671	7,71054E-07	2,55352E-05	5,544900957
AKT3	-3,427525656	1,119710513	-6,103885685	8,06293E-07	2,6651E-05	5,500532302
LRRC32	-3,269819233	2,272472648	-6,097879618	8,20398E-07	2,70653E-05	5,483314963
P2RY10	-2,405097789	-0,869389101	-6,091608866	8,3539E-07	2,75072E-05	5,465337226
FASLG	-2,367735267	-0,706220719	-6,075716406	8,74633E-07	2,87444E-05	5,419767472
SELPLG	-2,398562343	2,159266159	-6,072244543	8,8345E-07	2,89788E-05	5,409810931

AMPH	-1,988285603	-0,728702053	-6,066166215	8,99102E-07	2,94362E-05	5,39237844
ITGBL1	-2,553368559	-0,247493517	-6,058042004	9,20459E-07	3,00782E-05	5,369076095
ANKRD30BL	-1,926764074	-0,856314464	-6,048845145	9,45253E-07	3,07913E-05	5,342693962
GABRD	-1,668552672	-1,097554721	-6,048624085	9,45858E-07	3,07913E-05	5,342059786
CYTIP	-3,586622581	1,478799422	-6,044628467	9,56845E-07	3,10902E-05	5,330596884
WFDC1	-2,968958667	0,998911576	-6,040127711	9,69375E-07	3,14381E-05	5,317684067
ARHGAP20	-1,779188633	-1,082458021	-6,033569979	9,87929E-07	3,19796E-05	5,298868333
CRMP1	-2,762905492	0,564572928	-6,023928088	1,01586E-06	3,2822E-05	5,271200446
CALCRL	-4,081104063	1,461649975	-6,02196995	1,02163E-06	3,29465E-05	5,265581049
PCDH17	-3,444049087	0,38763563	-6,002470482	1,0809E-06	3,47929E-05	5,209614498
AEBP1	-4,122469484	4,050535969	-5,995547801	1,10277E-06	3,54306E-05	5,189742037
FPR1	-3,640160672	0,093551551	-5,994064732	1,10751E-06	3,55166E-05	5,185484476
SLC11A1	-2,878485363	1,338948247	-5,988009516	1,12709E-06	3,60772E-05	5,168100499
TNFRSF9	-2,887079724	0,017221549	-5,96305083	1,21151E-06	3,87078E-05	5,096433256
MMP3	-4,070519181	0,312386149	-5,960926	1,21899E-06	3,88745E-05	5,090330992
TMEM176B	-4,15800786	2,771660661	-5,956798198	1,23364E-06	3,92691E-05	5,078476011
IL18BP	-1,688161362	2,406073662	-5,949640826	1,25947E-06	4,00174E-05	5,057918865
DKK3	-3,662409779	2,600465429	-5,946645631	1,27045E-06	4,02916E-05	5,049315695
CCL8	-2,68604861	-0,35602559	-5,940920126	1,29168E-06	4,08899E-05	5,032869413
FLT4	-2,946286467	0,681182198	-5,911298284	1,40741E-06	4,44715E-05	4,947766083
CD79A	-3,225194744	0,396700368	-5,90560107	1,43083E-06	4,51288E-05	4,931395105
ARL11	-2,46347059	-0,534512592	-5,897643622	1,46421E-06	4,6044E-05	4,908527815
ADAM33	-3,197814998	0,270118051	-5,897411392	1,46519E-06	4,6044E-05	4,90786043
PIK3R5	-3,51126834	0,554973723	-5,890812105	1,49348E-06	4,68475E-05	4,888894725
TPSAB1	-3,61280465	-0,224112755	-5,8833268	1,52624E-06	4,76365E-05	4,867381278
MAP4K1	-2,560038187	1,023393605	-5,883169787	1,52693E-06	4,76365E-05	4,866929994
PDE10A	-2,514631386	-0,120347718	-5,870421466	1,58442E-06	4,93404E-05	4,83028675
CPA3	-3,574051436	-0,320722615	-5,867828097	1,59637E-06	4,9623E-05	4,822831971
PSTPIP1	-2,71235284	0,490313482	-5,864954723	1,60973E-06	4,9948E-05	4,814572109
AGAP2	-2,384271698	0,246945109	-5,857629355	1,64428E-06	5,09284E-05	4,793513527
CCRL2	-2,622952241	0,030015873	-5,847515701	1,69322E-06	5,22212E-05	4,76443721
VENTX	-1,577821895	-1,277057096	-5,846980008	1,69585E-06	5,22212E-05	4,76289705
LOC100499405	-2,040309413	-0,285145509	-5,846512763	1,69815E-06	5,22212E-05	4,761553676
BCL2A1	-3,995192578	1,146279686	-5,841541377	1,72281E-06	5,28852E-05	4,747260162
FCRL5	-2,829796169	-0,692850249	-5,837193225	1,74468E-06	5,3461E-05	4,734758083
ITGA8	-1,770417397	-1,222539635	-5,836325002	1,74908E-06	5,35006E-05	4,732261662
TSPYL5	-3,374549487	0,108518147	-5,828810663	1,78762E-06	5,45826E-05	4,710654822
KLRD1	-2,594992484	-0,406306065	-5,826629617	1,79896E-06	5,48318E-05	4,704383179
JAKMIP2	-1,617989334	-1,024265314	-5,823137869	1,81728E-06	5,52922E-05	4,69434237
FMO1	-1,819090112	-1,061576465	-5,821698007	1,82489E-06	5,54257E-05	4,690201855
PRKG1	-2,817350133	0,128288491	-5,8187155	1,84074E-06	5,58089E-05	4,681625115
LTA	-1,511124548	-1,002052873	-5,812269917	1,87549E-06	5,67624E-05	4,663089042
PIK3CD	-2,522540525	1,997118906	-5,810985168	1,88249E-06	5,68745E-05	4,659394286
GAL3ST4	-2,569495697	1,342974313	-5,807289824	1,90279E-06	5,73869E-05	4,648766813
GFRA1	-2,572258248	-0,534065916	-5,80490311	1,91601E-06	5,76847E-05	4,641902696
GRIK3	-2,249006943	-0,836378499	-5,800593258	1,94012E-06	5,82118E-05	4,629507408
CD300C	-1,743947133	-1,093863309	-5,800565137	1,94028E-06	5,82118E-05	4,629426529
CLIC2	-2,505573255	1,911413585	-5,794668131	1,97377E-06	5,91136E-05	4,612465947
LILRA5	-2,680135092	-0,767680787	-5,792773951	1,98465E-06	5,93167E-05	4,60701789
TMEM156	-1,991041921	-0,931374964	-5,792290048	1,98744E-06	5,93167E-05	4,605626073
CCL21	-3,860779097	-0,054118549	-5,791484866	1,99209E-06	5,93526E-05	4,603310173
SIGLEC11	-1,572544616	-1,321476025	-5,787300031	2,01643E-06	5,99741E-05	4,591273376

FAM65C	-2,286139615	0,987125251	-5,780993291	2,05368E-06	6,09767E-05	4,573132766
LOC100505702	-2,211013657	0,197702925	-5,775880698	2,08439E-06	6,17818E-05	4,558426461
NAALADL1	-2,628310876	-0,266024002	-5,763454534	2,16095E-06	6,39411E-05	4,522680912
GBP5	-3,86040661	2,561356567	-5,760107737	2,18205E-06	6,44547E-05	4,513052959
C5AR1	-2,961732413	1,486517645	-5,753140717	2,22664E-06	6,56591E-05	4,493009904
APOBR	-2,346192346	1,183879203	-5,746913946	2,26726E-06	6,67428E-05	4,4750958
SIGLEC5	-1,995886606	-1,10980503	-5,725779836	2,41078E-06	7,08464E-05	4,41428989
SLC9A9	-2,435876156	0,41854432	-5,711612528	2,51205E-06	7,35716E-05	4,373525195
TPSB2	-3,542590611	-0,281716118	-5,694804007	2,63777E-06	7,71222E-05	4,325157703
DNAJC5B	-2,038876992	-0,69878135	-5,675635841	2,78885E-06	8,12628E-05	4,269996701
TMEM176A	-3,691201563	2,369269365	-5,675457381	2,7903E-06	8,12628E-05	4,269483125
F2RL2	-2,624376999	-0,07007708	-5,675057383	2,79354E-06	8,12628E-05	4,268331998
LILRA2	-1,991694765	-1,11190095	-5,665568373	2,87165E-06	8,3394E-05	4,241023853
CTLA4	-3,227927821	0,045301011	-5,653868953	2,97097E-06	8,61332E-05	4,207353505
CCL19	-2,561583897	-0,826956384	-5,644296783	3,0548E-06	8,84146E-05	4,179804605
PREX1	-3,669806827	2,674248102	-5,640588764	3,0879E-06	8,92228E-05	4,169132707
GPR124	-3,4917187	2,15807095	-5,636650683	3,12346E-06	9,00989E-05	4,157798598
NOTCH4	-2,638358381	2,269666	-5,634304685	3,14483E-06	9,05432E-05	4,151046592
AVPR1A	-2,630670732	-0,019904193	-5,633517812	3,15203E-06	9,05432E-05	4,148781891
COL5A3	-3,120608401	0,854453444	-5,633234096	3,15463E-06	9,05432E-05	4,147965327
S1PR1	-3,212688756	1,458863032	-5,632456063	3,16178E-06	9,05973E-05	4,145726064
IGDCC4	-2,102540053	-0,258208235	-5,631445985	3,17107E-06	9,07127E-05	4,142818948
CNN1	-3,840449095	1,233625038	-5,609803202	3,37702E-06	9,6444E-05	4,080527666
TAGLN	-3,359023492	5,452321276	-5,608457996	3,39026E-06	9,66617E-05	4,076655907
RHOH	-3,074380787	0,659019214	-5,604799302	3,42652E-06	9,7534E-05	4,066125469
LOC606724	-1,644507507	-1,05226574	-5,598177654	3,49314E-06	9,92662E-05	4,047067003
TLR8	-2,445695961	-0,884900353	-5,592428275	3,55203E-06	0,000100726	4,03051906
POM121L9P	-1,660075056	-1,129096952	-5,592022704	3,55622E-06	0,000100726	4,029351739
C1QTNF1	-2,550509033	0,730930141	-5,587334913	3,60503E-06	0,000101941	4,015859248
WNT5A	-2,595925586	4,130298408	-5,582771599	3,6532E-06	0,000103134	4,002725025
PLA2G4C	-2,051307074	0,245627046	-5,581901223	3,66246E-06	0,000103226	4,00021989
GSTM5	-2,189274469	-0,945926588	-5,570491706	3,78603E-06	0,000106535	3,967380818
HAMP	-1,999785519	-1,025129034	-5,565290513	3,84374E-06	0,000107982	3,952410697
C1S	-3,766164993	4,660788931	-5,562684555	3,87298E-06	0,000108626	3,944910224
CD300E	-2,540326097	-0,837585284	-5,539255771	4,14614E-06	0,0001158	3,877478254
XCL2	-2,484857484	-0,865319591	-5,538508099	4,15517E-06	0,0001158	3,87532636
FAM167B	-2,091749063	0,454475562	-5,538469122	4,15564E-06	0,0001158	3,875214179
DES	-4,57597525	1,007142584	-5,536062496	4,18483E-06	0,000116425	3,868287624
IFNG	-2,567666078	-0,823915294	-5,52901447	4,27153E-06	0,000118542	3,848002732
FAM110D	-1,537311365	-0,643327637	-5,528758386	4,27471E-06	0,000118542	3,847265703
RAMP2	-2,804809915	2,008032189	-5,524237631	4,33131E-06	0,000119919	3,834254678
ACTG2	-3,56508927	1,879282772	-5,505632987	4,57222E-06	0,000126386	3,78071064
CPED1	-3,556714666	0,706879112	-5,502400807	4,61543E-06	0,000127375	3,771408698
GJA5	-3,000282098	1,170412585	-5,477366663	4,96419E-06	0,000136781	3,69936556
SEPT1	-1,866480132	1,270468933	-5,460586074	5,21263E-06	0,000142983	3,651077994
CD19	-2,08725865	-0,609691274	-5,460485085	5,21416E-06	0,000142983	3,6507874
ERG	-3,142747625	1,994331074	-5,454541391	5,30514E-06	0,000145016	3,633684714
TREM1	-3,080484927	-0,014297601	-5,444431572	5,46355E-06	0,000149109	3,604595245
BGN	-4,690474904	4,34762303	-5,443189724	5,48333E-06	0,000149314	3,601022109
LOC441081	-2,118245843	0,499893111	-5,442871927	5,48841E-06	0,000149314	3,600107724
CPZ	-3,331675303	1,171558607	-5,439393555	5,54425E-06	0,000150596	3,590099629
DDR2	-2,29954938	0,007793396	-5,433734459	5,63633E-06	0,000152855	3,573817449

TOX2	-2,260025927	-0,301195093	-5,425241516	5,77739E-06	0,000156189	3,549382699
FGL2	-3,768504721	1,872992547	-5,423993066	5,79842E-06	0,000156512	3,54579092
CES1	-3,014220881	0,344725052	-5,417465038	5,90964E-06	0,000159264	3,527010254
HTRA4	-1,579503762	-1,000441919	-5,414021852	5,96917E-06	0,000160617	3,517104735
HIGD1B	-1,976559254	-1,119468706	-5,4129105	5,98851E-06	0,000160886	3,513907587
ADAP2	-2,699069519	1,325247446	-5,394079788	6,32591E-06	0,000169494	3,459738519
AXL	-3,093463443	1,90947508	-5,384464761	6,50545E-06	0,000173691	3,432082137
MS4A1	-2,910216294	-0,652640186	-5,375333894	6,68067E-06	0,000178093	3,405820079
C19orf38	-1,940031404	-0,212150634	-5,371114797	6,76323E-06	0,000180015	3,393685757
ACP5	-3,426586708	2,824480395	-5,362953588	6,92582E-06	0,000184058	3,370214818
CCR6	-1,701439916	-0,234144075	-5,349651745	7,19925E-06	0,00019103	3,331963041
ENG	-2,945197517	4,373758404	-5,347896015	7,23614E-06	0,000191713	3,326914438
SH2D2A	-2,05805285	1,111384461	-5,343836294	7,32216E-06	0,000193694	3,315240989
GRIP2	-1,58409711	-0,582440005	-5,342563621	7,34933E-06	0,000194115	3,311581585
S1PR4	-1,930574906	-0,441686429	-5,317010822	7,91683E-06	0,000208077	3,238116523
TLR10	-2,298322608	-0,646954741	-5,316601347	7,92628E-06	0,000208077	3,23693941
HLA-DPA1	-4,666562626	4,767777621	-5,313457015	7,99916E-06	0,00020967	3,22790058
GPR82	-1,643846314	-1,224003092	-5,298598006	8,35273E-06	0,000218605	3,185189971
TNFRSF8	-1,74094977	-0,570178456	-5,295998419	8,41618E-06	0,000219598	3,177718389
LAYN	-2,634294048	0,982845892	-5,294589813	8,45076E-06	0,000220167	3,173669937
RFTN2	-2,040043383	-0,558405021	-5,291600887	8,5246E-06	0,000221551	3,165079711
GEM	-2,645971347	2,299048841	-5,291400074	8,52958E-06	0,000221551	3,164502581
NR5A2	-3,34795845	0,708204567	-5,283244288	8,7345E-06	0,000226191	3,141064119
PCDHB15	-1,522633024	-0,453367441	-5,277532399	8,88093E-06	0,000229637	3,124650249
ABCB1	-2,857318228	0,21315037	-5,276038425	8,91964E-06	0,000230292	3,120357287
XYLT1	-2,284606603	-0,049437442	-5,255335768	9,47364E-06	0,000243865	3,060875204
INHBA	-2,877841664	-0,086119679	-5,254127236	9,50703E-06	0,000244359	3,057403333
BTLA	-1,827987022	-0,960130679	-5,240048948	9,90467E-06	0,0002542	3,01696295
WIPF1	-3,190296464	3,269686619	-5,239468925	9,92141E-06	0,000254251	3,015296962
CD163L1	-1,950453571	-0,216228197	-5,2343093	1,00715E-05	0,000257714	3,000477613
MMP25	-2,400939937	0,085731166	-5,223494071	1,03936E-05	0,00026556	2,969417517
BCL11B	-2,151931224	-0,328458753	-5,222870562	1,04125E-05	0,000265649	2,967627004
CYP7B1	-1,713148874	-0,970859066	-5,215424362	1,06406E-05	0,000271067	2,946245085
PTGIS	-2,468347684	-0,152158936	-5,210391731	1,07975E-05	0,000274359	2,93179498
LINC00341	-1,602186485	-0,721635217	-5,210260902	1,08017E-05	0,000274359	2,931419347
RGS4	-3,592648981	0,873113611	-5,209749977	1,08177E-05	0,000274362	2,929952394
P2RX7	-1,919052643	-0,402281904	-5,201431571	1,10828E-05	0,000280672	2,906070284
LRCH2	-2,07793173	-0,794438095	-5,200894728	1,11001E-05	0,000280698	2,904529102
PLCB2	-2,866549094	2,014438729	-5,196592572	1,124E-05	0,000283402	2,892178803
GPR97	-2,485820675	0,079974973	-5,177620471	1,18779E-05	0,000298613	2,837724216
ZNF300P1	-1,978466743	-1,071296913	-5,16686427	1,22555E-05	0,000307657	2,806858055
HLA-DQA2	-3,28389515	0,352527623	-5,164538919	1,23387E-05	0,000309294	2,800185854
COL8A1	-3,207312044	0,334308322	-5,154145891	1,27175E-05	0,000318071	2,770367769
TMEM140	-2,182215512	1,911338332	-5,153587019	1,27382E-05	0,000318071	2,768764478
FHL1	-3,407331436	1,715490397	-5,153423501	1,27443E-05	0,000318071	2,76829538
APOBEC3H	-1,671617485	-0,402381025	-5,146693481	1,29963E-05	0,000323891	2,74898947
P2RY8	-2,282921381	-0,438459665	-5,139740035	1,32618E-05	0,000330032	2,729044838
ANO4	-1,978964149	-0,79842307	-5,124901514	1,38468E-05	0,000343999	2,686491046
LOC654433	-2,469267943	-0,032367395	-5,124498646	1,3863E-05	0,000343999	2,685335852
LRRN3	-2,26559769	-0,670304627	-5,122584755	1,39404E-05	0,000345016	2,679848025
CD1D	-2,435382237	0,182444604	-5,122494557	1,39441E-05	0,000345016	2,679589399
TM6SF1	-2,101080494	-0,273175235	-5,108197079	1,45362E-05	0,00035915	2,638599104
TIMP3	-3,878852977	3,262987597	-5,106388797	1,46128E-05	0,000360527	2,633415567

KLRC2	-1,962107018	-1,058191498	-5,102395595	1,47835E-05	0,000364216	2,621969433
DACT3	-2,221273791	0,388044496	-5,098259826	1,49624E-05	0,000368097	2,610115508
PLXNC1	-2,982329479	2,188812184	-5,094653617	1,51202E-05	0,0003711	2,599780134
ENPEP	-2,832813143	0,297637437	-5,094484615	1,51276E-05	0,0003711	2,599295793
SLC6A1	-1,567691139	-1,186416089	-5,088377242	1,53987E-05	0,000376963	2,581793715
PPP2R2B	-1,895551732	-0,552166865	-5,088115818	1,54104E-05	0,000376963	2,581044588
TMEM200A	-3,177394271	1,348025285	-5,07984723	1,57854E-05	0,000385589	2,55735234
TSHZ3	-3,113286215	0,83481144	-5,07597651	1,5964E-05	0,000389401	2,546262717
LOC643733	-2,246934713	-0,586422984	-5,072546833	1,6124E-05	0,000392747	2,536437367
TRAT1	-1,973349006	-1,053226687	-5,066490659	1,64105E-05	0,000398596	2,519089211
HEYL	-2,405469533	1,655125764	-5,064778771	1,64924E-05	0,000400021	2,514185809
STARD8	-2,414719947	0,717576331	-5,063699954	1,65442E-05	0,000400713	2,511095813
HLA-F	-3,852794289	2,823926958	-5,060025292	1,67219E-05	0,000403957	2,50057117
POU2AF1	-2,782751448	0,208904168	-5,059960262	1,6725E-05	0,000403957	2,500384924
RGCC	-2,722411611	2,933005568	-5,050209612	1,72059E-05	0,00041499	2,472461742
TBC1D10C	-2,177611753	1,686275252	-5,046611246	1,73868E-05	0,000418767	2,462158396
RNASE1	-3,329002028	4,437918743	-5,043768923	1,7531E-05	0,000421651	2,454020393
ZNF208	-1,772632253	-0,929427926	-5,042891098	1,75758E-05	0,000422139	2,451507144
PLXDC2	-3,019042867	2,453569552	-5,040350449	1,77061E-05	0,000424675	2,444233411
IGSF21	-1,508810549	-1,353343058	-5,036813663	1,78891E-05	0,000428467	2,434108434
GPR176	-1,94217143	0,798794974	-5,023737718	1,8582E-05	0,000444445	2,396681633
SCARF1	-1,996082784	1,479734405	-5,022690128	1,86387E-05	0,000445182	2,393683603
ADAMTSL1	-3,00772007	0,696202515	-5,002136594	1,97858E-05	0,000471926	2,334876595
MFAP4	-4,373374975	1,711552449	-5,000402944	1,98857E-05	0,000473653	2,329917559
PRKCDBP	-3,508239314	1,025643176	-4,985086735	2,07905E-05	0,000494521	2,286114628
HGF	-1,871353848	-0,81751642	-4,983304018	2,08984E-05	0,000496402	2,281017223
HVCN1	-1,993480171	0,730091699	-4,979915135	2,11052E-05	0,000500623	2,271327814
TTN	-1,524314481	-0,954408403	-4,978486033	2,1193E-05	0,000502014	2,267241992
RASSF2	-2,969671731	2,253316546	-4,97633748	2,13256E-05	0,000504462	2,261099505
ARHGAP6	-1,915917244	-0,472771727	-4,973628513	2,14941E-05	0,00050775	2,253355299
EDIL3	-2,614017004	-0,588580707	-4,971589371	2,16218E-05	0,000510066	2,247526269
HSD11B1	-2,260494037	-0,631345672	-4,965189216	2,20274E-05	0,000518925	2,229232812
CD72	-2,062022261	1,09456352	-4,963063949	2,21638E-05	0,000521425	2,223158817
NPTX2	-2,703961205	0,157219114	-4,961883753	2,22399E-05	0,000522501	2,21978596
MYLK	-3,135433569	4,273389348	-4,95539346	2,2663E-05	0,000531019	2,201239224
DPEP2	-1,802492699	-0,66737133	-4,955376704	2,26641E-05	0,000531019	2,201191348
THEMIS	-2,454100452	-0,532815842	-4,953812149	2,27673E-05	0,000532712	2,196720897
GPR18	-1,599328524	-1,193049317	-4,953233374	2,28056E-05	0,000532884	2,195067189
HOXD11	-2,029178134	-0,429129014	-4,943997953	2,34254E-05	0,000546625	2,168682441
PLN	-3,010357004	-0,55640057	-4,93991446	2,37048E-05	0,000552396	2,157018213
DOCK8	-3,062628155	2,239276535	-4,927808203	2,45527E-05	0,000571381	2,12244457
CDH11	-3,549792493	2,905347885	-4,92243833	2,49384E-05	0,000579573	2,107112462
TSPAN18	-2,618227837	0,287311717	-4,921291518	2,50215E-05	0,000580722	2,103838349
ESAM	-3,295713004	2,16143534	-4,912802953	2,56456E-05	0,000593606	2,079606824
SIGLEC8	-1,718936135	-1,248280265	-4,911984523	2,57066E-05	0,000594219	2,077270813
IKZF3	-2,862423747	1,923978111	-4,911449673	2,57465E-05	0,000594344	2,075744242
SEPT4	-2,231424085	0,974758563	-4,909857037	2,58658E-05	0,000596298	2,071198655
CHRD	-2,973284857	1,32269889	-4,905579888	2,61888E-05	0,000602938	2,058992085
GBP4	-3,04467972	3,175140749	-4,901154177	2,65273E-05	0,000609916	2,046363004
FCGR3B	-2,836213797	-0,483763405	-4,887668424	2,75858E-05	0,000633406	2,0078898
KNDC1	-1,617956701	-1,030664091	-4,855332186	3,0298E-05	0,000693831	1,915697483
C16orf45	-2,480492464	1,10532049	-4,854428849	3,03774E-05	0,000694727	1,913123249
COL1A2	-4,600019983	6,448511458	-4,853892912	3,04247E-05	0,000694885	1,911596025

N4BP2L1	-2,069545798	2,216844295	-4,844593032	3,12561E-05	0,000711986	1,885098597
MARCO	-2,375492516	-0,59403079	-4,841217796	3,15634E-05	0,000718036	1,875483602
MMRN2	-3,128836008	1,793561758	-4,838018979	3,18574E-05	0,000723769	1,866372065
HLX	-2,040194141	0,838470468	-4,834932172	3,21437E-05	0,000729311	1,857580409
HLA-DPB1	-4,270523457	4,384657937	-4,823389593	3,32371E-05	0,000751151	1,824712815
DLGAP1-AS1	-1,599763929	2,533535371	-4,820168235	3,35488E-05	0,000757201	1,815542042
SYDE1	-1,989358577	1,70820707	-4,819492223	3,36146E-05	0,000757693	1,813617643
CARD16	-3,106884569	2,043098297	-4,817779735	3,37818E-05	0,000759596	1,808742893
LAT	-2,080420827	2,065541305	-4,817724114	3,37873E-05	0,000759596	1,808584568
FHL5	-1,790823321	-1,036528181	-4,816746024	3,38832E-05	0,000760759	1,80580047
TMEM215	-2,116481437	-0,690284171	-4,813807063	3,41729E-05	0,000766265	1,797435329
IGF2	-4,400266538	2,778027305	-4,809148092	3,46373E-05	0,000775668	1,784176109
FCER1A	-2,232868196	-0,991314235	-4,797646347	3,58107E-05	0,000799865	1,751451011
COL6A1	-3,400222067	5,391756927	-4,795368747	3,60477E-05	0,000804116	1,744972138
RRN3P2	-1,958460888	-0,317286728	-4,772685341	3,84948E-05	0,000853998	1,680472948
LOC728392	-2,478350829	0,866430563	-4,769506112	3,88507E-05	0,00085996	1,671436809
TDO2	-2,239250947	-0,154492557	-4,76482416	3,93808E-05	0,000870574	1,658131319
P2RY6	-1,799813855	0,365832092	-4,762212129	3,96797E-05	0,000876056	1,65070918
APOL3	-2,238252188	2,403583325	-4,744660443	4,1747E-05	0,000919342	1,600852825
C2	-2,622048953	2,538799281	-4,740776319	4,22188E-05	0,000927359	1,589823869
COL22A1	-2,104571654	-0,485367316	-4,740330775	4,22732E-05	0,000927373	1,588558843
ZDBF2	-2,056034241	-0,30475689	-4,738611925	4,2484E-05	0,00093081	1,583678727
SIGLEC12	-1,541445962	-1,337025352	-4,73782434	4,25809E-05	0,000931747	1,581442733
TNXB	-2,75898431	0,897370625	-4,733771547	4,3083E-05	0,000940345	1,569937623
TM4SF18	-2,416553482	0,840983893	-4,732449395	4,32481E-05	0,000942753	1,56618464
SFMBT2	-2,719184985	0,842325109	-4,727211621	4,39082E-05	0,000955933	1,551318729
FAM26F	-2,793698286	1,438901185	-4,719371853	4,4915E-05	0,000976618	1,529072989
ARHGAP30	-2,247487947	2,17028466	-4,707165837	4,65283E-05	0,001010421	1,494450312
FOXS1	-2,734791509	0,047942583	-4,688308694	4,91344E-05	0,001064332	1,440992055
FBXL7	-3,47080377	1,07268821	-4,686473032	4,93957E-05	0,001067585	1,43579013
ZNF781	-1,629653328	-0,291715946	-4,686013705	4,94613E-05	0,001067585	1,434488541
DKK2	-1,963903038	-0,831245477	-4,685948717	4,94706E-05	0,001067585	1,434304387
CCL13	-2,386015326	-0,91474067	-4,684601176	4,96636E-05	0,001070408	1,430486011
APOBEC3G	-3,041721188	2,438818346	-4,683705219	4,97923E-05	0,001071841	1,427947348
PEG3	-2,293032611	-0,574133076	-4,682685612	4,99392E-05	0,001073661	1,42505843
APOD	-3,173336319	0,670704913	-4,681936778	5,00473E-05	0,001074645	1,42293678
JAM2	-3,295521412	0,546613824	-4,67821223	5,05887E-05	0,001084917	1,412385031
CMAHP	-2,906664878	1,137625595	-4,671850768	5,15269E-05	0,001103663	1,394366295
RLTPR	-1,756075655	0,313633801	-4,670905512	5,16678E-05	0,001105305	1,391689248
LHFP	-1,786047657	3,117985518	-4,667953949	5,21101E-05	0,001113384	1,383330799
LOC100505495	-2,854791519	1,041559119	-4,654102529	5,42365E-05	0,001156082	1,344118145
ARHGAP4	-2,129832597	2,899135346	-4,654062486	5,42428E-05	0,001156082	1,344004817
ST8SIA4	-3,575221366	1,642552118	-4,65335435	5,43538E-05	0,001157016	1,342000697
DPP6	-2,24282543	-0,847098042	-4,646378963	5,54593E-05	0,001176188	1,322262403
MME	-3,959648801	1,606353676	-4,645157681	5,56551E-05	0,00117889	1,318807099
SNORA25	-1,560036721	-0,772334739	-4,635641863	5,72047E-05	0,001210224	1,291890309
CD1A	-2,179867358	-1,017814654	-4,634381542	5,74131E-05	0,001213143	1,288326092
RERG	-2,759772749	0,141875322	-4,606077254	6,2297E-05	0,001313118	1,208329409
FILIP1L	-2,828528548	2,755947262	-4,603568839	6,27492E-05	0,001319143	1,20124439
GPSM3	-1,936510041	2,972894612	-4,603218021	6,28127E-05	0,001319143	1,200253563
ST6GALNAC3	-2,463890471	0,37624769	-4,595941323	6,41442E-05	0,001345466	1,179705087
RECK	-2,270153504	0,705007587	-4,593595775	6,45794E-05	0,001351965	1,173082908

ROBO3	-1,975271972	-0,237556896	-4,59295481	6,46988E-05	0,001352157	1,17127339
FAM65B	-2,365665092	0,783374137	-4,591956888	6,48851E-05	0,001354408	1,168456239
FGF7	-2,541793095	0,180728248	-4,589320376	6,538E-05	0,001361557	1,161013901
GALNT15	-1,838093981	-0,54956885	-4,58873521	6,54904E-05	0,001362089	1,15936221
ZMIZ1-AS1	-1,528018448	-0,181599458	-4,587003263	6,58181E-05	0,001367253	1,154473855
CFP	-1,755281293	0,042607385	-4,585103145	6,61794E-05	0,001373104	1,149111265
PCOLCE	-3,392903281	3,471168162	-4,570540586	6,9015E-05	0,001428494	1,108026912
NAPSB	-3,37817065	1,701367214	-4,569941746	6,91341E-05	0,001429242	1,106338007
CXCR2P1	-1,814689503	-1,177589494	-4,562263472	7,06799E-05	0,001459447	1,084686964
PRAM1	-1,745875459	-0,479657931	-4,56111207	7,09147E-05	0,001462541	1,081440899
PDLIM3	-3,130633651	0,620306361	-4,558889606	7,13699E-05	0,001468413	1,075175736
CLEC12A	-1,875771153	-1,169862756	-4,55403372	7,23747E-05	0,001485537	1,061489086
GNG7	-2,033552914	-0,506848437	-4,543284055	7,46492E-05	0,001530398	1,03120106
TNFRSF17	-1,936428667	-1,118178744	-4,538393905	7,57071E-05	0,001550241	1,017427574
TMEM26	-2,753848422	0,415861286	-4,53688861	7,60358E-05	0,001555121	1,013188413
ZNF626	-2,742377279	-0,203124519	-4,512276967	8,16135E-05	0,001661307	0,943919924
HECW2	-2,032979693	0,324232609	-4,499044372	8,47777E-05	0,00172368	0,906710514
KCTD12	-2,90390339	3,216548451	-4,497924274	8,5051E-05	0,001727198	0,903561936
PTPRN2	-2,239946227	0,27857257	-4,497496252	8,51557E-05	0,001727287	0,902358816
C3orf70	-1,854623171	-0,690512267	-4,493878349	8,60457E-05	0,001743285	0,892190317
VGLL3	-2,579914722	-0,004156585	-4,491750124	8,65735E-05	0,001751917	0,886209546
CACNA1H	-2,893605192	0,500545794	-4,490948525	8,67731E-05	0,001753896	0,883957041
LINC00667	-2,952018045	0,648960817	-4,487681269	8,75914E-05	0,001768361	0,874776911
EPB41L3	-3,286960918	1,318522524	-4,478906299	8,98273E-05	0,001811377	0,850128811
HLA-DQB2	-2,513379794	0,285882868	-4,477551629	9,01775E-05	0,001814221	0,84632461
CCL14	-2,276374313	-0,769962038	-4,477545477	9,01791E-05	0,001814221	0,846307336
NPL	-2,292208117	1,84107045	-4,459192301	9,50582E-05	0,001903485	0,794793005
DPYSL4	-2,129120774	-0,466641235	-4,457627824	9,5486E-05	0,001909729	0,790403968
IL33	-3,513346158	2,328377155	-4,457241851	9,55918E-05	0,001909729	0,789321201
TMEM200B	-2,466015987	0,685210771	-4,447592389	9,82755E-05	0,001961069	0,762258509
LOC100216479	-2,287762929	0,25403204	-4,43788256	0,000101051	0,002011795	0,735039997
GFI1	-1,881921909	0,199785374	-4,436080283	0,000101575	0,002019885	0,729989371
MYL9	-2,890715769	4,96214008	-4,433527919	0,000102321	0,002027698	0,722837536
CLEC3B	-2,124120567	-0,222296614	-4,428372952	0,000103845	0,002055526	0,708395995
NTNG2	-1,5145988	-0,905969393	-4,427517826	0,000104099	0,002058206	0,706000753
VASH1	-2,26267808	2,803159978	-4,420589	0,000106188	0,002094683	0,686596796
LPPR4	-2,381833773	0,442777196	-4,419363648	0,000106561	0,002099648	0,683165972
RASA3	-2,590667337	1,746500586	-4,413577116	0,000108343	0,002132316	0,666967459
COL10A1	-2,348230451	-0,815002805	-4,412991945	0,000108525	0,002133456	0,665329642
CST7	-2,962388592	0,677600589	-4,410657761	0,000109253	0,002142913	0,658797064
ST8SIA1	-1,710432526	-0,45166598	-4,410652328	0,000109255	0,002142913	0,65878186
SOGA3	-1,818308358	-0,859192211	-4,401114129	0,000112281	0,002197266	0,632096219
TBX2	-3,248230506	1,262767739	-4,395560384	0,000114081	0,002223576	0,616564462
PAG1	-2,023233033	2,388538691	-4,395374095	0,000114142	0,002223576	0,616043562
NPR2	-1,628658183	2,325593572	-4,393915741	0,00011462	0,002229293	0,611965908
GPR133	-1,522858921	-1,237592542	-4,393688029	0,000114694	0,002229293	0,611329239
LRRK2	-2,355626209	0,245469405	-4,384569534	0,000117728	0,002285674	0,585840994
EMB	-3,346281825	1,438979488	-4,379912955	0,000119307	0,002313731	0,572829733
CCL11	-2,097900729	-1,058797968	-4,375189	0,000120931	0,002337892	0,559633632
REN	-2,508075058	0,787520231	-4,37510394	0,000120961	0,002337892	0,559396054
VSTM4	-2,54361986	0,412000747	-4,368421697	0,000123295	0,002380344	0,540735603
CAMK1G	-1,624636778	-0,511667428	-4,363555839	0,000125023	0,002408304	0,527151875
AFF3	-3,096466274	1,098826927	-4,345793624	0,000131536	0,002521159	0,477597894

GPRASP1	-1,814479229	1,418008111	-4,345586314	0,000131614	0,002521159	0,477019827
F10	-1,822025334	-0,710019858	-4,335134955	0,000135603	0,002591816	0,447885974
PTPRB	-2,42740156	2,656515094	-4,328647978	0,000138139	0,00263736	0,429811987
CD1E	-1,569103509	-1,287386241	-4,319958381	0,00014161	0,002700623	0,40561183
TBXAS1	-2,007161113	1,657263143	-4,288344152	0,000154976	0,002948996	0,317673223
CD5	-2,636396928	0,477336533	-4,286641819	0,00015573	0,002960072	0,31294276
PROCR	-2,106961835	1,951558214	-4,282452159	0,000157601	0,002992333	0,301302584
CEACAM21	-2,58876643	-0,175778143	-4,277890684	0,000159663	0,00302815	0,288632804
TSPAN2	-2,65609435	-0,010515493	-4,277385992	0,000159893	0,003029144	0,287231211
MCAM	-2,03625802	4,469544064	-4,274730135	0,000161108	0,003042144	0,279856279
POSTN	-3,914892393	1,973199203	-4,261719644	0,00016719	0,003150095	0,243745643
TNFSF14	-2,287610188	0,439889682	-4,259073726	0,000168455	0,00317045	0,236405498
FFAR2	-2,155579773	-0,840391818	-4,255191944	0,000170327	0,003202184	0,225639111
FOXN4	-2,615989681	0,247609676	-4,253734782	0,000171035	0,003208489	0,221598255
KCNE4	-2,495631901	0,413014973	-4,246447828	0,000174619	0,003265059	0,201396422
C3orf80	-1,640742232	-1,116095216	-4,238524758	0,0001786	0,003332262	0,179441746
CLEC4E	-2,658941913	0,267275412	-4,237882061	0,000178927	0,003334747	0,177661335
PMP22	-1,985690771	3,374107886	-4,22285624	0,000186738	0,003469059	0,136057669
RGS2	-2,760662388	3,021634503	-4,214202824	0,000191388	0,003547778	0,112116532
GAS1	-2,707459125	0,875237597	-4,202531037	0,00019784	0,003651657	0,079846275
GBP2	-2,686704994	4,167089768	-4,190325881	0,000204815	0,003770802	0,046128306
FAM19A5	-2,766291991	0,469262161	-4,19009129	0,000204952	0,003770802	0,045480496
GBGT1	-1,993942978	0,383273707	-4,187011429	0,000206751	0,003791752	0,036976596
HNRNPUL2-BSCL2	3,455681	4,259850025	4,182016559	0,000209702	0,0038377	0,023188894
LILRA3	-1,757726623	-1,228885022	-4,179004253	0,000211502	0,003862426	0,014876081
PDZD4	-1,807106019	-0,742003234	-4,174671478	0,000214117	0,003906043	0,002922286
PTGIR	-1,70991317	-0,601945906	-4,168862896	0,000217673	0,003962517	-0,013097549
LGALS2	-2,069485839	-0,836771934	-4,168123812	0,000218129	0,003962601	-0,015135451
NEXN	-1,672992801	1,182163521	-4,167661899	0,000218415	0,003963463	-0,01640905
PDE4B	-2,704204713	2,024778484	-4,164239017	0,000220545	0,003997896	-0,025845419
NID1	-3,292257469	3,272673475	-4,154788751	0,000226531	0,004097783	-0,051886694
ITGA1	-2,515724915	3,422592564	-4,153188358	0,00022756	0,004112086	-0,05629505
LAX1	-1,800776471	-0,484582347	-4,148723426	0,000230457	0,004155703	-0,068591286
FCRLA	-1,708488565	-1,232148795	-4,143119898	0,000234143	0,00421466	-0,084017679
GIMAP2	-2,374728456	1,284072835	-4,143010198	0,000234216	0,00421466	-0,084319619
FMNL1	-1,606967968	2,740389623	-4,139349761	0,000236656	0,004254121	-0,094393328
HHEX	-1,877638131	0,644203706	-4,13607787	0,000238858	0,00428476	-0,103395515
FLRT2	-2,432057218	0,811319585	-4,129281596	0,000243496	0,004363423	-0,122087848
CD180	-1,928864517	0,640702851	-4,122695119	0,000248076	0,004431656	-0,140194426
GJA4	-3,22361641	1,244184789	-4,112599531	0,00025526	0,004544057	-0,167930942
NAP1L3	-1,824361909	-0,193894741	-4,112373194	0,000255423	0,004544057	-0,168552542
HEG1	-1,812877287	3,696190634	-4,099715138	0,000264726	0,004690169	-0,203299584
AOC3	-1,881726375	1,708841854	-4,091017209	0,00027131	0,004792027	-0,227156986
ZCCHC24	-1,71456728	2,345493767	-4,086669571	0,000274661	0,004846242	-0,239076242
BMP8A	-2,187901699	0,913056229	-4,081769607	0,000278486	0,004908707	-0,252505055
WT1	-2,295683189	0,265862708	-4,067711636	0,000289753	0,005096869	-0,291004619
POPDC2	-1,539484804	0,436224726	-4,066567392	0,000290689	0,005108124	-0,294136462
FAM49A	-2,020185599	1,700394839	-4,065981214	0,00029117	0,005111359	-0,295740751
GRAP	-2,126445917	2,016497592	-4,063272015	0,000293403	0,005140075	-0,303154516
COL4A1	-2,087242423	7,049041527	-4,046931747	0,00030723	0,005344248	-0,347837054
OLFML3	-2,485078533	2,653599474	-4,045865219	0,000308154	0,005354918	-0,350751507
ZNF334	-2,179073756	-0,576739841	-4,040102635	0,000313196	0,005437043	-0,366494461
TRO	-2,899886719	0,958708888	-4,039528561	0,000313703	0,005440354	-0,368062398

RASL12	-2,681347168	1,511172316	-4,03699643	0,000315947	0,005468264	-0,374977429
NNMT	-3,486199435	2,845152493	-4,032168904	0,00032027	0,005537512	-0,38815716
ARMCX1	-2,332653032	1,355994169	-4,030442462	0,000321829	0,005558902	-0,392869334
PLA2G7	-2,762675683	1,778128495	-4,029049415	0,000323094	0,005575144	-0,396671064
RAB31	-2,517417068	3,958557155	-4,021713689	0,000329831	0,005680016	-0,416683867
KIAA0125	-1,882725968	-1,166385349	-4,02014672	0,000331288	0,005699405	-0,42095724
MSRB3	-2,455715971	1,767295056	-4,017928016	0,000333361	0,005723642	-0,427007082
CDH5	-2,596039199	3,088123949	-4,015574196	0,000335575	0,005755913	-0,433424175
SIRPB2	-1,700901607	-0,622434034	-4,012355165	0,000338626	0,005802462	-0,442198076
VAMP5	-1,907163729	2,532773889	-4,007942574	0,000342852	0,005857393	-0,454221484
SYNE1	-2,198419525	2,621058356	-4,003300144	0,000347354	0,005928425	-0,466866516
CXCR7	-2,335492159	2,87210462	-4,002554631	0,000348082	0,005934974	-0,468896695
USHBP1	-2,030555268	0,361219416	-3,986496121	0,000364138	0,006178156	-0,512597175
RSPO1	-1,598994721	-1,287825939	-3,984239057	0,000366453	0,006211298	-0,51873476
ABCA6	-1,688614791	-0,507617416	-3,978543198	0,000372356	0,006292786	-0,534218275
STON1	-1,821816284	1,111284925	-3,976563677	0,00037443	0,006321625	-0,539597651
CHIT1	-1,824143886	-0,734672269	-3,975731004	0,000375305	0,006330201	-0,541860187
LOC339524	-1,520473884	-0,053391677	-3,96473842	0,000387054	0,006509234	-0,571714392
CYSLTR1	-1,620621382	-0,819484754	-3,961047958	0,000391078	0,006564092	-0,581730941
DNM3OS	-2,633551994	0,201084331	-3,958413774	0,000393976	0,006595208	-0,588878655
DPYD	-2,38654711	1,283988288	-3,95581459	0,000396855	0,006633893	-0,595929834
DYX1C1-CCPG1	2,903441206	1,317529521	3,955537926	0,000397163	0,006633893	-0,596680289
VEGFC	-2,099543959	1,753607525	-3,953156012	0,000399822	0,006665375	-0,603140528
KCNAB2	-2,028442565	2,212127707	-3,945790201	0,000408155	0,006758494	-0,623109804
TBC1D3	-1,955381303	-0,569044537	-3,943306806	0,000411002	0,006792583	-0,629839635
CALHM2	-2,09727379	1,247717295	-3,938148944	0,000416979	0,006858444	-0,643812493
CX3CR1	-1,614316274	-0,277367025	-3,936724946	0,000418644	0,006879258	-0,647669066
DOC2A	-2,081105387	-0,233713147	-3,933436389	0,000422513	0,006936227	-0,656573552
MYOCD	-1,539523719	-1,157199854	-3,913166785	0,000447148	0,00730126	-0,711401534
NDNF	-2,348397926	-0,0764548	-3,906705495	0,000455292	0,007402775	-0,728858347
DPT	-2,027388832	-0,832161525	-3,905312635	0,000457066	0,007418604	-0,732620197
ELFN1	-1,657798962	-0,690852722	-3,904484574	0,000458124	0,007421788	-0,734856413
C22orf34	-1,599525626	-0,880119095	-3,899448963	0,000464611	0,007519792	-0,748451742
CLDN5	-2,583100383	0,897647512	-3,895217882	0,00047013	0,007594844	-0,759870231
C1R	-2,417632223	5,289043893	-3,89023285	0,000476714	0,007694002	-0,77331785
LAMA2	-2,283708396	1,110031985	-3,884815639	0,000483972	0,007792033	-0,787924449
ECEL1P2	-2,114604366	-0,413945269	-3,884687039	0,000484146	0,007792033	-0,788271109
SELL	-2,321343149	1,348646431	-3,883522783	0,00048572	0,007810072	-0,791409356
P2RX1	-1,790272436	-0,713200735	-3,88129027	0,000488753	0,007840675	-0,797426158
RARB	-1,834024979	1,927523195	-3,878673058	0,000492332	0,007886934	-0,804478198
CLECL1	-1,649626981	-1,186894428	-3,877900327	0,000493394	0,007892868	-0,806559988
PSD	-1,958612861	1,32691065	-3,877736393	0,000493619	0,007892868	-0,807001619
CHRDL1	-1,98691879	-0,843833265	-3,871891785	0,000501725	0,008007609	-0,822742395
P2RX5	-1,547916866	-0,775272885	-3,868349072	0,000506702	0,008072072	-0,832279567
IGFBP7	-2,537147019	7,04986851	-3,867279961	0,000508213	0,008088664	-0,835157059
COL11A1	-1,94257509	-0,967281508	-3,865765018	0,000510362	0,008107951	-0,839234017
LAMA4	-2,740807896	3,802310013	-3,865761854	0,000510366	0,008107951	-0,83924253
PODN	-2,098889546	0,561119259	-3,857524573	0,000522207	0,008273161	-0,861400379
LAIR2	-1,504147745	-1,002446993	-3,855534742	0,000525107	0,008311462	-0,866750378
HLA-DQB1	-3,511017455	4,848828708	-3,847473941	0,000537018	0,008476607	-0,888413053
FRZB	-2,619601494	2,373429655	-3,841973483	0,000545296	0,008588928	-0,903185638
IL1B	-2,841189005	0,824895531	-3,83693385	0,000552989	0,008665174	-0,91671386
GZMM	-1,607704687	-0,688875438	-3,831318181	0,000561687	0,008785475	-0,931780768

MAFB	-1,538043092	3,424863011	-3,814212435	0,00058901	0,009179496	-0,977625913
FMO2	-1,685924068	-0,718956463	-3,81068041	0,000594811	0,009244803	-0,9870827
EBF1	-2,178006696	1,133848704	-3,81035391	0,00059535	0,009244837	-0,98795672
KANK3	-1,635328547	0,121788613	-3,808676117	0,000598128	0,009279599	-0,992447636
BATF3	-1,648720243	-0,159259161	-3,805137259	0,000604027	0,009354277	-1,001917626
CD36	-2,444667899	0,242060025	-3,804517687	0,000605066	0,009356284	-1,003575265
CCDC80	-2,275871991	4,053336594	-3,800298442	0,000612186	0,009446649	-1,014861021
ADAM8	-1,968539151	2,891876118	-3,797339725	0,000617228	0,009515919	-1,022772305
NOS3	-1,984152324	1,6934063	-3,790507091	0,000629025	0,009671827	-1,04103323
HLA-DRB5	-3,647378839	3,460548098	-3,7900844	0,000629762	0,009674522	-1,042162513
TXLNB	-1,549344832	-0,847055704	-3,788286478	0,000632907	0,009714159	-1,046965404
PEAR1	-1,919770644	0,520964974	-3,775580088	0,000655568	0,010008451	-1,080884292
ITGA4	-2,708694666	2,351411349	-3,771728721	0,000662591	0,010097771	-1,09115678
NFASC	-2,72565018	0,805923285	-3,769788216	0,000666157	0,010134185	-1,096331054
ADRA2C	-2,563618383	1,646488136	-3,766007167	0,00067316	0,010231678	-1,106410164
ADAMTS6	-2,171689384	1,753110714	-3,764928071	0,000675172	0,010244171	-1,109285995
SLC37A2	-2,301604365	0,690994861	-3,762378923	0,000679947	0,010307545	-1,116078329
MXRA8	-2,772270677	3,067936602	-3,744886993	0,000713613	0,010751643	-1,162639045
HOXD3	-1,697573196	-0,187417898	-3,740633987	0,00072204	0,010868427	-1,173947279
CD3G	-1,987173791	-0,669837104	-3,735638708	0,000732062	0,010991142	-1,1872228
RSPO3	-2,155430439	0,28666378	-3,735175231	0,000732999	0,010995619	-1,188454195
UQCRBP1	-1,937233069	4,761194795	-3,720569343	0,000763121	0,011378204	-1,227229664
LTBP2	-2,449920762	3,990785368	-3,715464692	0,000773929	0,01149186	-1,240767449
HLA-DRB1	-3,648277965	5,65146687	-3,712352168	0,000780593	0,011558545	-1,249018445
RBP5	-1,836054264	0,460219099	-3,688306442	0,000833982	0,012190187	-1,312669442
TBX3	-2,97009693	2,315408815	-3,685458207	0,000840536	0,012256447	-1,320198096
EFEMP1	-3,482843439	2,247641108	-3,68382648	0,000844313	0,012290712	-1,324510146
CRISPLD2	-1,520040344	3,257419	-3,678191245	0,000857485	0,012461391	-1,339396131
MEIS3	-2,06440579	0,857959846	-3,674435184	0,000866375	0,012571618	-1,349313043
PDE2A	-1,779500049	-0,274362883	-3,67366769	0,000868203	0,012585283	-1,351338916
JPH4	-1,711222183	-0,957704161	-3,671766528	0,000872746	0,012629877	-1,356356479
GLI1	-1,966941811	0,168083613	-3,665704185	0,000887387	0,012809467	-1,372349293
DLC1	-2,37711789	2,996802894	-3,664099987	0,000891301	0,012844433	-1,376579479
HIST1H4J	-2,555259658	1,031935864	-3,66348655	0,000892802	0,012850171	-1,378196886
SDPR	-2,47398681	0,905024824	-3,662453722	0,000895335	0,012859524	-1,380919822
HHIP	-2,552919509	0,269964176	-3,661053735	0,00089878	0,01289824	-1,384610235
JAKMIP1	-1,695490423	-0,684765766	-3,647286247	0,000933346	0,01333871	-1,420871369
BTN3A1	-1,718179016	4,767524383	-3,644516577	0,000940454	0,013384752	-1,428159483
HHIP-AS1	-1,839852301	-0,054025199	-3,64394681	0,000941922	0,013394585	-1,42965849
AGBL2	-1,776373965	0,7051621	-3,642736871	0,000945049	0,013427954	-1,432841416
MS4A2	-1,586828074	-1,291520208	-3,640903866	0,000949804	0,013471017	-1,437662585
GLT8D2	-2,06016604	1,353815095	-3,640664713	0,000950426	0,013471017	-1,438291532
PILRA	-1,954751244	1,697862901	-3,63965577	0,000953055	0,013497171	-1,440944761
ZIK1	-1,533761824	-0,816284102	-3,636733402	0,00096071	0,013594398	-1,448628045
DKFZp686D0853	-2,616703046	-0,758156066	-3,635345395	0,000964366	0,013597931	-1,452276411
LRRC36	-1,523372172	-0,162571588	-3,63175153	0,000973897	0,013668684	-1,461720202
NAIP	-1,525872661	4,325891741	-3,629504432	0,000979902	0,013730588	-1,467623074
INSR	-2,320381771	3,85276552	-3,625554568	0,000990545	0,013834692	-1,477995279
CCL3L3	-1,767776937	-1,12816919	-3,616575245	0,001015158	0,014155498	-1,501557324
FPR2	-1,648773467	-1,189666008	-3,610998496	0,001030742	0,014326397	-1,516178724
PLAT	-2,615501621	3,666157357	-3,604434103	0,001049382	0,014573721	-1,533377561
CXCL10	-2,835018629	2,891803924	-3,603915481	0,001050869	0,014582606	-1,534735805
F2R	-1,796842465	3,601797186	-3,598690215	0,00106596	0,014716564	-1,548415954

PTPRO	-2,278646712	-0,037978395	-3,598503221	0,001066504	0,014716564	-1,548905364
HCG27	-1,661829923	-0,1012482	-3,595290549	0,001075892	0,014822344	-1,557312084
KIF19	-1,999582387	0,228075769	-3,59404636	0,001079549	0,014860837	-1,560566955
MCOLN2	-1,9327693	0,644771476	-3,585948132	0,001103647	0,015132085	-1,581740828
MATK	-1,924802873	-0,475596329	-3,582664009	0,001113567	0,015228925	-1,590321866
GPR75-ASB3	2,03971275	0,889628482	3,579887693	0,001122021	0,015323011	-1,597573472
CCR7	-1,863153246	-0,159200764	-3,572890186	0,001143604	0,01556838	-1,615840087
CXCL11	-2,41161729	0,758669626	-3,571779636	0,001147066	0,015603177	-1,618737724
ATP8A1	-1,573397173	2,709951594	-3,570366145	0,001151487	0,015638612	-1,62242524
TCF4	-3,0637317	4,219685605	-3,56833482	0,00115787	0,015700531	-1,627723475
PCDH18	-2,828633813	2,36641591	-3,563559337	0,00117301	0,015843451	-1,640174149
PRELP	-2,344721206	1,166469369	-3,560158847	0,001183907	0,015934505	-1,649035598
IRF8	-2,92051014	1,569307419	-3,558861738	0,001188089	0,015971967	-1,652414826
CXCR1	-1,779924284	-0,995653881	-3,558026224	0,001190791	0,015995799	-1,654591227
MIR155HG	-1,840055059	0,458803045	-3,555458802	0,00119913	0,016095262	-1,661277649
GLIPR2	-2,513732233	3,350364126	-3,546350074	0,001229173	0,016396811	-1,684983106
FXYD5	-2,31955883	3,000909553	-3,543361635	0,001239188	0,016517068	-1,692754818
TWIST2	-1,643776659	-0,43603071	-3,543028724	0,001240308	0,016519217	-1,69362041
NBPF10	1,529304208	3,978378819	3,53473698	0,001268533	0,016804162	-1,715168178
PRR16	-1,678391381	0,045452262	-3,525705073	0,001299984	0,01708933	-1,738614511
MIAT	-3,411844712	1,899023206	-3,524613462	0,001303836	0,017113837	-1,741446507
NR3C1	-2,526894603	2,076980461	-3,523453561	0,001307941	0,017142205	-1,744455252
S1PR3	-2,280369418	2,66331468	-3,514841158	0,001338812	0,017479673	-1,76678202
P4HA3	-1,550573636	0,309608035	-3,509938765	0,001356699	0,017641377	-1,779480293
GAS6	-1,864615934	2,912337333	-3,50610473	0,001370847	0,017776628	-1,789405865
RMRP	-1,653762001	0,45918908	-3,505272051	0,001373939	0,017803313	-1,791560879
AKAP2	-1,715532018	3,36790379	-3,501794708	0,001386923	0,017931078	-1,800557977
C4A	-2,462877524	3,993683683	-3,499140317	0,001396913	0,018033167	-1,807423166
DTHD1	-1,614656084	-0,470135481	-3,496311386	0,001407637	0,018112931	-1,814737244
PI15	-2,113002589	-0,101238719	-3,494043609	0,001416291	0,018174334	-1,820598597
ANKRD36BP2	-1,547019104	-0,926593611	-3,492149379	0,001423559	0,018240414	-1,825493179
SOCS1	-1,550160302	1,49125121	-3,489134561	0,001435201	0,018321423	-1,833280873
LOC339803	-2,101614502	-0,193795601	-3,486775398	0,001444375	0,018417036	-1,83937284
SOWAHB	1,657570381	1,756377201	3,48665883	0,00144483	0,018417036	-1,8396738
ST6GAL2	-2,031729726	0,266177808	-3,483411379	0,001457555	0,018542937	-1,848056436
VAT1L	-1,588757875	-1,213227368	-3,48331416	0,001457937	0,018542937	-1,848307334
ITGB2-AS1	-1,94789388	0,459820364	-3,482532472	0,001461017	0,018568394	-1,850324559
GPR68	-1,604717883	0,154621891	-3,480279561	0,001469928	0,018648333	-1,856137294
RASD2	-1,634268283	-0,017187652	-3,480121541	0,001470556	0,018648333	-1,856544939
SFRP1	-3,509111253	2,499387248	-3,477661491	0,00148035	0,018744935	-1,862890073
RPPH1	-1,560828661	-0,243896508	-3,477262336	0,001481945	0,018751346	-1,863919411
GLIPR1	-1,937555826	2,887663513	-3,471302212	0,001505962	0,018916249	-1,879283082
DSC2	1,663089531	6,274510924	3,469642822	0,001512715	0,018987226	-1,883558466
ENTPD1	-2,181192626	3,655440327	-3,463957394	0,001536075	0,019211092	-1,898199896
C22orf15	-1,848271609	-0,604257329	-3,454608996	0,001575243	0,019600626	-1,922250921
HLA-DRA	-3,785108043	7,014979234	-3,453074909	0,001581762	0,019667528	-1,926194934
ANO1	-2,050924365	5,086539269	-3,451042208	0,00159044	0,019761157	-1,931419619
ABI3BP	-3,06357902	1,69090982	-3,449376078	0,001597587	0,019821354	-1,935701064
EMP3	-1,754660676	3,187141464	-3,443324917	0,001623804	0,020059925	-1,951242819
GATA3	-1,525278282	-0,08832281	-3,429806421	0,001683881	0,020639229	-1,985918745
SNAP25	-1,728727522	-0,345672124	-3,422940965	0,001715205	0,020993284	-2,003505265
OLFM1	-2,244684303	0,120032829	-3,4183799	0,001736325	0,021176523	-2,015179925

HLA-DOA	-2,5762224	2,01713872	-3,41278141	0,00176259	0,021421008	-2,029500223
CD82	1,611893371	4,902969885	3,402849184	0,001810131	0,021859938	-2,054879042
DACT1	-2,246880336	0,900376501	-3,39826481	0,001832488	0,022026296	-2,066581469
LOC100507463	-1,90256245	2,68264559	-3,397393698	0,001836767	0,022036744	-2,068804308
SUSD3	-1,76409106	0,584611981	-3,388232605	0,001882344	0,022408941	-2,092164843
LGI4	-1,582644649	-0,793821315	-3,388047362	0,001883276	0,022408941	-2,092636902
BNC2	-2,120629869	0,817008718	-3,386732541	0,001889909	0,022461098	-2,09598716
MDFIC	-2,181519266	2,043394018	-3,375586505	0,001947049	0,023013127	-2,124363579
CHST11	-2,289538961	2,817464035	-3,369867168	0,001977009	0,023306084	-2,13890724
PDE1A	-1,603879139	1,186836821	-3,368307651	0,001985255	0,023361224	-2,142870908
THBS4	-2,26708131	2,0587246	-3,360891212	0,002024925	0,023705796	-2,161708676
PATL2	-1,555256961	-0,149318595	-3,359661344	0,002031576	0,023751372	-2,164830644
LRRC4B	-1,809485264	-0,727652914	-3,353094472	0,002067448	0,024056438	-2,1814912
CD38	-1,647752005	0,580512646	-3,346986431	0,00210136	0,024396762	-2,196973766
HCLS1	-2,499929906	3,552865569	-3,34680714	0,002102363	0,024396762	-2,197428028
CBFA2T3	-1,527602141	-0,298500451	-3,345884885	0,002107532	0,024440274	-2,199764517
LCP1	-2,28918747	5,256768645	-3,339729334	0,002142345	0,024770984	-2,215351444
CCL2	-2,404181555	3,62392268	-3,339700681	0,002142508	0,024770984	-2,215423966
SCG5	-2,161500297	0,738584915	-3,338545142	0,002149105	0,024805452	-2,218348451
MUSTN1	-1,667394205	0,027214685	-3,331573326	0,002189322	0,025168431	-2,235982714
TTYH2	-1,632813747	0,650808505	-3,330548884	0,002195292	0,025220226	-2,238572409
NLRP1	-2,435369581	1,885944138	-3,328880893	0,002205046	0,025315393	-2,242788121
CCDC17	-1,518189296	1,304851884	-3,32846445	0,002207487	0,02532654	-2,243840489
RBMS3	-2,004680212	1,286124483	-3,316080529	0,002281293	0,025914344	-2,275106123
PTPN22	-2,201845587	0,674647274	-3,314779012	0,002289186	0,025971034	-2,278388789
FAM92B	-2,225898545	0,563157213	-3,314512074	0,002290808	0,025971034	-2,279061979
LOC389895	-1,954690148	-0,163779903	-3,309167979	0,002323513	0,026289898	-2,292533697
C19orf59	-1,598168575	-1,146494123	-3,3079779	0,002330857	0,026355677	-2,295532287
SLC15A3	-2,314338031	2,516455295	-3,299481871	0,002383936	0,026780018	-2,316924103
SPIB	-1,507535393	-0,41855862	-3,292761689	0,002426739	0,027129095	-2,333825578
CPXM2	-2,571619325	0,945599644	-3,29262556	0,002427614	0,027129095	-2,334167773
FBN1	-1,992667898	3,53041767	-3,289278047	0,002449216	0,027317326	-2,342580419
RUNDC3B	-1,802657201	-0,231132468	-3,285740819	0,002472243	0,027485149	-2,351465281
HOXD8	-2,408315018	1,443796434	-3,280735291	0,002505183	0,027779622	-2,364030218
CSPG4	-1,931268231	2,049615418	-3,277114773	0,00252927	0,027974665	-2,373112612
LINC00839	-1,843856671	-0,353432419	-3,275694415	0,00253878	0,028008024	-2,376674357
OGN	-1,947581285	-1,13395769	-3,268461026	0,002587744	0,028426841	-2,394801263
INS-IGF2	-2,387878471	-0,583717324	-3,266130689	0,00260371	0,02857775	-2,400636878
MAN1C1	-1,886677782	1,450324283	-3,264475789	0,002615106	0,028684543	-2,404779816
ITGA5	-2,581312426	4,162170694	-3,264142724	0,002617405	0,028691488	-2,405613497
TCF21	-1,572373915	-1,321561375	-3,263847538	0,002619444	0,028695578	-2,40635233
IL22RA2	-1,514339642	-1,350578512	-3,261103593	0,002638474	0,028830689	-2,413218673
ASB2	-1,774139214	1,260712719	-3,249092288	0,002723344	0,029626478	-2,443241481
CPNE5	-1,7159364	0,14805933	-3,248795988	0,002725471	0,02963089	-2,443981398
CACNA1C	-1,577440544	1,257402815	-3,243632835	0,002762777	0,02988675	-2,456869359
LOC100144604	-2,252982497	1,149093354	-3,231187903	0,002854716	0,030629951	-2,487891414
CHRDL2	-1,688353193	-1,027238179	-3,227854564	0,002879834	0,030871464	-2,496190396
ZNF521	-2,439450006	1,018732316	-3,220414689	0,00293666	0,031344183	-2,514697788
LPAR6	-2,018102844	3,662733035	-3,218268987	0,002953247	0,031471449	-2,520031412
CAV1	-2,010108617	3,687330034	-3,213812145	0,002987986	0,031763026	-2,531104136
TMOD2	-1,791327564	0,722683913	-3,206000434	0,003049818	0,032320561	-2,550493003
XCL1	-2,161183611	0,640973235	-3,201671286	0,003084608	0,032649072	-2,561227709

OLFML2A	-1,981899528	2,193441858	-3,193111487	0,003154516	0,033286717	-2,582431072
GBP1	-2,226246019	4,301217636	-3,192605451	0,003158696	0,033310412	-2,583683658
PPP1R14A	-1,741661031	1,392456464	-3,18728216	0,003202987	0,033623652	-2,596854173
GPR132	-1,500419534	0,301486689	-3,184163515	0,003229209	0,033805599	-2,604564863
SOCS3	-2,064134149	4,540138557	-3,177885608	0,003282618	0,034239828	-2,62007488
ISY1-RAB43	2,053194161	4,703199041	3,173751289	0,003318249	0,034548705	-2,630280388
NDUFA4L2	-2,528492768	2,458345799	-3,171018175	0,003342006	0,034775032	-2,637023271
GBP1P1	-1,561141907	-0,471393813	-3,16400073	0,003403748	0,035310812	-2,654322271
INPP5D	-2,038317157	2,794122065	-3,153540481	0,003497804	0,03598308	-2,680071303
C10orf54	-1,933429357	2,982851356	-3,150790625	0,003522937	0,036114366	-2,686832993
C2orf74	-1,757924756	0,892958096	-3,150767652	0,003523148	0,036114366	-2,68688947
PSMB9	-2,255277754	4,043009917	-3,144602921	0,003580124	0,036589504	-2,702036827
C1orf228	-1,548204872	1,08030149	-3,131000423	0,00370896	0,037593883	-2,73540446
FEZ1	-1,744533853	1,169145338	-3,119693137	0,003819404	0,038374539	-2,763083796
CR1	-1,644393859	0,027683983	-3,113087254	0,003885367	0,038801019	-2,779229943
TLE4	-1,73229336	1,608455767	-3,111251526	0,003903889	0,0388831	-2,783713618
ANGPT1	-1,714371531	-0,367647823	-3,11093442	0,003907097	0,038892558	-2,784487992
SLC24A3	-1,779962657	0,765325965	-3,110506104	0,003911435	0,038913238	-2,785533872
CSDC2	-1,764658893	0,04575656	-3,103232781	0,003985786	0,039515957	-2,80328251
GNG11	-2,446063294	3,955415516	-3,102339335	0,003995011	0,03958463	-2,805461204
STARD9	-1,583889331	1,459315082	-3,093718524	0,004085074	0,040222451	-2,826466083
ANKRD1	1,903648144	0,924675443	3,093076673	0,004091857	0,040266207	-2,828028723
MAF	-2,256795774	2,418267585	-3,092083564	0,004102371	0,040323595	-2,830446187
CUBN	-1,842163716	1,631509965	-3,086957393	0,004157056	0,040690113	-2,842917892
LYPLAL1	-2,408145187	1,361797287	-3,086407138	0,004162966	0,040690113	-2,844255972
EMILIN3	-1,513377559	-0,119053008	-3,083975036	0,004189188	0,040873659	-2,850168695
PAGE4	-1,962631588	-1,126432539	-3,08030801	0,004229021	0,0412156	-2,859078926
CHN1	-1,538351867	2,95803722	-3,064122132	0,004409174	0,0427055	-2,898339376
EHD2	-2,017014859	3,035747639	-3,059147874	0,004465985	0,043110277	-2,910382423
HSD17B3	-1,591716702	0,317167458	-3,05735217	0,004486665	0,043272366	-2,914727345
HLA-H	-1,994350282	4,013863467	-3,057035968	0,004490315	0,043272366	-2,915492289
GFPT2	-1,837141007	0,75392449	-3,055969648	0,004502647	0,043342699	-2,918071577
SERPINE1	-2,358816791	2,691116428	-3,053907088	0,004526592	0,043524536	-2,923059247
SNCAIP	-2,099601133	1,966180476	-3,052634066	0,004541431	0,043594196	-2,926136748
MOXD1	-2,604479107	2,963882075	-3,048209969	0,004593361	0,043921301	-2,936826452
CCDC78	-1,938386609	2,267998486	-3,047782486	0,004598408	0,043941998	-2,937858907
FCRL2	-1,548662287	-0,315010149	-3,046823801	0,004609747	0,044004683	-2,940174035
FAM20A	-2,580689615	2,55905711	-3,041022121	0,004678932	0,044480732	-2,954175998
PLAC9	-1,546763418	-1,259204681	-3,037963161	0,004715806	0,0447438	-2,961552708
FBLN2	-1,748958854	2,366301404	-3,036876163	0,004728975	0,044795205	-2,964173034
ZNF662	-1,78655362	0,413428801	-3,033767751	0,004766827	0,045079365	-2,971663356
GABRB3	-1,505719191	-0,837693175	-3,02476955	0,004878024	0,045901605	-2,993322488
HSPB6	-2,32502395	1,449685522	-3,020235905	0,004934975	0,046237874	-3,004221766
ADGB	-1,507507987	-0,850907499	-3,011781621	0,005042864	0,046977572	-3,02452246
CIITA	-1,581929475	2,395237688	-3,007822177	0,005094156	0,047284428	-3,034019157
LOC100132062	-1,842543857	-0,550528951	-3,00368166	0,005148321	0,047640646	-3,043942736
LOC100132287	-1,842543857	-0,550528951	-3,00368166	0,005148321	0,047640646	-3,043942736
AMY2B	-1,529628105	2,912296695	-3,002906803	0,005158518	0,047658177	-3,04579899
C10orf32-AS3MT	2,299884188	0,303031446	2,995281123	0,005259894	0,048387093	-3,064052916
C15orf48	-2,868190606	1,686441622	-2,989822395	0,005333617	0,048881393	-3,077103801
RGS10	-1,578047696	5,816060454	-2,980929058	0,005455821	0,049692816	-3,098337699

TEKT4	-1,769992417	-0,086448575	-2,97819255	0,005493953	0,049890106	-3,104864295
CD74	-2,285943382	9,234588414	-2,978020317	0,005496361	0,049890106	-3,105274958

Table S5. Genes included in card

ABL1	CTNNB1	FLT3	KIT	NOTCH1	RUNX1
AKT1	EGFR	GATA1	KRAS	NOTCH4	SMAD4
AKT2	ERBB2	GNA11	MAG	NRAS	SMARCB1
AKT3	ERBB3	GNAQ	MAP2K1	PDGFRA	SRC
ALK	ESR1	GNAS	MET	PIK3CA	STK11
APC	FBXW7	HRAS	MLH1	PIK3R1	TP53
BRAF	FGFR1	IDH1	MPL	PIK3R5	VHL
CDH1	FGFR2	IDH2	MSH6	PTEN	
CDKN2A	FGFR3	JAK1	MYC	RB1	
CSF1R	FGFR4	JAK3	NF2	RET	

Table S6. Mutational study

Sample	Only in primary tumor	Only in PDOX	Shared mutations
1	ERBB2_V477L	PIK3CA_R88Q; PTEN_E7X; PTEN_R130Q; RB1_E137X	PTEN_M134I; TP53_R273C
2	TP53_R213X		APC_V1377I; CDKN2A_H83Y; FGFR1_R609X; FGFR1_E612K; FGFR2_V463I; PIK3CA_R88Q; PIK3CA_R108C; PTEN_E7X; PTEN_R130Q; PTEN_F341V; TP53_R342X
3		FBXW7_R465C; FGFR4_P279T	PIK3R1_N564D
4		FGFR3_T394M; TP53_Q165K	KRAS_G13D; PIK3CA_E545G; PTEN_R130G; PTEN_T321fs
5			ERBB3_N62K; PTEN_R130G; PTEN_T321fs
6		CTNNB1_D32N; FGFR1_A21T; MSH6_T1085fs; PIK3R1_T576fs; TP53_Q165K	FGFR2_S252W; PTEN_S229X
7	FGFR2_N228H	FGFR2_S57L; JAK1_D145E; KRAS_Q61H; PIK3CA_E545K; PIK3R1_L466X; PTEN_E7X; RB1_K130T; STK11_Q37X; TP53_K132T	FGFR1_c_1430+7A>C; PIK3CA_E81K
8	STK11_G279fs	FGFR3_c_616-6G>A; NRAS_G12V	FGFR4_E316V; NRAS_G12D
9		PTEN_L182V	CTNNB1_G34R; PIK3CA_E542Q
10		FGFR4_A729V; PTEN_R130G; PTEN_Y177fs	EGFR_M793V; JAK1_K142fs; NOTCH1_L1678M; TP53_R342X
11	CDKN2A_R103Q; HRAS_E63del; STK11_G163D; TP53_R273C		MSH6_T1085fs; PTEN_L265fs; PTEN_T321fs
12	FBXW7_R465C; TP53_R280I	APC_R564X; JAK1_K142fs; TP53_H179R	ERBB2_R678Q; PIK3CA_Y1021C; PTEN_T321fs; TP53_R273C
13	APC_S1400L; CTNNB1_D32G; FGFR4_c_2154-5C>T; PIK3CA_R88Q	FGFR4_E330K; JAK1_D145E; TP53_F341V; TP53_R213X; TP53_D281E	ERBB2_T900S; PTEN_E299X
14			KRAS_G12C; PIK3CA_H1047R; PTEN_L265fs; PTEN_E291fs; STK11_P275L
15	APC_T1292M; FGFR2_R759X; FGFR2_c_940-4C>A; KIT_K558N; PTEN_E299X; TP53_R290C	FBXW7_R465H	TP53_R213X

SUPPORTING FIGURE LEGENDS

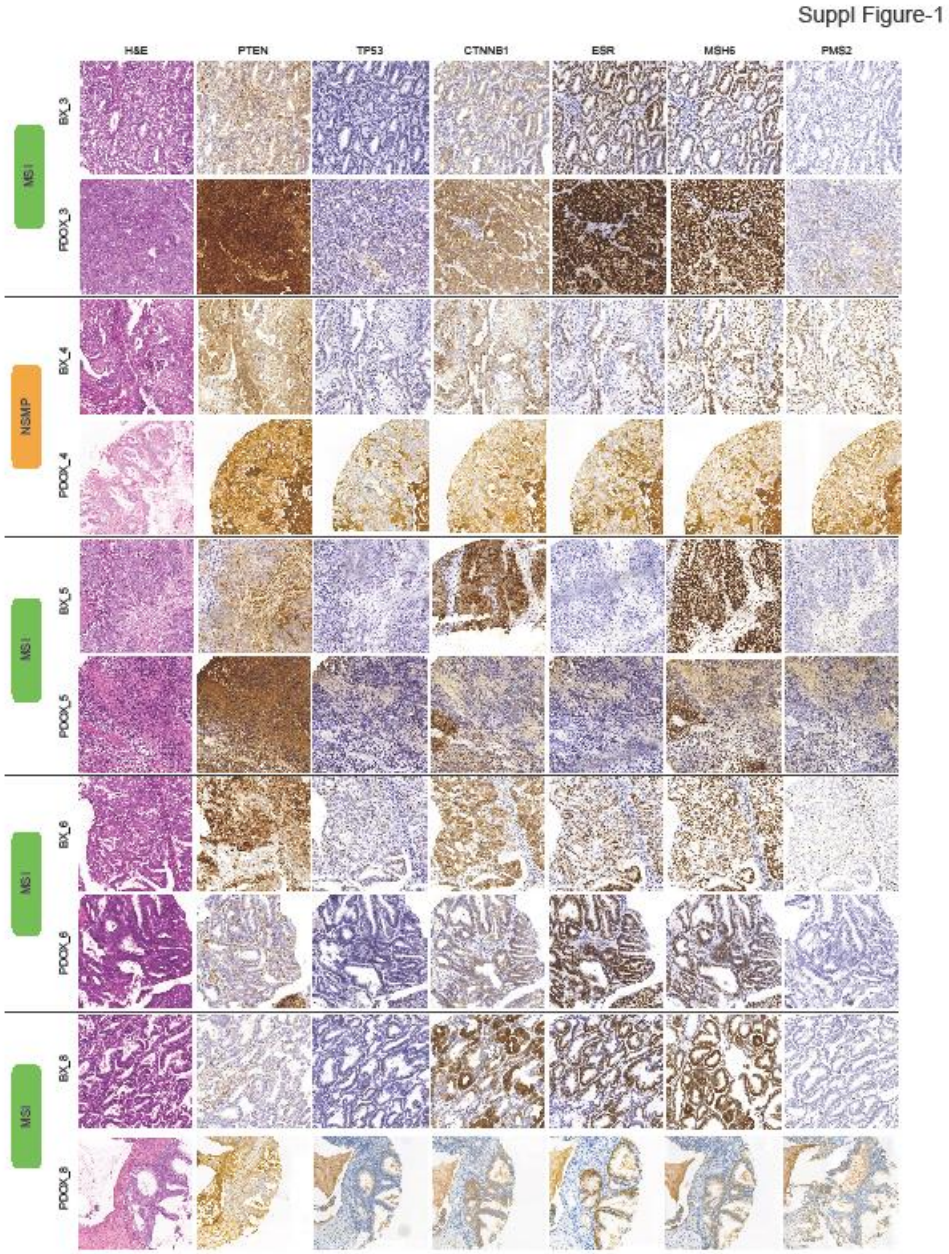

Figure S1. Morphological and immunohistochemical correlation between primary tumors (BXs) and PDOXs. Images illustrate HE stainings and detection by immunohistochemistry of PTEN, TP53, CTNNB1, ESR, MSH6 and PMS2 between BX and PDOX. BX3, BX5, BX6, BX8 (MSI) and BX4 (MSS).

Suppl Figure-2

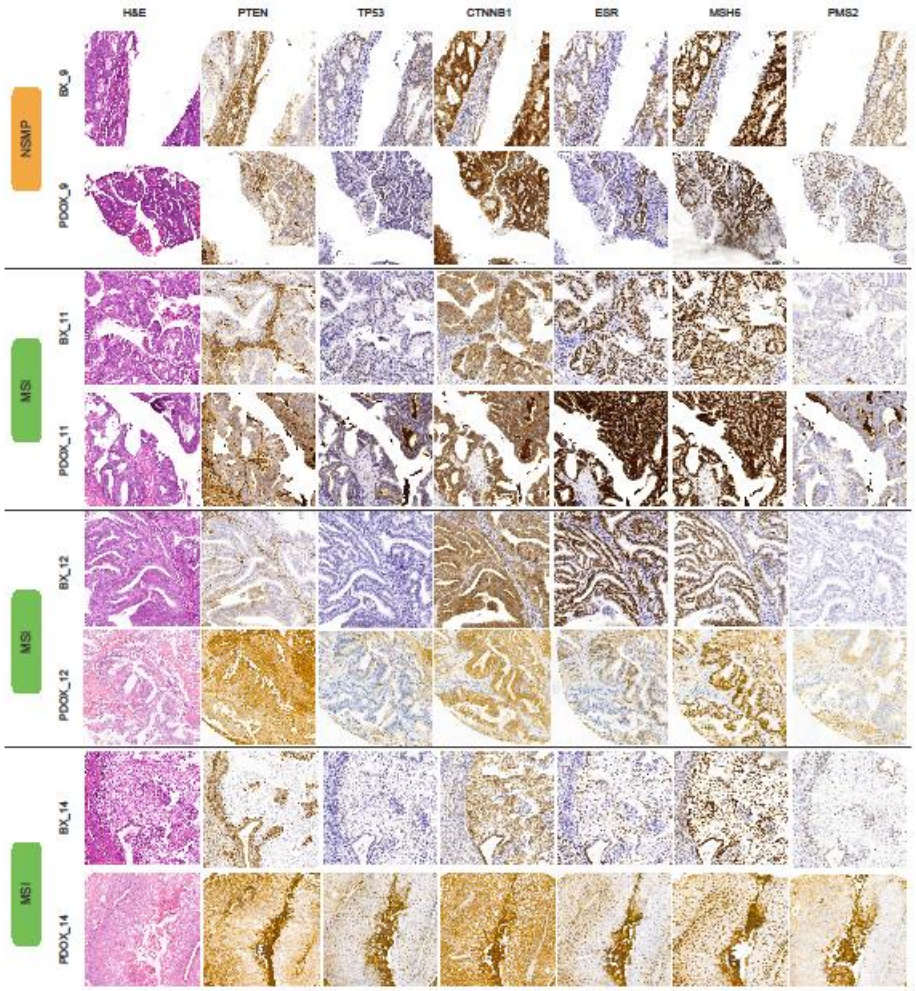

Figure S2. Morphological and immunohistochemical correlation between primary tumors (BXs) and PDOXs. Images illustrate HE stainings and detection by immunohistochemistry of PTEN, TP53, CTNNB1, ESR, MSH6 and PMS2 between BX and PDOX. BX11, BX12, BX14 (MSI) and BX9 (MSS).

Suppl Figure-3

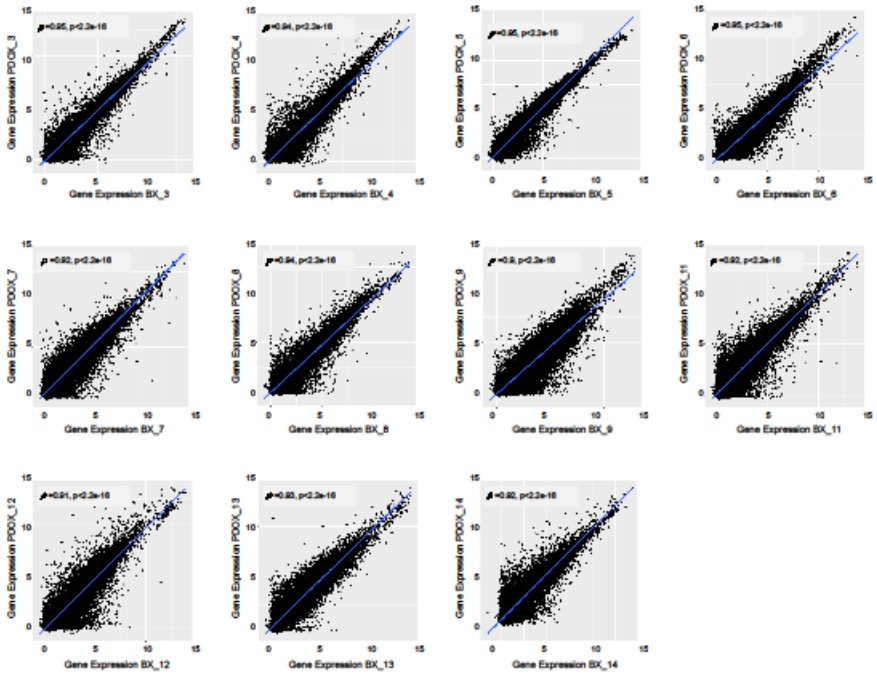

Figure S3. Transcriptomic analysis of BX and PDOX tumor pairs**.** Total RNA sequencing for the 15 pairs of BX/PDOX tumors was conducted and computationally analyzed. BX and PDOX pairs correlated extremely well at transcriptomic level. Spearman's correlation (rho) ρ values and P values indicate the strength and significance of the correlations, respectively.

Suppl Figure-4

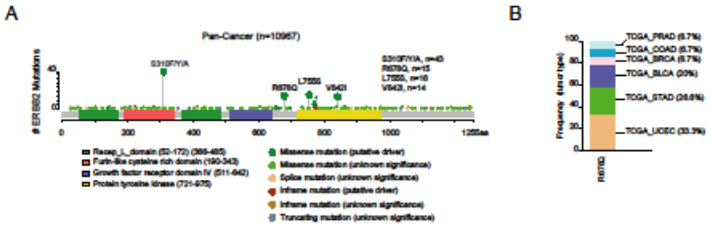

Figure S4. (A) Lollipop plot and analysis of the ERBB2 mutational landscape using the TCGA pancancer dataset (n=10,967) showing that ERBB2^{R678Q} is one of the most representative ERBB2 mutations. **(B)** Stacked bar chart illustrating the distribution of ERBB2^{R678Q} according to tumor types and the highest representation in endometrial cancer (TCGA_ucec).

DISCUSSIÓ

La resistència a la quimioteràpia, tant de forma endògena com adquirida en el curs del tractament és un dels principals problemes que hi ha en el maneig dels malalts amb càncer. Es necessiten nous models experimentals que ens ajudin a entendre a nivell molecular els mecanismes de quimioresistència, així com disposar d'eines preclíniques que ens permetin poder desenvolupar estratègies terapèutiques per a vèncer-la. Així mateix, també es necessiten aquests models preclínics amb resistència als tractaments de quimioteràpia per a ajudar a desenvolupar noves molècules perquè acabin convertint-se en fàrmacs que ens permetin millorar els tractaments.

Quan volem generar models tumorals de resistència, a partir de tumors humans implantats en ratolins, podem definir dues estratègies generals diferents: (i) generar els models aparellats sensibles/resistents als tractaments mitjançant la implantació de mostres tumorals obtingudes abans i després que el pacient rebi els tractaments; o bé (ii) derivar el model de resistència a partir del model generat amb la mostra obtinguda abans de començar el tractament, i generar la resistència *in vivo* a l'animal mitjançant l'exposició del tumor a cicles iteratius de concentracions creixents del/s fàrmac/s quimioteràpic/s (ex. Platí, 5-FU, etc.) amb què es tractarà el malalt com hem demostrat als treballs d'aquesta Tesi i en altres que hem publicat (Castillo-Avila et al., 2009; Juliachs et al., 2014; Byrne et al., 2017).

El primer abordatge requereix l'obtenció de tumor del pacient en diferents moments de la seva malaltia, la qual cosa no sempre resulta senzilla des del punt de vista tècnic i/o ètic ja que moltes vegades representa un risc important i possiblement innecessari per al pacient. No obstant això, avui dia amb la implementació d'estratègies de medicina de precisió que requereixen conèixer les característiques moleculars del tumor en cada moment de la seva evolució per a poder triar la millor opció terapèutica, resulta més factible obtenir aquestes mostres del tumor o la metàstasi a la recaiguda, fent possible, teòricament, la generació d'aquesta mena de models de resistència. Arribats a aquest punt, però, és important ressaltar que en aquestes circumstàncies la quantitat de teixit que s'obté és limitada i de vegades amb poca representació de tumor, cosa que fa difícil la generació d'aquests models. Una altra limitació a tenir en compte és que de vegades, per l'evolució de la malaltia, passa molt de temps entre la

obtenció de la mostra del tumor primari i la de la recaiguda, per la qual cosa no sempre és possible la coordinació entre els diferents professionals i, moltes vegades, entre els diferents hospitals en què els pacients són tractats per a aconseguir les parelles de models. A més a més hi ha el hàndicap d'haver de realitzar els passos d'implantació i perpetuació dels tumors dues vegades. Hem de tenir en compte que el principal factor limitant en aquest tipus de procediments són les taxes d'implantació i perpetuació que es puguin assolir i que el fet que hagi crescut amb èxit el tumor abans del tractament no implica que passi el mateix amb el tumor resistent.

En els treballs presentats en aquesta Tesi hem optat per la segona opció, és a dir, la de generar el model abans del tractament i evolucionar-lo posteriorment *in vivo* a model de resistència una vegada que el tumor primari està perpetuat al ratolí. Això ens ha permés generar parelles de tumors sensibles i resistents al cisplatí que ens han servit per a

i) estudiar mecanismes de resistència adquirida al cisplatí,

ii) provar tractaments basats en noves molècules en desenvolupament, com és el cas de la Lurbinectedina,

iii) provar tractaments usats en altres tipus de càncer en base a les alteracions moleculars demostrades en el model en el cas del Trastuzumab, o bé

iv) el reposicionament de DL-threo-PDMP, un inhibidor de la glucosilceramida sintasa (GCS) indicat per al tractament de malalties metabòliques com la malatia de Gaucher, la de Niemann-Pick o la diabetis mellitus, per al tractament de tumors refractaris al cisplatí.

En resum, en moltes d'aquestes circumstàncies el que hem aconseguit és, en certa manera, una re-sensibilització dels tumors resistents al cisplatí mitjançant diferents estratègies.

En el cas dels TTCG també hem aconseguit generar 4 models a la recaiguda a partir de biòpsies de metàstasis ganglionars, pulmonars i cerebrals de pacients ja tractats amb cisplatí, però en aquests models no disposem de la parella prèvia al tractament perquè no vam tenir accés a la mostra del tumor primari.

Tot i que no és el tema d'aquesta Tesi, per tal d'il·lustrar la dificultat que representa obtenir models aparellats a partir de tumor previ al tractament i de tumor resistent a la recidiva, vull comentar que malgrat haver adoptat una estratègia d'implantació massiva de carcinomes ovàrics al llarg dels anys i haver aconseguit generar més de 150 models de PDOX de càncer d'ovari diferents, només en dos casos hem obtingut la parella de models sensible / resistent procedent de la mateixa pacient. De totes maneres, és important ressaltar que aquests models preclínics obtinguts post-quimioteràpia, malgrat no disposar del model del tumor primari generat previ al tractament del pacient, són d'un gran valor ja que incorporen les alteracions que són conseqüència dels processos de selecció que es van produint entre les cèl·lules tumorals en els pacients en el curs del tractament.

Al primer treball (165) s'ha generat un model ortotòpic de carcinoma serós d'alt grau ovàric i la seva parella resistent al cisplatí. Aquesta parella de models s'ha emprat per a provar l'eficàcia d'una nova molècula que estava en desenvolupament, el PM01183, anomenat en el nostre article com lurbinectedina.

L'estructura de l'ADN té dues fenedures ben definides anomenades solcs major i menor. Les proteïnes i els fàrmacs que s'uneixen a l'ADN poden contactar amb la molècula a través de les bases presents a algun dels dos solcs (166,167). El cisplatí i altres agents alquilants s'uneixen a l'ADN a través del solc major, mentre que altres fàrmacs quimioteràpics com ara la mitomicina C, la cromomicina A3 o la trabectedina ho fan pel solc menor, formant adductes (168–171). La lurbinectedina és un fàrmac sintètic derivat de la trabectedina, amb què comparteix aquest mecanisme d'acció, però amb millors propietats farmacocinètiques i farmacodinàmiques (172–175). Per tractar-se un tumor resistent a un determinat fàrmac s'hauria d'emprar una molècula que tingui un mecanisme d'acció diferent i que no tingui resistència creuada amb aquella primera molècula (176). Aquest treball, basat en l'ús de lurbinectedina, sembla apuntar en la direcció que una estratègia útil per a tractar carcinomes d'ovari resistents o refractaris al cisplatí podria fonamentar-se en l'ús de fàrmacs que interaccionin amb els solcs major i menor de la molècula d'ADN. Els resultats obtinguts indiquen que el tractament amb lurbinectedina en monoteràpia obté

resultats semblants al tractament amb cisplatí en el carcinoma serós d'ovari sensible a aquest darrer fàrmac i per tant podria ser emprat com tractament de primera línia en aquest tipus de neoplàsia. Però la conclusió més rellevant que es pot obtenir d'aquest model preclínic és que els tractaments amb lurbinectedina en monoteràpia o en combinació amb cisplatí són útils en el carcinoma d'ovari resistent al cisplatí. Això s'ha demostrat des del punt de vista macroscòpic, constatant la reducció de volum i pes dels tumors, i histològic objectivant-se criteris de regressió histopatològica atribuïble al tractament quimioteràpic en carcinomes d'ovari (177). Aquesta resposta s'ha pogut objectivar tant a curt termini, o sigui en el moment d'acabar la quimioteràpia, com en aquells experiments en que s'ha valorat la resposta a llarg termini, setmanes després del final del tractament, donant la idea que aquest tractament pot aconseguir una resposta més duradora en el temps. Aquests resultats obren la possibilitat a emprar lurbinectedina en segona línia en aquelles malaltes que tinguin tumors resistents o refractaris al tractament estàndard.

Aquest treball amb els nostres models preclínics va ser important per a l'aprovació de la lurbinectedina per les agències reguladores FDA i EMA, a l'hora d'autoritzar un assaig clínic en fase II en càncer d'ovari resistent al platí (Poveda et al., 2017).En aquest assaig es va demostrar que lurbinectedina era un fàrmac actiu en càncer d'ovari resistent / refractari al platí. En base a aquest estudi es va desenvolupar l'assaig en fase III (estudi CORAIL) que va avaluar si la lurbinectedina millorava la supervivència lliure de progressió (PFS) en comparació amb la doxorubicina liposomal pegilada (PLD) o el topotecà en pacients amb càncer d'ovari resistent al platí. No es va complir l'objectiu principal de millora de la PFS. La lurbinectedina va mostrar una eficàcia antitumoral similar i es va tolerar millor que l'estàndard d'atenció actual en pacients amb càncer d'ovari resistent al platí (179). Des de la pròpia companyia es creu que l'assaig clínic CORAIL no va sortir tan positiu com s'esperava perquè en el seu moment es van plantejar uns objectius erronis. En càncer d'ovari actualment s'estan avaluant en diferents assaigs clínics fase I i II (estudi POLA) la combinació de lurbinectedina amb inhibidors de PARP, en context de tumors amb HRD (deficients en recombinació homòloga), així com combinacions amb altres

quimioteràpics, teràpies dirigides i immunoteràpia (180) , amb la idea de posicionar el fàrmac en el tractament d'aquest tipus de càncer.

Però on realment de moment ha demostrat la seva potència la lurbinectedina ja com a fàrmac (ZEPZELCA™) ha estat en carcinoma de cèl·lula petita de pulmó. Ha rebut l'estatus de medicament orfe per al tractament d'aquest tipus de tumor per part de les autoritats reguladores de diversos països d'arreu del món i va ser aprovat als Estats Units el juny de 2020 per al tractament de pacients adults amb carcinoma de cèl·lula petita de pulmó metastàtic amb progressió de la malaltia administrat amb o després de quimioteràpia a base de platí (181,182).

En treballs realitzats en els darrers anys s'ha demostrat que la lurbinectedina és un inhibidor de la ARN polimerasa II, que és un enzim essencial per a la transcripció que és troba sobreactivada en les cèl·lules tumorals. La seva inhibició dona lloc a una progressió retardada a través de la fase S, aturada del cicle cel·lular a la Fase G2/M i acaba produint mort cel·lular. A més, lurbinectedina interacciona amb el microambient tumoral, reduint el nombre de macròfags associats al tumor i inhibint la secreció de citocines i quimiocines (183). Totes aquestes característiques estan sent explotades per a definir noves combinacions de lurbinectedina tant amb quimioteràpia, amb teràpies dirigides com amb immunoteràpia.

Al segon treball (184)es va generar una col·lecció important i fins a aquesta data inexistent, de models ortotòpics de tumors testiculars de cèl·lules germinals. Aquests models conservaven moltes de les característiques dels tumors primaris dels que derivaven, incloent l'heterogeneïtat tumoral, amb diferents components histològics presents al mateix tumor, la secreció de marcadors sèrics, com alfa-fetoproteïna i la subunitat beta de la gonadotrofina coriònica humana, que permetia fer-ne un seguiment en temps real de la resposta als tractaments i la sensibilitat al tractament amb cisplatí. En cinc d'aquests models, de manera anàloga a com ho havíem fet en càncer epitelial d'ovari, es va generar la corresponent parella de tumor resistent al cisplatí mitjançant l'exposició a cicles iteratius de tractament amb dosis creixents del fàrmac. Els tumors generats després d'aquest procés deixaven de respondre fins i tot a dosis altes de cisplatí. Mitjançant matrius d'hibridació genòmica comparada (CGH) es va demostrar que hi havia zones recurrents de guanys i pèrdues als tumors resistents al cisplatí

comparat amb les seves respectives parelles sensibles. Per a aquest estudi ens vàrem centrar en la regió 9q32-q33.1, que estava guanyada en tres dels tumors resistents. Per a veure si aquest guany de material genòmic, que de manera recurrent es guanyava als tumors que s'havien fet resistents al platí *in vivo* en els ratolins, tenia rellevància clínica es va estudiar una sèrie de 75 pacients amb tumors de cèl·lules germinals metastàtics tractats de manera homogènia i es va demostrar que l'amplificació de 9q32-q33.1 s'associava amb un temps de progressió de la malaltia més curt i amb un risc de mort més elevat. Aquest fet és molt rellevant perquè ens valida aquests models preclínics de resistència ja que reprodueixen un mecanisme genètic/genòmic que també succeeix en els tumors primaris dels pacients.

A continuació es va estudiar l'expressió dels 60 gens i 2 miARNs presents a la regió 9q32-q33.1 tant als tumors originals sensibles al cisplatí com a les seves parelles resistents. Es van identificar cinc gens que estaven sobreregulats o infraregulats en tots els tumors resistents (*GCS*, *ZNF883*, *CTR1*, *ATP6V1G1* i *FLJ31713*). Els estudis de dsRNAi (interferència amb RNA de cadena doble) a C. elegans que silenciava els tres gens ortòlegs conservats (*GCS*, *CTR1* i *ATP6V1G1*) confirmaven el paper rellevant dels tres, ressaltant el paper de GCS. Així, analitzant les dades dels tumors i del cuc vàrem decidir que d'aquest cinc gens seleccionavem *GCS* per a fer una prova de concepte per a buscar noves estratègies terapèutiques per a vèncer la resistència al cisplatí. A part de què aquest gen estava sobreregulat a tots els tumors resistents, era molt interessant perquè a més a més es disposava d'inhibidors específics de l'enzim GCS (glucosil ceramida sintasa) i que ja s'estaven usant en la pràctica clínica per a altres malalties (185,186) .

Aquest és un exemple clar del potencial d'aquests models no només per a ajudar al desenvolupament preclínic de noves molècules como la lurbinectedina, sinó també per a descobrir noves indicacions de fàrmacs ja en ús en altres malalties, dit d'una altra manera, és un exemple clar de reposicionament de fàrmacs. Aquest ús és molt rellevant ja que els estudis de toxicitat d'aquestes molècules ja estan fets i això pot contribuir a accelerar i optimitzar l'arribada de nous fàrmacs per al tractament del càncer. A més, el nostre estudi remarca la rellevància de l'activitat del enzim GCS en el procés biològic de protecció de les

cèl·lules tumorals davant l'exposició al cisplatí, i senyala la importància del metabolisme dels esfingolípids en la resistència al cisplatí, tant en el TTGC com en càncer epitelial d'ovari.

Al tercer treball (139) hem desenvolupat una metodologia basada en la implantació de fragments tumorals sòlids, no disgregats, de forma ortotòpica al pulmó de ratolins immunodeficients. Els tumors que hem implantat no són tumors primaris humans, sinó que son els petits tumors que es generen en diversos models GEMM després de la inducció d'un oncogen (*KRAS*) o d'una traslocació (EML4-ALK). Tècnicament aquest procediment d'implantació ortotòpica, possiblement sigui el més complex ja que fixem el tumor amb el fil de sutura al parènquima pulmonar. Els tumors de pulmó generats en models GEMM induïts per un sol oncogen presenten certes limitacions com ara la poca heterogeneïtat histològica i genètica i la manca d'invasivitat local i de capacitat metastàtica. En aquest treball demostrem que mitjançant la implantació ortotòpica seqüencial de fragments d'aquests tumors s'ha aconseguit generar tumors que tenen un patró d'infiltració local i de disseminació metastàtica similar a l'observat en la malaltia humana. També s'ha incrementat de manera important l'heterogeneïtat tumoral, obtenint-se tumors amb diferents patrons histològics tal i com es veu en els tumors de pulmó humans (84). Així mateix, la implantació successiva de tumors afavoreix l'aparició de mutacions en oncogens i la pèrdua d'expressió de gens supressors tumorals de manera semblant al que passa en el carcinoma de pulmó no cèl·lula petita humà en estadis avançats. El model ha permès obtenir diferents línies cel·lulars de càncer de pulmó *KRAS* mutat amb *TP53* no mutat que no es podien derivar dels tumors primàriament generats en els models de ratolins dissenyats genèticament. Aquestes línies cel·lulars seran molt útils a l'hora d'avaluar el potencial de nous fàrmacs en un context genètic molt més controlat i definit que el què es pot fer en línies cel·lulars derivades dels tumors primaris humans. A més, a partir d'aquestes línies s'ha pogut demostrar que partint d'un clon únic es pot reproduir l'heterogeneïtat tumoral present en tumors humans. Finalment, s'ha demostrat en aquests models una resposta a les teràpies estàndard similar a la que s'observa en la clínica, tant en cas de quimioteràpia clàssica (model K-RASG12V), com en el cas de teràpies dirigides (crizotinib en el model EML4-ALK).

Al quart treball (187) hem desenvolupat una col·lecció d'ortoxenografts derivats del pacient (PDOX) de 15 pacients amb carcinoma endometrioide d'endometri. Després d'una extensa caracterització histològica, genètica i transcriptòmica comparativa tant del tumor primari de la pacient donant com del PDOX del ratolí, clarament hem demostrat que aquests models preclínics conserven la major part de les característiques del seu tumor original. A més, també hem demostrat que els PDOX són entitats dinàmiques i que poden presentar característiques evolutives intrigants com ara la desdiferenciació a mesura que van creixent *in vivo*.

Com ja he anat indicant al llarg de la discussió, els models de xenograft derivats del pacient (PDX) i mès concretament els models ortotòpics (PDOX/orthoxenografts) han resorgit en els últims anys com a poderoses eines per a la investigació del càncer. Els models PDX s'han revelat com a models preclínics extraordinaris i precisos, amb un alt valor predictiu de resposta als fàrmacs, superant en general als models *in vitro*. A més a més, quan s'han inclòs els PDX en assaigs clínics o co-clínics, han augmentat la taxa d'èxit de l'aprovació dels compostos. Globalment aquests models s'han convertit en uns recursos innovadors per a refinar les decisions de tractament en el futur i per a accelerar el desenvolupament de nous fàrmacs, així com per a la implementació de la medicina personalitzada o de precisió basada en les característiques moleculars individuals dels tumors.

Encara que en aquest treball presentem dades sobre un nombre reduït de models, i centrat en el carcinoma endometrioide, cal destacar que el banc de PDOX d'endometri que hem generat en els darrers 10 anys és d'uns 150 models que inclouen tots els tipus histològics més freqüents de càncer d'endometri (carcinomes endometrioides, serosos, de cèl·lules clares i carcinosarcomes), representació dels quatre tipus moleculars de càncer d'endometri, així com també alguns models generats a partir de tumors resistents a la recaiguda. Algun d'aquests models els hem usat en altres treballs que no presentem en aquesta Tesi, per a avaluar el paper de l'autofàgia en el càncer d'endometri (188), l'estrès oxidatiu en carcinoma serós d'endometri (189) o noves estratègies d'immunoteràpia en carcinoma d'endometri amb dèficit de proteïnes reparadores (190)

En aquest treball hem demostrat que els PDOX també són una font de teixit molt interessant `per a la generació de tumoroides, essent la seva generació molt més eficient quan es fa partint del PDOX que del tumor primari. En l'actual època de la medicina de precisió o personalitzada, aquests organoides poden ser utilitzats per avaluar *in vitro* els tractaments que poden arribar a ser més efectius per a tractar un tumor concret en base a les seves alteracions genètiques. Així, i com a prova de concepte hem seleccionat un PDOX que té la mutació en el gen *HER2*^{R678Q} , i que es troba enriquida als tumors d'endometri, i hem demostrat la utilitat de l'ús del binomi PDOX-tumoroide a l'hora d'avaluar la utilitat terapèutica del trastuzumab (inhibidor de HER2), demostrant col·lectivament la rellevància dels models PDOX per explorar noves vies terapèutiques per als pacients amb càncer d'endometri.

Al llarg del treball, a la introducció ja he fet una descripció rigorosa i extensa dels diferents tipus de models preclínics, focalitzant-me majoritàriament en els PDX i els PDOX/orthoxenografts, descrivint-ne les virtuts, limitacions i usos. Per tot això considero que seria repetitiu tornar a emfatitzar aquests aspectes a la discussió general d'aquesta Tesi. A més, molts d'aquests aspectes també estan àmpliament discutits en els quatre treballs que configuren aquesta Tesi.

Al llarg d'aquesta Tesi, he destacat la importància de disposar de bons models preclínics no només per aprofundir en el coneixement de les bases moleculars del desenvolupament i progressió del càncer (treball 3 a CPNCP), sinó també com a eines preclíniques que ens ajudin a identificar marcadors pronòstics (treball 2 a TTGC), així com en el desenvolupament de noves molècules (treball 1), l'ús de fàrmacs ja en utilitzats en el tractament d'altres tumors (treball 4), o en el reposicionament de fàrmacs ja en ús en altres malalties (treball 2). Aquests models preclínics no són fàcils de generar tècnicament, i requereixen la coordinació de molts professionals sanitaris que participen del diagnòstic i tractament dels pacients amb càncer. Aquest treball no es podria fer sense la col·laboració dels pacients que ens donen el seu consentiment per a fer recerca amb el remanent dels seus tumors una vegada s'han estudiat d'acord amb l'estàndard clínic assistencial. Disposar d'aquests models és una finestra cap al futur, ja que ens permetran generar i validar noves opcions terapèutiques que puguin millorar el tractament i la qualitat de vida dels pacients. L'ampli

coneixement que es té actualment en temps real de les alteracions genètiques dels tumors, així com l'arribada de potents eines d'intel·ligència artificial estan incrementant de manera exponencial la nostra capacitat de generar hipòtesis de tractament (ex: bessons digitals, noves molècules, noves combinacions de fàrmacs,...). És en aquest context que pensem que cada cop es fa més rellevant i necessari disposar de bons models preclínics, com els que descrivim en aquesta Tesi, com a eines en què avaluar totes aquestes noves hipòtesis.

CONSIDERACIONS FINALS

Com a patòleg, m'ha representat una veritable satisfacció poder ajudar a generar aquests models, poder-los validar histopatològicament i poder usar-los com a eines. Si bé aquests models tenen limitacions ja comentades anteriorment, com ara el fet que es desenvolupin en una espècie animal diferent de la del tumor original i, a més a més, en un entorn d'immunodeficiència, un dels aspectes que més m'ha sorprès en fer l'estudi comparatiu entre els tumors primaris i els PDOX ha estat l'enorme similitud que hi ha entre tots dos, similitud que sovint he trobat a faltar analitzant altres experiments en què els tumors es generaven a partir de línies cel·lulars o inclús en PDX subcutanis.

Durant els anys del desenvolupament d'aquesta Tesi he participat a més a més en la generació i caracterització de molts altres tipus de models PDOX generats majoritàriament en el grup del Dr. Villanueva. Models que hem fet servir en estudis realitzats en col·laboració amb altres grups tan nacionals com internacionals. Vull ressaltar aquest aspecte de col·laboració, ja que aquests models han permès fer i publicar estudis de molt alta rellevància per a millorar el tractament dels pacients (191–193).

CONCLUSIONS

1. S'han generat i caracteritzat des del punt de vista clínico-patològic models PDOX/Orthoxenografts de càncer epitelial d'ovari, de tumors testiculars de cèl·lules germinals i de carcinomes endometrioides d'endometri, models que recapitulen les principals característiques de la malaltia humana.

2. A partir de l'evolució de models PDOX/Orthoxenografts de càncer epitelial d'ovari i de tumors testiculars de cèl·lules germinals s'han obtingut models de resistència adquirida al tractament amb cisplatí.

3. El model PDOX/Orthoxenografts aparellat de carcinoma serós d'alt grau d'ovari sensible i resistent al platí ha contribuït al desenvolupament preclínic de la molècula lurbinectedina.

4. L'amplificació gènica de 9q32-q33.1 és un marcador de mal pronòstic en tumors testiculars de cèl·lules germinals.

5. S'ha identificat una cohort de gens potencialment implicats en la resistència al platí gràcies a l'estudi combinat amb diferents models preclínics. Això ha facilitat com a prova de concepte el disseny d'una teràpia de re-sensibilització al platí mitjançant el reposicionament d'un fàrmac emprat en la pràctica clínica en algunes malalties metabòliques.

6. S'han generat al·loempelts ortotòpics (orthoallografts) de tumors de ratolins modificats genèticament que han permès i) estudiar els estadis inicials de la progressió tumoral en adenocarcinoma de pulmó, ii) reproduir les característiques clínico-patològiques de la malaltia humana en termes d'heterogeneïtat tumoral, invasivitat local i capacitat de disseminació metastàtica i, iii) obtenir per primera vegada línies cel·lulars derivades d'aquests tumors que s'han demostrat útils en l'avaluació pre-clínica de diferents aproximacions terapèutiques.

7. Els PDOX/Orthoxenografts de carcinoma endometrioide d'endometri han permès la caracterització transcriptòmica i del perfil mutacional, facilitant el disseny de noves teràpies dirigides contra aquests tumors.

BIBLIOGRAFIA

1. Slamon DJ, Leyland-Jones B, Shak S, Fuchs H, Paton V, Bajamonde A, et al. Use of chemotherapy plus a monoclonal antibody against HER2 for metastatic breast cancer that overexpresses HER2. N Engl J Med [Internet]. 2001 Mar 15 [cited 2022 Dec 4];344(11):783–92. Available from: https://pubmed.ncbi.nlm.nih.gov/11248153/

2. Perez EA, Romond EH, Suman VJ, Jeong JH, Sledge G, Geyer CE, et al. Trastuzumab plus adjuvant chemotherapy for human epidermal growth factor receptor 2-positive breast cancer: planned joint analysis of overall survival from NSABP B-31 and NCCTG N9831. J Clin Oncol [Internet]. 2014 Nov 20 [cited 2022 Dec 4];32(33):3744–52. Available from: https://pubmed.ncbi.nlm.nih.gov/25332249/

3. O'Sullivan CC, Swain SM. Pertuzumab : evolving therapeutic strategies in the management of HER2-overexpressing breast cancer. Expert Opin Biol Ther [Internet]. 2013 May [cited 2022 Dec 4];13(5):779–90. Available from: https://pubmed.ncbi.nlm.nih.gov/23530718/

4. Hochhaus A, Larson RA, Guilhot F, Radich JP, Branford S, Hughes TP, et al. Long-Term Outcomes of Imatinib Treatment for Chronic Myeloid Leukemia. N Engl J Med [Internet]. 2017 Mar 9 [cited 2022 Dec 4];376(10):917–27. Available from: https://pubmed.ncbi.nlm.nih.gov/28273028/

5. Kalmanti L, Saussele S, Lauseker M, Müller MC, Dietz CT, Heinrich L, et al. Safety and efficacy of imatinib in CML over a period of 10 years: data from the randomized CML-study IV. Leukemia [Internet]. 2015 May 11 [cited 2022 Dec 4];29(5):1123–32. Available from: https://pubmed.ncbi.nlm.nih.gov/25676422/

6. Hehlmann R. CML--Where do we stand in 2015? Ann Hematol [Internet]. 2015 Apr 1 [cited 2022 Dec 4];94 Suppl 2(2):103–5. Available from: https://pubmed.ncbi.nlm.nih.gov/25814076/

7. Sung H, Ferlay J, Siegel RL, Laversanne M, Soerjomataram I, Jemal A, et al. Global Cancer Statistics 2020: GLOBOCAN Estimates of Incidence and Mortality Worldwide for 36 Cancers in 185 Countries. CA Cancer J Clin [Internet]. 2021 May [cited 2022 Dec 6];71(3):209–49. Available from: https://pubmed.ncbi.nlm.nih.gov/33538338/

8. Webb PM, Green AC, Jordan SJ. Trends in hormone use and ovarian cancer incidence in US white and Australian women: implications for the future. Cancer Causes and Control [Internet]. 2017 May 1 [cited 2024 May 1];28(5):365–70. Available from: https://link-springer-com.sire.ub.edu/article/10.1007/s10552-017-0868-0

9. Cabasag CJ, Arnold M, Butler J, Inoue M, Trabert B, Webb PM, et al. The influence of birth cohort and calendar period on global trends in ovarian cancer incidence. Int J Cancer [Internet]. 2020 Feb 1 [cited 2022 Jul 21];146(3):749–58. Available from: https://pubmed.ncbi.nlm.nih.gov/30968402/

10. Webb PM, Jordan SJ. Global epidemiology of epithelial ovarian cancer. Nature Reviews Clinical Oncology | [Internet]. 2024 [cited 2024 May 1];21:389–400. Available from: https://doi.org/10.1038/s41571-024-00881-3

11. Jervis S, Song H, Lee A, Dicks E, Tyrer J, Harrington P, et al. Ovarian cancer familial relative risks by tumour subtypes and by known ovarian cancer genetic susceptibility variants. J Med Genet [Internet]. 2014 Feb 1 [cited 2024 May 1];51(2):108–13. Available from: https://jmg-bmj-com.sire.ub.edu/content/51/2/108

12. Flaum N, Crosbie EJ, Edmondson RJ, Smith MJ, Evans DG. Epithelial ovarian cancer risk: A review of the current genetic landscape. Clin Genet [Internet]. 2020 Jan 1 [cited 2024 May 4];97(1):54–63. Available from: https://onlinelibrary-wiley-com.sire.ub.edu/doi/full/10.1111/cge.13566

13. Jones MR, Kamara D, Karlan BY, Pharoah PDP, Gayther SA. Genetic epidemiology of ovarian cancer and prospects for polygenic risk prediction. Gynecol Oncol [Internet]. 2017 Dec 1 [cited 2024 Jun 2];147(3):705–13. Available from: https://pubmed.ncbi.nlm.nih.gov/29054568/

14. Jensen KC, Mariappan MR, Putcha G V., Husain A, Chun N, Ford JM, et al. Microsatellite instability and mismatch repair protein defects in ovarian epithelial neoplasms in patients 50 years of age and younger. Am J Surg Pathol [Internet]. 2008 Jul [cited 2024 May 4];32(7):1029–37. Available from: https://pubmed.ncbi.nlm.nih.gov/18469706/

15. Norquist BM, Harrell MI, Brady MF, Walsh T, Lee MK, Gulsuner S, et al. Inherited Mutations in Women With Ovarian Carcinoma. JAMA Oncol [Internet]. 2016 Apr 1 [cited 2024 May 4];2(4):482–90. Available from: https://jamanetwork-com.sire.ub.edu/journals/jamaoncology/fullarticle/2479125

16. Soong TR, Howitt BE, Miron A, Horowitz NS, Campbell F, Feltmate CM, et al. Evidence for lineage continuity between early serous proliferations (ESPs) in the Fallopian tube and disseminated high-grade serous carcinomas. J Pathol [Internet]. 2018 Nov 1 [cited 2024 Jun 2];246(3):344–51. Available from: https://pubmed.ncbi.nlm.nih.gov/30043522/

17. Kuhn E, Kurman RJ, Vang R, Sehdev AS, Han G, Soslow R, et al. TP53 mutations in serous tubal intraepithelial carcinoma and concurrent pelvic high-grade serous carcinoma--evidence supporting the clonal relationship of the two lesions. J Pathol [Internet]. 2012 Feb [cited 2024 Jun 2];226(3):421–6. Available from: https://pubmed.ncbi.nlm.nih.gov/21990067/

18. Ahmed AA, Etemadmoghadam D, Temple J, Lynch AG, Riad M, Sharma R, et al. Driver mutations in TP53 are ubiquitous in high grade serous carcinoma of the ovary. J Pathol [Internet]. 2010 May [cited 2024 Jun 2];221(1):49–56. Available from: https://pubmed.ncbi.nlm.nih.gov/20229506/

19. Vang R, Levine DA, Soslow RA, Zaloudek C, Shih IM, Kurman RJ. Molecular Alterations of TP53 are a Defining Feature of Ovarian High-Grade Serous Carcinoma: A Rereview of Cases Lacking TP53 Mutations in The Cancer Genome Atlas Ovarian Study. Int J Gynecol Pathol [Internet]. 2016 Jan 1 [cited 2024 Jun 2];35(1):48–55. Available from: https://pubmed.ncbi.nlm.nih.gov/26166714/

20. Aziz S, Kuperstein G, Rosen B, Cole D, Nedelcu R, McLaughlin J, et al. A genetic epidemiological study of carcinoma of the fallopian tube. Gynecol Oncol [Internet]. 2001 [cited 2024 Jun 2];80(3):341–5. Available from: https://pubmed.ncbi.nlm.nih.gov/11263928/

21. Levine DA, Argenta PA, Yee CJ, Marshall DS, Olvera N, Bogomolniy F, et al. Fallopian tube and primary peritoneal carcinomas associated with BRCA mutations. J Clin Oncol [Internet]. 2003 Nov 15 [cited 2024 Jun 2];21(22):4222–7. Available from: https://pubmed.ncbi.nlm.nih.gov/14615451/

22. Cheung A, Ellenson L, Gilks C, Kim KR, Kong C, Lax S, et al. Tumours of the Ovary. In: WHO Classification of Tumours Editorial Board Female Genital Tumours [Internet]. 5th ed. Lyon (France): International Agency for Research on Cancer; 2020. p. 31–167. Available from: https://publications.iarc.fr/592

23. Köbel M, Kalloger SE, Huntsman DG, Santos JL, Swenerton KD, Seidman JD, et al. Differences in Tumor Type in Low-stage Versus High-stage Ovarian Carcinomas. International Journal of Gynecological Pathology [Internet]. 2010 May [cited 2017 Jun 20];29(3):203–11. Available from: http://www.ncbi.nlm.nih.gov/pubmed/20407318

24. WHO Classification of Tumours Editorial Board. Female genital tumours. 5th ed. Vol. 4. Lyon (France): International Agency for Research on Cancer; 2020.

25. Brierley JD, Gospodarowicz MK, Wittekind C. The TNM Classification of Malignant Tumours, 8th Edition [Internet]. Wiley-Blackwell; 2016. Available from: https://www.uicc.org/resources/tnm-classification-malignant-tumours-8th-edition

26. Amin MB, Edge SB, Greene FL, Byrd DR, Brookland RK, Washington MK, et al. AJCC Cancer Staging Manual. 8th Edition [Internet]. Springer Cham; 2017. Available from: https://link.springer.com/book/9783319406176

27. Ledermann JA, Raja FA, Fotopoulou C, Gonzalez-Martin A, Colombo N, Sessa C. Newly diagnosed and relapsed epithelial ovarian carcinoma: ESMO Clinical Practice Guidelines for diagnosis, treatment and follow-up. Annals of Oncology [Internet]. 2013 Oct 1 [cited 2017 Jun 20];24(suppl 6):vi24–32. Available from: https://academic.oup.com/annonc/article-lookup/doi/10.1093/annonc/mdt333

28. du Bois A, Lück HJ, Meier W, Adams HP, Möbus V, Costa S, et al. A randomized clinical trial of cisplatin/paclitaxel versus carboplatin/paclitaxel as first-line treatment of ovarian cancer. J Natl Cancer Inst [Internet]. 2003 Sep 3 [cited 2022 Jul 11];95(17):1320–30. Available from: https://pubmed.ncbi.nlm.nih.gov/12953086/

29. Ozols RF, Bundy BN, Greer BE, Fowler JM, Clarke-Pearson D, Burger RA, et al. Phase III trial of carboplatin and paclitaxel compared with cisplatin and paclitaxel in patients with optimally resected stage III ovarian cancer: A Gynecologic Oncology Group study. Journal of Clinical Oncology. 2003 Sep 1;21(17):3194–200.

30. Vergote I, Tropé CG, Amant F, Kristensen GB, Ehlen T, Johnson N, et al. Neoadjuvant chemotherapy or primary surgery in stage IIIC or IV ovarian cancer. N Engl J Med [Internet]. 2010 Sep 2 [cited 2017 Jun 20];363(10):943–53. Available from: http://www.nejm.org/doi/abs/10.1056/NEJMoa0908806

31. Burger RA, Brady MF, Bookman MA, Fleming GF, Monk BJ, Huang H, et al. Incorporation of Bevacizumab in the Primary Treatment of Ovarian Cancer. https://doi.org/101056/NEJMoa1104390 [Internet]. 2011 Dec 29 [cited 2022 Jul 12];365(26):2473–83. Available from: https://www.nejm.org/doi/10.1056/NEJMoa1104390

32. Aghajanian C, Blank S V., Goff BA, Judson PL, Teneriello MG, Husain A, et al. OCEANS: A randomized, double-blind, placebo-controlled phase III trial of chemotherapy with or without

bevacizumab in patients with platinum-sensitive recurrent epithelial ovarian, primary peritoneal, or fallopian tube cancer. Journal of Clinical Oncology. 2012 Jun 10;30(17):2039–45.

33. Pujade-Lauraine E, Hilpert F, Weber B, Reuss A, Poveda A, Kristensen G, et al. Bevacizumab combined with chemotherapy for platinum-resistant recurrent ovarian cancer: The AURELIA open-label randomized phase III trial. Journal of Clinical Oncology. 2014 May 1;32(13):1302–8.

34. Disilvestro P, Banerjee S, Colombo N, Scambia G, Kim BG, Oaknin A, et al. Overall Survival With Maintenance Olaparib at a 7-Year Follow-Up in Patients With Newly Diagnosed Advanced Ovarian Cancer and a BRCA Mutation: The SOLO1/GOG 3004 Trial. J Clin Oncol [Internet]. 2023 Jan 20 [cited 2024 Jun 2];41(3):609–17. Available from: https://pubmed.ncbi.nlm.nih.gov/36082969/

35. González-Martín A, Pothuri B, Vergote I, DePont Christensen R, Graybill W, Mirza MR, et al. Niraparib in Patients with Newly Diagnosed Advanced Ovarian Cancer. N Engl J Med [Internet]. 2019 Dec 19 [cited 2024 Jun 2];381(25):2391–402. Available from: https://pubmed.ncbi.nlm.nih.gov/31562799/

36. Moore K, Colombo N, Scambia G, Kim BG, Oaknin A, Friedlander M, et al. Maintenance Olaparib in Patients with Newly Diagnosed Advanced Ovarian Cancer. N Engl J Med [Internet]. 2018 Dec 27 [cited 2024 Jun 2];379(26):2495–505. Available from: https://pubmed.ncbi.nlm.nih.gov/30345884/

37. Kyrgiou M, Salanti G, Pavlidis N, Paraskevaidis E, Ioannidis JPA. Survival Benefits With Diverse Chemotherapy Regimens for Ovarian Cancer: Meta-analysis of Multiple Treatments. JNCI Journal of the National Cancer Institute [Internet]. 2006 Nov 15 [cited 2017 Jun 20];98(22):1655–63. Available from: http://www.ncbi.nlm.nih.gov/pubmed/17105988

38. Oosterhuis JW, Looijenga LHJ. Testicular germ-cell tumours in a broader perspective. Nat Rev Cancer [Internet]. 2005 Mar [cited 2022 Jul 15];5(3):210–22. Available from: https://pubmed.ncbi.nlm.nih.gov/15738984/

39. Germà-Lluch JR, Garcia del Muro X, Maroto P, Paz-Ares L, Arranz JA, Gumà J, et al. Clinical pattern and therapeutic results achieved in 1490 patients with germ-cell tumours of the testis: the experience of the Spanish Germ-Cell Cancer Group (GG). Eur Urol [Internet]. 2002 Dec [cited 2017 Jun 20];42(6):553–62; discussion 562-3. Available from: http://www.ncbi.nlm.nih.gov/pubmed/12477650

40. Maxwell Parkin D, Bray F, Ferlay J, Pisani P. Estimating the world cancer burden: Globocan 2000. Int J Cancer [Internet]. 2001 Oct 15 [cited 2022 Jul 14];94(2):153–6. Available from: https://pubmed.ncbi.nlm.nih.gov/11668491/

41. Bray F, Ferlay J, Devesa SS, McGlynn K a, Møller H. Interpreting the international trends in testicular seminoma and nonseminoma incidence. Nat Clin Pract Urol [Internet]. 2006 Oct [cited 2014 Jul 30];3(10):532–43. Available from: http://www.ncbi.nlm.nih.gov/pubmed/17031378

42. Power DA, Brown RSD, Brock CS, Payne HA, Majeed A, Babb P. Trends in testicular carcinoma in England and Wales, 1971-99. BJU Int. 2001;87(4):361–5.

43. McDowall ME, Balarajan R. Testicular cancer mortality in England and Wales 1971-80: variations by occupation. J Epidemiol Community Health (1978) [Internet]. 1986 [cited 2022 Jul 14];40(1):26–9. Available from: https://pubmed.ncbi.nlm.nih.gov/3711767/

44. Mortensen MS, Lauritsen J, Gundgaard MG, Agerbæk M, Holm NV, Christensen IJ, et al. A nationwide cohort study of stage I seminoma patients followed on a surveillance program. Eur Urol [Internet]. 2014 Dec 1 [cited 2022 Jul 14];66(6):1172–8. Available from: https://pubmed.ncbi.nlm.nih.gov/25064686/

45. Daugaard G, Gundgaard MG, Mortensen MS, Agerbæk M, Holm NV, Rørth M, et al. Surveillance for stage I nonseminoma testicular cancer: outcomes and long-term follow-up in a population-based cohort. J Clin Oncol [Internet]. 2014 Dec 1 [cited 2022 Jul 14];32(34):3817–23. Available from: https://pubmed.ncbi.nlm.nih.gov/25267754/

46. Dieckmann KP, Loy V. Prevalence of contralateral testicular intraepithelial neoplasia in patients with testicular germ cell neoplasms. J Clin Oncol [Internet]. 1996 [cited 2022 Jul 14];14(12):3126–32. Available from: https://pubmed.ncbi.nlm.nih.gov/8955658/

47. Harland SJ, Cook PA, Fossa SD, Horwich A, Mead GM, Parkinson MC, et al. Intratubular germ cell neoplasia of the contralateral testis in testicular cancer: defining a high risk group. J Urol [Internet]. 1998 [cited 2022 Jul 14];160(4):1353–7. Available from: https://pubmed.ncbi.nlm.nih.gov/9751353/

48. Akre O, Ekbom A, Hsieh CC, Trichopoulos D, Adami HO. Testicular nonseminoma and seminoma in relation to perinatal characteristics. J Natl Cancer Inst [Internet]. 1996 Jul 3 [cited 2022 Jul 14];88(13):883–9. Available from: https://pubmed.ncbi.nlm.nih.gov/8656440/

49. Møller H, Skakkebæk NE. Testicular cancer and cryptorchidism in relation to prenatal factors: case-control studies in Denmark. Cancer Causes Control [Internet]. 1997 [cited 2022 Jul 14];8(6):904–12. Available from: https://pubmed.ncbi.nlm.nih.gov/9427433/

50. Goedert JJ, Coté TR, Virgo P, Scoppa SM, Kingma DW, Gail MH, et al. Spectrum of AIDS-associated malignant disorders. Lancet [Internet]. 1998 Jun 20 [cited 2022 Jul 14];351(9119):1833–9. Available from: https://pubmed.ncbi.nlm.nih.gov/9652666/

51. Birkeland SA, Storm HH, Lamm LU, Barlow L, Blohmé I, Forsberg B, et al. Cancer risk after renal transplantation in the Nordic countries, 1964-1986. Int J Cancer [Internet]. 1995 [cited 2022 Jul 14];60(2):183–9. Available from: https://pubmed.ncbi.nlm.nih.gov/7829213/

52. Richiardi L, Akre O, Bellocco R, Ekbom A. Perinatal determinants of germ-cell testicular cancer in relation to histological subtypes. Br J Cancer [Internet]. 2002 Aug 27 [cited 2022 Jul 15];87(5):545–50. Available from: https://pubmed.ncbi.nlm.nih.gov/12189554/

53. Hanna NH, Einhorn LH. Testicular cancer--discoveries and updates. N Engl J Med [Internet]. 2014 Nov 20 [cited 2022 Jul 15];371(21):2005–16. Available from: https://pubmed.ncbi.nlm.nih.gov/25409373/

54. Rapley EA, Turnbull C, Al Olama AA, Dermitzakis ET, Linger R, Huddart RA, et al. A genome-wide association study of testicular germ cell tumor. Nat Genet [Internet]. 2009 Jul [cited 2022 Jul 15];41(7):807–10. Available from: https://pubmed.ncbi.nlm.nih.gov/19483681/

55. Ottesen AM, Skakkebæk NE, Lundsteen C, Leffers H, Larsen J, Rajpert-De Meyts E. High-resolution comparative genomic hybridization detects extra chromosome arm 12p material in most cases of carcinoma in situ adjacent to overt germ cell tumors, but not before the invasive tumor development. Genes Chromosomes Cancer [Internet]. 2003 Oct 1 [cited 2022 Jul 15];38(2):117–25. Available from: https://pubmed.ncbi.nlm.nih.gov/12939739/

56. Shen H, Shih J, Hollern DP, Wang L, Bowlby R, Tickoo SK, et al. Integrated Molecular Characterization of Testicular Germ Cell Tumors. Cell Rep [Internet]. 2018 Jun 12 [cited 2022 Jul 15];23(11):3392–406. Available from: https://pubmed.ncbi.nlm.nih.gov/29898407/

57. Bagrodia A, Lee BH, Lee W, Cha EK, Sfakianos JP, Iyer G, et al. Genetic Determinants of Cisplatin Resistance in Patients With Advanced Germ Cell Tumors. J Clin Oncol [Internet]. 2016 Nov 20 [cited 2022 Jul 15];34(33):4000–7. Available from: https://pubmed.ncbi.nlm.nih.gov/27646943/

58. WHO Classification of Tumours Editorial Board. Urinary and male genital tumours [Internet] [Internet]. Lyon (France): International Agency for Research on Cancer: (WHO classification of tumours series, 5th ed.; vol. 8); 2022. Available from: https://tumourclassification.iarc.who.int/chapters/36

59. Berney DM, Looijenga LHJ, Idrees M, Oosterhuis JW, Rajpert-De Meyts E, Ulbright TM, et al. Germ cell neoplasia in situ (GCNIS): evolution of the current nomenclature for testicular pre-invasive germ cell malignancy. Histopathology [Internet]. 2016 Jul 1 [cited 2022 Jul 17];69(1):7–10. Available from: https://pubmed.ncbi.nlm.nih.gov/26918959/

60. Kao CS, Ulbright TM, Young RH, Idrees MT. Testicular embryonal carcinoma: a morphologic study of 180 cases highlighting unusual and unemphasized aspects. Am J Surg Pathol [Internet]. 2014 [cited 2022 Jul 17];38(5):689–97. Available from: https://pubmed.ncbi.nlm.nih.gov/24503753/

61. Lobo J, Costa AL, Vilela-Salgueiro B, Rodrigues Â, Guimarães R, Cantante M, et al. Testicular germ cell tumors: revisiting a series in light of the new WHO classification and AJCC staging systems, focusing on challenges for pathologists. Hum Pathol [Internet]. 2018 Dec 1 [cited 2022 Jul 17];82:113–24. Available from: https://pubmed.ncbi.nlm.nih.gov/30041024/

62. Jacobsen GK, Barlebo H, Olsen J, Schultz HP, Starklint H, Søgaard H, et al. Testicular germ cell tumours in Denmark 1976-1980. Pathology of 1058 consecutive cases. Acta Radiol Oncol [Internet]. 1984 [cited 2022 Jul 17];23(4):239–47. Available from: https://pubmed.ncbi.nlm.nih.gov/6093440/

63. Alvarado-Cabrero I, Hernández-Toriz N, Paner GP. Clinicopathologic analysis of choriocarcinoma as a pure or predominant component of germ cell tumor of the testis. Am J Surg Pathol [Internet]. 2014 Jan [cited 2022 Jul 17];38(1):111–8. Available from: https://pubmed.ncbi.nlm.nih.gov/24145647/

64. Mead GM. International Germ Cell Consensus Classification: a prognostic factor-based staging system for metastatic germ cell cancers. International Germ Cell Cancer Collaborative Group. J Clin Oncol [Internet]. 1997 [cited 2022 Jul 16];15(2):594–603. Available from: https://pubmed.ncbi.nlm.nih.gov/9053482/

65. Mortensen MS, Lauritsen J, Gundgaard MG, Agerbæk M, Holm NV, Christensen IJ, et al. A nationwide cohort study of stage I seminoma patients followed on a surveillance program. Eur Urol [Internet]. 2014 Dec 1 [cited 2022 Jul 17];66(6):1172–8. Available from: https://pubmed.ncbi.nlm.nih.gov/25064686/

66. Honecker F, Aparicio J, Berney D, Beyer J, Bokemeyer C, Cathomas R, et al. ESMO Consensus Conference on testicular germ cell cancer: diagnosis, treatment and follow-up. Ann Oncol [Internet]. 2018 Aug 1 [cited 2022 Jul 17];29(8):1658–86. Available from: https://pubmed.ncbi.nlm.nih.gov/30113631/

67. Kier MG, Lauritsen J, Mortensen MS, Bandak M, Andersen KK, Hansen MK, et al. Prognostic Factors and Treatment Results After Bleomycin, Etoposide, and Cisplatin in Germ Cell Cancer: A Population-based Study. Eur Urol [Internet]. 2017 Feb 1 [cited 2022 Jul 17];71(2):290–8. Available from: https://pubmed.ncbi.nlm.nih.gov/27649970/

68. Scandura G, Wagner T, Beltran L, Alifrangis C, Shamash J, Berney DM. Pathological predictors of metastatic disease in testicular non-seminomatous germ cell tumors: which tumor-node-metastasis staging system? Mod Pathol [Internet]. 2021 Apr 1 [cited 2022 Jul 17];34(4):834–41. Available from: https://pubmed.ncbi.nlm.nih.gov/33319858/

69. Feldman DR. Treatment options for stage I nonseminoma. J Clin Oncol [Internet]. 2014 Dec 1 [cited 2022 Jul 17];32(34):3797–800. Available from: https://pubmed.ncbi.nlm.nih.gov/25366681/

70. Daugaard G, Gundgaard MG, Mortensen MS, Agerbæk M, Holm NV, Rørth M, et al. Surveillance for stage I nonseminoma testicular cancer: outcomes and long-term follow-up in a population-based cohort. J Clin Oncol [Internet]. 2014 Dec 1 [cited 2022 Jul 17];32(34):3817–23. Available from: https://pubmed.ncbi.nlm.nih.gov/25267754/

71. Blok JM, Pluim I, Daugaard G, Wagner T, Jóźwiak K, Wilthagen EA, et al. Lymphovascular invasion and presence of embryonal carcinoma as risk factors for occult metastatic disease in clinical stage I nonseminomatous germ cell tumour: a systematic review and meta-analysis. BJU Int [Internet]. 2020 Mar 1 [cited 2022 Jul 17];125(3):355–68. Available from: https://pubmed.ncbi.nlm.nih.gov/31797520/

72. Trabert B, Chen J, Devesa SS, Bray F, Mcglynn KA. International patterns and trends in testicular cancer incidence, overall and by histologic subtype, 1973-2007. Andrology [Internet]. 2015 Jan 1 [cited 2022 Jul 17];3(1):4–12. Available from: https://pubmed.ncbi.nlm.nih.gov/25331326/

73. Dela Cruz CS, Tanoue LT, Matthay RA. Lung cancer: epidemiology, etiology, and prevention. Clin Chest Med [Internet]. 2011 Dec [cited 2024 Jun 3];32(4):605–44. Available from: https://pubmed.ncbi.nlm.nih.gov/22054876/

74. Siegel RL, Miller KD, Fuchs HE, Jemal A. Cancer statistics, 2022. CA Cancer J Clin. 2022 Jan;72(1):7–33.

75. Smith CJ, Perfetti TA, Garg R, Hansch C. IARC carcinogens reported in cigarette mainstream smoke and their calculated log P values. Food and Chemical Toxicology [Internet]. 2003 Jun 1 [cited 2024 Jun 3];41(6):807–17. Available from: https://pubmed.ncbi.nlm.nih.gov/12738186/

76. Le Calvez F, Mukeria A, Hunt JD, Kelm O, Hung RJ, Tanière P, et al. TP53 and KRAS mutation load and types in lung cancers in relation to tobacco smoke: distinct patterns in never, former, and current smokers. Cancer Res [Internet]. 2005 Jun 15 [cited 2024 Jun 3];65(12):5076–83. Available from: https://pubmed.ncbi.nlm.nih.gov/15958551/

77. Pao W, Hutchinson KE. Chipping away at the lung cancer genome. Nat Med [Internet]. 2012 Mar 6 [cited 2017 Jul 22];18(3):349–51. Available from: http://www.nature.com/doifinder/10.1038/nm.2697

78. Pao W, Girard N. New driver mutations in non-small-cell lung cancer. Lancet Oncol [Internet]. 2011 Feb [cited 2017 Jul 22];12(2):175–80. Available from: http://linkinghub.elsevier.com/retrieve/pii/S1470204510700875

79. Ding L, Getz G, Wheeler DA, Mardis ER, McLellan MD, Cibulskis K, et al. Somatic mutations affect key pathways in lung adenocarcinoma. Nature [Internet]. 2008 Oct 23 [cited 2017 Jul 22];455(7216):1069–75. Available from: http://www.ncbi.nlm.nih.gov/pubmed/18948947

80. Stewart BW, Wild CP. World cancer report 2014. World Health Organization [Internet]. 2014;1–2. Available from: http://www.videnza.org/wp-content/uploads/World-Cancer-Report-2014.pdf

81. Travis WD, Brambilla E, Burke AP, Marx A, Nicholson AG. Introduction to the 2015 World Health Organization Classification of Tumors of the Lung, Pleura, Thymus, and Heart. Journal of Thoracic

Oncology [Internet]. 2015 Sep 26 [cited 2024 Jun 2];10(9):1240–2. Available from: http://www.jto.org/article/S155608641533570X/fulltext

82. Travis WD, Brambilla E, Nicholson AG, Yatabe Y, Austin JHM, Beasley MB, et al. The 2015 World Health Organization Classification of Lung Tumors: Impact of Genetic, Clinical and Radiologic Advances Since the 2004 Classification. Journal of Thoracic Oncology. 2015 Sep 1;10(9):1243–60.

83. Pesch B, Kendzia B, Gustavsson P, Jöckel KH, Johnen G, Pohlabeln H, et al. Cigarette smoking and lung cancer-relative risk estimates for the major histological types from a pooled analysis of case-control studies. Int J Cancer [Internet]. 2012 Sep 1 [cited 2017 Jul 22];131(5):1210–9. Available from: http://doi.wiley.com/10.1002/ijc.27339

84. Travis WD, Brambilla E, Riely GJ. New Pathologic Classification of Lung Cancer: Relevance for Clinical Practice and Clinical Trials. Journal of Clinical Oncology [Internet]. 2013 Mar 10 [cited 2017 Jul 22];31(8):992–1001. Available from: http://ascopubs.org/doi/10.1200/JCO.2012.46.9270

85. Travis WD, Brambilla E, Riely GJ. New pathologic classification of lung cancer: relevance for clinical practice and clinical trials. J Clin Oncol [Internet]. 2013 Mar 10 [cited 2017 Jul 22];31(8):992–1001. Available from: http://ascopubs.org/doi/10.1200/JCO.2012.46.9270

86. Nelson GS, Pink A, Lee S, Han G, Morris D, Ogilvie T, et al. Gynecologic Oncology MMR de fi ciency is common in high-grade endometrioid carcinomas and is associated with an unfavorable outcome. Gynecol Oncol [Internet]. 2013;131(2):309–14. Available from: http://dx.doi.org/10.1016/j.ygyno.2013.08.003

87. Pignon JP, Tribodet H, Scagliotti G V., Douillard JY, Shepherd FA, Stephens RJ, et al. Lung adjuvant cisplatin evaluation: a pooled analysis by the LACE Collaborative Group. J Clin Oncol [Internet]. 2008 [cited 2024 Jun 2];26(21):3552–9. Available from: https://pubmed.ncbi.nlm.nih.gov/18506026/

88. R A, A A, S B, JP H, DH J, T LC, et al. Adjuvant chemotherapy, with or without postoperative radiotherapy, in operable non-small-cell lung cancer: two meta-analyses of individual patient data. Lancet [Internet]. 2010 [cited 2024 Jun 2];375(9722):1267–77. Available from: https://pubmed.ncbi.nlm.nih.gov/20338627/

89. Lanni TB, Grills IS, Kestin LL, Robertson JM. Stereotactic radiotherapy reduces treatment cost while improving overall survival and local control over standard fractionated radiation therapy for medically inoperable non-small-cell lung cancer. Am J Clin Oncol [Internet]. 2011 Oct [cited 2024 Jun 9];34(5):494–8. Available from: https://pubmed.ncbi.nlm.nih.gov/20805737/

90. Depierre A, Milleron B, Moro-Sibilot D, Chevret S, Quoix E, Lebeau B, et al. Preoperative chemotherapy followed by surgery compared with primary surgery in resectable stage I (except T1N0), II, and IIIa non-small-cell lung cancer. J Clin Oncol [Internet]. 2002 Jan 1 [cited 2024 Jun 4];20(1):247–53. Available from: https://pubmed.ncbi.nlm.nih.gov/11773176/

91. Gilligan D, Nicolson M, Smith I, Groen H, Dalesio O, Goldstraw P, et al. Preoperative chemotherapy in patients with resectable non-small cell lung cancer: results of the MRC LU22/NVALT 2/EORTC 08012 multicentre randomised trial and update of systematic review. Lancet [Internet]. 2007 Jun 9 [cited 2024 Jun 4];369(9577):1929–37. Available from: https://pubmed.ncbi.nlm.nih.gov/17544497/

92. Felip E, Rosell R, Maestre JA, Rodríguez-Paniagua JM, Morán T, Astudillo J, et al. Preoperative chemotherapy plus surgery versus surgery plus adjuvant chemotherapy versus surgery alone in early-stage non-small-cell lung cancer. J Clin Oncol [Internet]. 2010 Jul 1 [cited 2024 Jun 4];28(19):3138–45. Available from: https://pubmed.ncbi.nlm.nih.gov/20516435/

93. Alduais Y, Zhang H, Fan F, Chen J, Chen B. Non-small cell lung cancer (NSCLC): A review of risk factors, diagnosis, and treatment. Medicine [Internet]. 2023 Feb 22 [cited 2024 Jun 2];102(8):E32899. Available from: https://pubmed.ncbi.nlm.nih.gov/36827002/

94. Soria JC, Ohe Y, Vansteenkiste J, Reungwetwattana T, Chewaskulyong B, Lee KH, et al. Osimertinib in Untreated EGFR-Mutated Advanced Non-Small-Cell Lung Cancer. N Engl J Med [Internet]. 2018 Jan 11 [cited 2024 Jun 10];378(2):113–25. Available from: https://pubmed.ncbi.nlm.nih.gov/29151359/

95. Kwak EL, Bang YJ, Camidge DR, Shaw AT, Solomon B, Maki RG, et al. Anaplastic lymphoma kinase inhibition in non-small-cell lung cancer. N Engl J Med [Internet]. 2010 Oct 28 [cited 2024 Jun 10];363(18):1693–703. Available from: https://pubmed.ncbi.nlm.nih.gov/20979469/

96. Katayama R, Kobayashi Y, Friboulet L, Lockerman EL, Koike S, Shaw AT, et al. Cabozantinib overcomes crizotinib resistance in ROS1 fusion-positive cancer. Clin Cancer Res [Internet]. 2015 Jan 1 [cited 2024 Jun 10];21(1):166–74. Available from: https://pubmed.ncbi.nlm.nih.gov/25351743/

97. Drilon A, Laetsch TW, Kummar S, DuBois SG, Lassen UN, Demetri GD, et al. Efficacy of Larotrectinib in TRK Fusion-Positive Cancers in Adults and Children. N Engl J Med [Internet]. 2018 Feb 22 [cited 2024 Jun 10];378(8):731–9. Available from: https://pubmed.ncbi.nlm.nih.gov/29466156/

98. Drilon A, Hu ZI, Lai GGY, Tan DSW. Targeting RET-driven cancers: lessons from evolving preclinical and clinical landscapes. Nat Rev Clin Oncol [Internet]. 2018 Mar 1 [cited 2024 Jun 10];15(3):151–67. Available from: https://pubmed.ncbi.nlm.nih.gov/29134959/

99. Paik PK, Felip E, Veillon R, Sakai H, Cortot AB, Garassino MC, et al. Tepotinib in Non-Small-Cell Lung Cancer with MET Exon 14 Skipping Mutations. N Engl J Med [Internet]. 2020 Sep 3 [cited 2024 Jun 10];383(10):931–43. Available from: https://pubmed.ncbi.nlm.nih.gov/32469185/

100. Skoulidis F, Li BT, Dy GK, Price TJ, Falchook GS, Wolf J, et al. Sotorasib for Lung Cancers with KRAS p.G12C Mutation. N Engl J Med [Internet]. 2021 Jun 24 [cited 2024 Jun 10];384(25):2371–81. Available from: https://pubmed.ncbi.nlm.nih.gov/34096690/

101. Planchard D, Smit EF, Groen HJM, Mazieres J, Besse B, Helland Å, et al. Dabrafenib plus trametinib in patients with previously untreated BRAFV600E-mutant metastatic non-small-cell lung cancer: an open-label, phase 2 trial. Lancet Oncol [Internet]. 2017 Oct 1 [cited 2024 Jun 10];18(10):1307–16. Available from: https://pubmed.ncbi.nlm.nih.gov/28919011/

102. Veluswamy R, Mack PC, Houldsworth J, Elkhouly E, Hirsch FR. KRAS G12C-Mutant Non-Small Cell Lung Cancer: Biology, Developmental Therapeutics, and Molecular Testing. J Mol Diagn [Internet]. 2021 May 1 [cited 2024 Jun 10];23(5):507–20. Available from: https://pubmed.ncbi.nlm.nih.gov/33618059/

103. Da Cunha Santos G, Shepherd FA, Tsao MS. EGFR mutations and lung cancer. Annu Rev Pathol [Internet]. 2011 Feb 28 [cited 2024 Jun 10];6:49–69. Available from: https://pubmed.ncbi.nlm.nih.gov/20887192/

104. Calle EE, Rodriguez C, Walker-Thurmond K, Thun MJ. Overweight, obesity, and mortality from cancer in a prospectively studied cohort of U.S. adults. N Engl J Med [Internet]. 2003 Apr 24 [cited 2024 Jun 9];348(17):1625–38. Available from: https://pubmed.ncbi.nlm.nih.gov/12711737/

105. Broeke SWT, Klift HMV, Tops CMJ, Aretz S, Bernstein I, Buchanan DD, et al. Cancer Risks for PMS2-Associated Lynch Syndrome. J Clin Oncol [Internet]. 2018 Oct 10 [cited 2024 Jun 9];36(29):2961–8. Available from: https://pubmed.ncbi.nlm.nih.gov/30161022/

106. Ring KL, Bruegl AS, Allen BA, Elkin EP, Singh N, Hartman AR, et al. Germline multi-gene hereditary cancer panel testing in an unselected endometrial cancer cohort. Mod Pathol [Internet]. 2016 Nov 1 [cited 2024 Jun 9];29(11):1381–9. Available from: https://pubmed.ncbi.nlm.nih.gov/27443514/

107. Bonadona V, Bonaïti B, Olschwang S, Grandjouan S, Huiart L, Longy M, et al. Cancer risks associated with germline mutations in MLH1, MSH2, and MSH6 genes in Lynch syndrome. JAMA [Internet]. 2011 Jun 8 [cited 2024 Jun 9];305(22):2304–10. Available from: https://pubmed.ncbi.nlm.nih.gov/21642682/

108. Møller P, Seppälä TT, Bernstein I, Holinski-Feder E, Sala P, Evans DG, et al. Cancer risk and survival in path_MMR carriers by gene and gender up to 75 years of age: a report from the Prospective Lynch Syndrome Database. Gut [Internet]. 2018 [cited 2024 Jun 9];67(7):1306–16. Available from: https://pubmed.ncbi.nlm.nih.gov/28754778/

109. Colombo N, Creutzberg C, Amant F, Bosse T, González-Martón A, Ledermann J, et al. ESMO-ESGO-ESTRO Consensus Conference on Endometrial Cancer: diagnosis, treatment and follow-up. Ann Oncol [Internet]. 2016 Jan 1 [cited 2024 Jun 9];27(1):16–41. Available from: https://pubmed.ncbi.nlm.nih.gov/26634381/

110. Lacey J V., Sherman ME, Rush BB, Ronnett BM, Ioffe OB, Duggan MA, et al. Absolute risk of endometrial carcinoma during 20-year follow-up among women with endometrial hyperplasia. J Clin Oncol [Internet]. 2010 Feb 10 [cited 2024 Jun 9];28(5):788–92. Available from: https://pubmed.ncbi.nlm.nih.gov/20065186/

111. Makker V, MacKay H, Ray-Coquard I, Levine DA, Westin SN, Aoki D, et al. Endometrial cancer. Nat Rev Dis Primers [Internet]. 2021 Dec 1 [cited 2024 Jun 9];7(1). Available from: https://pubmed.ncbi.nlm.nih.gov/34887451/

112. Suryo Rahmanto Y, Shen W, Shi X, Chen X, Yu Y, Yu ZC, et al. Inactivation of Arid1a in the endometrium is associated with endometrioid tumorigenesis through transcriptional reprogramming. Nat Commun [Internet]. 2020 Dec 1 [cited 2024 Jun 9];11(1). Available from: https://pubmed.ncbi.nlm.nih.gov/32483112/

113. Gao Y, Lin P, Lydon JP, Li Q. Conditional abrogation of transforming growth factor-β receptor 1 in PTEN-inactivated endometrium promotes endometrial cancer progression in mice. J Pathol [Internet]. 2017 Sep 1 [cited 2024 Jun 9];243(1):89–99. Available from: https://pubmed.ncbi.nlm.nih.gov/28657664/

114. Jarboe EA, Pizer ES, Miron A, Monte N, Mutter GL, Crum CP. Evidence for a latent precursor (p53 signature) that may precede serous endometrial intraepithelial carcinoma. Mod Pathol [Internet]. 2009 [cited 2024 Jun 9];22(3):345–50. Available from: https://pubmed.ncbi.nlm.nih.gov/19151662/

115. Getz G, Gabriel SB, Cibulskis K, Lander E, Sivachenko A, Sougnez C, et al. Integrated genomic characterization of endometrial carcinoma. Nature [Internet]. 2013 [cited 2024 Jun 9];497(7447):67–73. Available from: https://pubmed.ncbi.nlm.nih.gov/23636398/

116. Concin N, Matias-Guiu X, Vergote I, Cibula D, Mirza MR, Marnitz S, et al. ESGO/ESTRO/ESP guidelines for the management of patients with endometrial carcinoma. Int J Gynecol Cancer [Internet]. 2021 Jan 1 [cited 2024 Jun 9];31(1):12–39. Available from: https://pubmed.ncbi.nlm.nih.gov/33397713/

117. Bokhman J V. Two pathogenetic types of endometrial carcinoma. Gynecol Oncol [Internet]. 1983 [cited 2024 Jun 10];15(1):10–7. Available from: https://pubmed.ncbi.nlm.nih.gov/6822361/

118. Talhouk A, McConechy MK, Leung S, Yang W, Lum A, Senz J, et al. Confirmation of ProMisE: A simple, genomics-based clinical classifier for endometrial cancer. Cancer [Internet]. 2017 Mar 1 [cited 2024 Jun 9];123(5):802–13. Available from: https://pubmed.ncbi.nlm.nih.gov/28061006/

119. Talhouk A, McConechy MK, Leung S, Li-Chang HH, Kwon JS, Melnyk N, et al. A clinically applicable molecular-based classification for endometrial cancers. Br J Cancer [Internet]. 2015;113(2):299–310. Available from: http://www.nature.com/doifinder/10.1038/bjc.2015.190

120. Kommoss S, McConechy MK, Kommoss F, Leung S, Bunz A, Magrill J, et al. Final validation of the ProMisE molecular classifier for endometrial carcinoma in a large population-based case series. Ann Oncol [Internet]. 2018 May 1 [cited 2024 Jun 9];29(5):1180–8. Available from: https://pubmed.ncbi.nlm.nih.gov/29432521/

121. Berek JS, Matias-Guiu X, Creutzberg C, Fotopoulou C, Gaffney D, Kehoe S, et al. FIGO staging of endometrial cancer: 2023. Int J Gynaecol Obstet [Internet]. 2023 Aug 1 [cited 2024 Jun 9];162(2):383–94. Available from: https://pubmed.ncbi.nlm.nih.gov/37337978/

122. Brooks RA, Fleming GF, Lastra RR, Lee NK, Moroney JW, Son CH, et al. Current recommendations and recent progress in endometrial cancer. CA Cancer J Clin [Internet]. 2019 Jul [cited 2024 Jun 9];69(4):258–79. Available from: https://pubmed.ncbi.nlm.nih.gov/31074865/

123. MacKay HJ, Freixinos VR, Fleming GF. Therapeutic Targets and Opportunities in Endometrial Cancer: Update on Endocrine Therapy and Nonimmunotherapy Targeted Options. Am Soc Clin Oncol Educ Book [Internet]. 2020 May [cited 2024 Jun 9];40(40):245–55. Available from: https://pubmed.ncbi.nlm.nih.gov/32239967/

124. Green AK, Feinberg J, Makker V. A Review of Immune Checkpoint Blockade Therapy in Endometrial Cancer. Am Soc Clin Oncol Educ Book [Internet]. 2020 May [cited 2024 Jun 9];40(40):238–44. Available from: https://pubmed.ncbi.nlm.nih.gov/32213091/

125. Abu-Rustum NR, Chi DS, Leitao M, Oke EA, Hensley ML, Alektiar KM, et al. What is the incidence of isolated paraaortic nodal recurrence in grade 1 endometrial carcinoma? Gynecol Oncol [Internet]. 2008 Oct [cited 2024 Jun 9];111(1):46–8. Available from: https://pubmed.ncbi.nlm.nih.gov/18657853/

126. Metindir J, Dilek GB. The role of omentectomy during the surgical staging in patients with clinical stage I endometrioid adenocarcinoma. J Cancer Res Clin Oncol [Internet]. 2008 Oct [cited 2024 Jun 9];134(10):1067–70. Available from: https://pubmed.ncbi.nlm.nih.gov/18386056/

127. Rabinovich A. Neo-adjuvant chemotherapy for advanced stage endometrial carcinoma: a glimmer of hope in select patients. Arch Gynecol Obstet [Internet]. 2016 Jan 1 [cited 2024 Jun 9];293(1):47–53. Available from: https://pubmed.ncbi.nlm.nih.gov/26288978/

128. Miller DS, Filiaci VL, Mannel RS, Cohn DE, Matsumoto T, Tewari KS, et al. Carboplatin and Paclitaxel for Advanced Endometrial Cancer: Final Overall Survival and Adverse Event Analysis of a Phase III Trial (NRG Oncology/GOG0209). J Clin Oncol [Internet]. 2020 Nov 20 [cited 2024 Jun 9];38(33):3841–50. Available from: https://pubmed.ncbi.nlm.nih.gov/33078978/

129. Fleming GF. Second-Line Therapy for Endometrial Cancer: The Need for Better Options. J Clin Oncol [Internet]. 2015 Nov 1 [cited 2024 Jun 9];33(31):3535–40. Available from: https://pubmed.ncbi.nlm.nih.gov/26195695/

130. Fader AN, Roque DM, Siegel E, Buza N, Hui P, Abdelghany O, et al. Randomized Phase II Trial of Carboplatin-Paclitaxel Compared with Carboplatin-Paclitaxel-Trastuzumab in Advanced (Stage III-IV) or Recurrent Uterine Serous Carcinomas that Overexpress Her2/Neu (NCT01367002): Updated Overall Survival Analysis. Clin Cancer Res [Internet]. 2020 Aug 1 [cited 2024 Jun 9];26(15):3928–35. Available from: https://pubmed.ncbi.nlm.nih.gov/32601075/

131. Marabelle A, Fakih M, Lopez J, Shah M, Shapira-Frommer R, Nakagawa K, et al. Association of tumour mutational burden with outcomes in patients with advanced solid tumours treated with pembrolizumab: prospective biomarker analysis of the multicohort, open-label, phase 2 KEYNOTE-158 study. Lancet Oncol [Internet]. 2020 Oct 1 [cited 2024 Jun 9];21(10):1353–65. Available from: https://pubmed.ncbi.nlm.nih.gov/32919526/

132. Hidalgo M, Amant F, Biankin a. V., Budinska E, Byrne a. T, Caldas C, et al. Patient-Derived Xenograft Models: An Emerging Platform for Translational Cancer Research. Cancer Discov [Internet]. 2014;4:998–1013. Available from: http://cancerdiscovery.aacrjournals.org/content/4/9/998.full

133. Abaan OD, Polley EC, Davis SR, Zhu YJ, Bilke S, Walker RL, et al. The exomes of the NCI-60 panel: a genomic resource for cancer biology and systems pharmacology. Cancer Res [Internet]. 2013 Jul 15 [cited 2024 Jun 8];73(14):4372–82. Available from: https://pubmed.ncbi.nlm.nih.gov/23856246/

134. Gillet JP, Calcagno AM, Varma S, Marino M, Green LJ, Vora MI, et al. Redefining the relevance of established cancer cell lines to the study of mechanisms of clinical anti-cancer drug resistance. Proc Natl Acad Sci U S A [Internet]. 2011 Nov 15 [cited 2024 Jun 8];108(46):18708–13. Available from: https://pubmed.ncbi.nlm.nih.gov/22068913/

135. Hausser HJ, Brenner RE. Phenotypic instability of Saos-2 cells in long-term culture. Biochem Biophys Res Commun [Internet]. 2005 Jul 22 [cited 2024 Jun 8];333(1):216–22. Available from: https://pubmed.ncbi.nlm.nih.gov/15939397/

136. Herpers B, Eppink B, James MI, Cortina C, Cañellas-Socias A, Boj SF, et al. Functional patient-derived organoid screenings identify MCLA-158 as a therapeutic EGFR × LGR5 bispecific antibody with efficacy in epithelial tumors. Nat Cancer [Internet]. 2022 Apr 1 [cited 2024 Jun 8];3(4):418–36. Available from: https://pubmed.ncbi.nlm.nih.gov/35469014/

137. Fiebig HH, Neumann HA, Henss H, Koch H, Kaiser D, Arnold H. Development of three human small cell lung cancer models in nude mice. Recent Results Cancer Res [Internet]. 1985 [cited 2024 Jun 8];97:77–86. Available from: https://pubmed.ncbi.nlm.nih.gov/2986247/

138. Tentler JJ, Tan AC, Weekes CD, Jimeno A, Leong S, Pitts TM, et al. Patient-derived tumour xenografts as models for oncology drug development. Nat Rev Clin Oncol [Internet]. 2012 Jun [cited 2024 Jun 8];9(6):338–50. Available from: https://pubmed.ncbi.nlm.nih.gov/22508028/

139. Ambrogio C, Carmona FJ, Vidal A, Falcone M, Nieto P, Romero OA, et al. Modeling lung cancer evolution and preclinical response by orthotopic mouse allografts. Cancer Res. 2014;74(21).

140. Calles A, Rubio-Viqueira B, Hidalgo M. Primary human non-small cell lung and pancreatic tumorgraft models--utility and applications in drug discovery and tumor biology. Curr Protoc Pharmacol [Internet]. 2013 [cited 2024 Jun 8];Chapter 14(SUPPL.61). Available from: https://pubmed.ncbi.nlm.nih.gov/23744711/

141. Kim MP, Evans DB, Wang H, Abbruzzese JL, Fleming JB, Gallick GE. Generation of orthotopic and heterotopic human pancreatic cancer xenografts in immunodeficient mice. Nat Protoc [Internet]. 2009 [cited 2024 Jun 8];4(11):1670–80. Available from: https://pubmed.ncbi.nlm.nih.gov/19876027/

142. Hidalgo M, Amant F, Biankin A V., Budinská E, Byrne AT, Caldas C, et al. Patient-derived xenograft models: an emerging platform for translational cancer research. Cancer Discov [Internet]. 2014 [cited 2024 Jun 8];4(9):998–1013. Available from: https://pubmed.ncbi.nlm.nih.gov/25185190/

143. Byrne AT, Alférez DG, Amant F, Annibali D, Arribas J, Biankin A V., et al. Interrogating open issues in cancer precision medicine with patient-derived xenografts. Nat Rev Cancer [Internet]. 2017 Apr 1 [cited 2024 Jun 8];17(4):254–68. Available from: https://pubmed.ncbi.nlm.nih.gov/28104906/

144. Marques Da Costa ME, Zaidi S, Scoazec JY, Droit R, Lim WC, Marchais A, et al. A biobank of pediatric patient-derived-xenograft models in cancer precision medicine trial MAPPYACTS for relapsed and refractory tumors. Commun Biol [Internet]. 2023 Dec 1 [cited 2024 Jun 8];6(1). Available from: https://pubmed.ncbi.nlm.nih.gov/37723198/

145. Némati F, Sastre-Garau X, Laurent C, Couturier J, Mariani P, Desjardins L, et al. Establishment and characterization of a panel of human uveal melanoma xenografts derived from primary and/or metastatic tumors. Clin Cancer Res [Internet]. 2010 Apr 15 [cited 2024 Jun 8];16(8):2352–62. Available from: https://pubmed.ncbi.nlm.nih.gov/20371695/

146. Zhang X, Claerhout S, Prat A, Dobrolecki LE, Petrovic I, Lai Q, et al. A renewable tissue resource of phenotypically stable, biologically and ethnically diverse, patient-derived human breast cancer xenograft models. Cancer Res [Internet]. 2013 Aug 1 [cited 2024 Jun 8];73(15):4885–97. Available from: https://pubmed.ncbi.nlm.nih.gov/23737486/

147. Dong X, Guan J, English JC, Flint J, Yee J, Evans K, et al. Patient-derived first generation xenografts of non-small cell lung cancers: promising tools for predicting drug responses for personalized chemotherapy. Clin Cancer Res [Internet]. 2010 Mar 1 [cited 2024 Jun 8];16(5):1442–51. Available from: https://pubmed.ncbi.nlm.nih.gov/20179238/

148. Johnson JI, Decker S, Zaharevitz D, Rubinstein L V., Venditti JM, Schepartz S, et al. Relationships between drug activity in NCI preclinical in vitro and in vivo models and early clinical trials. Br J Cancer [Internet]. 2001 May 18 [cited 2024 Jun 8];84(10):1424–31. Available from: https://pubmed.ncbi.nlm.nih.gov/11355958/

149. Martinez-Marti A, Felip E, Matito J, Mereu E, Navarro A, Cedrés S, et al. Dual MET and ERBB inhibition overcomes intratumor plasticity in osimertinib-resistant-advanced non-small-cell lung cancer (NSCLC). Ann Oncol [Internet]. 2017 Oct 1 [cited 2024 Jun 8];28(10):2451–7. Available from: https://pubmed.ncbi.nlm.nih.gov/28961841/

150. Creus-Bachiller E, Fernández-Rodríguez J, Magallón-Lorenz M, Ortega-Bertran S, Navas-Rutete S, Romagosa C, et al. Expanding a precision medicine platform for malignant peripheral nerve sheath tumors: New patient-derived orthotopic xenografts, cell lines and tumor entities. Mol Oncol [Internet]. 2024 Apr 1 [cited 2024 Jun 8];18(4):895–917. Available from: https://pubmed.ncbi.nlm.nih.gov/37798904/

151. Castellsagué J, Gel B, Fernández-Rodríguez J, Llatjós R, Blanco I, Benavente Y, et al. Comprehensive establishment and characterization of orthoxenograft mouse models of malignant peripheral nerve sheath tumors for personalized medicine. EMBO Mol Med [Internet]. 2015 May [cited 2024 Jun 8];7(5):608–27. Available from: https://pubmed.ncbi.nlm.nih.gov/25810463/

152. Fernández-Rodríguez J, Morales La Madrid A, Gel B, Castañeda Heredia A, Salvador H, Martínez-Iniesta M, et al. Use of patient derived orthotopic xenograft models for real-time therapy guidance in a pediatric sporadic malignant peripheral nerve sheath tumor. Ther Adv Med Oncol [Internet]. 2020 [cited 2024 Jun 8];12. Available from: https://pubmed.ncbi.nlm.nih.gov/32670419/

153. Keysar SB, Astling DP, Anderson RT, Vogler BW, Bowles DW, Morton JJ, et al. A patient tumor transplant model of squamous cell cancer identifies PI3K inhibitors as candidate therapeutics in defined molecular bins. Mol Oncol [Internet]. 2013 [cited 2024 Jun 8];7(4):776–90. Available from: https://pubmed.ncbi.nlm.nih.gov/23607916/

154. Migliardi G, Sassi F, Torti D, Galimi F, Zanella ER, Buscarino M, et al. Inhibition of MEK and PI3K/mTOR suppresses tumor growth but does not cause tumor regression in patient-derived xenografts of RAS-mutant colorectal carcinomas. Clin Cancer Res [Internet]. 2012 May 1 [cited 2024 Jun 8];18(9):2515–25. Available from: https://pubmed.ncbi.nlm.nih.gov/22392911/

155. Bertotti A, Migliardi G, Galimi F, Sassi F, Torti D, Isella C, et al. A molecularly annotated platform of patient-derived xenografts ('xenopatients') identifies HER2 as an effective therapeutic target in cetuximab-resistant colorectal cancer. Cancer Discov [Internet]. 2011 Nov [cited 2024 Jun 8];1(6):508–23. Available from: https://pubmed.ncbi.nlm.nih.gov/22586653/

156. Julien S, Merino-Trigo A, Lacroix L, Pocard M, Goeŕé D, Mariani P, et al. Characterization of a large panel of patient-derived tumor xenografts representing the clinical heterogeneity of human colorectal cancer. Clin Cancer Res [Internet]. 2012 Oct 1 [cited 2024 Jun 8];18(19):5314–28. Available from: https://pubmed.ncbi.nlm.nih.gov/22825584/

157. Bardelli A, Corso S, Bertotti A, Hobor S, Valtorta E, Siravegna G, et al. Amplification of the MET receptor drives resistance to anti-EGFR therapies in colorectal cancer. Cancer Discov [Internet]. 2013 [cited 2024 Jun 8];3(6):658–73. Available from: https://pubmed.ncbi.nlm.nih.gov/23729478/

158. Dancey JE, Bedard PL, Onetto N, Hudson TJ. The genetic basis for cancer treatment decisions. Cell [Internet]. 2012 Feb 3 [cited 2024 Jun 8];148(3):409–20. Available from: https://pubmed.ncbi.nlm.nih.gov/22304912/

159. Garraway LA. Genomics-driven oncology: framework for an emerging paradigm. J Clin Oncol [Internet]. 2013 May 20 [cited 2024 Jun 8];31(15):1806–14. Available from: https://pubmed.ncbi.nlm.nih.gov/23589557/

160. Diaz LA, Williams RT, Wu J, Kinde I, Hecht JR, Berlin J, et al. The molecular evolution of acquired resistance to targeted EGFR blockade in colorectal cancers. Nature [Internet]. 2012 Jun 28 [cited 2024 Jun 8];486(7404):537–40. Available from: https://pubmed.ncbi.nlm.nih.gov/22722843/

161. Garber K. Personal mouse colonies give hope for pancreatic cancer patients. J Natl Cancer Inst [Internet]. 2007 Jan 17 [cited 2024 Jun 8];99(2):105–7. Available from: https://pubmed.ncbi.nlm.nih.gov/17227991/

162. Byrne AT, Alférez DG, Amant F, Annibali D, Arribas J, Biankin A V., et al. Interrogating open issues in cancer precision medicine with patient-derived xenografts. Nat Rev Cancer [Internet]. 2017;17(4):254–68. Available from: http://www.nature.com/doifinder/10.1038/nrc.2016.140

163. Castillo-Avila W, Piulats JM, Garcia Del Muro X, Vidal A, Condom E, Casanovas O, et al. Sunitinib inhibits tumor growth and synergizes with cisplatin in orthotopic models of cisplatin-sensitive and cisplatin-resistant human testicular germ cell tumors. Clin Cancer Res [Internet]. 2009 May 15 [cited 2014 Jul 30];15(10):3384–95. Available from: http://www.ncbi.nlm.nih.gov/pubmed/19417025

164. Juliachs M, Muñoz C, Moutinho CA, Vidal A, Condom E, Esteller M, et al. The PDGFRβ-AKT pathway contributes to CDDP-acquired resistance in testicular germ cell tumors. Clinical Cancer Research. 2014;20(3).

165. Vidal A, Munoz C, Guillen MJ, Moreto J, Puertas S, Martinez-Iniesta M, et al. Lurbinectedin (PM01183), a New DNA Minor Groove Binder, Inhibits Growth of Orthotopic Primary Graft of Cisplatin-Resistant Epithelial Ovarian Cancer. Clinical Cancer Research [Internet]. 2012; Available from: http://gateway.webofknowledge.com/gateway/Gateway.cgi?GWVersion=2&SrcAuth=ORCID&SrcApp=OrcidOrg&DestLinkType=FullRecord&DestApp=WOS_CPL&KeyUT=WOS:000311906600025&KeyUID=WOS:000311906600025

166. Pabo CO, Sauer RT. Protein-DNA Recognition. Annu Rev Biochem [Internet]. 1984 Jun [cited 2017 Jun 28];53(1):293–321. Available from: http://www.ncbi.nlm.nih.gov/pubmed/6236744

167. Rohs R, West SM, Sosinsky A, Liu P, Mann RS, Honig B. The role of DNA shape in protein?DNA recognition. Nature [Internet]. 2009 Oct 29 [cited 2017 Jun 28];461(7268):1248–53. Available from: http://www.ncbi.nlm.nih.gov/pubmed/19865164

168. Susbielle G, Blattes R, Brevet V, Monod C, Käs E. Target practice: aiming at satellite repeats with DNA minor groove binders. Curr Med Chem Anticancer Agents [Internet]. 2005 Jul [cited 2017 Jun 28];5(4):409–20. Available from: http://www.ncbi.nlm.nih.gov/pubmed/16101491

169. Guan Y, Sakai R, Rinehart KL, Wang AH. Molecular and crystal structures of ecteinascidins: potent antitumor compounds from the Caribbean tunicate Ecteinascidia turbinata. J Biomol Struct Dyn [Internet]. 1993 Apr [cited 2017 Jun 28];10(5):793–818. Available from: http://www.ncbi.nlm.nih.gov/pubmed/8318161

170. Kishi K, Yazawa K, Takahashi K, Mikami Y, Arai T. Structure-activity relationships of saframycins. J Antibiot (Tokyo) [Internet]. 1984 Aug [cited 2017 Jun 28];37(8):847–52. Available from: http://www.ncbi.nlm.nih.gov/pubmed/6480503

171. Pommier Y, Kohlhagen G, Bailly C, Waring M, Mazumder A, Kohn KW. DNA sequence- and structure-selective alkylation of guanine N2 in the DNA minor groove by ecteinascidin 743, a potent antitumor compound from the Caribbean tunicate Ecteinascidia turbinata. Biochemistry [Internet]. 1996 Oct 15 [cited 2017 Jun 28];35(41):13303–9. Available from: http://pubs.acs.org/doi/abs/10.1021/bi960306b

172. Manzanares I, Cuevas C, García-Nieto R, Marco E, Gago F. Advances in the chemistry and pharmacology of ecteinascidins, a promising new class of anti-cancer agents. Curr Med Chem Anticancer Agents [Internet]. 2001 Nov [cited 2017 Jun 28];1(3):257–76. Available from: http://www.ncbi.nlm.nih.gov/pubmed/12678757

173. Bueren-Calabuig JA, Giraudon C, Galmarini CM, Egly JM, Gago F. Temperature-induced melting of double-stranded DNA in the absence and presence of covalently bonded antitumour drugs: insight from molecular dynamics simulations. Nucleic Acids Res [Internet]. 2011 Oct [cited 2017 Jun 28];39(18):8248–57. Available from: https://academic.oup.com/nar/article-lookup/doi/10.1093/nar/gkr512

174. Leal JFM, Martínez-Díez M, García-Hernández V, Moneo V, Domingo A, Bueren-Calabuig JA, et al. PM01183, a new DNA minor groove covalent binder with potent in vitro and in vivo anti-tumour activity. Br J Pharmacol [Internet]. 2010 Nov [cited 2017 Jun 28];161(5):1099–110. Available from: http://doi.wiley.com/10.1111/j.1476-5381.2010.00945.x

175. Soares DG, Machado MS, Rocca CJ, Poindessous V, Ouaret D, Sarasin A, et al. Trabectedin and Its C Subunit Modified Analogue PM01183 Attenuate Nucleotide Excision Repair and Show Activity toward Platinum-Resistant Cells. Mol Cancer Ther [Internet]. 2011 Aug 1 [cited 2017 Jun 28];10(8):1481–9. Available from: http://www.ncbi.nlm.nih.gov/pubmed/21622731

176. Dunton CJ. New options for the treatment of advanced ovarian cancer. Semin Oncol [Internet]. 1997 Feb [cited 2017 Jul 10];24(1 Suppl 5):S5-2-S5-11. Available from: http://www.ncbi.nlm.nih.gov/pubmed/9122739

177. Sassen S, Schmalfeldt B, Avril N, Kuhn W, Busch R, Höfler H, et al. Histopathologic assessment of tumor regression after neoadjuvant chemotherapy in advanced-stage ovarian cancer. Hum Pathol [Internet]. 2007 Jun [cited 2014 Jul 30];38(6):926–34. Available from: http://www.ncbi.nlm.nih.gov/pubmed/17397905

178. Poveda A, del Campo JM, Ray-Coquard I, Alexandre J, Provansal M, Guerra Alía EM, et al. Phase II randomized study of PM01183 versus topotecan in patients with platinum-resistant/refractory advanced ovarian cancer. Ann Oncol [Internet]. 2017 Jun 1 [cited 2024 Jun 7];28(6):1280–7. Available from: https://pubmed.ncbi.nlm.nih.gov/28368437/

179. Gaillard S, Oaknin A, Ray-Coquard I, Vergote I, Scambia G, Colombo N, et al. Lurbinectedin versus pegylated liposomal doxorubicin or topotecan in patients with platinum-resistant ovarian cancer: A multicenter, randomized, controlled, open-label phase 3 study (CORAIL). Gynecol Oncol [Internet]. 2021 Nov 1 [cited 2024 Jun 7];163(2):237–45. Available from: https://pubmed.ncbi.nlm.nih.gov/34521554/

180. Poveda A, Lopez-Reig R, Oaknin A, Redondo A, Rubio MJ, Guerra E, et al. Phase 2 Trial (POLA Study) of Lurbinectedin plus Olaparib in Patients with Advanced Solid Tumors: Results of Efficacy, Tolerability, and the Translational Study. Cancers (Basel) [Internet]. 2022 Feb 1 [cited 2024 Jun 7];14(4). Available from: https://pubmed.ncbi.nlm.nih.gov/35205662/

181. Trigo J, Subbiah V, Besse B, Moreno V, López R, Sala MA, et al. Lurbinectedin as second-line treatment for patients with small-cell lung cancer: a single-arm, open-label, phase 2 basket trial. Lancet Oncol [Internet]. 2020 May 1 [cited 2024 Jun 7];21(5):645–54. Available from: https://pubmed.ncbi.nlm.nih.gov/32224306/

182. Markham A. Lurbinectedin: First Approval. Drugs [Internet]. 2020 Sep 1 [cited 2024 Jun 7];80(13):1345–53. Available from: https://pubmed.ncbi.nlm.nih.gov/32816202/

183. Gadducci A, Cosio S. Trabectedin and lurbinectedin: Mechanisms of action, clinical impact, and future perspectives in uterine and soft tissue sarcoma, ovarian carcinoma, and endometrial carcinoma. Front Oncol [Internet]. 2022 Nov 3 [cited 2024 Jun 7];12. Available from: https://pubmed.ncbi.nlm.nih.gov/36408147/

184. Piulats JM, Vidal A, García-Rodríguez FJ, Muñoz C, Nadal M, Moutinho C, et al. Orthoxenografts of Testicular Germ Cell Tumors Demonstrate Genomic Changes Associated with Cisplatin Resistance and Identify PDMP as a Resensitizing Agent. Clin Cancer Res [Internet]. 2018 Aug 1 [cited 2022 Jul 14];24(15):3755–66. Available from: https://pubmed.ncbi.nlm.nih.gov/29618620/

185. Patterson MC, Vecchio D, Prady H, Abel L, Wraith JE. Miglustat for treatment of Niemann-Pick C disease: a randomised controlled study. Lancet Neurol [Internet]. 2007 Sep [cited 2024 Apr 22];6(9):765–72. Available from: https://pubmed.ncbi.nlm.nih.gov/17689147/

186. Bennett LL, Mohan D. Gaucher disease and its treatment options. Ann Pharmacother [Internet]. 2013 Sep 1 [cited 2024 Apr 22];47(9):1182–93. Available from: https://pubmed.ncbi.nlm.nih.gov/24259734/

187. Devis-Jauregui L, Vidal A, Plata-Peña L, Santacana M, García-Mulero S, Bonifaci N, et al. Generation and Integrated Analysis of Advanced Patient-Derived Orthoxenograft Models (PDOX) for the Rational Assessment of Targeted Therapies in Endometrial Cancer. Adv Sci (Weinh) [Internet]. 2022 Jan 4 [cited 2024 Jun 7];10(1). Available from: https://pubmed.ncbi.nlm.nih.gov/36373729/

188. Eritja N, Chen BJ, Rodríguez-Barrueco R, Santacana M, Gatius S, Vidal A, et al. Autophagy orchestrates adaptive responses to targeted therapy in endometrial cancer. Autophagy [Internet].

2017 Mar 4 [cited 2024 Jun 7];13(3):608–24. Available from: https://pubmed.ncbi.nlm.nih.gov/28055301/

189. Lopez-Mejia IC, Pijuan J, Navaridas R, Santacana M, Gatius S, Velasco A, et al. Oxidative stress-induced FAK activation contributes to uterine serous carcinoma aggressiveness. Mol Oncol [Internet]. 2023 Jan 1 [cited 2024 Jun 7];17(1):98–118. Available from: https://pubmed.ncbi.nlm.nih.gov/36409196/

190. Etxeberria I, Bolaños E, Quetglas JI, Gros A, Villanueva A, Palomero J, et al. Intratumor Adoptive Transfer of IL-12 mRNA Transiently Engineered Antitumor CD8$^+$ T Cells. Cancer Cell. 2019;36(6).

191. Ambrogio C, Gómez-López G, Falcone M, Vidal A, Nadal E, Crosetto N, et al. Combined inhibition of DDR1 and Notch signaling is a therapeutic strategy for KRAS-driven lung adenocarcinoma. Nat Med [Internet]. 2016 Mar 1 [cited 2024 Jun 13];22(3):270–7. Available from: https://pubmed.ncbi.nlm.nih.gov/26855149/

192. Fernandes Neto JM, Nadal E, Bosdriesz E, Ooft SN, Farre L, McLean C, et al. Multiple low dose therapy as an effective strategy to treat EGFR inhibitor-resistant NSCLC tumours. Nat Commun [Internet]. 2020 Dec 1 [cited 2024 Jun 13];11(1). Available from: https://pubmed.ncbi.nlm.nih.gov/32572029/

193. Dias MH, Friskes A, Wang S, Fernandes Neto JM, van Gemert F, Mourragui S, et al. Paradoxical activation of oncogenic signaling as a cancer treatment strategy. Cancer Discov [Internet]. 2024 Apr 30 [cited 2024 Jun 13];OF1–26. Available from: https://pubmed.ncbi.nlm.nih.gov/38533987/